Phase change dispersions as high performance heat transfer fluids

Poppy O'Neill

N°d'ordre NNT : 2022ISAL0073

THESE de DOCTORAT **DE L'**INSA LYON,
membre de l'Université de Lyon

Ecole Doctorale N° 162
Mécanique, Énergétique, Génie Civil, Acoustique (MEGA)
Spécialité/ discipline de doctorat : Thermique et Énergétique

Soutenue publiquement le 02/09/2022, par :
Poppy O'Neill

Phase change dispersions as high performance heat transfer fluids

Devant le jury composé de :

BELLETTRE, Jérôme	Professeur (Polytech Nantes)	Président
SIROUX, Monica	Professeure (INSA-Strasbourg)	Rapporteure
KIND, Matthias	Professeur (Karlsruher Institut Für Technologie	Rapporteur
REVELLIN , Rémi	Professeur (INSA Lyon)	Directeur de thèse
BONJOUR, Jocelyn	Professeur (INSA Lyon)	Co-directeur de thèse
FISCHER, Ludger	Professeur (HSLU, Luzern)	Directeur de thèse
STAMATIOU, Anastasia	Maître de conférences (HSLU)	Invitée
HABERSCHILL, Philippe	Maître de conférences (HSLU)	Invitée

Département FEDORA – INSA Lyon - Ecoles Doctorales

SIGLE	ECOLE DOCTORALE	NOM ET COORDONNEES DU RESPONSABLE
CHIMIE	**CHIMIE DE LYON** **https://www.edchimie-lyon.fr** Sec. : Renée EL MELHEM Bât. Blaise PASCAL, 3e étage secretariat@edchimie-lyon.fr	**M. Stéphane DANIELE** C2P2-CPE LYON-UMR 5265 Bâtiment F308, BP 2077 43 Boulevard du 11 novembre 1918 69616 Villeurbanne **directeur@edchimie-lyon.fr**
E.E.A.	**ÉLECTRONIQUE, ÉLECTROTECHNIQUE, AUTOMATIQUE** **https://edeea.universite-lyon.fr** Sec. : Stéphanie CAUVIN Bâtiment Direction INSA Lyon Tél : 04.72.43.71.70 secretariat.edeea@insa-lyon.fr	**M. Philippe DELACHARTRE** INSA LYON Laboratoire CREATIS Bâtiment Blaise Pascal, 7 avenue Jean Capelle 69621 Villeurbanne CEDEX Tél : 04.72.43.88.63 **philippe.delachartre@insa-lyon.fr**
E2M2	**ÉVOLUTION, ÉCOSYSTÈME, MICROBIOLOGIE, MODÉLISATION** **http://e2m2.universite-lyon.fr** Sec. : Bénédicte LANZA Bât. Atrium, UCB Lyon 1 Tél : 04.72.44.83.62 secretariat.e2m2@univ-lyon1.fr	**Mme Sandrine CHARLES** Université Claude Bernard Lyon 1 UFR Biosciences Bâtiment Mendel 43, boulevard du 11 Novembre 1918 69622 Villeurbanne CEDEX **sandrine.charles@univ-lyon1.fr**
EDISS	**INTERDISCIPLINAIRE SCIENCES-SANTÉ** **http://ediss.universite-lyon.fr** Sec. : Bénédicte LANZA Bât. Atrium, UCB Lyon 1 Tél : 04.72.44.83.62 secretariat.ediss@univ-lyon1.fr	**Mme Sylvie RICARD-BLUM** Institut de Chimie et Biochimie Moléculaires et Supramoléculaires (ICBMS) - UMR 5246 CNRS - Université Lyon 1 Bâtiment Raulin - 2ème étage Nord 43 Boulevard du 11 novembre 1918 69622 Villeurbanne Cedex Tél : +33(0)4 72 44 82 32 **sylvie.ricard-blum@univ-lyon1.fr**
INFOMATHS	**INFORMATIQUE ET MATHÉMATIQUES** **http://edinfomaths.universite-lyon.fr** Sec. : Renée EL MELHEM Bât. Blaise PASCAL, 3e étage Tél : 04.72.43.80.46 infomaths@univ-lyon1.fr	**M. Hamamache KHEDDOUCI** Université Claude Bernard Lyon 1 Bât. Nautibus 43, Boulevard du 11 novembre 1918 69 622 Villeurbanne Cedex France Tél : 04.72.44.83.69 **hamamache.kheddouci@univ-lyon1.fr**
Matériaux	**MATÉRIAUX DE LYON** **http://ed34.universite-lyon.fr** Sec. : Yann DE ORDENANA Tél : 04.72.18.62.44 yann.de-ordenana@ec-lyon.fr	**M. Stéphane BENAYOUN** Ecole Centrale de Lyon Laboratoire LTDS 36 avenue Guy de Collongue 69134 Ecully CEDEX Tél : 04.72.18.64.37 **stephane.benayoun@ec-lyon.fr**
MEGA	**MÉCANIQUE, ÉNERGÉTIQUE, GÉNIE CIVIL, ACOUSTIQUE** **http://edmega.universite-lyon.fr** Sec. : Stéphanie CAUVIN Tél : 04.72.43.71.70 Bâtiment Direction INSA Lyon mega@insa-lyon.fr	**M. Jocelyn BONJOUR** INSA Lyon Laboratoire CETHIL Bâtiment Sadi-Carnot 9, rue de la Physique 69621 Villeurbanne CEDEX **jocelyn.bonjour@insa-lyon.fr**
ScSo	**ScSo*** **https://edsciencessociales.universite-lyon.fr** Sec. : Mélina FAVETON INSA : J.Y. TOUSSAINT Tél : 04.78.69.77.79 melina.faveton@univ-lyon2.fr	**M. Christian MONTES** Université Lumière Lyon 2 86 Rue Pasteur 69365 Lyon CEDEX 07 **christian.montes@univ-lyon2.fr**

*ScSo : Histoire, Géographie, Aménagement, Urbanisme, Archéologie, Science politique, Sociologie, Anthropologie

Acknowledgements

This PhD thesis was carried out with funding from the ED MEGA grant, for which I am grateful. I would like to thank Professor Jocelyn Bonjour, Professor Rémi Revellin, Professor Ludger Fischer and Dr. Anastasia Stamatiou who all co-supervised this thesis, for their wisdom, support, patience and dedication, without which, this work would not be possible.

Additionally, I would like to thank Silvan von Arx and Philippe Haberschill for their knowledge and expertise in the field, in the design and operation of test-rigs and their fundamental grasp on the topic. Alongside this, I would like to extend my appreciation to all my colleagues and fellow students at CETHIL, INSA Lyon and at the CCTES, HSLU for their support and motivating words throughout the whole PhD process.

Finally, words cannot express the gratitude I have towards my family, Mum, Dad, Lucy and Arton. Thank you all so much for your love, support and encouragement at every step of the way. This thesis is dedicated to all of you, alongside Hugh Frederick Hurst.

Summary

This research focuses on the heat transfer, transport, and rheological behaviour of novel two-phase fluids. These two-phase fluids consist of phase change material dispersed into a continuous phase and are subsequently named phase change dispersions. The optimal formulation procedure for phase change dispersions with high stabilities, low supercooling degrees and high apparent specific heat capacities is presented and discussed. The thermophysical behaviour of phase change dispersions with different hydrophilic head group sizes was examined. Firstly, a surfactant was chosen on accounts of its bulky substituent groups and the thermophysical properties were compared to the results from a standard surfactant system. Thermal analysis of differential scanning calorimetry and the EasyMax thermal cycling unit showed that the supercooling degree to be 13 K with the standard surfactant system, and 4 K with the bulky surfactant, suggesting the surfactant had nucleating-inducing behaviour. However, the bulky surfactant resulted in a more viscous phase change dispersion, which separated after thermal cycling. Consequently, smaller co-surfactants were added to allow higher packing densities to increase stability, and decrease the viscosity, whilst keeping the nucleating ability of the original surfactant. This optimised surfactant system showed a supercooling reduction of 9 K and thermal stability during extended cycling. Overall, the results demonstrate an innovative approach in fine-tuning the thermophysical properties of a phase change dispersion with the use of co-surfactants. Two of the formulations were then chosen for subsequent comparison for the heat transfer behaviour to observe the effect that surfactants have on the transport and heat transfer properties during heating. The heat transfer and rheological behaviour of two-phase change dispersion formulations during melting was investigated in a cylindrical tube in the Competence Centre for Thermal Energy Storage (CCTES), where the effects of formulation transport properties and operational parameters on the heat transfer and rheological behaviour were assessed. This was performed through using a test-rig to measure the bulk fluid and inner wall temperatures of the phase change dispersions flowing through a cylindrical tube under the constant heat flux boundary condition. The temperature measurements allowed for the calculation of the local heat transfer coefficients and the apparent specific heat capacities. Preliminary tests with water were performed and the experimental test-rig was validated with known correlations. Results from the experiments with the two-phase change dispersion formulations are presented and discussed for

the turbulent and transition flow regime. It was observed that the apparent specific heat capacity, that correlates with the amount of heat that was absorbed through the phase change of the phase change material particles, resulted in a higher heat transfer coefficient. The crystallisation and cooling heat transfer and rheological behaviour of one of the phase change dispersion formulations was subsequently examined through calculation of heat balances in a rectangular duct in the Centre d'Énergetique et de Thermique de Lyon (CETHIL) at INSA Lyon. Whilst, during crystallisation an increase in the heat transfer coefficients was observed, and an increase in the heat transfer coefficient with increasing mass flow rate (and subsequently shear rate and mass flow rate), an interesting peculiarity was discovered, that the transition from laminar to turbulent with two-phase non-Newtonian fluids was much lower than predicted for Newtonian single-phase fluids. By regression of the experimental results, correlations for the local and average Nusselt numbers for laminar flow have been presented, using both the modified Reynolds number and the Prandtl number. A theoretical analysis of the heat transfer behaviour is presented, giving rise to future research questions about the shear-rate dependence of the thermal conductivity in non-Newtonian fluids and the balance of the inertial forces. A numerical model for the thermal behaviour studies of a phase change dispersion during its cooling in laminar flow through a rectangular duct was developed and is based on the quasi-homogeneous single fluid approach. The evolution of the experimental and theoretical values for the phase change dispersions average temperature, heat flux through the wall and the heat transfer coefficients between the wall and the fluid shows good agreement and the model satisfactorily predicts the behaviour, with variations of less than 5%.

Résumé

Cette recherche porte sur le transfert de chaleur, le transport et le comportement rhéologique de nouveaux fluides à deux phases. Ces fluides diphasiques sont constitués d'un matériau à changement de phase dispersé dans une phase continue et sont par la suite appelés dispersions à changement de phase. La procédure de formulation optimale pour les dispersions à changement de phase avec des stabilités élevées, de faibles degrés de surfusion et des capacités thermiques spécifiques apparentes élevées est présentée et discutée. Le comportement thermophysique des dispersions à changement de phase avec différentes tailles de groupes de tête hydrophiles a été examiné. Tout d'abord, un tensioactif a été choisi en raison de ses groupes substituants volumineux et les propriétés thermophysiques ont été comparées aux résultats d'un système tensioactif standard. L'analyse thermique par calorimétrie à balayage différentiel et l'unité de cycle thermique EasyMax ont montré que le degré de surfusion était de 13 K avec le système tensioactif standard, et de 4 K avec le tensioactif volumineux, ce qui suggère que le tensioactif avait un comportement d'induction de nucléation. Cependant, l'agent tensioactif volumineux a donné lieu à une dispersion à changement de phase plus visqueuse, qui s'est séparée après le cycle thermique. Par conséquent, des co-surfactants plus petits ont été ajoutés pour permettre des densités de tassement plus élevées afin d'augmenter la stabilité et de diminuer la viscosité, tout en conservant la capacité de nucléation du surfactant original. Ce système tensioactif optimisé a montré une réduction de la surfusion de 9 K et une stabilité thermique pendant un cycle prolongé. Dans l'ensemble, les résultats démontrent une approche innovante dans le réglage fin des propriétés thermophysiques d'une dispersion à changement de phase avec l'utilisation de co-surfactifs. Deux des formulations ont ensuite été choisies pour une comparaison ultérieure du comportement de transfert thermique afin d'observer l'effet des tensioactifs sur les propriétés de transport et de transfert thermique pendant le chauffage. Le transfert de chaleur et le comportement rhéologique des formulations de dispersion à changement de phase pendant la fusion ont été étudiés dans un tube cylindrique au Centre de compétence pour le stockage de l'énergie thermique (CCTES), où les effets des propriétés de transport de la formulation et des paramètres opérationnels sur le transfert de chaleur et le comportement rhéologique ont été évalués. Les effets des propriétés de transport de la formulation et des paramètres opérationnels sur le transfert de chaleur et le comportement rhéologique ont été évalués. Pour ce faire, un banc d'essai a été utilisé pour mesurer les températures du fluide en vrac et de la paroi interne des dispersions à changement de phase s'écoulant dans un tube cylindrique dans des conditions de flux thermique constant. Les mesures de température ont permis de calculer les coefficients de transfert de chaleur locaux et les capacités thermiques spécifiques apparentes. Des tests préliminaires avec de l'eau ont été effectués et le banc d'essai expérimental a été validé avec des corrélations connues.

Les résultats des expériences avec les formulations de dispersion à changement de phase sont présentés et discutés pour le régime d'écoulement turbulent et de transition. Il a été observé que la capacité thermique spécifique apparente, qui est en corrélation avec la quantité de chaleur absorbée par le changement de phase des particules de matériau à changement de phase, a donné lieu à un coefficient de transfert de chaleur plus élevé. Le transfert de chaleur de cristallisation et de refroidissement et le comportement rhéologique de l'une des formulations de dispersion à changement de phase ont ensuite été examinés par le calcul des bilans thermiques dans un conduit rectangulaire au Centre d''Energétique et de Thermique de Lyon (CETHIL) à l'INSA de Lyon.

Alors que, pendant la cristallisation, une augmentation des coefficients de transfert de chaleur a été observée, et une augmentation du coefficient de transfert de chaleur avec l'augmentation du débit massique (et par la suite du taux de cisaillement et du débit massique), une particularité intéressante a été découverte, à savoir que la transition du laminaire au turbulent avec des fluides biphasés non-newtoniens était beaucoup plus faible que celle prédite pour les fluides monophasés newtoniens. Par régression des résultats expérimentaux, des corrélations pour les nombres de Nusselt locaux et moyens pour un écoulement laminaire ont été présentées, en utilisant à la fois le nombre de Reynolds modifié et le nombre de Prandtl. Une analyse théorique du comportement de transfert de chaleur est présentée, donnant lieu à de futures questions de recherche sur la dépendance de la conductivité thermique au taux de cisaillement dans les fluides non-newtoniens et l'équilibre des forces d'inertie. Un modèle numérique pour l'étude du comportement thermique d'une dispersion à changement de phase pendant son refroidissement dans un écoulement laminaire à travers un conduit rectangulaire a été développé et est basé sur l'approche du fluide unique quasi-homogène. L'évolution des valeurs expérimentales et théoriques pour la température moyenne des dispersions à changement de phase, le flux de chaleur à travers la paroi et les coefficients de transfert de chaleur entre la paroi et le fluide montre un bon accord et le modèle prédit de manière satisfaisante le comportement, avec des variations de moins de 5%.

Nomenclature

Abbreviations

COP Coefficient of performance

DSC Differential scanning calorimetry

FOM Figure of merit

HLB Hydrophillic-lipophillic balance

HTF Heat transfer fluid

$HVAC$ Heating, ventilation and air conditioning

LHS Latent heat storage

MCR Modular compact rheometer

NA Nucleating agent

NIR Near-infrared spectroscopy

NTU Number of transfer units

PCD Phase change dispersion

PCE Phase change emulsion

PCM Phase change material

PEC Performance evaluation criterion

$PIDS$ Polarisation intensity differential scattering

PIR Polyisocyanurate

PSD Particle size distribution

PVC Polyvinyl chloride

RTD Resistance temperature detector

TES Thermal energy storage

THB Thermal hot bridge

US Ultrasound

Dimensionless numbers

Nu Nusselt number $Nu = \frac{hl}{\lambda}$

Pr Prandtl number $Pr = \frac{cp\mu}{\lambda}$

Re Reynolds number $Re = \frac{\rho ul}{\mu}$

Ste Stefan number $Ste = \frac{cp\Delta T}{\Delta h}$

Greek characters

α Thermal diffusivity ($m^2\ s^{-1}$)

$\dot{\gamma}$ Shear rate (s^{-1})

β Sphericity factor (-)

γ Intermittency factor (-)

Δp Pressure drop (Pa)

Δh Latent heat capacity ($J\ kg^{-1}$)

ϵ Heat transfer effectiveness (-)

λ Thermal conductivity ($W\ m^{-1}\ K^{-1}$)

μ Dynamic viscosity (Pa s)

ρ Density ($kg\ m^{-3}$)

τ Shear stress (Pa)

ψ Mass content (-)

τ_0 Minimal shear stress (Pa)

τ_q Time lag of heat flux (s)

τ_t Time lag of temperature gradient (s)

Φ Particle volume fraction (-)

ϕ Local heat flux (W m^{-2})

Latin characters

A Inner area (m)

a Width (m)

b Channel height (m)

C Capacity ratio (-)

cp Specific heat capacity at constant pressure (J kg^{-1} K^{-1})

$cp*$ Modified specific heat capacity at constant pressure (J kg^{-1} K^{-1})

$\tilde{cp}$ Apparent specific heat capacity (J kg^{-1} K^{-1})

D Diameter (m)

D_h Hydraulic diameter (m)

e Thickness (m)

f Friction factor (-)

g Gravitational acceleration (m s^{-2})

h Heat transfer coefficient (W m^{-2} K^{-1})

i' Rate of irreversibility (W)

J Colborn factor (-)

K Consistency factor (Pa s^n)

l Characteristic length (m)

L Latent heat of melting (J kg^{-1})

$L*$ Latent heat capacity (J kg^{-1})

M Merit Number (-)

m Mass (kg)

$\dot{m}$ Mass flow rate (kg s^{-1})

n Flow behavioural index (-)

P Pumping power (W)

P_{el} Electrical power input (W)

Q Heat flow (W)

q Heat flux (W m^{-2})

q_f Heat flux calculated through Fourier's law (W m^{-2})

$q3$ Volume fraction (%)

r Installation location (-)

S Time derivative (K^2s^-1)

t Time (s)

T Temperature (K)

u Velocity (m s^{-1})

x Coordinate in the axial location (m)

$x*$ Dimensionless axial location (-)

$y+$ Wall co-ordinate (-)

z Empirical shape factor (-)

Subscripts

amb Ambient

avg Average

bulk Bulk

copper Copper

crit Critical

cryst Crystallisation

en Enhanced

et Ethanol

exp Experimental

f Reference

fluid Fluid

gain Rate of increase due to PCM addition

in Inlet

inner Inner

jacket Jacket

laminar Laminar

losses Heat losses

melting Melting

MR Metzner and Reed

out Outlet

outer Outer

PCD Phase change dispersion

PCM Phase change material

pipe Pipe

plate Plate

reactor Reactor

t Total

total Total

turbulent Turbulent

w Wall

water Water

x Axial location

List of Figures

3 Materials and Methodology for thermophysical analysis

4 Formulation of Phase Change Dispersions

5 Heat Transfer and Rheology during melting

List of Tables

Contents

Chapter 1

Introduction and Scope

The rising cooling demand is having a profound effect on power generation and distribution capacity, especially during the peak demand periods, whether diurnal or seasonal. CO_2 emissions from space cooling have almost tripled between 1990 and 2020 and to meet the current energy demands, alternative strategies to reduce CO_2 emissions needs to be employed [1]. Two effective ways to achieve this include the further development of renewable energy sources and subsequently to increase the efficiency of thermal installations [2, 3]. Despite this, moving from fossil fuels to sustainable energy sources, such as wind or solar power, results in imbalances between energy production and demand. Thermal energy storage (TES) is a potential technology that can be used to improve the efficiency and reliability of thermal facilities by reducing peak loads and aiding the intermittency issues with renewable energy sources [4, 5]. TES involves using phase change materials (PCMs), which exploit the latent heat of phase change to enhance thermal capacity. Whilst PCMs have improved the thermal capacity of a wide-range of domestic and industrial facilities, the large-scale use of PCMs still requires extra infrastructure, as bulk PCMs cannot be transported in their solid phase, and subsequently a secondary heat transfer fluid (HTF) is generally needed to charge/discharge the PCM storage to where the heat is required [6, 7]. Thermal resistances between the PCM and the HTF further reduces the heat transfer performance and prevents the PCM storage system from reaching the full storage potential [6].

Methods to reduce the PCMs' resistance to the heat flow can be classified into static and dynamic solutions [7]. Static solutions involve both geometry and system modifications such as increasing the heat transfer area, through multi-tubed configurations [8, 9, 10] and finned surfaces in the PCM container [11, 12] or solutions through the direct enhancement of the thermal conductivity of the PCM [13, 14, 15, 16]. Dynamic solutions involve direct contact storages. In direct contact systems, there is no separation between the interface of the PCM and the HTF, whereby the PCM can directly exchange

the thermal energy into the HTF. Here, it is also possible to distinguish between two different classifications. The first solution is to have the HTF flow directly through the PCM, which has a high compactness factor, with the drawbacks of pressure build ups and changes in volume [17, 18]. The second solution is for the PCM to circulate with the HTF, which, with the help of surfactants, results in a dispersed PCM phase flowing in a continuous HTF, named a phase change dispersion (PCD) [19, 20, 21]. PCDs are particularly attractive HTFs on accounts of their enhanced heat capacities and isothermal phase change temperatures [19]. Due to their ability to isothermally release/absorb heat, PCDs also have the potential to be used as HTFs in temperature stabilisation applications, such as in the cooling of electronics [22, 23, 24, 25, 26] and in the machining industry [27, 28]. Additionally, it is envisioned that PCDs can be used improve the performance of refrigeration by being used as secondary refrigerants [29, 30, 31, 32].

Despite the plethora of applications PCDs can be integrated as replacement HTFs in, there are current limitations of implementing PCDs into the cooling network. The main shortcomings include issues with long term stability, during cycling and storage, problems of supercooling and a general lack of understanding of their fundamental heat transfer and rheological behaviour [19, 20, 33, 34].

PCDs are required to show long-term stability both in storage and under thermal and mechanical loads [20, 19]. The stability of PCDs is dependent on many factors, such as the surfactant system and concentration of surfactant, the operational temperature, the viscosity of the continuous phase and the droplet sizes of the PCM [19, 35]. Whilst the stability of a PCD can be increased in different ways, the most employed method is by creating small particle sizes, resulting in a more thermodynamically stable PCDs [35, 36, 37]. However, smaller particle sizes increase the degree of supercooling of the PCM droplets, since supercooling is a stochastic phenomenon. Supercooling is a mechanism by which the PCM droplets need to be cooled below their melting point to initiate crystallisation, which limits the feasibility of implementing PCDs into cooling technologies as the latent heat is released at a lower temperature or within a larger temperature range [37, 38]. Methods to combat supercooling have been the centre of PCD research for quite some time, with most techniques focusing on seeding [22, 39, 19]. Seeding involves mixing additives, named nucleating agents (NA), within the PCM droplets to induce heterogeneous nucleation. In literature, several classes of materials have been identified as potential NAs, namely compounds from the same chemical class as the PCM, but with a higher melting point and nanoparticles. Despite the promising results demonstrated in literature on the supercooling reducing effects of NAs and the subsequent improvements in the heat storage capacities, it has been reported that after a certain amount of thermo-mechanical cycles the efficacy of nucleating agents reduces [22]. Concerning the issue of a lack of understanding of the physical mechanisms and phenomena governing the heat transfer and rheological performance of PCDs, for the investigation of PCDs as HTFs,

the behaviour during heating and cooling of the PCD must be understood. Thus far in literature, a detailed explanation of the physical phenomena governing the performance of PCDs is extremely limited.

1.1 Objectives

The main objective of this work is the analysis of different formulation and operational conditions on the heat transfer and rheological performance of phase change dispersions in various energy systems. This involves both as indirect refrigerants, by exploiting the latent heat release during crystallisation and as heat transfer fluids for temperature stabilisation applications through utilising the latent heat release during melting. In order to analyse the effect of different operational conditions of phase change dispersions for both applications, an understanding of how to formulate a stable phase change dispersion with excellent thermophysical properties is required. This should be set as a benchmark for future phase change dispersion development.

Additionally, to permit the design of heat exchangers and piping that will host phase change dispersions the knowledge of the heat transfer and rheological behaviour of phase change dispersions needs to be expanded upon.

1.2 Structure of the thesis

This thesis consists of eight chapters. Chapter 1 has presented the introduction to the topic, the general scope and the motivation for the study. Chapter 2 introduces the background and reviews the state-of-the-art studies of phase change dispersions and the relevant theory. In chapter 3 a description of the analytical techniques used to achieve the thermophysical characterisation of the developed phase change dispersions is given. Chapter 4 discusses how to formulate phase change dispersions in a way to eliminate their two major drawbacks, supercooling and issues with stability. In chapter 5, an experimental investigation in to the heat transfer and rheological performance of two phase change dispersions during melting is presented and in chapter 6 an experimental study on the heat transfer and rheological performance of a phase change dispersion during crystallisation is shown. Chapter 7 presents preliminary results from a numerical investigation of the same phase change dispersion used in chapter 6, with the same geometry and boundary conditions. Finally, chapter 8 displays the main conclusions arising from this work, and suggestions for future areas of research. The framework of all the experiments were carried out at the competence centre of thermal energy storage (CCTES) at the Hochschule Luzern in Switzerland and at the Centre d'Énergetique et de Thermique de Lyon (CETHIL) at INSA Lyon in France.

References

[1] IEA. *Global Energy Review 2021*. IEA, Paris, 2021. URL: https://www.iea.org/reports/global-energy-review-2021.

[2] Armin Razmjoo, Seyedali Mirjalili, Mehdi Aliehyaei, Poul Alberg Østergaard, Abolfazl Ahmadi, and Meysam Majidi Nezhad. "Development of smart energy systems for communities: Technologies, policies and applications". In: *Energy* 248 (2022), p. 123540.

[3] AG Olabi and Mohammad Ali Abdelkareem. "Renewable energy and climate change". In: *Renewable and Sustainable Energy Reviews* 158 (2022), p. 112111.

[4] VV Tyagi, K Chopra, B Kalidasan, Aditya Chauhan, U Stritih, Sanjeev Anand, AK Pandey, Ahmet Sarı, and Richa Kothari. "Phase change material based advance solar thermal energy storage systems for building heating and cooling applications: A prospective research approach". In: *Sustainable Energy Technologies and Assessments* 47 (2021), p. 101318.

[5] GV Brahmendra Kumar and K Palanisamy. "Review of energy storage system for microgrid". In: *Microgrid Technologies* (2021), pp. 57–90.

[6] D Cabaleiro, F Agresti, L Fedele, S Barison, C Hermida-Merino, S Losada-Barreiro, S Bobbo, and MM Piñeiro. "Review on phase change material emulsions for advanced thermal management: Design, characterization and thermal performance". In: *Renewable and Sustainable Energy Reviews* 159 (2022), p. 112238.

[7] NHS Tay, Mingyang Liu, M Belusko, and F Bruno. "Review on transportable phase change material in thermal energy storage systems". In: *Renewable and Sustainable Energy Reviews* 75 (2017), pp. 264–277.

[8] Mehdi Esapour, Arash Hamzehnezhad, A Ali Rabienataj Darzi, and Mahmoud Jourabian. "Melting and solidification of PCM embedded in porous metal foam in horizontal multi-tube heat storage system". In: *Energy conversion and management* 171 (2018), pp. 398–410.

[9] Hadi Bashirpour-Bonab. "Investigation and optimization of PCM melting with nanoparticle in a multi-tube thermal energy storage system". In: *Case Studies in Thermal Engineering* 28 (2021), p. 101643.

[10] Mustafa S Mahdi, Hameed B Mahood, Ahmed A Alammar, and Anees A Khadom. "Numerical investigation of PCM melting using different tube configurations in a shell and tube latent heat thermal storage unit". In: *Thermal Science and Engineering Progress* 25 (2021), p. 101030.

[11] Tushar Sathe and AS Dhoble. "Thermal analysis of an inclined heat sink with finned PCM container for solar applications". In: *International Journal of Heat and Mass Transfer* 144 (2019), p. 118679.

[12] Sourav Khanna, KS Reddy, and Tapas K Mallick. "Optimization of finned solar photovoltaic phase change material (finned pv pcm) system". In: *International Journal of Thermal Sciences* 130 (2018), pp. 313–322.

[13] Long Zhang, Kechao Zhou, Quiping Wei, Li Ma, Wentao Ye, Haichao Li, Bo Zhou, Zhiming Yu, Cheng-Te Lin, Jingting Luo, et al. "Thermal conductivity enhancement of phase change materials with 3D porous diamond foam for thermal energy storage". In: *Applied Energy* 233 (2019), pp. 208–219.

[14] Hafiz Muhammad Ali. "Recent advancements in PV cooling and efficiency enhancement integrating phase change materials based systems–A comprehensive review". In: *Solar Energy* 197 (2020), pp. 163–198.

[15] Weixiong Wu, Wei Wu, and Shuangfeng Wang. "Form-stable and thermally induced flexible composite phase change material for thermal energy storage and thermal management applications". In: *Applied Energy* 236 (2019), pp. 10–21.

[16] Piao Cheng, Xiao Chen, Hongyi Gao, Xiaowei Zhang, Zhaodi Tang, Ang Li, and Ge Wang. "Different dimensional nanoadditives for thermal conductivity enhancement of phase change materials: Fundamentals and applications". In: *Nano Energy* 85 (2021), p. 105948.

[17] Stefan Krimmel, Anastasia Stamatiou, Jörg Worlitschek, and Heimo Walter. "Experimental characterization of the heat transfer in a latent direct contact thermal energy storage with one nozzle in labor scale". In: *International Journal of Mechanical Engineering* 3 (2018).

[18] JIN Guang, ZHAO Wenxiu, ZHAO Jun, and GUO Shaopeng. "Development and research status on the technology of direct contact thermal energy storage". In: *Energy Storage Science and Technology* 8.3 (2019), p. 477.

[19] Poppy O'neill, Ludger Fischer, Rémi Revellin, and Jocelyn Bonjour. "Phase change dispersions: A literature review on their thermo-rheological performance for cooling applications". In: *Applied Thermal Engineering* 192 (2021), p. 116920.

[20] Fangxian Wang, Wenzhu Lin, Ziye Ling, and Xiaoming Fang. "A comprehensive review on phase change material emulsions: Fabrication, characteristics, and heat transfer performance". In: *Solar Energy Materials and Solar Cells* 191 (2019), pp. 218–234.

[21] Naixing Yang, Juan Wang, Shiwei Xu, Jianxiao Zheng, Liangliang Wang, and Juan Yu. "A comparative assessment of the battery liquid-cooling system employing two coolants: Phase change material emulsion and water". In: *International Journal of Energy Research* 46.5 (2022), pp. 6498–6516.

[22] Ludger Fischer, Ernesto Mura, Poppy O'Neill, Silvan Von Arx, Jörg Worlitschek, Geng Qiao, Qi Li, and Yulong Ding. "Thermophysical properties of a phase change dispersion for cooling around 50 C". In: *International Journal of Refrigeration* 119 (2020), pp. 410–419.

[23] Ludger Fischer, Ernesto Mura, Poppy O'Neill, Silvan von Arx, Jörg Worlitschek, Geng Qiao, Qi Li, and Yulong Ding. "Heat transfer performance potential with a high-temperature phase change dispersion". In: *Energies* 14.16 (2021), p. 4899.

[24] Ludger Fischer, Ernesto Mura, Geng Qiao, Poppy O'Neill, Silvan von Arx, Qi Li, and Yulong Ding. "HVDC Converter Cooling System with a Phase Change Dispersion". In: *Fluids* 6.3 (2021), p. 117.

[25] Qi Li, Geng Qiao, Ernesto Mura, Chuan Li, Ludger Fischer, and Yulong Ding. "Experimental and numerical studies of a fatty acid based phase change dispersion for enhancing cooling of high voltage electrical devices". In: *Energy* 198 (2020), p. 117280.

[26] Qi Li, Ludger Fischer, Geng Qiao, Ernesto Mura, Chuan Li, and Yulong Ding. "High performance cooling of a HVDC converter using a fatty acid ester-based phase change dispersion in a heat sink with double-layer oblique-crossed ribs". In: *International Journal of Energy Research* 44.7 (2020), pp. 5819–5840.

[27] Ludger J Fischer, Silvan von Arx, Ueli Wechsler, Simon Züst, and Jörg Worlitschek. "Phase change dispersion, potentially a new class of heat transfer fluids". In: *Journal of Physics: Conference Series*. Vol. 745. 3. IOP Publishing. 2016, p. 032133.

[28] Ludger J Fischer, Silvan von Arx, Ueli Wechsler, Simon Züst, and Jörg Worlitschek. "Phase change dispersion properties, modeling apparent heat capacity". In: *International Journal of Refrigeration* 74 (2017), pp. 240–253.

[29] Virginia Vasile, Horia Necula, Adrian Badea, Rémi Revellin, Jocelyn Bonjour, and Phillipe Haberschill. "Experimental study of the heat transfer characteristics of a paraffin-in-water emulsion used as a secondary refrigerant". In: *International Journal of Refrigeration* 88 (2018), pp. 1–7.

[30] Peng Zhang and ZW Ma. "An overview of fundamental studies and applications of phase change material slurries to secondary loop refrigeration and air conditioning systems". In: *Renewable and Sustainable Energy Reviews* 16.7 (2012), pp. 5021–5058.

[31] Virginia Vasile, Jocelyn Bonjour, Rémi Revellin, Philippe Haberschill, Adrian Badea, and Horia Necula. "New technology in comfort cooling applications: Experimental study on paraffin in water emulsion". In: *2017 International Conference on Energy and Environment (CIEM)*. IEEE. 2017, pp. 157–161.

[32] Mohamed Najib El Boujaddaini, Philippe Haberschill, and Abdelaziz Mimet. "Rheological behaviour and concentration distribution of paraffin slurry in horizontal rectangular channel". In: *HEFAT 2010* (2010).

[33] Liu Yang, Shuli Liu, and Hongfei Zheng. "A comprehensive review of hydrodynamic mechanisms and heat transfer characteristics for microencapsulated phase change slurry (MPCS) in circular tube". In: *Renewable and Sustainable Energy Reviews* 114 (2019), p. 109312.

[34] Kasra Ghasemi, Syeda Tasnim, and Shohel Mahmud. "PCM, nano/microencapsulation and slurries: A review of fundamentals, categories, fabrication, numerical models and applications". In: *Sustainable Energy Technologies and Assessments* 52 (2022), p. 102084.

[35] Fangxian Wang, Xiaoming Fang, and Zhengguo Zhang. "Preparation of phase change material emulsions with good stability and little supercooling by using a mixed polymeric emulsifier for thermal energy storage". In: *Solar energy materials and solar cells* 176 (2018), pp. 381–390.

[36] Samira Abedi, Naureen S Suteria, Chau-Chyun Chen, and Siva A Vanapalli. "Microfluidic production of size-tunable hexadecane-in-water emulsions: Effect of droplet size on destabilization of two-dimensional emulsions due to partial coalescence". In: *Journal of colloid and interface science* 533 (2019), pp. 59–70.

[37] Liu Liu, Jianlei Niu, and Jian-Yong Wu. "Preparation of Stable Phase Change Material Emulsions for Thermal Energy Storage and Thermal Management Applications: A Review". In: *Materials* 15.1 (2021), p. 121.

[38] Allan Takudzwa Muzhanje, MA Hassan, Shinichi Ookawara, and Hamdy Hassan. "An overview of the preparation and characteristics of phase change materials with nanomaterials". In: *Journal of Energy Storage* 51 (2022), p. 104353.

[39] Jingjing Shao, Jo Darkwa, and Georgios Kokogiannakis. "Review of phase change emulsions (PCMEs) and their applications in HVAC systems". In: *Energy and buildings* 94 (2015), pp. 200–217.

Chapter 2

Literature study into phase change dispersions

2.1 Introduction

Cold technologies are essential for a variety of domestic, commercial and industrial applications. They are employed in the preservation of food and medical equipment, comfort cooling in cars, residences and commercial buildings and in the cooling of electronic and industrial equipment. Despite its plethora of usages, the cold energy market is an often over-looked energy-consuming sector. The use of energy for space cooling is the fastest growing area of energy usage in buildings and it has more than tripled between 1990 and 2016 [1]. Worldwide, almost one fifth of all electricity utilised in buildings is used for cooling [1]. Current aims to reduce this electrical usage include technologies implemented to increase the coefficient of performance (COP) of cold systems. In recent years, this has involved the incorporation of phase change materials (PCM) into cold systems to act as latent heat stores (LHS) [2, 3, 4]. LHS exploits the heat of phase change of materials to store and release significant amounts of energy as a material changes phase. The isothermal nature of phase change allows PCM systems to be fine-tuned to temperature-sensitive applications such as air-conditioning (5 to 15 °C), refrigeration (0 to 4 °C) and freezing (less than 0 °C). However, there are instances where it is much more efficient to use PCM in the form of particles within another fluid. For example, where heat transfer rate is to be maximized, and where it is beneficial to have the PCM in a pump-able form. Using PCM in conjunction with a heat transfer fluid (HTF), generally water, results in a two-phase fluid with a high specific heat capacity [5]. The high specific heat capacity is due to the fluid not only using the sensible heat, as with a normal HTF, but with the additional latent heat during the phase change process [5, 6]. It is expected that because of this, the fluid will have better heat transfer characteristics than for a single-phase HTF, within a limited temperature range around the phase change temperature of the

PCM. This is beneficial in a number of applications as improved heat transfer and storage characteristics, such as an increase in the specific heat capacity, allows for a smaller volumetric flow of the HTF to be used. This suggests that less pumping power is required in the system and thus smaller thermal resistances are achieved and therefore higher heat transfer efficiencies [7]. Essentially, this could lower the operational and investment costs of the cold-chain network. To date, there are a couple of reported usages of PCDs that have been implemented into the cooling network. Fischer et al. [8] retrofitted an existing cooling circuit using PCM dispersed in water as the heat transfer fluid to isothermally cool a machine spindle. Additionally, Shibutani [9] installed micro-encapsulated slurries into a pre-existing chiller unit in Narita Airport in Tokyo and found higher storage densities than using water as the HTF. Despite this, PCDs are still to be considered in the developmental stage and are not yet commercialised.

To date, there are four different types of fluid incorporated with PCM: ice slurries, clathrate hydrate slurries, micro-encapsulated PCM slurries and PCDs [10, 5, 11]. The first three suffer from high operational costs, associated with shape stabilisation and encapsulation. Additionally, they suffer with problems of stability and consistency during extended cycling periods [10, 5, 11]. On the other hand, PCDs, or formerly named in literature as phase change emulsions (PCE), are dispersions of two immiscible liquids, stabilised with a surfactant. PCDs have simple preparation techniques, smaller thermal resistances (as a result of having no encapsulation shell) and lower production costs [10, 5, 11]. PCDs can be characterised by the size of the dispersed droplets. Currently, there are three different droplet sizes of the dispersed phase used for cooling purposes; emulsions (1-10 μm), mini-emulsions (20-200 nm) and micro-emulsions (10-100 nm) [12]. These sizes are given as reference values and as discussed by Mclements [13], other factors, such as preparation technique and thermodynamic stability should be taken into consideration when assigning categories to emulsion types. Emulsions with droplet sizes above 1 µm are currently the most studied but it is nano-emulsions that show the most promising characteristics such as long-term stability and low viscosities [14].

So far, the integration of PCDs into cooling systems has been limited due to a range of both material and heat transfer limitations. Material properties of the PCM such as supercooling, a phenomenon by which a solution starts crystallising below its freezing point and therefore requires a lower temperature to freeze, significantly limits the application of PCDs into cooling systems. Additives, named nucleating agents, are added to dispersions to prevent this from occurring, however their ability to function after multiple cycles and during storage is unknown. Additionally, PCDs suffer from instability when cycled due to thinning and disruption of the liquid film between droplets (coalescence), an irreversible process. Furthermore, to ensure the correct design of heat exchangers and systems with PCD, a comprehensive understanding of the heat transfer performance of PCDs is required. Whilst for single-phase Newtonian fluids an in depth understanding

of heat transfer is known, this is not the case for PCD. Numerical models have been presented [15, 7, 16, 6], but they are yet to be experimentally validated. Despite this, recent literature and reviews have almost predominantly focused on the characterisation and heat transfer properties of microencapsulated phase change material slurries [17, 18, 19, 20, 21]. Whilst, there are some reviews which discuss some properties of phase change dispersions [22, 19, 23], this chapter will focus exclusively on the thermophysical properties, heat transfer performance and rheology of PCDs. Specifically, this chapter will focus on PCDs made for cooling applications such as: HVAC, which as discussed by Huang et al. [24] requires a PCD with a phase change temperature between 0-20 °C, cooling of machining tools as discussed by Fischer et al. [8] with a temperature range of 20-30 °C, refrigeration with a phase change temperature of 0-6 °C and furthermore the cooling of electronic equipment which can require a phase change temperature of up to 50 °C [25, 26].

2.2 Phase change dispersions

As aforementioned, a PCD consists of a dispersed phase which is composed of PCM particles that are stabilised and dispersed in a continuous phase with the aid of surfactants. A diagram of a typical PCD droplet can be seen in Figure 1 and a list of the formulation properties and components of the PCDs discussed in this review can be found in Table 2.1. The most commonly investigated PCDs are oil-in-water, where a hydrophobic PCM is dispersed in a hydrophilic (generally water) continuous phase. In literature, the most commonly reported class of PCM for use in PCDs are paraffins, on account of their high latent heats. In Table 2, a list of some of the PCDs investigated in literature can be found. Table 2 is ordered based on increasing melting point of the PCDs, it also shows (when presented by the author of the study) the thermal conductivity, in both the emulsion form (when the PCM is liquid) and suspension form (when the PCM is solid), the mean particle size of the PCM droplets in the PCD, the viscosity in emulsion and suspension form, and the latent heat capacity of the PCD. The latent heat capacity of a PCD is defined as:

$$L^* = \psi L \tag{2.1}$$

where ψ is the mass fraction of PCM used in the PCD and L is the latent heat of melting. Due to the distinctive melting points of paraffins, and because of the high cost for pure paraffins, many commercial PCM paraffins are blends of different paraffins to obtain the desired application temperatures.

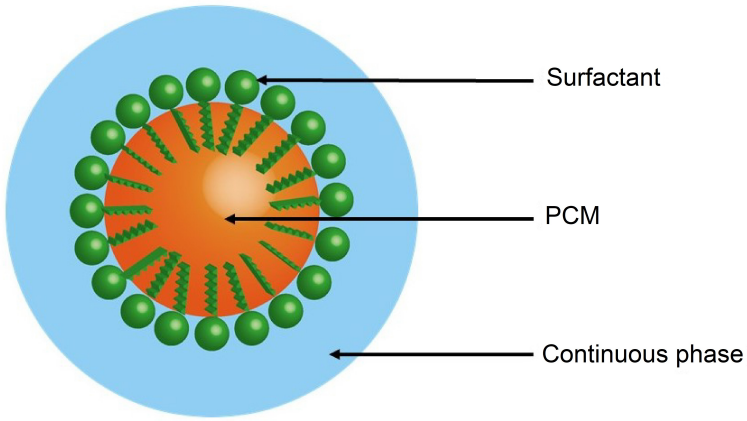

Figure 2.1: A dispersed particle within a PCD showing the PCM, surfactant layer and the continuous phase. The figure was adapted from Fischer et al. [8].

Table 2.1: PCDs listed in literature alongside the PCM used in the formulation, ordered on increasing melting temperatures with some relevant thermophysical properties.

PCM	**Melting Temperature (°C)**	**wt.%**	**λ suspension (W m^{-1} K^{-1})**	**λ emulsion (W m^{-1} K^{-1})**	**Mean Particle size (μm)**	**μ suspension (mPa s)**	**μ emulsion (mPa s)**	**Latent heat capacity (J g^{-1})**	**[Ref]**
Tetradecane	4.6	30			51		7.5	73	[**20**]
Tetradecane	4.8	20			0.2		4.2	43	[**19**]
n-alkanes	5	30	0.38			7.3	5.5	60	[**26**]
Tetradecane	5.1	30			51	6	3.8	32	[**30**]
Tetradecane	5.9	10			0.5			19.3	[**12**]
Tetradecane	6	40			17			66.3	[**18**]
RT6	6.1	30		0.48		10	25	40	[**29**]
RT6	8	30			0.5	20	20	75	[**24**]
RT10	8.2	25	0.4		4		21	41	[**25**]
RT10	9	30			5			43	[**23**]
RT10	9.3	30			5			36	[**10**]
n-alkanes	9.5	50			2	24.3	22.3	78.9	[**22**]
RT10	9.7	30		0.46				38	[**29**]
RT10	10	30			0.5	40	20	50	[**24**]
Hexadecane	16.5	10			100				[**7**]
Hexadecane	17.5	10	0.56	0.54	0.2	2.9	1.7	22.9	[**21**]
Hexadecane	17.5	20	0.52	0.48	0.3		4.1	45.8	[**21**]
Hexadecane	17.5	30	0.49	0.47	0.3		16.5	68.7	[**21**]
Hexadecane	18.2	10			0.5				[**12**]
Hexadecane	19.4	50			1.8		45	73.4	[**28**]
RT20	22	30			0.5	80	20	44	[**24**]
RT25HC	23	26			1			41	[**8**]
Octadecane/Hexadecane (50:50)	24	16	0.52	0.48	0.3	4.4	3.1	24	[**27**]
Octadecane	27	10	0.5	0.45	0.5				[**12**]
Octadecane	27.2	10	0.56	0.54	0.18	3.4	1.8	24.3	[**21**]
Octadecane	27.2	20	0.52	0.48	0.2		4.1	48.6	[**21**]
Octadecane	27.2	30	0.49	0.41	0.23			72.9	[**21**]

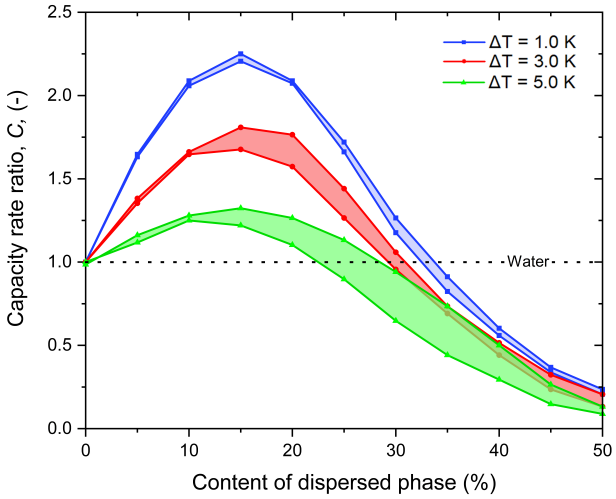

Figure 2.2: Heat capacity rate ratio, C, for a laminar flow in a pipe versus mass content of PCM within the PCD, ψ, based on Equation 2. For each assumed temperature difference, ΔT, (1, 3 and 5 K), the two curves of the same colour show the upper and lower limits of C. The two limits are calculated from: $T_{melting} \pm \Delta T$, where $\Delta T = 1, 3, 5$. The figure was adapted from Fischer et al. [29]

Paraffins however, are derived from non-sustainable oil feed stocks and can be flammable [27]. In recent years, research has focused on finding more sustainable PCMs for PCDs. Zhang et al. [28] investigated fatty acids, on accounts of their abundance, low cost, chemical inertness and non-toxicity. Four mixtures of fatty acids and eutectics thereof, were investigated. The thermophysical properties of the fatty acids as PCM can be found in [28]. From literature studies, 30 wt.% of the dispersed phase is most commonly investigated (see Table 2). Huang et al. [24] studied different weight percentages of paraffin dispersions and found 30 wt.% to be the minimum paraffin content for a specific heat capacity to be twice that of water during melting. However, Fischer et al. [29] found that 15 wt.% was optimal when considering the capacity rate ratio against the content of dispersed phase, where the capacity rate ratio for a laminar flow regime is defined to be:

$$C = \frac{\mu_{water}}{\mu_{PCD}} \frac{cp_{PCD}}{cp_{water}} \tag{2.2}$$

where μ_{water} and μ_{PCD} are the dynamic viscosities of water and the PCD respectively and cp_{PCD} and cp_{water} are the specific heat capacities of the PCD and water respectively. Figure 2 shows the capacity rate ratio, C, against the mass content of the PCM in the PCD, where it can be observed that a maximum C is obtained at 15 wt.%.

2.3 Physical properties

There are certain criteria that a PCD must fulfil to be considered useful as a HTF. These criteria include [29, 14, 30, 31]:

- high specific heat capacity (generally listed as twice that of water for the desired temperature range)
- high latent heat capacity
- high heat transfer rate
- low pressure drop in operation
- high storage stability
- high stability under thermal and mechanical loads during cycling
- high phase change enthalpy
- small degree of supercooling

These criteria will be discussed in the following sections of this review.

2.3.1 Stability

PCDs should demonstrate long-term stability, both in storage and under shear stress thermal cycling. A dispersion is considered stable if there is no distinct growth in droplet size over continuous cycling or if there is no phase separation during storage of the dispersion [32, 10, 33]. There are currently five known mechanisms by which dispersions can destabilise: creaming, sedimentation, coalescence, Ostwald ripening and phase inversion [31]. These mechanisms of destabilisation are outlined in Figure 3. Often times, destabilisation mechanisms are accelerated by thermal and mechanical cycling, which is why it is extremely important for researchers to focus on investigating stability over multiple thermal cycles. Within oil-in-water dispersions, the most commonly observed mode of destabilisation is creaming, due to oils (typically paraffins) having lower densities than water [15, 5]. Abedi et al. [34] stated that there are two major shortcomings in studying the stability of dispersions and that is the indirect measurement techniques and poly-disperse droplet sizes. To overcome this, Abedi et al. [34] produced dispersions with controlled and narrow particle size distributions using micro-fluidics. Zou et al. [35] suggested two methods for overcoming the destabilisation of dispersions, the first is to use an optimal concentration of PCM in the dispersion. High concentrations of PCM have a greater probability for agglomeration or precipitation, but reducing the concentration of PCM significantly will reduce the total heat capacity of the dispersion [35]. The second

method proposed by Zou et al. [35] is in accordance with Stokes law. Stokes law predicts that a stable dispersion will have a high viscosity, small density difference between the two phases and small droplet diameters. From these properties, reducing the droplet size is the most feasible. Zou et al. [35] stated that reducing the droplet size causes a large reduction in the gravitational force in the dispersion, suggesting that the Brownian motion may overcome the gravitational force. It has been suggested that PCDs with droplet sizes between 20-500 nm offer high stabilities and have greater longevity [36, 37]. Huang et al. [24] additionally discovered that creaming can be reduced by decreasing the droplet size of dispersions or increasing the viscosity of the dispersion. This was also found by Zhang et al. [36]. The greater stability of more viscous continuous phases was attributed to the retardation of aggregation of the PCM droplets. Lu and Tassou [38] used Xanthan gum as a thickener and found a reduced creaming destabilisation in their PCD. Despite this, for practical use thickeners cannot be used in industrial or commercial PCD systems due to the increased pumping power needed to pump a more viscous fluid. Abedi et al. [34] found that dispersions with a smaller droplet size are more stable due to the probability of particle coalescence being reduced. Despite this, smaller droplet sizes are associated with higher PCD viscosities for a given mass or volume of fluid and also an increased supercooling [24]. It is suggested by the author of this review that a compromise on droplet size should be reached to ensure good stability, low viscosities and lower supercooling degrees. Surfactants are often used to prevent instability in emulsions. From a literature search, it can be found that quite a large range of surfactants have been utilised to prevent destabilisation. Tween variations, which are non-ionic polyethoxylated surfactants, are commonly used for oil-in-water dispersions. Golemanov et al. [39] used a series of Tween surfactants (Tween20, 40, 60 and 80) and compared them to other surfactants. It was concluded that Tween 40 and Tween 60 were the most effective surfactants at stabilising paraffin-in-water dispersions, which was attributed to the fact that their chain length was small enough to allow the formation of dense interfacial layers surrounding the PCM, which were stabilised due to the steric effect [39]. Lu and Tassou [38] showed that non-ionic surfactants were better than ionic surfactants for dispersion stability and additionally reducing toxicity. More recently, this was confirmed by Chen and Zhang [5]. Tokiwa et al. [40] found that the concentration of the surfactant is also an important factor when considering PCD stability as the concentration of surfactant needs to be sufficient to ensure the entire surface of the PCM droplets are coated.

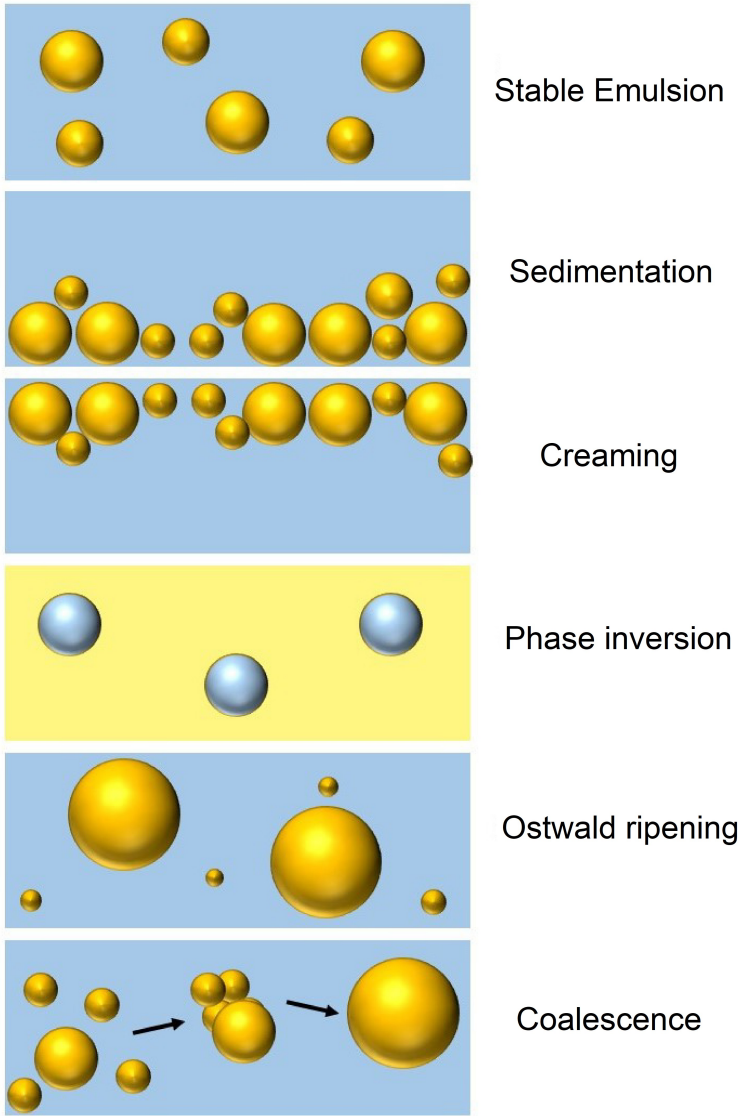

Figure 2.3: Schematic showing a stable emulsion alongside the destabilisation mechanisms.

Stability during storage

Huang et al. [24] stated that the most important factor to take into consideration when trying to increase PCD stability is PCM concentration. They found that after one month, distinct layering was observed in PCDs containing 16-60 wt.% paraffin, but creaming was not evident in the dispersions with 65-75 wt.% paraffin. However, practically, PCDs with such high paraffin concentrations cannot be used in cooling systems as a result of the high viscosity associated with PCDs with higher PCM concentrations. Günther et al. [37] prepared a 30 wt.% hexadecane dispersion and found that creaming occurred in only a few days. Another study performed by Huang et al. [41] found that after two years of storage, no significant destabilization was observed. Chen and Zhang [5] investigated the effect of HLB on the storage stability of their PCD and found that a dispersion with a HLB of 12.0 had a stabilisation period of greater than 210 days, but a dispersion with a HLB of 15.0 began to destabilise after 65 days. Despite this, Shao et al. [42] still found that after a storage period of 270 days there was an increased mean droplet size from 3.1 μm to 3.4 μm which was indicative that coalescence had occurred. Fischer et al. [26] showed that when their PCD was below its melting temperature (suspension form), the lifespan was 300 days, and when it was above its melting temperature (emulsion form), the lifespan was 25 days. Cabaleiro et al. [43] produced PCDs with droplet sizes between 90 - 120 nm and it was found that after 30 days in storage, the average droplet diameter had not increased, suggesting high stability. This was attributed to the droplets being small enough that Brownian motion ensured that the droplets moved throughout the sample and didn't cream to the top of the sample during storage [43]. As discussed by Chen and Zhang [5], who formulated nanoscale PCDs, smaller particle sizes tend to improve the stability of dispersions, however they also increase viscosity and degree of supercooling.

Stability during cycling

Huang et al. [24] performed cycling tests on a PCD with 35 wt.% paraffin, 2.5 wt.% surfactant and 2.5 wt.% nucleating agent. The cycling involved a heating/cooling cycle, which was repeated 50 times for 6 days. They found that the particle sizes slightly increased after cycling, and supercooling was observed. It was assumed by the authors that this was due to the nucleation agent separating from the dispersion. It was concluded however, that due to the viscosity remaining the same throughout cycling, that the PCD was stable to mechanical and thermal cycling. This was attributed to the mechanical energy provided in the pumping system preventing creaming from occurring. Another study by Huang et al. [41] found that dispersions of 30 wt.% RT10 and RT20 respectively also had an increased particle size distribution after thermal-mechanical cycling. Schalbart et al. [44] investigated the preparation methods of dispersions and their effects on stability. It was found that methods, which produced a narrow droplet size distribution, generated

dispersions that were stable against creaming for more than 6 months, however during cycling Ostwald ripening was observed which increased the droplet size and decreased the viscosity. Additionally, it has been suggested by Wang et al. [11] that the addition of co-surfactants ensures good stability of the dispersion. They found that a mass ratio of 50:50 polyvinyl alcohol to PEG-600 had good stability after 50 cooling-heating cycles. Although not applied specifically to PCD systems yet, research in emulsion chemistry has found that Pickering emulsions could offer increased stabilisation in PCDs. This involves stabilising the surfactants with amphipathic solid nanoparticles [36, 33]. More recently however, alternative additives, other than surfactants are being used to safeguard the stability of emulsions and prevent against creaming, for example, Zhang et al. [36] concluded that the addition of SiO_2 nanoparticles increased the stability of a paraffin-in-water emulsion.

2.3.2 Supercooling

For a material to crystallise, nucleation must occur. However, the process of nucleation has a potential energy barrier, which must be overcome for nucleation and thus crystallisation to initiate. This energy barrier is a function of the radius of a nucleus formed in the solution and it is not until a critical radius is reached that the energy barrier can be overcome and nucleation is initiated [45]. However, if a nucleus is smaller than this critical radius, nucleation will not occur, as the nucleus will collapse. The process of nucleation and supercooling is discussed extensively in [46]. The barrier to nucleation though, can also be overcome through thermal energy fluctuations, which are stochastic events that render nucleation a probabilistic phenomenon [47]. Because of this, nucleation is highly dependent on temperature. There are two kinds of nucleation, homogeneous and heterogeneous. Homogeneous nucleation occurs in an ideally pure solution, where no external contaminates can act as heterogeneous nucleators. Due to the stochastic nature of homogeneous nucleation, a larger volume of material suggests a higher probability for nucleation to occur. However, within a dispersion, the PCM volume is dramatically reduced compared to a bulk solution, hence reducing the likelihood of homogeneous nucleation occurring, resulting in large supercooling degrees. This is particularly obvious in the case of nano-sized emulsions, whereby in the small and isolated droplets, the probability of their being an external contaminant is lower, and thus crystallisation proceeds via homogeneous nucleation [43].

It is well observed that large degrees of supercooling limits the application of PCDs in cooling systems as the latent heat contributing to the large heat capacities of dispersions is released over a broad temperature range, rather than being released as a sharp peak over a narrow temperature range, this is outlined in Figure 4. Figure 2.4 shows an example of a typical DSC curve for crystallisation of two different PCDs, one of the curves represents an "ideal" PCD with little to no supercooling, and the other curve represents a PCD

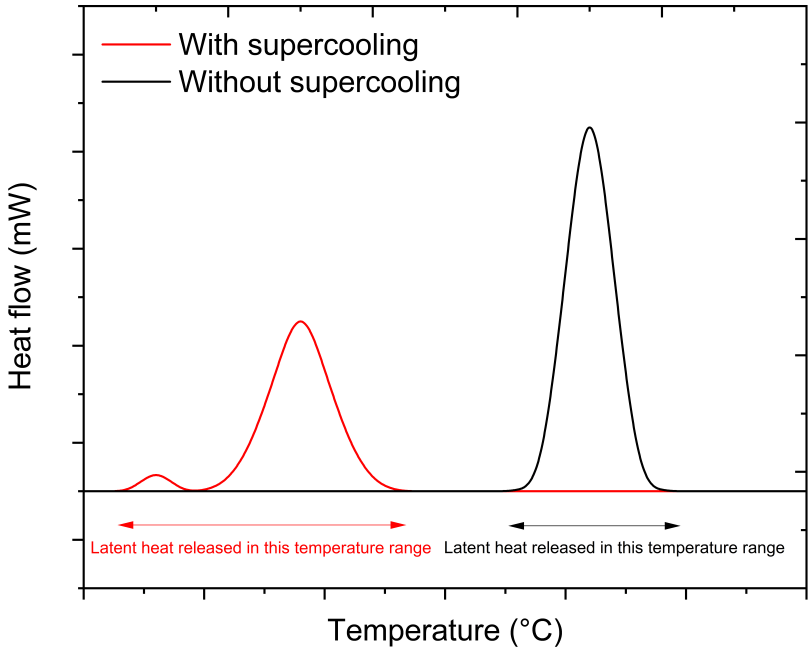

Figure 2.4: Example of a DSC curve showing the crystallisation curves of two PCDs, the solid black line shows an "ideal" PCD with no supercooling, whereby the latent heat is released over a small ΔT. The red dashed-line shows a PCD with supercooling, whereby the latent heat is released over a broad temperature range.

with a large supercooling degree. Within PCDs, there tends to be large degrees of supercooling, over a broad temperature range, as a result of the different crystallisation temperatures of different PCM droplets within the PCD (as a result of different particle size distributions and local droplet temperatures). A narrow crystallisation temperature of PCM within the PCD is essential for PCDs acting as HTF for temperature stability and for applications which require isothermal conditions. Large degrees of supercooling also suggest that the PCM within the PCD crystallises at lower temperatures, meaning a lower temperature from the chiller is required to crystallise the PCM which increases the energy consumption of PCD systems and reduces their efficiency [10]. Methods to combat supercooling have been the centre of PCM and PCD research for quite some time. Huang et al. [24, 41] performed a two part investigation on supercooling in tetradecane and hexadecane dispersions.

Effect of droplet size

Huang et al. [24] discovered that a 30 wt.% tetradecane-in-water emulsion with a droplet diameter of 1-10 μm had a supercooling degree of 7 K. Large supercooling degrees were also found by Günther et al. [37], Lu and Tassou [38], Hagelstein and Gschwander [48]

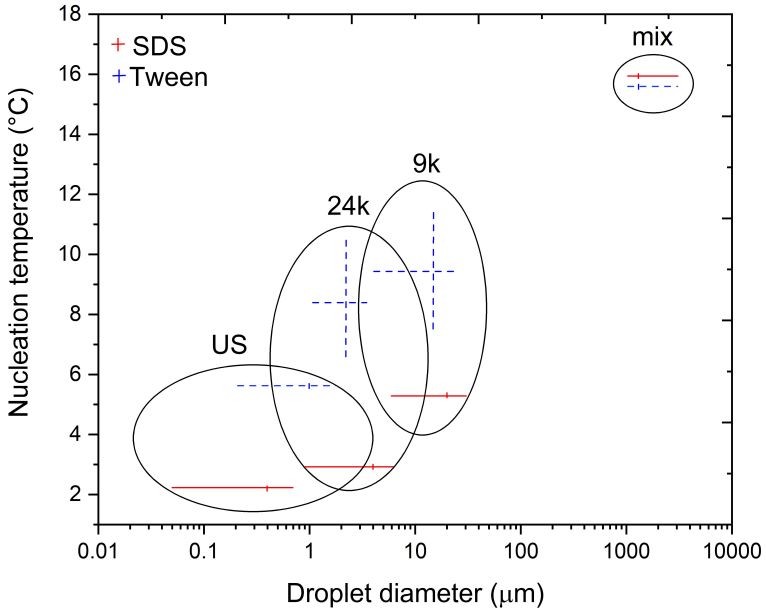

Figure 2.5: Nucleation temperature for hexadecane PCDs with varying hexadecane droplet diameters, which were prepared with different methods, ultrasound (US), homogenisier at 24,000 rpm and 9,000 rpm from [37]

and Wang et al. [11]. To investigate the claim that particle size influences the degree of supercooling, Günther et al. [37] prepared dispersions with droplet sizes ranging from 0.2 to 20 μm using different methods, ultrasound and different frequencies. For the smaller droplet sizes, supercooling on the scale of 15 K was observed, and for the larger particle sizes a supercooling of 5 K was observed. Figure 5 shows the nucleation temperature against droplet diameter for PCDs with different production methods and surfactants used. From Figure 5, it is evident that the larger the droplet size, the higher the nucleation temperature and thus the lower the supercooling degree

Effect of surfactant used

Günther et al. [37] concluded that interfacial phenomena between the surfactant and the PCM has an effect on the initiation of crystallisation due to surfactants having a large impact on the thermal properties of the dispersion. Functionalising the surfactant ensures that each dispersed particle contains a nucleation seed, therefore suggesting that each individual dispersed particle should crystallise. Hagelstein and Gschwander [48] used polyvinyl alcohol as a surfactant to reduce the supercooling of hexadecane dispersions from 12 K to 2 K. Lu and Tassou [38] also found that using hexadecanol, as a co-surfactant, reduced supercooling by 3 K compared to when just Tween 20 was used. Hexadecanol was also used by Zhang et al. [28] as a co-surfactant in a capric acid/lauric acid in water dispersion, and here it was found that the supercooling degree was reduced from 20 K to 10 K.

Effect of additives

Additives are often added to PCDs to induce heterogeneous nucleation. Huang et al. [41] added a paraffin with a phase change temperature of 50 °C (which is a paraffin with a higher melting point than the PCMs used in the PCD) to the dispersion as a nucleating agent. Adding a higher melting point paraffin was also found to be effective by Lu and Tassou [38]. Zhang et al. [28] used multi-wall carbon nano-tube (MWCNT) particles that resulted in the supercooling being reduced by 46% from 6.4 to 3.5 K. Fischer et al. [29] investigated varying amounts of Myristic acid in a RT25HC-in-water dispersion and found that increasing the amount of Myristic acid in the PCD decreased the degree of supercooling. Furthermore, a time-cycling dependency has been observed on the efficacy of nucleating agents, whereby after a certain amount of thermo-mechanical cycles the nucleating agents stops or reduces its impact on the crystallisation temperature [26]. It is therefore suggested that these cycling effects of nucleating agents and efficacy in reducing supercooling is researched more in depth.

2.3.3 Heat Capacity

Utilising PCDs as a HTF requires an increase in the total heat capacity compared to the specific heat of water at the desired application temperature. When comparing the total heat capacity of a PCD with water, the applied temperature range (around the phase change temperature) needs also to be considered on an application by application basis, depending on the operational conditions. When considering PCDs, the total heat capacity of the PCD is defined as [29]:

$$cp_{PCD,total} = (1 - \psi)cp_{water} + \psi\frac{L_{melting,PCD}}{\Delta T} \tag{2.3}$$

and is it generally calculated over a 6 K temperature difference around the melting point of the PCM within the PCD as found with DSC analysis (unless otherwise stated) [49]. Generally, the cp_{total} is higher for PCDs than for water as a result of the increase in the specific heat capacity during the phase change of the PCM. In fact, it is the increased total heat capacities of PCDs over single-phase HTF which stands as the basis for the development of PCDs. Chen and Zhang [5] concluded in their study that due to the high total heat capacity of their PCDs, the dispersion was particularly attractive for practical applications such as cooling and air-conditioning. This is because, as found in a study by Lu and Tassou [38], that amongst other parameters, the total heat capacity was found to have a great influence on the heat transfer of the PCD. To increase the total heat capacity, increasing the mass content of PCM within the dispersion is effective. Sivapalan et al. [50] found that a 10 wt.%, 20 wt.% and 33 wt.% paraffin wax PCD possessed a total heat capacity which was 7, 31 and 43% higher than water respectively. Huang et al. [51]

investigated a PCD composition of 50 wt.% and 30 wt.% of RT10 which had total heat capacities which were 2.7 and 2.0 times higher than water respectively for the applied range of 5-11 °C, i.e a 6 K temperature range. In another investigation, Huang et al. [41] found that their Cryosol 6, Cryosol 10 and Cryosol 20 PCDs had a latent heat capacity that was 3 times, 2 times and 1.8 times higher than that of water respectively, also in a 6 K temperature range. Despite this, increasing the mass fraction of PCM decreases the thermal conductivity of the PCDs and increases the viscosity, and thus when creating a PCD all parameters discussed in this review must be balanced and analysed using figures of merit, which is discussed further in section 5.

2.3.4 Thermal conductivity

Currently, one of the major drawbacks of dispersions is that paraffins have low thermal conductivities therefore dispersions in general have lower thermal conductivities than traditional single phase HTF. Shao et al. [42] measured the thermal conductivity of a 25 wt.% RT10 in water PCD to be 30% less than water at the same temperature. Whilst an increase in thermal conductivity is not necessary in terms of heat transfer into the dispersed particles to melt them (due to their small size), it is important in terms of the overall heat transfer mechanism within PCDs. Currently, this is unknown and therefore represents a major research gap in the study of PCDs. It has also been stated that the thermal conductivity of PCDs varies non-linearly with the size of the PCM droplets, concentration of PCM, fluid properties and temperature, making correlations for describing the thermal conductivity difficult to produce [52]. Yu et al. [53] explained that the thermal conductivity of dispersions depends not only on the concentration of the PCM within the dispersion but is a complex mixture of: the particle size and distribution, the particle shapes and orientations, the Brownian motion of the droplets, the aggregation of the droplets, the dispersions continuous phases's interfacial layer, additives, pH and temperature. This section will further explore the effects of different parameters on a dispersion's thermal conductivity.

Effect of PCM concentration

Paraffins have lower thermal conductivities than water, and thus when higher concentrations of paraffins are used, the thermal conductivity of the PCDs will be lower than when smaller concentrations of paraffins are used. Kawanami et al. [14] found that the thermal conductivity of a PCD decreased linearly with increasing PCM concentration. Lu and Tassou [38] also observed that with increasing the PCM concentration, the thermal conductivity of the sample decreased. Chen and Zhang [5] found that at the same temperature, the thermal conductivity of the PCD decreases with an increase in mass concentration of the PCM, which is due to the paraffins having a lower thermal conductivity

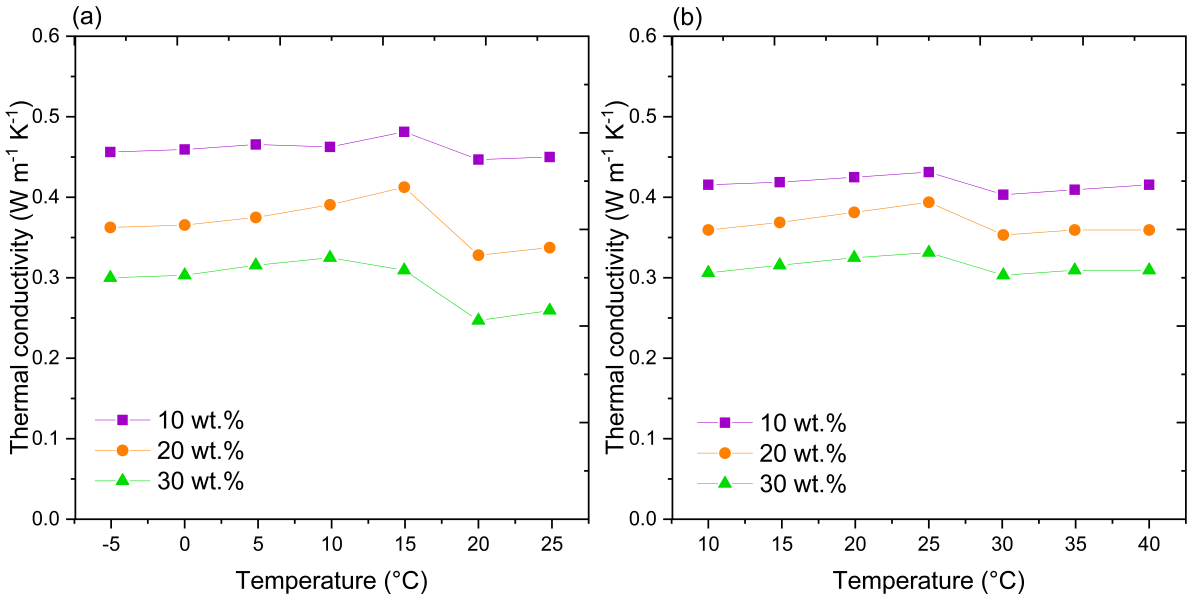

Figure 2.6: Variation of the thermal conductivity of (a) a hexadecane-based PCD and (b) an octadecane-based PCD at different temperatures and weight percentages of the dispersed PCM. Figure was adapted from Chen et al. [5].

than the base fluid (water). Figure 6 shows the results from Chen and Zhang [5] for two different dispersions with varying temperatures, mass contents and during the melting region. In Figure 6 it can be seen that for both the octadecane and hexadecane based PCDs, the 10 wt.% PCD has the highest thermal conductivity across all temperatures, and 30 wt.% has the lowest thermal conductivity.

Effect of phase change

The operational temperature of the PCD has an influence on the thermal conductivity for example, Wang et al. [11] found that for a 20 wt.% dispersion, the thermal conductivity at 30 °C was 0.49 W m^{-1} K^{-1} and at 60 °C was 0.61 W m^{-1} K^{-1}. However, phase change has a significant impact, after the PCD melts, there is a sharp decrease in the thermal conductivity due to the decreased thermal conductivity of liquids compared to solids. Chen and Zhang [5] found a large decrease in the thermal conductivity at the melting temperature, due to the PCM changing phase from a solid to a liquid. It has also been suggested that the thermal conductivities of dispersions have been overestimated during melting, due to the large amount of heat absorbed by the dispersion under isothermal conditions [54]. Figure 6 shows the significant decrease in the thermal conductivity during melting of two different dispersions prepared in [5].

Effect of droplet size

Additionally, experimental work by Liu et al. [55] highlighted that the thermal conductivity of paraffin-in-water dispersions vary with the PCM droplet size and that the thermal conductivity can be increased by reducing the droplet size. However, it should be noted that droplet size should be chosen when taking into consideration other factors such as supercooling, stability and viscosity.

Effect of additives

Current methods to increase the thermal conductivity of dispersions involve the addition of nanoparticles. For example, Zou et al. [35] investigated adding 1 wt.% of aluminium nanoparticles into a paraffin emulsion and found a 30% increase in the thermal conductivity, so that the thermal conductivity almost rivalled that of pure water. Ho and Gao [56] added 5 and 10 wt.% of Al_2O_3 nanoparticles which showed a 2 and 6% increase in the thermal conductivity of the PCD compared to without the nanoparticles. At 60 °C, an increase in 17% of the thermal conductivity was achieved, which was suggested by the authors to be due to the enhanced Brownian motion with the addition of the nanoparticles in the base fluid having a much lower viscosity at increased temperatures [56]. However, it has been noted that the addition of nanoparticles adds extra cost and reduces the fraction of paraffin used (and thus the total heat capacity) and as a result have been rendered unsuitable for use in most dispersion systems. Ho and Gao [56] found that by adding 10 wt.% of Al_2O_3, that the latent heat of fusion decreased from 243 kJ kg^{-1} (with no nanoparticles) to 212 kJ kg^{-1}.

Calculating the thermal conductivity of PCDs

Due to the different components in PCDs having different thermal conductivities, equations have been produced from researchers to quantify the effective thermal conductivities of PCDs for different mass fractions of PCM used. The effective thermal conductivity is most often calculated by modified versions of the first-order approximation Maxwell equation [57]:

$$\lambda_{PCD} = \frac{\lambda_{PCM} + 2\lambda_{water} + 2(\lambda_{PCM} - \lambda_{water})\phi)}{\lambda_{PCM} + 2\lambda_{water} - 2(\lambda_{PCM} - \lambda_{water})\phi)}\lambda_{water} \tag{2.4}$$

where $\lambda_{PCD}, \lambda_{PCM}, \lambda_{water}$ are the thermal conductivities of the dispersion, PCM and water respectively and ϕ is the particle volume fraction. The Maxwell equation is an empirical equation based on the effective medium theory. It has been suggested by Cabaleiro et al. [43] that the Maxwell equation does not take into account scale-related phenomena, for nano-sized PCM droplets which include; interfacial resistance, Brownian motion, droplet-continuous phase interactions or the flow of the droplets.

Kawanami et al. [14] used the Hamilton and Crosser equation to evaluate the thermal conductivity [58]:

$$\frac{\lambda_{PCD}}{\lambda_{water}} = \frac{(\lambda_{PCM} + (z-1)\lambda_{water} - (z-1)\phi(\lambda_{water} - \lambda_{PCM})}{(\lambda_{PCM} + (z-1)\lambda_{water} + \phi(\lambda_{water} - \lambda_{PCM}))} \tag{2.5}$$

where $z = 3/\beta$ and β is a sphericity factor, which was assumed to be 1. Within literature, it has been noted that an increase of thermal conductivity exists in oil-in-water dispersions and that this increase, alongside droplet size has not been considered in current equations for calculating the effective thermal conductivities of PCDs [55]. However, Liu et al. [55] proposed a new semi-empirical equation of the effective thermal conductivity, which takes into account the droplet size of the PCM [55]:

$$\lambda_{PCD} = \frac{(\lambda_{PCM} + 0.9023\lambda_{water} + 0.0051\phi(\lambda_{water} - \lambda_{PCM})(1 + 0.0512\frac{T}{T_f})(1 - 0.0215\frac{d_{PCM}}{d_{water}})}{(\lambda_{PCM} + 0.8699\lambda_{water} + 1.6824\phi(\lambda_{water} - \lambda_{PCM})(1 + 0.00194\frac{T}{T_f})(1 - 0.0001\frac{d_{PCM}}{d_{water}}))} \tag{2.6}$$

for the following conditions: 20 °C $\leq T \leq$ 70 °C, 0.5% $\leq \phi \leq$ 4.0,%, 0.5 µm $\leq$ d $\leq$ 0.9 µm where T_f is the reference temperature of 20 °C. Liu et al. [55] investigated the dual-phase-lag heat conduction which combines the micro-structural effects occurring between PCM droplets into delayed temporal responses into the macroscopic formulation of the entire PCDs. The dual-phase lag heat conduction was quantified based on the time lag ratio suggested by Kang et al. [59]:

$$\frac{\tau_q}{\tau_t} = \frac{S\pi\lambda^2}{4aq^2} \tag{2.7}$$

where τ_q describes the thermal inertia in short-time responses, τ_t is the delayed time caused by heat transport mechanisms in micro-scale, S is the time derivative, q is the heat flux and a is the thermal diffusivity. When $\tau_q/\tau_t \geq 1$ the governing equation of the dual-phase-lag heat conduction is hyperbolic and therefore is transported by thermal waves. When $\tau_q/\tau_t \leq 1$ the thermal conductivity is dominated by non-Fourier heat conduction and when $\tau_q/\tau_t = 0$, the governing equation is the classical diffusion equation employing Fourier's law. Liu et al. [55] found all their investigated dispersions had τ_q/τ_t between 0.1 and 0.3 suggesting that a diffusion-dominated non-Fourier heat conduction could exist in oil-in-water emulsions. Further investigation into this for other dispersions is suggested by the authors.

2.3.5 Rheology and viscosity

It is important to investigate the rheology of dispersion systems as viscosity influences the heat transfer, stability and pumping power requirements of dispersions [8]. Delgado et al.

[60] showed that due to the high viscosity of their 60 wt.% paraffin in water dispersion, the natural convective heat transfer was highly reduced. Additionally, Chen et al. [61] found that PCDs had higher viscosities than water, which led to drastic increases in the required pumping power in their feasibility studies. Increased viscosities of PCDs has also shown to increase the pressure drop in comparison to water [5, 11]. Wang et al. [11] found that although the PCDs had double the storage capacity of water, due to the higher viscosity and thus higher pressure drop of the PCDs, the power consumption for the PCDs system was found to be higher than for water. This increase in viscosity was originally attributed to solely the weight percentage of PCM employed, with an increasing concentration of PCM leading to an increased viscosity. For example, Ho et al. [62] investigated 1-10 wt.% n-Eicosane-in-water dispersions and reported pressure drops which were up to 200% for 10 wt.% compared to 1 wt.% highlighting the dependency of the pressure drop and viscosity on the concentration of the dispersed phase. However, more recently it has been suggested that the temperature of the PCD is operated at and the concentration of surfactant are two other important factors [28, 38]. These results are promising as it suggests that PCDs can be fine-tuned to create compromised rheological properties, whereby optimising the composition of the PCD allows for smaller viscosities and pressure drops whilst still retaining high heat transfer properties and stabilities. The majority of the dispersions tested in literature show extremely high viscosities compared to water, for example, Inaba and Morita [63] produced a 5 wt.% and 40 wt.% tetradecane-in-water emulsion and found the dispersions had viscosities of 31.1 mPa·s and 2.5 Pa·s, which are 1167 and 21 times higher than the viscosity of water respectively. Additionally, Zhao and Shi [64] found dispersions of 16 wt.% and 50 wt.% tetradecane-in-water had apparent viscosities of 24.5 mPa·s and 150 mPa·s which is 16 and 100 times the apparent viscosity of water respectively. Shao et al. [42] also observed a viscosity for a 30 wt.% paraffin-in-water dispersion, which was 13 times higher than that of water. The high viscosities of these dispersions render them unviable for HVAC and cooling applications due to the increase in the pump energy consumption. Additionally, this causes a switch from the turbulent to laminar flow regime resulting in a decreased heat transfer coefficient. However, more recently, Chen et al. [61] prepared a PCD with 30 wt.% paraffin and found a viscosity of 8.46 mPa·s which is only 5.6 times higher than water.

Effect of PCM concentration

One of the most well-known and investigated factors in the viscosity of dispersions is the concentration of the dispersed phase [15, 41]. Within literature, there are two competing notions concerning the influence of concentration and shear rate on the rheological properties of fluids. To determine whether a fluid exhibits Newtonian or non-Newtonian behaviour, one examines the relationship between the shear stress and shear rate that is

usually presented using the Ostwald formula [65]:

$$\tau = K\dot{\gamma}^{(n-1)} \tag{2.8}$$

where n is the fluid behaviour index and describes the degree of non-Newtonian behaviour exhibited and K is the consistency index, where the larger the value of K, the more viscous the fluid is. A value of $n = 1$ indicates Newtonian behaviour, $n \geq 1$ shear-thickening behaviour and $n \leq 1$ shear-thinning behaviour. Morimoto and Kumano [15] defined n experimentally and found that after melting the dispersions displayed Newtonian behaviour with $n = 0.95$, which was attributed to the liquid state of the particles becoming more deformable which created a more Newtonian behaviour. The first competing notion in literature, is that at and below a 30 wt.% of dispersed phase, PCDs demonstrate Newtonian behaviour, and above this concentration non-Newtonian behaviour is observed [54]. Vasile et al. [66] investigated the rheology of a 30 wt.% paraffin-in-water emulsion and found that the emulsion exhibited Newtonian behaviour with measurements performed on a rheometer in both the cone and plate geometry. Morimoto et al. [15] discovered that dispersions with 10-30 wt.% paraffin were considered to be Newtonian, whereas a dispersion containing 40 wt.% paraffin was considered non-Newtonian. This was attributed to higher concentrations of dispersed phase having a greater probability of generating aggregation-type structures, which cause more non-Newtonian behaviours. Chen et al. [61] also found that the friction factor of the 30 wt.% conformed to the classical formula of [61]:

$$f = \frac{64}{Re} \tag{2.9}$$

for laminar flow in circular pipes which confirmed its Newtonian behaviour. Conversely, the second notion is that all concentrations of paraffins show non-Newtonian behaviour. Huang et al. [67] investigated a larger range of paraffin concentrations, 15-75 wt.% and discovered that they all exhibited non-Newtonian behaviour and that the degree of non-Newtonian behaviour and viscosity dramatically increased once the paraffin concentration surpassed 50 wt.%. In another investigation by Huang et al. [41] dispersions containing RT10 with weight percentages of 15 to 50% all exhibited non-Newtonian behaviour. Lu and Tassou [38] also found that non-Newtonian behaviour was observed for a dispersion of 30 wt.% RT6 and a dispersions of 6 wt.% RT25. The conflict in these findings can be attributed to other factors that contribute to the rheology of dispersions such as surfactant type and concentration, temperature and shear rate.

Effect of surfactant choice

The role the surfactant plays in influencing the viscosity of PCDs is attributed to the micelle structure, which is formed by the surfactant interface. This indicates that the

viscosity is dependent on both the surfactant type and their respective concentrations. Zhang et al. [28] investigated the effects of three commonly used surfactants, SDS, Tween 80 and Tween 20 on the viscosity of a 30 wt.% hexadecane dispersion. It was concluded that there was great variation in the viscosities by just changing the type of surfactant used. Zhao and Shi [64] built on the idea of the surfactant influence by investigating the effect of the surfactant concentration on the viscosity. The surfactant concentration was varied from 2.6 to 4.7 wt.% and a corresponding dynamic viscosity change of 0.00055 Pa·s to 0.00294 Pa·s was observed at 20 °C. This can be explained by recognising that as the surfactant concentration increases, there will be an increased attraction strength of the surfactant monolayer. This increased attraction requires more energy to be transported than a smaller attraction strength, thus increasing the viscosity [64]. It is suggested by the authors that due to the complex surfactant system now employed in dispersions, as seen in the previous section, with co-surfactants and using a variety of surfactants mixed together that rheological properties are properly understood and tested for multi-component dispersion compositions.

Effect of temperature

Lu and Tassou [38] discovered that the viscosity of their PCD was heavily dependent on the temperature, where a decrease in temperature led to an increase in viscosity until the crystallisation temperature was reached. This was attributed to the presence of surfactants, as the liquid paraffin droplets remain smooth and flexible until their crystallisation point and therefore make little contribution to the friction. This was also confirmed by Huang et al. [24] who discovered that the viscosity of all the tested dispersions increased with the increasing frozen fraction of the RT10 paraffin in the dispersion, therefore as the temperature decreased the viscosity increased. This has been attributed to the fact that solid particles are less likely to deform under shear stress like liquid droplets, therefore increasing the viscosity. The variation of the viscosity with temperature was also found to be reduced for dispersions with lower paraffin concentrations, caused by the difference in water content [66]. Chen et al. [61] revealed that viscosities decrease with an increase in temperature, and the larger the mass fraction of the PCM, the quicker this effect is observed. For example, at 0°C the viscosity of a 30 wt.% hexadecane dispersion was 42 mPa·s and at 30°C was 17 mPa·s, whereas the 10 wt.% hexadecane dispersion had a viscosity of 4 mPa·s at 0°C and 2 mPa·s at 30°C . The temperature dependency of viscosity is due to the tendency of droplets to aggregate at lower temperatures, as explained by Zhang et al [28]. Zhang et al. [28] performed further experimentation on a capric/lauric acid-in-water dispersion and found that the cohesion of PCM droplets influenced the viscosity. This was attributed to temperature increases causing an increased distance between the PCM droplets thus reducing the attractive forces holding them together. In turn, this

reduces the shear stress by deformation and therefore a reduced viscosity is shown

2.3.6 Physical properties summary

It is evident to see that all the aforementioned physical properties of PCDs; stability (during cycling and storage), degree of supercooling, heat capacity, thermal conductivity and viscosity are influenced by the formulation and physical and operational parameters and conditions used when creating and testing PCDs. These parameters include the concentration of PCM used, the effect of temperature, the effect of PCM droplet size and the effect of chemical additives. It is important to understand the dual-nature that some of these parameters and conditions have on the physical properties of PCDs for future optimisation of PCD formulations and to glean information on how these parameters can be balanced to create a HTF which fulfils the requirements outlined in Section 3. Additionally, the hysteresis between the cooling and heating cycles of such behaviour is poorly reported, and the authors believe a thorough investigation into the thermal cycling of all physical properties should be conducted.

2.4 Heat transfer

Unlike micro-encapsulated phase change slurries, limited investigations, both experimentally and numerically have been performed on PCDs. Experimental studies for PCDs as potential HTF are essential as they not only have the potential to demonstrate the benefits of using PCDs, but also they help to understand the heat transfer processes and mechanisms that occur in PCDs. Ultimately, this allows predictive correlations to be produced for heat exchanger design and optimisation. The phase change process of PCDs occurs over a temperature range where the PCDs have a much higher specific heat capacity (during phase change) than a single-phase fluid. This means that PCDs have a much larger ability to transport heat. Zhao and Shi [64] provide a theoretical analysis of this and found that convective heat transfer can be increased if the flow rate of the fluid is increased, the temperature gradient is increased and certain material properties, such as the specific heat is increased.

This section on heat transfer will be separated into the different operational parameters that can be controlled when performing experiments with PCDs. Ma et al. [68] explained the physical reason for the influence of physical operational parameters on the melting heat transfer performance of PCDs. The author stated that during melting, a liquid layer of melting PCM droplets near the tube wall impedes the heat transfer from the wall to the bulk of the fluid. This effectively reduces the heat transfer from the wall to the bulk, and certain operational parameters such as the flow rate, imposed temperature or heat flux at the wall and mass concentration of PCM effect the rate at which this liquid layer

develops. [68]. This is discussed further in section 4.1.

Furthermore, for implementation of PCDs into industrial and commercial systems, a complete understanding of both the melting and crystallisation heat transfer behaviour is required to understand the complete cycle of PCDs. Therefore, in this section the effect of the operational parameters are further split into melting and crystallisation experiments. Additionally, forced convection is more highly studied than natural convection, due to the usefulness of forced convection in temperature stability and refrigeration applications and this is the focus of this chapter. Despite this, natural convection is still the focus of a few research articles, where the motivation is energy storage owing to the latent heat of phase change for PCDs [60, 69].

2.4.1 Melting

Generally, authors focus their heat transfer experiments on the melting behaviour of PCDs because during crystallisation the supercooling phenomena makes the heat transfer behaviour difficult to predict.

Effect of the wall heat flux

Morimoto and Kumano [15] found that a higher applied wall heat flux decreased the local heat transfer coefficient due to a faster melting PCD. Ma et al. [68] explained this by stating that the mass fraction of un-melted PCM is larger at lower heating powers at the same axial location as higher heating powers and therefore the liquid layer of melted PCM, which usually hinders heat transfer develops slower at lower heat fluxes. Ho et al. [6] varied the heat flux in their divergent mini-channels and found that with PCDs, when the wall heat flux was decreased that the dimensionless wall temperature would also decrease, suggesting a greater degree of melting. However, Ho et al. [6] discovered that the heat flux had a minor effect on the average Nusselt number (Nu). Morimoto and Kumano [15] showed that the enhancement ratio of Nu (of the PCD to the base fluid) was decreased as the wall heat flux was increased. This was most likely due to the latent heat absorption decreasing as the wall heat flux increased. This effect was shown through the following relation for the modified specific heat capacity (cp^*) inside the thermal boundary layer [15]:

$$cp^* \approx cp + \frac{L}{(T_w - T_{in})} \tag{2.10}$$

where L is the latent heat of melting for the PCDs, T_w is the wall temperature and T_{in} is the bulk inlet flow temperature. From Equation 10 when a low heat flux is applied, almost all the heat is allocated to the latent heat of the PCM because the temperature difference between the main flow and the wall temperature is relatively small. On the other hand, when a high wall heat flux is applied, the heat is transferred under the form

of sensible heat because the wall temperature is relatively high and the temperature of the PCD increases even though the PCM particles are melting. This was also validated with numerical results [15].

Effect of the mass flow rate

It is important to note that in all experimental and numerical investigations on the heat transfer of PCDs, the flow regime is always described as turbulent or laminar, which is a classification generally attributed to single-phase fluids, such as water. However, for PCDs, laminar and turbulent flow regimes are more difficult to define without a set of standard PCD formulations (including set droplet sizes and PCM concentrations) and there is little discussion on the validity of describing PCDs as flowing in the turbulent or laminar flow regime, especially when they have a non-Newtonian behaviour: the laminar turbulent transition of such fluids remains a non fully solved scientific issue.

Ho et al. [6] found that when a higher mass flow rate was used, the dimensionless wall temperature increased because the effective heat exchange duration between the PCDs and the wall was too short. However, this occurs at a critical Reynolds number (Re) and generally, an increase in Re number in the turbulent flow regime increases the heat transfer behaviour. Ho et al. [6] found that an increase in Re number increased the average Nu due to thinning of the thermal boundary layer resulting in an increased heat transfer rate. Ma et al. [68] also stated that an increase in Re increased the local heat transfer coefficients due to greater thinning of the thermal boundary layer. Morimoto and Kumano [70] suggested that the thermal boundary layer development was suppressed largely at higher flow rates, attributing to higher heat transfer coefficients. Despite this, Roy and Avanic [71] numerically found that in the laminar flow regime, the dimensionless wall temperature was independent of the Re used for their octadecane-in-water PCD. This is what is observed for single-phase fluids, such as water and further indicates the need for more research in attributing PCDs to the turbulent or laminar flow regime. Saarinen et al. [72] discovered similar results in the turbulent regime where for Re = 2300-6000, Nu enhancement did not increase a great deal. However, at Re = 7000, the highest Nu enhancements of 13-15% were obtained. Additionally, the same results could be seen for the convective heat transfer coefficients. Therefore, Re = 7000 was classified as a critical Re by the authors [72].

Effect of the PCM concentration

Cho et al. [73] numerically investigated a PCD in a mini-channel and found that increasing the concentration of the PCM in the PCD decreased the wall temperature increase along the channel compared to the base fluid. Cho et al. [73] attributed this to an increased melting time of the PCM when the concentration of the PCM is higher. Furthermore,

Morimoto and Kumano [15] numerically investigated the heat transfer behaviour of a PCD, in laminar flow, and found that the numerically obtained Nu agreed with the experimentally obtained results for 20 and 30 wt.% PCM based PCDs. However, the numerical model showed much lower values for the Nusselt number at 10 wt.% than the experimental results, they concluded that heat transfer promotion mechanisms occurred in PCDs with low PCM concentrations. Ma et al. [68] found that the local heat transfer coefficient increased with the mass concentration of PCM used whereby the local heat transfer coefficient of a 20 wt.% PCM dispersion was found to be 1.4 times higher than a 10 wt.% PCM dispersion at the same Reynolds number. Overall, despite the increase in the heat transfer performance with an increase in the concentration of PCM (at the same Re), a compromise of the mass fractions of PCMs used in PCDs needs to found by weighing up the increase in thermal performance and the additional increase in viscosity and pumping power required. This is discussed further in section 2.5.

Other notable effects

Wen and Ding [74] numerically found that during melting, a non-uniform particle size distribution resulted in higher Nusselt numbers because of particle migration and Brownian motion. During melting, Ma et al. [68] found that although the development of the thermal boundary layer is faster in smaller tubes than in larger tubes that the Nusselt number increased in smaller tubes. This was attributed to greater particle-wall interactions in smaller tubes.

2.4.2 Crystallisation

To date, very few studies have been performed examining the heat transfer behaviour during crystallisation. As aforementioned, the supercooling makes analysis and creating correlations more difficult.

Effect of the flow regime

Morimoto et al. [75] found that a turbulent flow regime caused an increase in the heat transfer promotion effect. Despite Roy and Avanic [71] finding that during melting the heat transfer coefficient was independent of the Reynolds number in laminar flow, Vasile et al. [66] discovered that the average heat transfer coefficient increased as the Re increase in a laminar flow regime for crystallisation.

Effect of the PCM concentration

Zhao and Shi [64] discovered that in a coiled circular tube that Nu increased as the mass fraction of the PCM was increased. Inaba and Morita [63] experimentally investigated

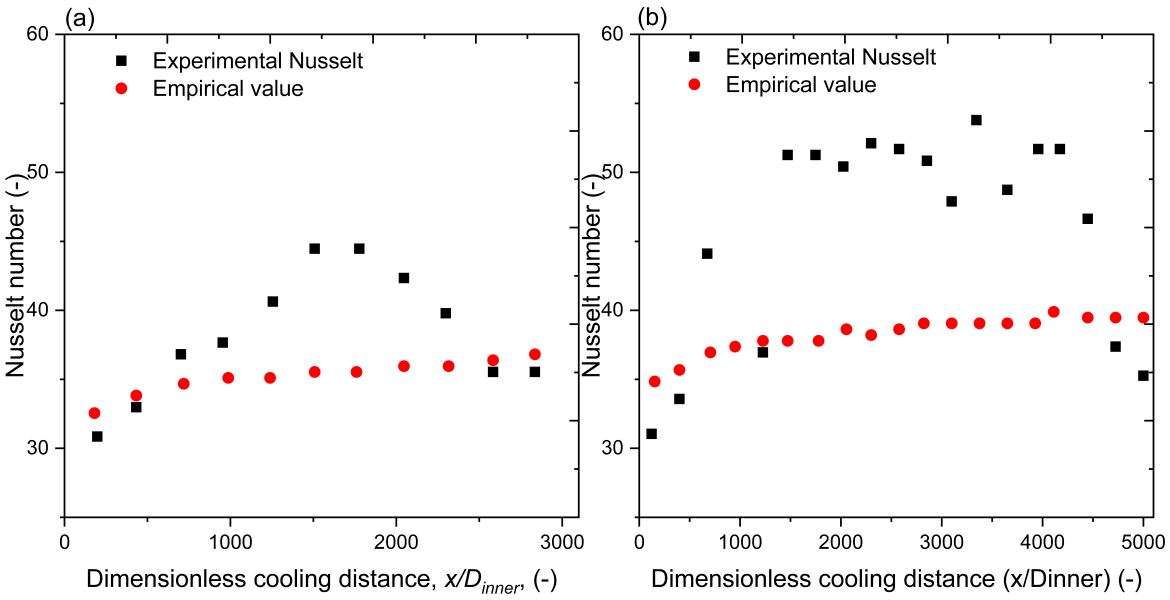

Figure 2.7: The local Nusselt number versus the dimensionless distance from inlet and the empirical correlation for single-phase fluid for (a) a PCD with Tween 80 as the surfactant and for (b) a PCD with Tween 60 as the surfactant. Figure was adapted from Morimoto et al. [15].

a tetradecane-in-water PCD in a double-tube coiled heat exchanger and showed that an increase in the concentration of the PCM in the PCD resulted in an increase in the Nu.

Other notable effects

Alongside the main operational parameters, several other parameters have been noticed to affect the heat transfer behaviour of PCDs. Inaba and Morita [63] stated that a decrease in the temperature difference between the PCDs and the fluid cooling it down increases the heat transfer performance of the PCDs. Zhao and Shi [64] found that the Nusselt number for the solid dispersed phase (after phase change) was larger than for the liquid dispersed phase (before phase change). The two explanations which were presented are, firstly that the emulsion becomes a solid/liquid two phase fluid when the emulsion temperature falls below the freezing point and the mixing and disturbing effects caused by small particles improve the convective heat transfer in the thermal boundary layer. Secondly, the emulsion's effective thermal conductivity has a somewhat higher value when the dispersed phase becomes solid particles. Inaba and Morita [63] also found that for the solidified PCM a larger Nusselt enhancement was obtained due to the higher thermal conductivities in the solid phase. Morimoto et al. [75] investigated two different PCDs with different surfactants, they plotted the Nusselt number for each PCD versus the dimensionless cooling distance alongside the Dittus–Boelter equation (from [75] for a single-phase fluid, as shown in Figure 7. From Figure 7, the initiation of solidification

time is different for each different surfactant used and the deviation between the empirical equation for a single-phase fluid and the Nusselt number's experimentally observed are greater for the PCD with Tween 60 surfactant than Tween 80 surfactant. This deviation suggests that surfactants can also play a role in the heat transfer performance of PCDs during crystallisation and this is something which needs to be further researched.

2.4.3 Heat transfer summary

Overall, the lack of experiments, both numerically and experimentally can be seen for crystallisation of PCDs. This creates a problem because in all usages of PCDs, knowledge of the full melting-crystallisation cycle is needed to design and optimise systems. Additionally, there are generally few research articles published on the heat transfer behaviour of PCDs, and few standardised methods of experimentation, due to different geometries and boundary conditions chosen for experiments. It is also acknowledged by the authors that due to the lack of research on defining and validating flow regimes as laminar or turbulent in the case of PCDs that the transition flow regime remains a non fully solved scientific issue and the heat transfer performance during this transition is unknown. Overall, this makes having a comprehensive understanding of the heat transfer and the factors which affect the heat transfer performance of PCDs very difficult, especially when studies focus primarily on the melting and few correlations exist describing the heat transfer during crystallisation.

2.5 Figures of merit

To choose the appropriate PCD for a specific application, the heat transfer capabilities of the dispersion compared to its base fluid or the standard HTF must be calculated. Figures of merits aim to characterise this comparison and comparison criteria are used to set the conditions under which the figure of merit comparison takes place. Additionally, an important aspect of experimental research into PCDs is to produce predictive equations for heat transfer coefficients, which eventually permits the effective design of heat exchangers and pipe geometries. For these equations to be applied to real applications, non-dimensional parameters are used to represent heat transfer coefficients, thermophysical properties and geometric configurations. For heat transfer fluids, the most commonly used dimensionless numbers are Nusselt, Prandtl (Pr) and Reynolds. When choosing an appropriate PCD, there are three main parameters, which are of the upmost importance; these are highlighted at each point of the triangle in Figure 8. Firstly, the heat transfer coefficient, h, this is a direct measurement of the heat transfer performance of a fluid and is thus vital in the generation of a figure of merit for PCD performance characterisation. Secondly, the pressure drop, Δp, which increases due to the increased viscosity of the

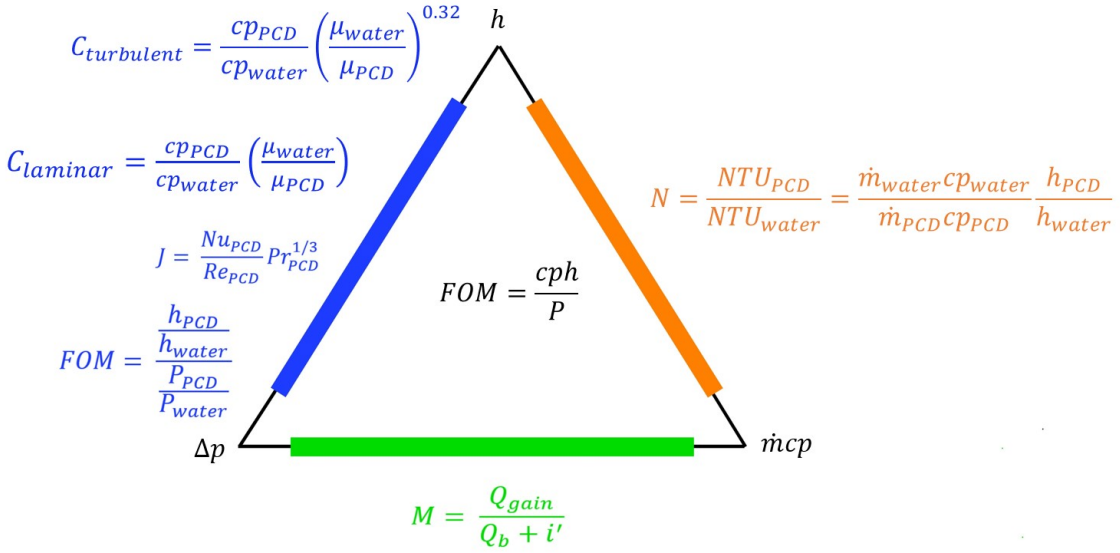

Figure 2.8: A depiction of the three key parameters for PCD comparison and their respective figures of merit

phase change of the PCD and impairs the applicability of PCDs. Finally, the capacity flow rate, which is taken into account because of the increase in specific heat capacity of the PCDs during phase change. The figures of merit found in literature are colour coded with the respective operational parameters that they take into consideration in Figure 8.

2.5.1 Comparison criteria

Within literature, the most frequently used comparison criteria are *Re*, flow velocity and pumping power. Whilst *Re* number is often used as a comparison criterion, it is generally an inappropriate choice because comparison under the same *Re* suggests that the flow velocity for the less viscous base fluid (water) is lower than for the more viscous PCD, which indicates that under the constant Re comparison criterion the observed effect is a mixture of both the flow velocity effects and the thermophysical properties of the PCDs and base fluids respectively [53]. Additionally, constant *Re* for comparison omits the increase in pumping power required with a more viscous PCD which is pumped at a higher flow velocity to reach the same *Re* as the less viscous base fluid. However, under the constant flow velocity comparison criterion, the flow velocity effect, which is inherently present under the constant *Re* comparison criterion, is eliminated. A PCD with the same velocity (or mass flow) as the base fluid will have a larger specific heat capacity flow due to the available latent heat [53]. Temperature increase will be lower and driving temperature difference higher, which results in larger heat transfers even though the heat transfer coefficient might be smaller. Even though the pumping power for PCDs is higher than for the base fluid, it has been found that in many applications the pumping

power difference between a PCD and its base fluid is small at the same flow velocity. Furthermore, the constant pumping power comparison, which compares the heat transfer under the condition that the PCDs and base fluid require the same amount of pumping power suggests that the flow velocity for the more viscous PCD is slightly lower than for the base fluid [53]. However, the constant pumping power comparison criteria represents the most explicit choice of criteria and should be used when the relevant information is known.

2.5.2 Nusselt number based figures of merit

Nu is a dimensionless form of the heat transfer coefficient that should be used to depict the convective heat transfer performance of HTF. Bonjour et al. [76] used the Colborn Factor (J), to assess the heat transfer versus the necessary pressure drop for a specific flow where J is defined as follows:

$$J = \frac{Nu_{PCD}}{Re_{PCD} Pr_{PCD}^{\frac{1}{3}}} \tag{2.11}$$

It is useful because it shows the dependency of heat exchange on Re and therefore the optimal surface depends on the Re of interest and thus the Colburn Factor. Nu can be interpreted as the ratio between the convective heat transfer (including advection and diffusion) to the conductive heat transfer within a fluid. Nu is useful in defining the heat transfer mechanisms which occur in PCDs.

2.5.3 Heat transfer coefficient based figures of merit

Often times the figure of merit of comparing heat transfer coefficients, is referred to the heat transfer effectiveness and is defined as the ratio of the convective heat transfer coefficient for the PCDs relative to the convective heat transfer coefficient of the base fluid as below [74, 77]:

$$\epsilon = \frac{h_{PCD}}{h_{water}} \tag{2.12}$$

where h_{PCD} and h_{water} are the heat transfer coefficients for the PCD and the base fluid (water) respectively at the same mass flow rate. From this, an enhanced heat transfer ability of the PCD is observed when $\epsilon \geq 1$. Memon et al. [78] investigated different PCDs by using the heat transfer effectiveness ratio, and found that the maximum ratio was reached when all the particles of the PCM were melted inside the dispersion. It was further concluded that this ratio could be further enhanced by minimising the sensible heat region at the inlet of the flow channel, which would allow the remaining length of the channel to be represented by the latent heat effect. In turn, this would permit a lower temperature increase along the channel and a greater temperature control within

the channel. This can be shown non-dimensionally in the form of the Stefan number (Ste), which represents the ratio of the sensible heat to latent heat as shown in Equation 13.

$$Ste = \frac{cp\Delta T}{L} \tag{2.13}$$

for the boundary condition of constant wall temperature or defined as [16]:

$$Ste = \frac{cp(q/\lambda)}{\psi L_{PCM}} \tag{2.14}$$

For the boundary condition of constant wall heat flux. The Stefan number has been used in some investigations to determine the melting time. Morimoto et al. [70] used a modified Stefan number and discovered that the Nusselt number increases when the modified Stefan number decreased meaning that the Nusselt number was found to increase when the heat allocated to the latent heat of phase change increased. Ma et al. [68] also used the Stefan number to investigate the optimal heat input to use to obtain the best heat transfer performance of their PCDs.

Ho et al. [77] went further and discussed the dependence of ϵ on Re and found a critical velocity to enhance ϵ . At extremely high Re, the sensible heat dominates over the latent heat of the PCDs due to the particles only partially melting due to higher flow velocity, whereas at slightly lower Re, the PCM particles within the slurry have more time to absorb the surrounding heat and are therefore more likely to fully melt. It is suspected by Memon et al. [78] that the maximum value of the effectiveness ratio is obtained when the sensible region at the inlet is minimised, and that the peak in effectiveness ratio is when the flow through the length of the channel is dominated by latent heat of phase change of the PCM. Further investigation into this by use of Ste is recommended by the author for future research.

2.5.4 Pumping power based figures of merit

Whilst an increase in the heat transfer coefficient is advantageous for PCDs, an increase in the pumping power is detrimental for their use as HTF. As a result of this, the two quantities can be combined to form a new figure of merit which shows the ratio of the heat transfer coefficient increase to the pumping power enhancement and is defined as [53]:

$$FOM = \frac{h_{PCD}/h_{water}}{P_{PCD}/P_{water}} \tag{2.15}$$

If this figure of merit is utilised under the constant pumping power comparison criterion, then it reduces to the ratio of heat transfer coefficients between the PCDs and the base fluid, see Equation 12. When the figure of merit is higher, it is indicative that there is a

greater heat transfer increase when using the PCDs than pumping power penalty.

Memon et al. [78] defined a figure of merit based on the pumping power and heat transfer named Merit number (M). It uses a measure of the irreversibility of the heat transfer and frictional losses due to the addition of the PCM particles within a fluid. Subsequently, it represents the ratio of the enhancement in heat transfer due to PCM addition to the total of the heat transfer to the top wall of the channel and the irreversibility. M is defined as:

$$M = \frac{Q_{gain}}{Q_b + i^{'}} \tag{2.16}$$

where Q_{gain} is the rate of increase of heat absorption in the dispersion due to the addition of the PCM, Q_b is the heat transfer rate of the bulk fluid to the wall and $i^{'}$ is the rate of irreversibility the definitions of both can be found in [78]. The irreversibility depends on the volumetric entropy generation rate which is defined in [79]. It is expected that at higher heat flux to mass ratios, the lower concentration of dispersions will show higher M values, this is suspected because the heat transfer enhancement is smaller than the increase in irreversibility, due to higher pressure-drops and viscosities.

2.5.5 Heat capacity based figures of merit

In laminar flow regimes, Prasher et al. [80] suggested the following F.O.M. ratio [80]:

$$\frac{C_\mu}{C_\lambda} = \frac{\frac{\mu_{PCD} - \mu_{water}}{\mu_{water}}}{\frac{\lambda_{PCD} - \lambda_{water}}{\lambda_{water}}} \tag{2.17}$$

where it was stated that for $\frac{C_\mu}{C_\lambda} \geq 4$, the PCD is considered better in terms of the heat transfer compared to the base fluid (water). Fischer et al. [29] also investigated this figure of merit, and named it the heat capacity rate ratio, C. This can be seen in Equation 2. The derivation for C can be seen in [29]. It was discussed that C cannot be applied directly to turbulent flow. This is because the derivation of this equation involves calculating the pressure drop in the pipe, and then equating the pressure drop of water and PCDs. This is possible in laminar flow, however due to the exponent in the pressure drop calculation in a pipe for turbulent flow this cannot be equated.

2.5.6 Figures of merit summary

Overall, the heat transfer and rheological performance of new HTF need to be compared to the heat transfer performance of existing HTF. For choosing an appropriate HTF, the three main parameters which need to be considered are the heat transfer coefficient, the pressure drop and the capacity flow rate. As discussed in Sections 3 and 4, there are many factors which need to be considered when formulating and using PCDs as an

enhanced HTF. Figures of merit aim to quantify these parameters and allow a direct comparison between different HTF on their performance for specific applications under certain comparison criteria.

2.6 Conclusions and Future directions

This chapter has focused on a review that highlighted the types of PCDs that have been investigated in the literature, alongside their thermophysical, rheological and heat transfer properties. It clearly demonstrates that the increased heat capacities shown by dispersions renders them strong candidates for HTF. The thermophysical properties of paraffins as phase change material in dispersions are widely reported for a broad temperature range within the cooling domain; however, low thermal conductivities indicate that other classes of materials should be investigated to increase the heat transfer capabilities. Currently, the application of PCDs into systems for cooling has been limited on accounts of large degrees of supercooling of dispersions because of their microscopic geometries and stability observed both in storage and during cycling. Additionally, from this review, it has been highlighted that out of the functional latent heat transfer fluids developed, phase change dispersions are the least investigated, particularly in terms of heat transfer and the mechanisms of heat transfer. Whilst numerical models have been developed in both laminar and turbulent flow, experimental validation is still required. It has been suggested that for PCDs to become prevalent as heat transfer fluids, a more comprehensive understanding and validation of their heat transfer performance is required. This is in order to design correct heat exchangers and optimise the cooling system geometries. Additionally, the heat transfer performance of PCDs undergoing crystallisation needs more attention that melting due to the lack of studies performed during solidification. On top of this, an effective model to describe the rheology of dispersions should be generated as currently literature offers conflicting experimental results, most likely due to different test set-ups and data collection methods. Furthermore, this review highlights the need to be careful in designing PCDs for cooling applications, due to the positive and negatives effects each parameter can have on the PCDs as a fluid overall.

Whilst the current standard PCM used in PCDs is paraffins, as can be seen by Table 2.1, the global standards for improving sustainability amongst energy solutions will encourage researchers to investigate bio-based PCM for use in PCDs, such as fatty acids and esters. New PCMs will require new literature in terms of formulation such as; effective surfactant systems and nucleating agents. One of the main future directions of the formulation of PCDs, will be more attention given to the finding of novel and efficient nucleating agents, and testing whether these nucleating agents hold up over thermo-mechanical cycling and

storage. Particularly, the use of surfactants to initiate nucleation (reduce supercooling) will be a future direction of PCD formulation research. Once a greater understanding of the interfacial tension, and crystallisation kinetics of phase change dispersions has been achieved, and more research has been performed, carefully selecting surfactant systems to induce nucleation will become more commonplace when formulating PCDs. Additionally, this balance between choosing the appropriate surfactant system for stability and for inducing nucleation will have to also be investigated. Furthermore, once supercooling has been successfully reduced within phase change dispersions, more attention should be geared towards investigating the heat transfer behaviour of PCDs during crystallisation and the author's believe that as more PCDs are pushed into the developmental stage, that more research will focus on crystallisation as a complete understanding of the heating-melting cycle will need to be considered for implementation into cooling systems.

References

[1] Paris IEA. "The Future of Cooling". In: (). URL: https://www.iea.org/reports/the-future-of-cooling.

[2] M. Caliano, N. Bianco, G. Graditi, and L. Mongibello. "Analysis of a phase change material-based unit and of an aluminum foam/phase change material composite-based unit for cold thermal energy storage by numerical simulation". In: *Appl. Energy* 256 (2019), p. 113921.

[3] T. Yang, C. Wang, Q. Sun, W. Qie, and W. Ronald. "Study on the application of latent heat cold storage in a refrigerated warehouse". In: *Energy Procedia* 142 (2017), pp. 3546–3552.

[4] X. Xu, X. Zhang, and S. Liu. "Experimental study on cold storage box with nanocomposite phase change material and vacuum insulation panel". In: *Int. J. Energy Res.* 42.14 (2018), pp. 4429–4438.

[5] J. Chen and P. Zhang. "Preparation and characterization of nano-sized phase change emulsions as thermal energy storage and transport media". In: *Appl. Energy* 190 (2017), pp. 868–879. DOI: https://doi.org/10.1016/j.apenergy.2017.01.012.

[6] C. Ho, C. Huang, C. Qin, and w. Yan. "Thermal performance of phase change nano-emulsion in a rectangular minichannel with wall conduction effect". In: *Int. Commun. Heat Mass Transf.* 110 (2020), p. 104438.

[7] F. Wang, J. Cao, Z. Ling, Z. Zhang, and X. Fang. "Experimental and simulative investigations on a phase change material nano-emulsion-based liquid cooling thermal management system for a lithium-ion battery pack". In: *Energy* 207 (2020), p. 118215.

[8] L. Fischer, S. von Arx, U. Wechsler, S. Züst, and J. Worlitschek. "Phase change dispersion properties, modeling apparent heat capacity". In: *Int. J. Refrig.* 74 (2017), pp. 240–253. ISSN: 0140-7007. DOI: https://doi.org/10.1016/j.ijrefrig.2016.10.008.

[9] S. Shibutani. "PCM-micro capsule slurry thermal storage system for cooling in Narita Airport". In: *Proc. 3rd Expert. Meet. Work. IEA Annex 17., IEA,Lublijana* 2002 (2020), p. 118215.

[10] G. Zhang, Z. Yu, G. Cui, B. Dou, W. Lu, and X. Yan. "Fabrication of a novel nano phase change material emulsion with low supercooling and enhanced thermal conductivity". In: *Renewable Energy* 151 (2020), pp. 542–550. DOI: https://doi.org/10.1016/j.renene.2019.11.044.

[11] F. Wang, X. Fang, and Z. Zhang. "Preparation of phase change material emulsions with good stability and little supercooling by using a mixed polymeric emulsifier for thermal energy storage". In: *Sol. Energy Mater Sol. Cells* 176 (2018), pp. 381–390.

[12] E. Shchukina, M. Graham, Z. Zheng, and D. Shchukin. "Nanoencapsulation of phase change materials for advanced thermal energy storage systems". In: *Chem. Soc. Rev.* 47.11 (2018), pp. 4156–4175.

[13] D. McClements. "Nanoemulsions versus microemulsions: terminology, differences, and similarities". In: *Soft matter* 8.6 (2012), pp. 1719–1729.

[14] T. Kawanami, K. Togashi, K. Fumoto, S. Hirano, P. Zhang, K. Shirai, and S. Hirasawa. "Thermophysical properties and thermal characteristics of phase change emulsion for thermal energy storage media". In: *Energy* 117 (2016), pp. 562–568. DOI: https://doi.org/10.1016/j.energy.2016.04.021.

[15] T. Morimoto and H. Kumano. "Flow and heat transfer characteristics of phase change emulsions in a circular tube: Part 1. Laminar flow". In: *Int. J. Heat Mass Transf.* 117 (2018), pp. 887–895. DOI: https://doi.org/10.1016/j.ijheatmasstransfer.2017.10.055.

[16] Qi Li, Geng Qiao, Ernesto Mura, Chuan Li, Ludger Fischer, and Yulong Ding. "Experimental and numerical studies of a fatty acid based phase change dispersion for enhancing cooling of high voltage electrical devices". In: *Energy* 198 (2020), p. 117280.

[17] L. Chai, R. Shaukat, L. Wang, and H Wang. "A review on heat transfer and hydrodynamic characteristics of nano/microencapsulated phase change slurry (N/MPCS) in mini/microchannel heat sinks". In: *Appl. Therm. Eng.* 135 (2018), pp. 334–349.

[18] Z. Qiu, X. Ma, P. Li, X. Zhao, and A. Wright. "Micro-encapsulated phase change material (MPCM) slurries: Characterization and building applications". In: *Renew. Sustain. Energy Rev.* 77 (2017), pp. 246–262.

[19] M. Delgado, A. Lázaro, J. Mazo, and B. Zalba. "Review on phase change material emulsions and microencapsulated phase change material slurries: materials, heat transfer studies and applications". In: *Renew. Sustain. Energy Rev* 16.1 (2012), pp. 253–273.

[20] M. Jurkowska and I. Szczygieł. "Review on properties of microencapsulated phase change materials slurries (mPCMS)". In: *Appl. Therm. Eng.* 98 (2016), pp. 365–373.

[21] Z. Chen and G. Fang. "Preparation and heat transfer characteristics of microencapsulated phase change material slurry: a review". In: *Renew. Sustain. Energy Rev* 15.9 (2011), pp. 4624–4632.

[22] F. Wang, W. Lin, Z. Ling, and X. Fang. "A comprehensive review on phase change material emulsions: Fabrication, characteristics, and heat transfer performance". In: *Sol. Energy Mater Sol. Cells.* 191 (2019), pp. 218–234.

[23] Jingjing Shao, Jo Darkwa, and Georgios Kokogiannakis. "Review of phase change emulsions (PCMEs) and their applications in HVAC systems". In: *Energy and buildings* 94 (2015), pp. 200–217.

[24] L. Huang, M. Petermann, and C. Doetsch. "Evaluation of paraffin/water emulsion as a phase change slurry for cooling applications". In: *Energy* 34.9 (2009), pp. 1145–1155. ISSN: 0360-5442. DOI: https://doi.org/10.1016/j.energy.2009.03.016.

[25] Q. Li, L. Fischer, G. Qiao, E. Mura, C. Li, and Y. Ding. "High performance cooling of a HVDC converter using a fatty acid ester-based phase change dispersion in a heat sink with double-layer oblique-crossed ribs". In: *Int. J. Energy Res.* 44.7 (2020), pp. 5819–5840.

[26] L. Fischer, E. Mura, P. O'Neill, S. von Arx, J. Worlitschek, G. Qiao, Q. Li, and Y. Ding. "Thermophysical properties of a phase change dispersion for cooling around 50 °C". In: *Int J Refrig* 119 (2020), pp. 410–419. DOI: https://doi.org/10.1016/j.ijrefrig.2020.05.013.

[27] R. Ravotti, O. Fellmann, N. Lardon, L. Fischer, A. Stamatiou, and J. Worlitschek. "Synthesis and Investigation of Thermal Properties of Highly Pure Carboxylic Fatty Esters to Be Used as PCM". In: *Appl. Sci.* 8.7 (June 2018), p. 1069. ISSN: 2076-3417. DOI: 10.3390/app8071069.

[28] x. Zhang, J. Niu, S. Zhang, and J. Wu. "PCM in Water Emulsions: Supercooling Reduction Effects of Nano-Additives, Viscosity Effects of Surfactants and Stability". In: *Adv. Eng. Mater.* 17.2 (2015), pp. 181–188. DOI: https://doi.org/10.1002/adem.201300575.

[29] L. Fischer, A. Stamatiou, S. von Arx, M. Pfister, S. Züst, and J. Worlitschek. "Investigation of heat transfer in phase change dispersions (PCD)". In: *JP Journal of Heat and Mass Transfer.* 14(4) (2017), pp. 485–510. DOI: https://doi.org/10.17654/HM014040485.

[30] S. Nižetić, M. Jurčević, M. Arıcı, A. Arasu, and G. Xie. "Nano-enhanced phase change materials and fluids in energy applications: A review". In: *Renew. Sust. Energ. Rev.* 129 (2020), p. 109931. DOI: https://doi.org/10.1016/j.rser.2020.109931.

[31] F. Wang, W. Lin, Z. Ling, and X. Fang. "A comprehensive review on phase change material emulsions: Fabrication, characteristics, and heat transfer performance". In: *Sol. Energy Mater Sol. Cells* 191 (2019), pp. 218–234. DOI: https://doi.org/10.1016/j.solmat.2018.11.016.

[32] F. Wang, C. Zhang, J. Liu, X. Fang, and Z. Zhang. "Highly stable graphite nanoparticle-dispersed phase change emulsions with little supercooling and high thermal conductivity for cold energy storage". In: *Appl. Energy* 188 (2017), pp. 97–106. DOI: https://doi.org/10.1016/j.apenergy.2016.11.122.

[33] X. Zhang, J. Niu, and J. Wu. "Evaluation and manipulation of the key emulsification factors toward highly stable PCM-water nano-emulsions for thermal energy storage". In: *Sol. Energy Mater Sol. Cells* 219 (2021), p. 110820. DOI: https://doi.org/10.1016/j.solmat.2020.110820.

[34] S. Abedi, N. Suteria, C. Chen, and S. Vanapalli. "Microfluidic production of size-tunable hexadecane-in-water emulsions: Effect of droplet size on destabilization of two-dimensional emulsions due to partial coalescence". In: *J. Colloid Interface Sci.* 533 (2019), pp. 59–70. DOI: https://doi.org/10.1016/j.jcis.2018.08.045.

[35] D. Zou, Z. Feng, R. Xiao, K. Qin, J. Zhang, W. Song, and Q. Tu. "Preparation and flow characteristic of a novel phase change fluid for latent heat transfer". In: *Sol. Energy Mater Sol. Cells* 94.12 (2010), pp. 2292–2297. DOI: https://doi.org/10.1016/j.solmat.2010.07.028.

[36] X. Zhang, J. Niu, and J. Wu. "Development and characterization of novel and stable silicon nanoparticles-embedded PCM-in-water emulsions for thermal energy storage". In: *Appl. Energy* 238 (2019), pp. 1407–1416. DOI: https://doi.org/10.1016/j.apenergy.2019.01.159.

[37] E. Günther, T. Schmid, H. Mehling, S. Hiebler, and L. Huang. "Subcooling in hexadecane emulsions". In: *Int J Refrig* 33.8 (2010). Phase Change Materials and Slurries for Refrigeration and Air Conditioning, pp. 1605–1611. DOI: https://doi.org/10.1016/j.ijrefrig.2010.07.022.

[38] W. Lu and S.A. Tassou. "Experimental study of the thermal characteristics of phase change slurries for active cooling". In: *Appl. Energy* 91.1 (2012), pp. 366–374. DOI: https://doi.org/10.1016/j.apenergy.2011.10.004.

[39] K. Golemanov, S. Tcholakova, N. Denkov, and T. Gurkov. "Selection of Surfactants for Stable Paraffin-in-Water Dispersions, undergoing Solid Liquid Transition of the Dispersed Particles". In: *Langmuir* 22.8 (2006), pp. 3560–3569. DOI: 10.1021/la053059y.

[40] Y. Tokiwa, H. Sakamoto, T. Takiue, M. Aratono, H. Matsubara, and C. Bain. "Effect of Surface Freezing on Stability of Oil-in-Water Emulsions". In: *Langmuir.* 34.21 (2018), pp. 6205–6209. DOI: 10.1021/acs.langmuir.8b01088.

[41] L. Huang, C. Doetsch, and C. Pollerberg. "Low temperature paraffin phase change emulsions". In: *Int. J. Refrig.* 33.8 (2010), pp. 1583–1589.

[42] J. Shao, J. Darkwa, and G. Kokogiannakis. "Development of a novel phase change material emulsion for cooling systems". In: *Renew. Energy* 87 (2016), pp. 509–516.

[43] D.Cabaleiro, F. Agresti, S. Barison, M. Marcos, J. Prado, S. Rossi, S.Bobbo, and L. Fedele. "Development of paraffinic phase change material nanoemulsions for thermal energy storage and transport in low-temperature applications". In: *Appl. Therm. Eng.* 159 (2019), p. 113868.

[44] P. Schalbart, M. Kawaji, and K. Fumoto. "Formation of tetradecane nanoemulsion by low-energy emulsification methods". In: *Int. J. Refrig.* 33.8 (2010), pp. 1612–1624.

[45] Y. Wu, M. Alivand, G. Hu, G. Stevens, and K. Mumford. "Nucleation kinetics of glycine promoted concentrated potassium carbonate solvents for carbon dioxide absorption". In: *Chem. Eng. J.* 381 (2020), p. 122712.

[46] J. Coupland. "Crystallization of Lipids in Oil-in-Water Emulsion States". In: *Crystallization of lipids: Fundamentals and applications in food, cosmetics, and pharmaceuticals* (2018), p. 431.

[47] T. El Rhafiki, T. Kousksou, A. Jamiland S. Jegadheeswaran, S. Pohekar, and Y. Zeraouli. "Crystallization of PCMs inside an emulsion: Supercooling phenomenon". In: *Sol. Energy Mater Sol. Cells* 95.9 (2011), pp. 2588–2597.

[48] G. Hagelstein and S. Gschwander. "Reduction of supercooling in paraffin phase change slurry by polyvinyl alcohol". In: *Int. J. Refrig.* 84 (2017), pp. 67–75.

[49] G. Höhne, W. Hemminger, and H. Flammersheim. *Differential scanning calorimetry.* Springer Science & Business Media, 2013.

[50] B. Sivapalan, M. Neelesh Chandran, S. Manikandan, M. Saranprabhu, S. Pavithra, and K. Rajan. "Paraffin wax–water nanoemulsion: A superior thermal energy storage medium providing higher rate of thermal energy storage per unit heat exchanger volume than water and paraffin wax". In: *Energy Convers. Manag.* 162 (2018), pp. 109–117.

[51] L. Huang, P. Noeres, M. Petermann, and C. Doetsch. "Experimental study on heat capacity of paraffin/water phase change emulsion". In: *Energy Convers. Manag.* 51.6 (2010), pp. 1264–1269.

[52] T. Kousksou, T. El Rhafiki, M. Mahdaoui, P. Bruel, and Y. Zeraouli. "Crystallization of supercooled PCMs inside emulsions: DSC applications". In: *Sol. Energy Mater Sol. Cells* 107 (2012), pp. 28–36.

[53] W. Yu, D. France, E. Timofeeva, D. Singh, and J. Routbort. "Comparative review of turbulent heat transfer of nanofluids". In: *Int. J. Heat Mass Transf.* 55.21-22 (2012), pp. 5380–5396.

[54] H. Xu, R. Yang, Y. Zhang, Z. Huang, J. Lin, and X. Wang. "Thermal physical properties and key influence factors of phase change emulsion". In: *Chinese Sci. Bull.* 50.1 (2005), pp. 88–93.

[55] F. Liu, Q. Chen, Z. Kang, W. Pan, D. Zhang, and L. Wang. "Non-Fourier heat conduction in oil-in-water emulsions". In: *Int. J. Heat Mass Transf.* 135 (2019), pp. 323–330.

[56] C. Ho and J. Gao. "Preparation and thermophysical properties of nanoparticle-in-paraffin emulsion as phase change material". In: *Int. Commun. Heat Mass.* 36.5 (2009), pp. 467–470.

[57] J. Maxwell. "Electricity and Magnetism". In: *Clarendon Press, Oxford, UK* (1873).

[58] R. Hamilton and O. Crosser. "Thermal Conductivity of Heterogeneous Two-Component Systems". In: *Ind. Eng. Chem.* 1.3 (1962), pp. 187–191.

[59] Z. Kang, P. Zhu, D. Gui, and L. Wang. "A method for predicting thermal waves in dual-phase-lag heat conduction". In: *Int. J. Heat Mass Transf.* 115 (2017), pp. 250–257.

[60] M. Delgado, A. Lázaro, J. Mazo, C. Peñalosa, P. Dolado, and B. Zalba. "Experimental analysis of a low cost phase change material emulsion for its use as thermal storage system". In: *Energy Convers. Manag.* 106 (2015), pp. 201–212.

[61] B. Chen, X. Wang, Y. Zhang, H. Xu, and R. Yang. "Experimental research on laminar flow performance of phase change emulsion". In: *Appl. Therm. Eng.* 26.11-12 (2006), pp. 1238–1245.

[62] C. Ho, C. Lee, and M. Yamada. "Experiments on laminar cooling characteristics of a phase change nanofluid flow through an iso-flux heated circular tube". In: *Int. J. Heat Mass Transf.* 118 (2018), pp. 1307–1315.

[63] H. Inaba and S. Morita. "Flow and cold heat-storage characteristics of phase-change emulsion in a coiled double-tube heat exchanger". In: *J. Heat. Trans.* 117 (1995), p. 440.

[64] Z. Zhao and Y. Shi. "Experimental investigations of flow resistance and convection heat transfer and prediction of cold heat-storage characteristics for a phase-change emulsion in a coiled circular tube". In: *Heat Transf. Eng.* 26.6 (2005), pp. 32–44.

[65] F. Ostwald. "The theory of solutions". In: *Z. Phys. Chem.* 2 (1888), pp. 36–37.

[66] Virginia Vasile, Horia Necula, Adrian Badea, Rémi Revellin, Jocelyn Bonjour, and Phillipe Haberschill. "Experimental study of the heat transfer characteristics of a paraffin-in-water emulsion used as a secondary refrigerant". In: *International Journal of Refrigeration* 88 (2018), pp. 1–7.

[67] L. Huang and M. Petermann. "An experimental study on rheological behaviors of paraffin/water phase change emulsion". In: *Int. J. Heat Mass Transf.* 83 (2015), pp. 479–486.

[68] F. Ma, J. Chen, and P. Zhang. "Experimental study of the hydraulic and thermal performances of nano-sized phase change emulsion in horizontal mini-tubes". In: *Energy* 149 (2018), pp. 944–953.

[69] H. Inaba, C. Dai, and A. Horibe. "Natural convection heat transfer of microemulsion phase-change-material slurry in rectangular cavities heated from below and cooled from above". In: *Int. J. Heat Mass Transf.* 46.23 (2003), pp. 4427–4438.

[70] M. Takashi and Hiroyuki K. "Flow and heat transfer characteristics of phase change emulsions in a circular tube: Part 2. Turbulent flow". In: *Int. J. Heat Mass Transf.* 117 (2018), pp. 903–911.

[71] S. Roy and B. Avanic. "Laminar forced convection heat transfer with phase change material suspensions". In: *Int. Commun. Heat Mass Transf.* 28.7 (2001), pp. 895–904.

[72] S. Saarinen, S. Puupponen, A. Meriläinen, A. Joneidi, A. Seppälä, K. Saari, and T. Ala-Nissila. "Turbulent heat transfer characteristics in a circular tube and thermal properties of n-decane-in-water nanoemulsion fluids and micelles-in-water fluids". In: *Int. J. Heat Mass Transf.* 81 (2015), pp. 246–251.

[73] Y. Cho, E. Choi, and H. Lorsch. *A novel concept for heat transfer fluids used in district cooling systems*. Tech. rep. Drexel Univ., Philadelphia, PA (United States). Dept. of Mechanical ..., 1991.

[74] D. Wen and Y. Ding. "Experimental investigation into convective heat transfer of nanofluids at the entrance region under laminar flow conditions". In: *Int. J Heat Mass Transf.* 47.24 (2004), pp. 5181–5188.

[75] T. Morimoto, K. Suzuki, and H. Kumano. "Heat transfer characteristics of phase change emulsions with solidification of phase change material particles in a circular tube". In: *Int. J. Refrig.* 114 (2020), pp. 1–9.

[76] J. Bonjour, R. Revellin, P. Haberschill, V. Vasile, A. Badea, and H. Necula. "Theoretical evaluation of the use of Phase Change Material Emulsions and Figures of Merit". In: *2019 International Conference on ENERGY and ENVIRONMENT (CIEM)*. IEEE. 2019, pp. 520–523.

[77] J. Ho, N. Wijeysundera, S. Rajasekar, and T. Chandratilleke. "Performance of a compact, spiral coil heat exchanger". In: *Heat Recovery Systems and CHP* 15.5 (1995), pp. 457–468.

[78] S. Memon, M. Sajid, M. Malik, A. Alquaity, M. Rehman, T. Cheema, M. Kwak, and C. Park. "Investigation of the Thermal Performance of Salt Hydrate Phase Change of Nanoparticle Slurry Flow in a Microchannel". In: *J. Chem.* (2019).

[79] L. Yeh, R. Chu, and W. Janna. "Thermal Management of Microelectronic Equipment: Heat Transfer Theory, Analysis Methods, and Design Practices. ASME Press Book Series on Electronic Packaging". In: *Appl. Mech. Rev.* 56.3 (2003), B46–B48.

[80] R. Prasher, D. Song, and J. Wang. "Measurements of nanofluid viscosity and its implications for thermal applications". In: *Appl. Phys. Lett.* 89 (2006), p. 133108.

Chapter 3

Materials and Methodology for thermophysical analysis

Throughout the subsequent chapters, thermophysical characterisation of different PCD formulations are reported. This chapter is dedicated to the description of the analytical techniques used to achieve this characterisation. It is to be noted that the experimental test-rigs used to determine the heat transfer behaviour of different PCDs presented in Chapters 5 and 6 will be described in the respective chapters for ease.

3.1 Methodology

3.1.1 Differential Scanning Calorimeter

Differential scanning calorimetry was used in this investigation to determine the inlet conditions which should be used in the experimental test-rigs, the peak melting temperature of the PCDs, the enthalpy of melting/crystallisation and the specific heat capacities. The differential scanning calorimeter (DSC) employed was the Mettler Toledo (Columbus, OH, USA) DSC 832 which, has a reported uncertainty of ± 8% for the melting enthalpy. The sample mass and heating/cooling rates used in the DSC measurements were varied and will be discussed in the relevant results section.

3.1.2 Thermal Cycling

For extended thermal cycling, the Mettler Toledo (Columbus, OH, USA) EasyMax 102 unit was used to observe the thermal profiles of the PCDs with larger volumes than in the DSC. Each PCD sample, which was cycled using the EasyMax, was approximately 100 mL. The EasyMax works by pre-setting a temperature profile (with specific heating and cooling ramp rates) using the Mettler Toledo softwareTM (v. 5.4). Due to the larger volume sizes allowed in the EasyMax, compared to the DSC for example, emulsion

destabilisation processes, such as: creaming, coalescence and phase separation can be observed. Additionally, the EasyMax permits agitation using an in-house 3D-printer stirrer bar. The EasyMax thermal cycling unit and an example of one of the 3D stirrer bars can be seen in Figure 3.1.

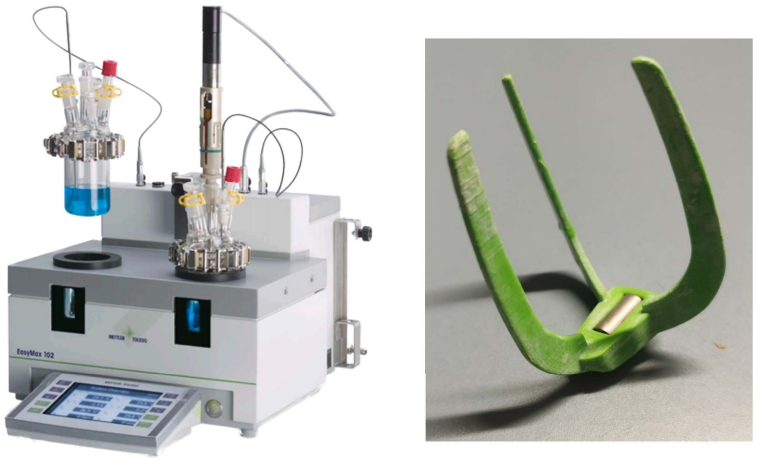

Figure 3.1: The EasyMax Thermal Cycling unit from Mettler Toledo (left) and the 3D printed stirrer bar (right)

3.1.3 Particle Size Distribution

To investigate the particle size distribution (PSD) of all dispersions presented in this thesis, a Beckman-Coulter LS13320 with Polarisation Intensity Differential Scattering (PIDS) and laser diffraction was used. The PSD is a great property to investigate the quality of a PCD, with narrower PSD suggesting a more highly stable dispersion. The measuring range of the Beckman-Coulter LS13320 is within the range of 0.04-2000 μm.

3.1.4 Viscosity

The dynamic viscosity (μ) of the PCDs were determined using the MCR 302 Anton Paar Rheometer. The dynamic viscosity of the PCDs were investigated under different applied shear rates and temperatures. According to the manufacturer, the uncertainty of the viscosity measurements are ± 3%. The validity of the experiments were tested in the temperature range used in this investigation, by measuring the dynamic viscosity values of water between 5-30℃ at a range of shear rates. An example of the dynamic viscosity of water at 1 s^{-1} and between 5-30℃ measured with the rheometer and values taken from CoolProp [1] are shown in Figure 3.2.

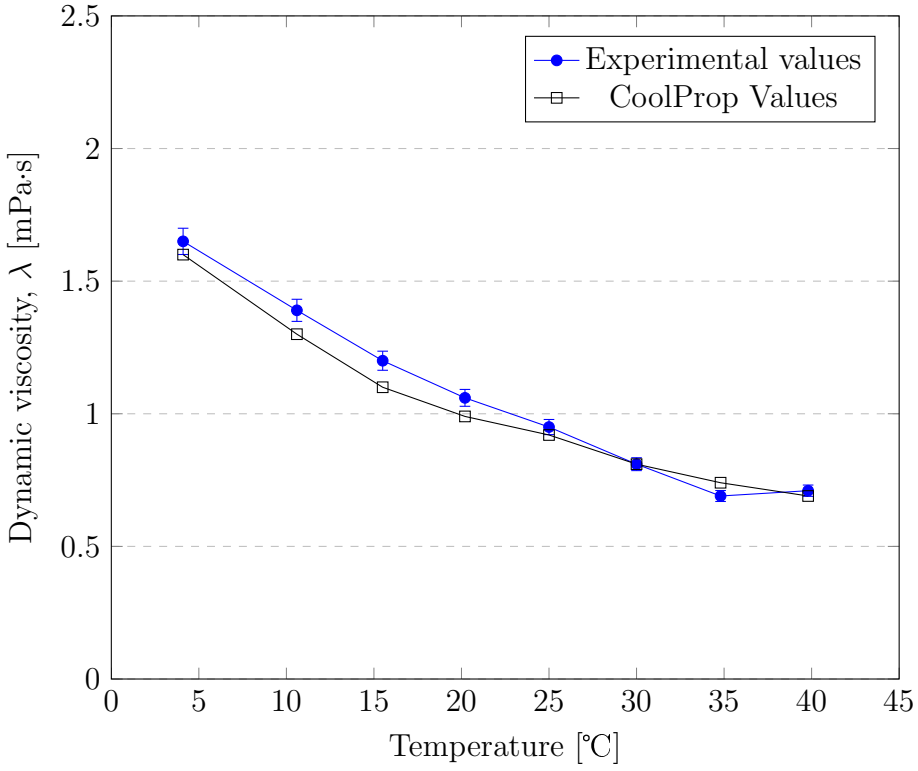

Figure 3.2: Validation of Dynamic viscosity measurements with the Anton Paar Rheometer by comparing the dynamic viscosity of water at different temperatures to the CoolProp values [1]. Additionally, the errors bars of the uncertainty given by the manufacturer is shown.

3.1.5 Density measurements

The density of the PCDs were measured in order to accurately calculate the Reynolds numbers of the PCDs at the respective temperatures used in the test-rig experiments. The density of the formulated PCDs were measured with the DM40 Density meter from Mettler Toledo. The density measurements were performed over the temperature ranges of 5—30℃ in both the heating and cooling direction (so from 30℃ being cooled down to 5℃ and vice versa). The measuring range of the instrument is 0—3000 kgm^{-3} and the error of the density meter as given by the manufacturer is $\pm$0.1 kgm^{-3}.

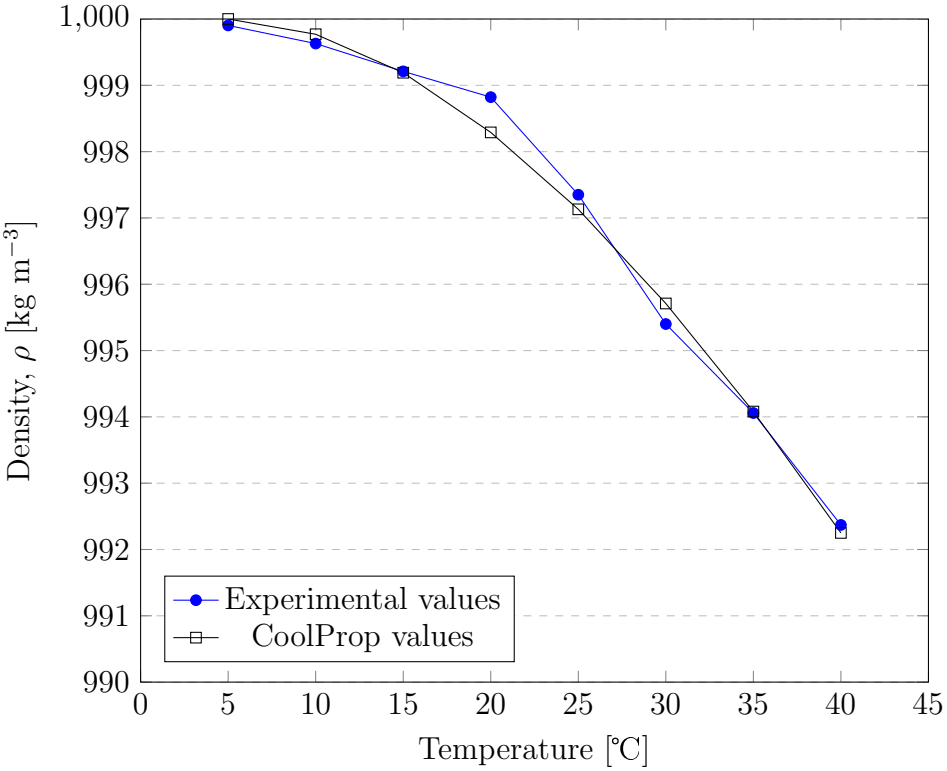

Figure 3.3: Validation of the density measurements by comparing the experimentally measured densities of water at different temperatures against the CoolProp [1]. Additionally, the errors bars of the uncertainty given by the manufacturer are shown.

3.1.6 Thermal conductivity measurements

The transient hot bridge method was used to determine the thermal conductivity of the formulated PCDs with the Linseis THB-100 (Germany). Determining the thermal conductivity of PCDs at different temperatures is essential for accurate calculation of Nusselt numbers and Prandtl numbers. Additionally, it serves as an additional method to calculate the thermal diffusivity (α). The working principle of the thermal hot bridge method is that the wire in the sensor, which is comprised of a strip heater and a temperature sensor is connected in a bridge circuit, between two identical samples of PCDs from the same batch. The potential difference on the bridge diagonal corresponds to the temperature difference. The measuring range of the instrument is 0.01-100 $Wm^{-1}K^{-1}$ with a measurement uncertainty of ± 2%. Figure 3.4 shows the experimentally measured values of the thermal conductivity of water between 5—40℃ and values taken from CoolProp [1].

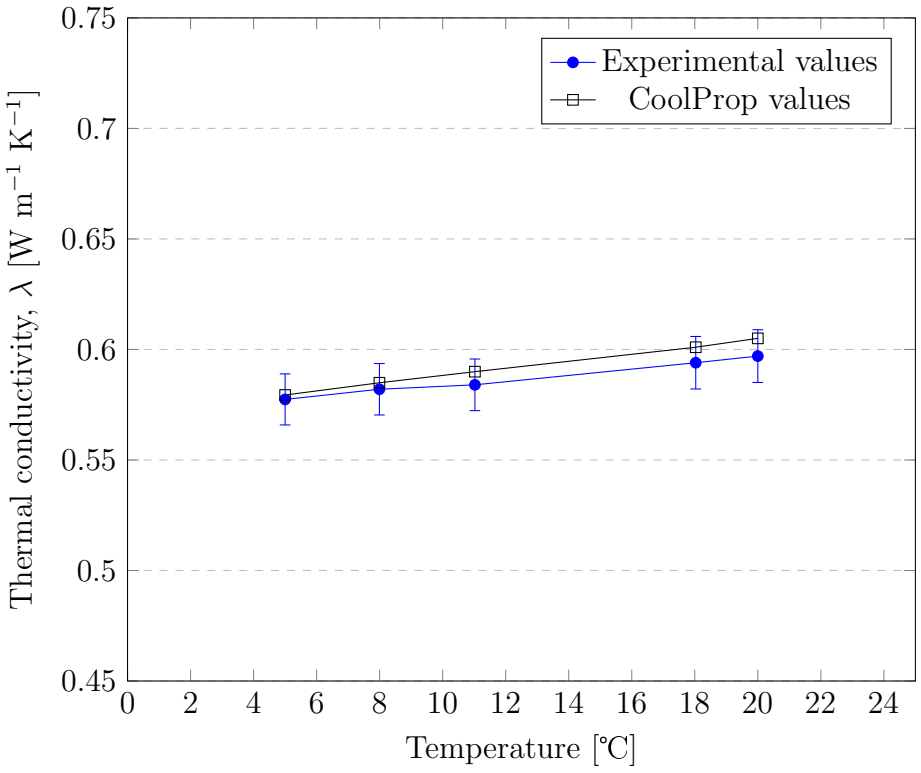

Figure 3.4: The thermal conductivity of formulation 1 during the cooling process measured with the THB and the thermal conductivities of water as found with Coolprop [1] are shown as a comparison.

3.1.7 Storage stability: LumiSizer Optical Centrifuge

The stability against creaming, sedimentation and coalescence of the PCDs was studied using the LUMiSizer optical centrifuge from LUM GmBH. The LUMiSizer is a pre-calibrated centrifuge that scatters light transmissions through the entire PCD sample. During operation, the PCD is placed into a sample probe and the centrifuge exposes it up to 2300 times the gravitational acceleration (g). To calculate the lifespan of the sample at $g = 9.81ms^{-2}$, the duration of the measurement is multiplied with the applied gravitational acceleration. A schematic of the LUMiSizer can be seen in Figure 3.5.

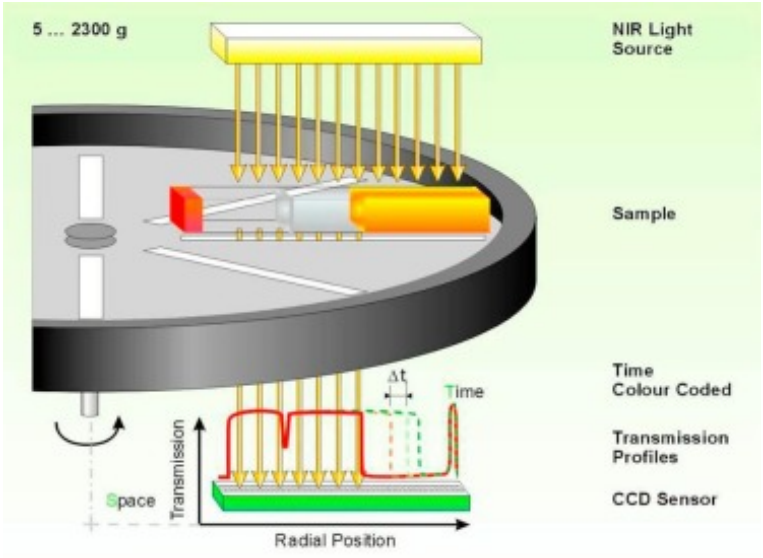

Figure 3.5: Schematic of the operational principle of the LumiSizer optical centrifuge. Figure adapated from [2].

For the experimental investigation into the stability of different PCD formulations, the PCD samples were exposed to different gravitational accelerations. This was to allow for the future operational design of the PCD system. The LumiSizer works on the premise that during sampling, the intensity of transmitted light is detected in time and space, and subsequently resolved and then converted into a transmission profile. An example of a transmission profile can be seen in Figure 3.6.

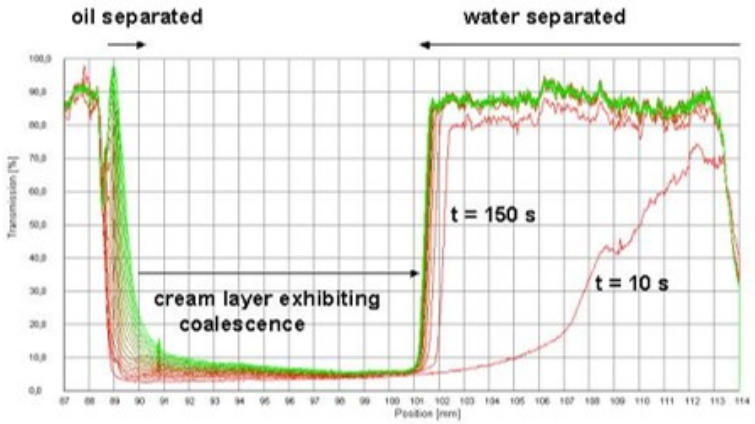

Figure 3.6: An example of a LumiSizer transmission profile for a typical emulsion destabilisation process. Figure adapated from [3].

Transmission profiles show the changes in concentration of the sample over the length of the sample holder over the calculated time. Furthermore, from the transmission profiles, an instability-index, which quantifies the shelf-life of the PCDs, is calculated. Low values of the instability index indicate that the PCDs are relatively stable. A PCD is

considered sufficiently stable as long as the instability index does not exceed 10% of the final instability index value (the maximum possible instability).

3.1.8 Interfacial tension measurements

The drop shape analyser DSA-30 from Krüss GmbH (Hamburg, Germany) was used to determine the interfacial tensions between PCM and water phases, and to study the effect of different surfactant systems on this interfacial tension. The measurements are based on the pendant drop technique, which can be seen in Figure 3.7. In the case of determining the interfacial tension between oil droplets in water, an inverted J needle is used (as a result of the density differences between the oil and water).

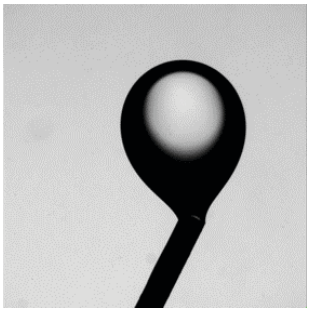

Figure 3.7: Droplet of Ethyl palmitate in water highlighting the measuring procedure of the interfacial tension in the pendant drop method.

The experimental set-up for determining the interfacial tension is shown in Figure 3.8. The measurement principle proceeded as so; the continuous phase chamber was filled with 15 mL of deionised water (or if testing the effect of different surfactants, the correct mass fraction of surfactant and water was pre-combined and subsequently added to the continuous phase chamber). The PCM was then introduced into a stainless steel J-needle with a diameter of 2.01 mm. The tensiometer was validated for both determining the surface tension of water in air, and for measuring the interfacial tension of ethyl palmitate in water. The results of this calibration can be seen in Figure 3.79, alongside the values obtained from literature [4]. The set-up of the tensiometer can be seen in Figure 3.6.

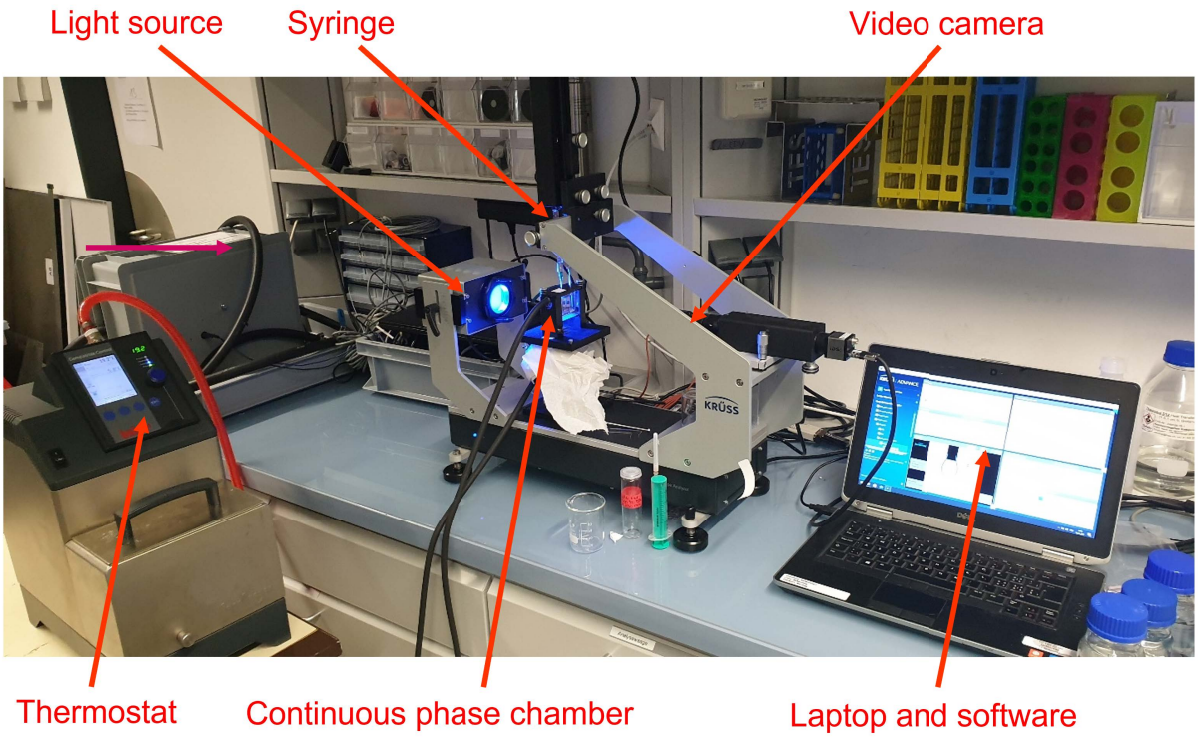

Figure 3.8: Set-up of the tensiometer experiments, showing the important measuring components

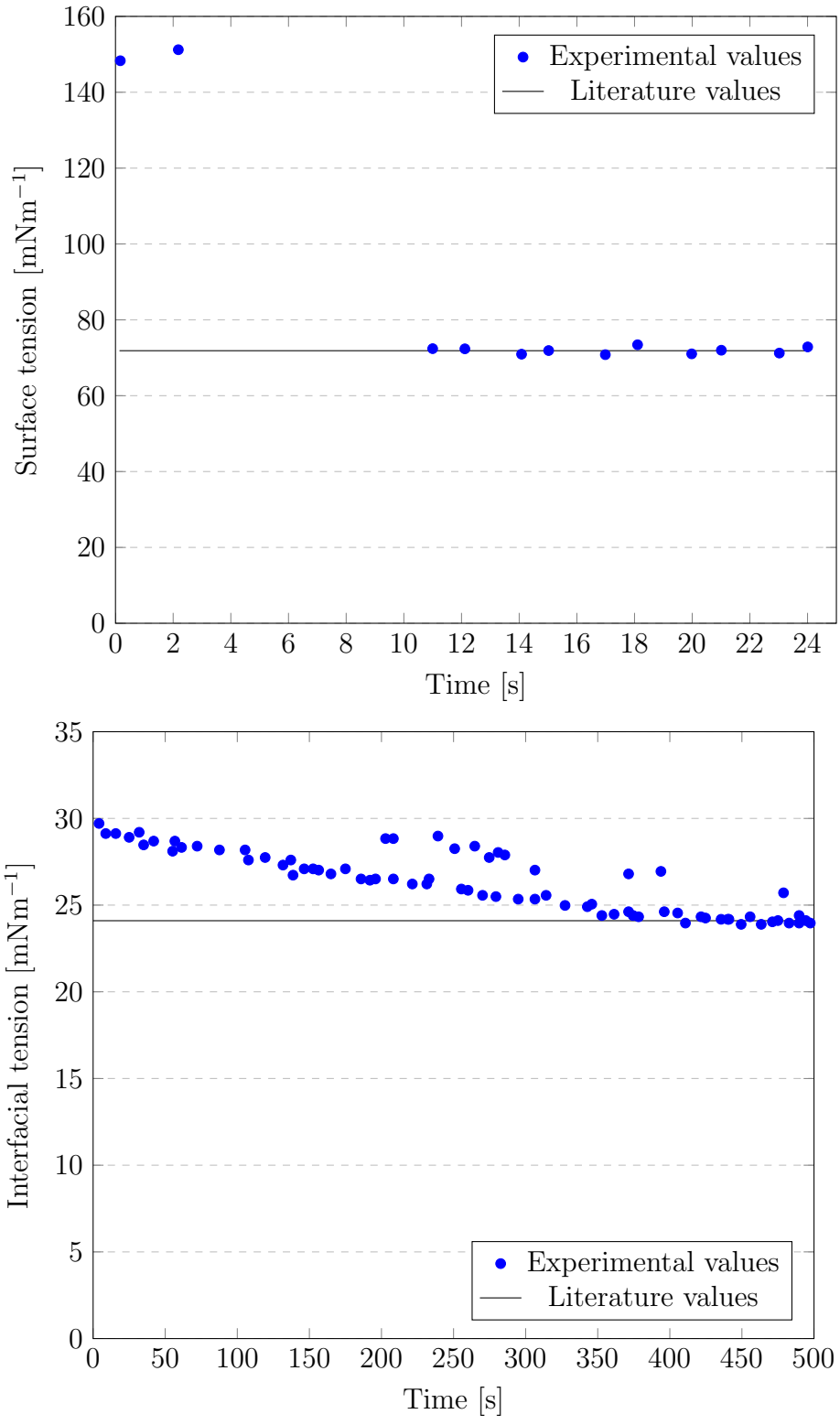

Figure 3.9: Validation of Top: the surface tension measurements with water in air and Bottom: The interfacial tension measurements with Ethyl Palmitate in water.

3.1.9 Optical analysis: Microscopy

The optical microscope which was initially used to determine the internal structure of the formulated PCDs was the Dinolite digital microscope. Additionally, attached to the microscope, a hot-stage was attached to allow for the cooling and heating up of samples through a controlled Peltier element.

References

[1] Ian H. Bell, Jorrit Wronski, Sylvain Quoilin, and Vincent Lemort. "Pure and Pseudo-pure Fluid Thermophysical Property Evaluation and the Open-Source Thermophysical Property Library CoolProp". In: *Industrial & Engineering Chemistry Research* 53.6 (2014), pp. 2498–2508.

[2] Ludger Fischer, Ernesto Mura, Poppy O'Neill, Silvan Von Arx, Jörg Worlitschek, Geng Qiao, Qi Li, and Yulong Ding. "Thermophysical properties of a phase change dispersion for cooling around 50 C". In: *International Journal of Refrigeration* 119 (2020), pp. 410–419.

[3] T. Sobisch. Jan. 1970. URL: `http://appliedcolloidssurfactants.blogspot.com/2004/12/characterization-and-optimization-of.html`.

[4] Rudolph Albert Peters. "Interfacial tension and hydrogen-ion concentration". In: *Proceedings of the Royal Society of London. Series A, Containing Papers of a Mathematical and Physical Character* 133.821 (1931), pp. 140–154.

Chapter 4

Formulation of stable and nucleating-inducing interfaces in phase change dispersions

Despite PCDs presenting as attractive HTFs, on accounts of their enhanced heat capacities and isothermal phase change temperatures, their implementation into the cooling network has currently been limited due to issues with stability and supercooling. Consequently, this chapter discusses the effect of PCDs preparation method, the surfactant system itself and its relative concentration on both the stability and supercooling behaviour of PCDs.

4.1 Formulation of stable interfaces

From an application point of view, PCDs are required to be stable both during thermo-mechanical cycling and during storage. Therefore the study of the formation of stable interfaces between the PCM droplets and the water continuous phase is of the upmost importance when studying the formulation of PCDs.

4.1.1 The effect of preparation method on PCD stability

To determine the optimum emulsification technique for producing stable PCDs, different methods of homogenising were employed. The testing of different homogenising techniques required an efficient screening strategy and continuous analysis of the particle size distribution, thermal behaviour and viscosity. Additionally, to investigate the effect of the preparation method on the PCD stability, different PCDs had to be produced and this was kept consistent until the rotor-stator homogeniser process (last process) in Figure 3.1.

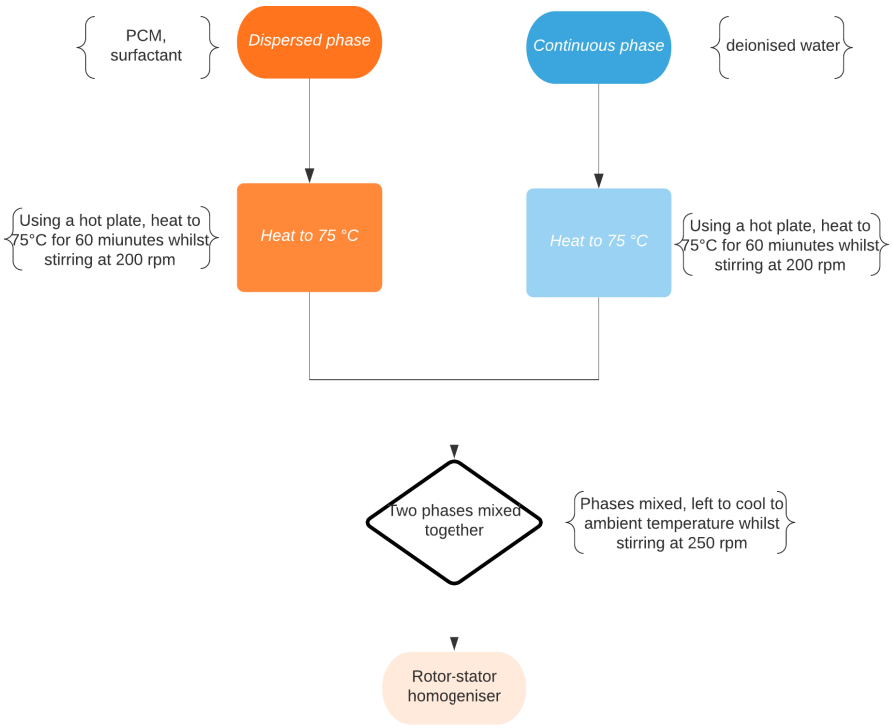

Figure 4.1: Flow chart schematic for PCD preparation

For each screening test, the flow chart presented in Figure 4.1 was followed and for each screening test 0.2 kg of PCD was produced. For determining the optimum homogenising technique, a Polytron 10-35 GT lab rotor-stator from Kinematica was used.

Two methods of homogenising were carried out to determine which was better for a mono-modal particle size distribution and for greater PCD stability. The first method was during homogenising using the rotor-stator homogeniser, to strap the beaker and leave the beaker stationary as the rotor-stator was homogenising the PCDs, as highlighted by Figure 4.2a. The second method involved moving the beaker up and down the shaft of the rotor-stator whilst homogenising the PCDs, this is shown in Figure 4.2b. This was to observe in which method the better vortex, and subsequently the better mixing of the two phases was found.

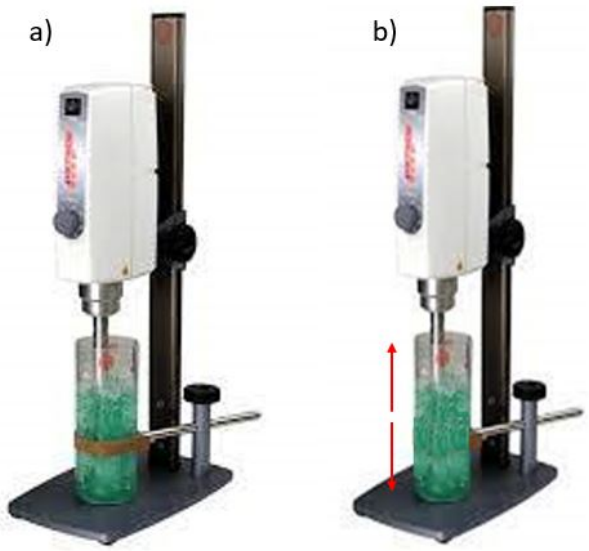

Figure 4.2: Schematic showing the procedure for the two different methods of homogenisation; stationary (left) and straight up and down (right).

Six experiments were performed with six different PCDs, formulated as shown in Figure 4.1. The relative composition of each formulation was as follows; PCM phase was 16 wt.% of Crodatherm-24, surfactant was 4 wt.% of EE360 and the continuous phase was 80 wt.% of water. The two different methods were tried for three different rotational speeds of the rotor-stator homogeniser as outlined in table 4.1 for a duration of five minutes.

Table 4.1: The six experiments performed to determine the appropriate homogenising technique. For both of the two methods, 3 different homogenising speeds; 1500, 3500 and 5500 rpm were used.

Sample Number	Homogeniser time (min)	Homogeniser speed (rpm)	Homogeniser method
1	5	1500	Stationary
2	5	1500	Moving up and down
3	5	3500	Stationary
4	5	3500	Moving up and down
5	5	5500	Stationary
6	5	5500	Moving up and down

The particle size distributions and microscope images of each of the formulation techniques for each sample (1-6 in Table 4.1) can be seen in Figures 4.3, 4.4 and 4.5 respectively.

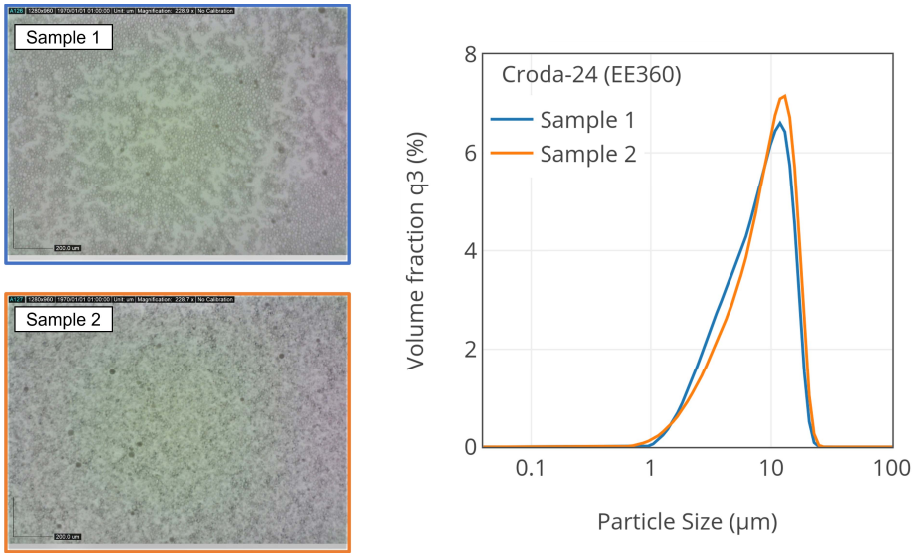

Figure 4.3: Microscope images and particle size distributions of samples 1 and 2 from Table 4.1

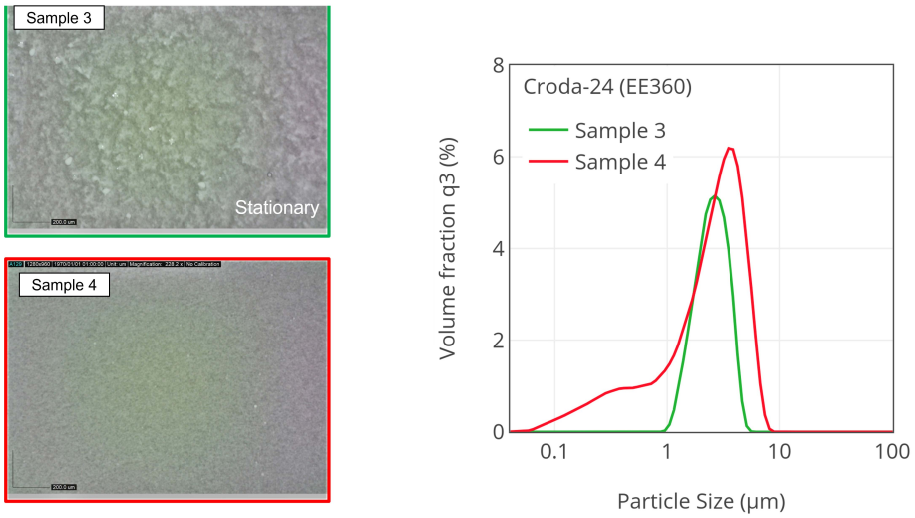

Figure 4.4: Microscope images and particle size distributions of samples 3 and 4 from Table 4.1

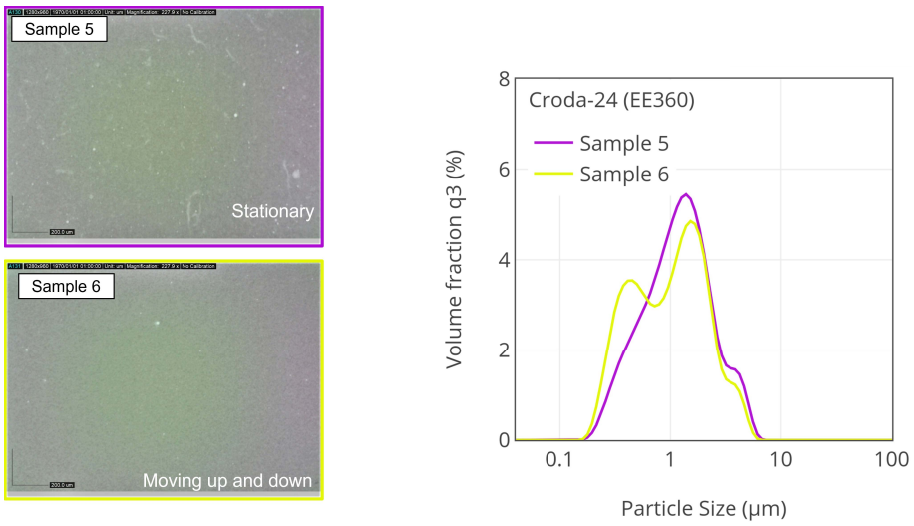

Figure 4.5: Microscope images and particle size distributions of samples 5 and 6 from Table 4.1

At the lowest homogeniser speed (1500 rpm), the difference in technique does not seem to have much effect on the particle size distributions or the internal structures of the PCDs as seen in Figure 4.3. However this is not the case for all the different homogeniser speeds used. For example, as shown in Figure 4.4, for the homogeniser speed of 3500 rpm, there is a wider particle size distribution for the up and down method compared to the stationary method. The internal structure also appears different from the microscope images. This effect can also be seen with samples 5 and 6 and seen in Figure 4.5, it appears that sample 5, which was produced with the stationary method has much a much more homogeneous particle size distribution than for the method of up and down. Unfortunately, the microscope images give little information about the relative internal structure of either of the samples due to the resolution of the microscope. Whilst the initial particle size distributions give some indication about the stability of the PCDs, with smaller more mono-modal particle size distributions suggesting a greater stability, for further inspection of the stability, the samples were thermally cycled on the EasyMax thermal cycling unit for an extended period of time, to see if there was a significant change in the crystallisation behaviour over the thermal cycling. The crystallisation behaviour gives quite a good indication of the stability of PCDs, with a changing crystallisation temperature over time evidencing destabilisation processes occurring within the samples, for example an increase in the particle size due to coalescence would present as a smaller degree of supercooling. Figure 4.6 shows the crystallisation onset temperature for each sample versus time.

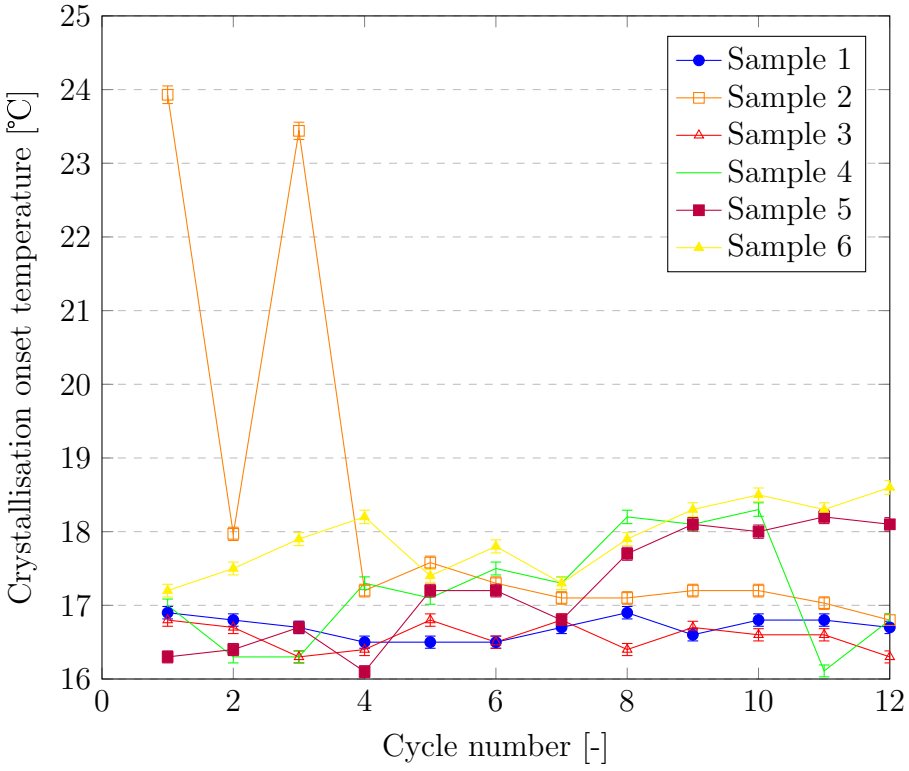

Figure 4.6: Crystallisation onset temperatures versus cycle number from easymax thermal cycling tests for samples 1-6 from Table 4.1.

Figure 4.6 shows the cycle number (which was every 80 minutes) of each sample being cycled from 40℃to 5℃against the crystallisation onset temperature. Figure 4.6 shows that samples 4, 5 and 6 all show an increase in the crystallisation onset temperature with an increase in the cycle number. This suggests that coalescence occurred, and was expected from looking at the particle size distributions in Figures 4.4 and 4.5, due to the non-uniform particle size distributions suggesting unstable PCDs. Despite this, it is sample 2 which shows the greatest destabilisation, with a high crystallisation onset temperature from the first couple of cycles and then a reduction in the crystallisation onset temperature. This indicates that destabilisation of sample 2 occurred during the first cycles and for closer inspection the internal structure of sample 2 was looked at under the microscope and can be seen in Figure 4.7.

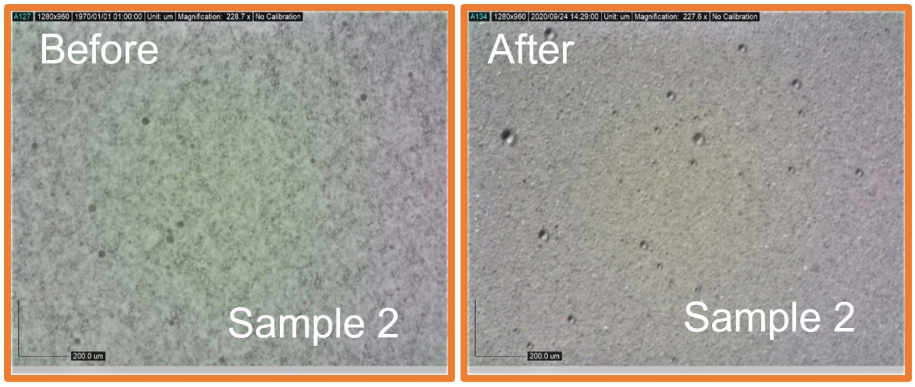

Figure 4.7: Microscope images of sample 2 from Table 4.1, before and after thermal cycling on the Easymax thermal cycling unit.

Figure 4.7 highlights that the internal structure of sample 2 changed during thermal cycling, with larger droplets alongside smaller droplets being seen in the after cycling microscope image. This indicates that Ostwald ripening and coalescence occurred during the thermal cycling of sample 2. The last method to determine the effect of the two different preparation techniques on the stability was investigating the storage stability of each sample through the means of an optical centrifuge, which produces bar charts of the instability indexes (with higher relative instability indexes indicating a higher-degree of destabilisation has occurred throughout the measuring time). The results from the optical centrifuge can be seen in Figure 4.8.

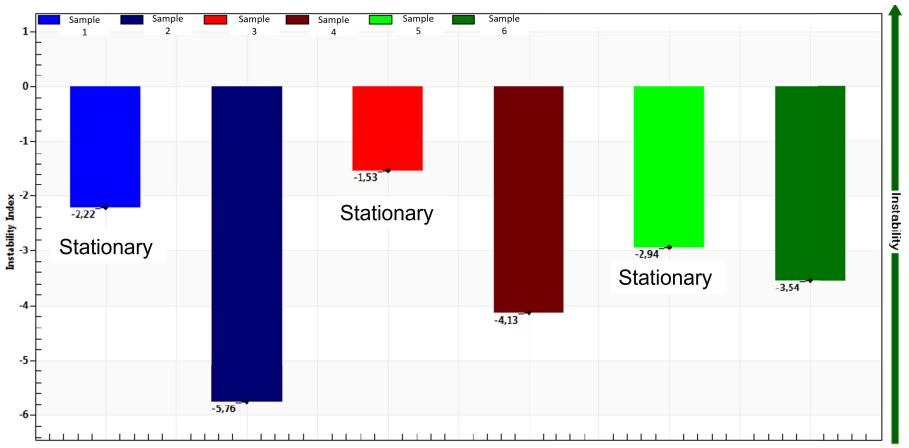

Figure 4.8: Instability indexes calculated by the optical centrifuge for each sample in Table 4.1

Within the optical centrifuge experiments, each sample was subjected to 2300 g for 20 hours at a temperature of 30°C(so each sample was in the emulsion form). Figure 4.8 shows the maximum instability of each sample over the duration of the measurement. The higher the absolute value of the instability index, the greater variations in concentration along the measuring path the sample displayed. As is evident from Figure 4.8, all three

of the stationary samples showed lower instability indexes than the moving up-and-down method suggesting the stationary method creates more stable emulsions against creaming and other gravitational destabilisation mechanisms. Interestingly, the samples with the most mono-modal particle size distribution from Figures 4.3-4.5, for example, sample 3, display the lowest instability index. Normally it is assumed that a narrower and more mono-modal particle size distribution results in a more thermodynamically stable PCDs, this is due to better surface-coverage of the PCM droplet with the surfactant. This finding can be used as a future guide to select the most promising PCD preparation method. Overall, this short investigation shows the importance of picking the correct emulsification technique for producing PCDs, and how just by simply changing the position of the vortex during emulsification can affect the stabilities and longevities of PCDs. It can be seen that the method of production affects the relative stabilities of the PCDs, but a clear link cannot be elucidated between the homogenising speed (shear rate) and the stabilities, and therefore an investigation into the best homogenising speed (shear rate) was performed. Ideally, the lowest amount of shear rate to produce the most stable emulsion would be optimal, to reduce the energy input in producing the PCDs. Table 4.2 shows the different shear rates and their relative revolutions per minute (rpm). To ensure fair testing, each sample consisted of the same material (PCM was Crodatherm-24 and the surfactant was EE360) and was homogenised for the same amount of time, 5 minutes using the stationary method as aforementioned.

Table 4.2: The different operational conditions for each experiment to determine the best shear rate for producing the most stable PCD

Sample number	Homogeniser speed (min^{-1})	Shear rate (s^{-1})
1	500	2616
2	1500	7848
3	2500	13080
4	3500	18312
5	4500	23544
6	5500	28776
7	6500	34008
8	7500	39240
9	8500	44472
10	9500	49704

After each PCD was produced according to Table 4.2, the particle size distributions were measured and can be seen in Figure 4.9, which shows the particle size distributions of each sample and the average droplet size obtained for each sample.

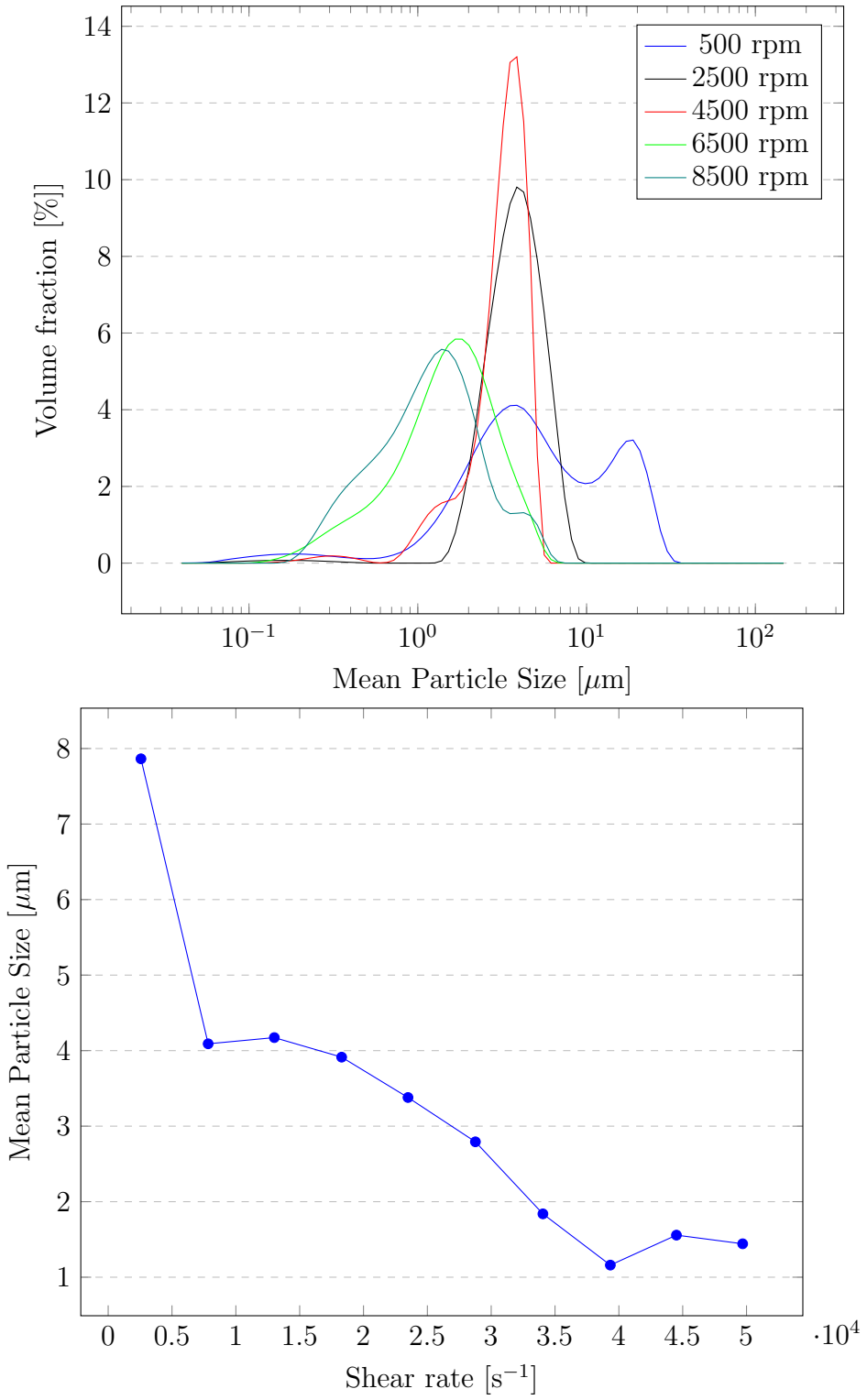

Figure 4.9: Left: The particle size distribution against homogeniser speed used of samples 1-10 as outlined by Table 4.2 and Right: The mean particle size of each sample against the shear rate employed during their production.

From Figure 4.9, it can be seen that generally as the shear rate is increased, the average droplet size decreases, which is what is expected. This suggests that higher-energy (higher

shear-rate) emulsification methods result in PCDs with greater stabilities. An additional observation can be made, not only does the size of the particles decrease as the shear rate increases, but also the degree of homogeneity also increases. Sample 1 appears much more in-homogeneous than sample 10, however from the particle size distribution graph, the most homogeneous samples appear to be at 4500 rpm (shear rate = 23, 544). Whilst above this shear rate the particle size continues to decrease, the degree of in-homogeneity also starts to increase again. According to Stoke's law [1], the smaller the particles the more storage-stable they will be, as the speed the PCM droplets coalesce is proportional to their diameter squared. To further determine if this is the case in PCDs, the samples were subsequently subjected to thermal cycling and the particle sizes were compared before and after cycling. As aforementioned, during thermal cycling, it is generally easy to observe if destabilisation processes are occurring within the PCDs by a change in the crystallisation temperature. Since crystallisation is a stochastic phenomenon, the larger the droplet size, the higher the temperature of crystallisation (lower degree of supercooling). Therefore, if there is a significant change in the temperature of crystallisation during thermal cycling, the droplet size is changing and thus the sample is not stable. The crystallisation onset temperature versus the sample number was plotted against the cycle number for each sample and can be observed in Figure 4.10.

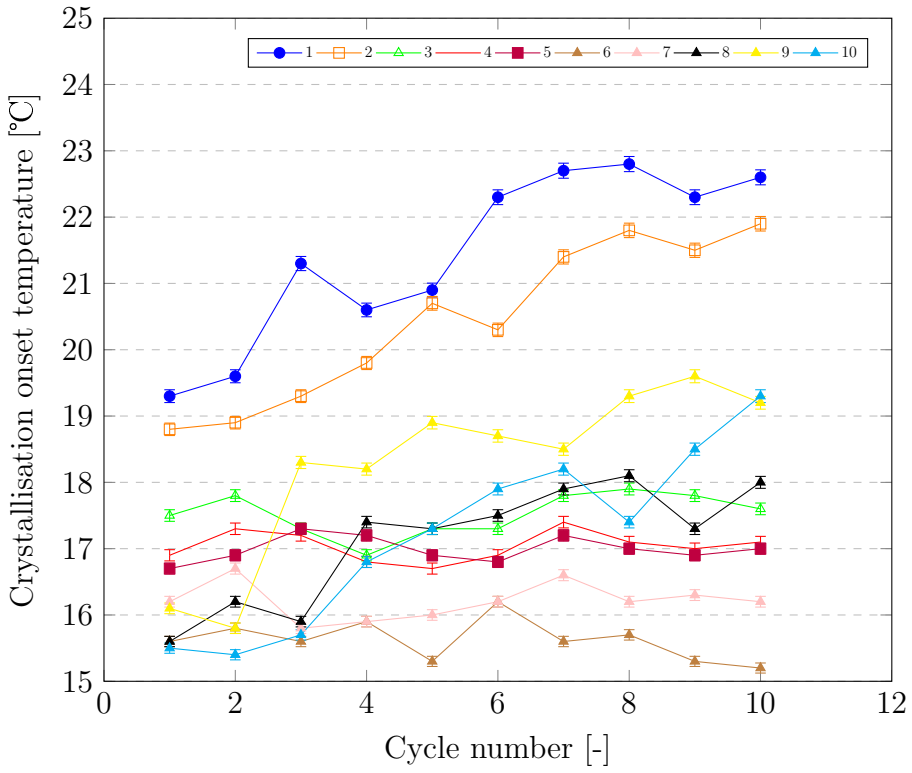

Figure 4.10: Crystallisation onset temperatures versus cycle number from easymax thermal cycling tests for samples 1-10 from Table 4.2.

Figure 4.10 shows two main effects; the first is that there is a trend between the shear-rate applied during sample preparation (from Table 4.2), the particle size distribution (From Figure 4.9) and the crystallisation onset temperature. The higher the shear-rates applied, the smaller the average particle size and the lower the crystallisation onset temperature (higher degrees of supercooling), this is to expected and is discussed in the following section of this chapter. The second effect displayed is the samples 1 and 2, which were produced with low shear rates, show the greatest increase of the crystallisation onset temperature over the cycle number, and subsequently the highest degree of destabilisation during thermal cycling. Samples 3, 4, 5, 6 and 7 show no specific increase in the crystallisation onset temperature over the 10 cycles, and they also show relatively mono-modal particle size distributions from Figure 4.9, which indicates that they are stable. Despite this, samples 8, 9 and 10 show destabilisation, with an increase in the crystallisation onset temperature over cycling and from Figure 4.9 they show less mono-modal particle size distributions. From the thermal cycling in Figure 4.10, the best shear-rates were those for samples 3,4,5,6 and 7. However, further investigation into stabilities of the samples with respect to storage were performed by taking photographs of each sample right after they were produced and after storage for 48 hours. During this 48 hour period the samples were left undisturbed and the before and after photographs can be seen in Figure 4.11 for each sample.

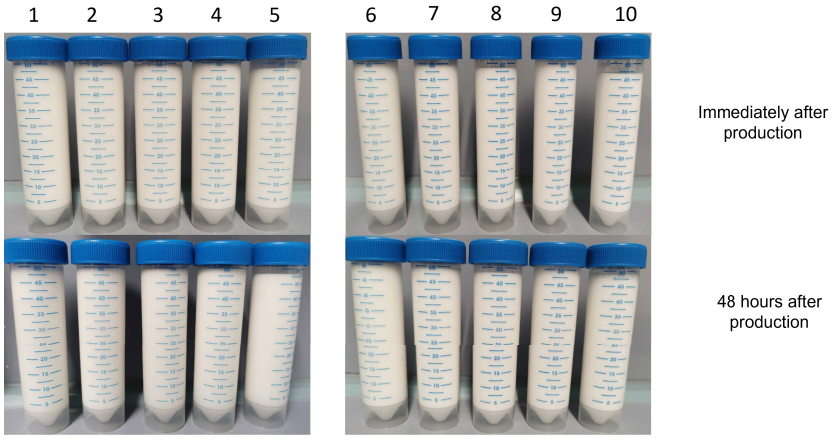

Figure 4.11: Photographs of samples 1-10 from Table 4.2 before and after 48 hours of storage to observe the storage-stability

After the 48 hour period, no obvious destabilisation had occurred (no separation of the PCM and water layers) and so the samples were subjected to the optical centrifugation, which accelerates the gravitational separation process. Table 4.3 shows the instability indexes for each sample from Table 4.2. Table 4.3 shows the sample 7 had the lowest instability index, which means that this sample was the most stable during the centrifuging process. Additionally, sample 7 showed a relatively mono-modal particle size distribution

Table 4.3: Instability indexes from the LuMiSizer Optical centrifuge experiments with samples 1-10

Sample Number	Instability index
1	9.23
2	9.47
3	4.32
4	3.76
5	4.98
6	2.33
7	1.78
8	5.67
9	6.22
10	6.91

in Figure 4.9 and no change in temperature at the onset of crystallisation in Figure 4.10. Due to this, it was decided that for subsequent formulations, the rpm of 6500, (34,008 s^{-1}) would be used for future PCD formulation to ensure complete emulsification and the correct droplet size and stability. Whilst it is recognised that many other factors effect the stability, this was the first step in choosing one of the correct formulation parameters for the future design of PCD formulations.

4.2 The effect of the surfactant and its relative concentration

The properties of emulsions are essentially determined by the surfactant monolayer film which is separating the oil and water phases within the emulsion [2]. The structure and formation of emulsions can be explained by the mixed-film theory, in which an interfacial film is considered a duplex film consisting of different properties on the polar and apolar sides of the water and PCM boundary respectively [2, 3, 4]. The phase behaviour and microstructure of emulsions further depend on two interfacial parameters, the spontaneous film curvature, which is the optimal curvature of the amphiphilic film, and the elasticity, which is also known as the bending modulus, of the amphiphilic film (how rigid or flexible the film is) [3]. Additionally, the compatibility between the oil phase and the alkyl chains of the surfactant will influence the formation of emulsions by strongly affecting the bending modulus of the interfacial layer, with increased molecular comparability (between the oil phase and the alkyl chain) the bending modulus of the interfacial layer is drastically reduced [4]. Some compounds, like short-chain fatty acids, are amphiphilic or amphiphathic, e.g. they have one part which has an affinity for non-polar media (e.g. the oil phase) and one part that has an affinity for polar media such as water. The energetically most favourable orientation for these molecules is at surfaces or interfaces so that each part of the surfactant molecule can reside in an environment for which it has

the greatest affinity, see Figure 4.12 [5, 6, 7].

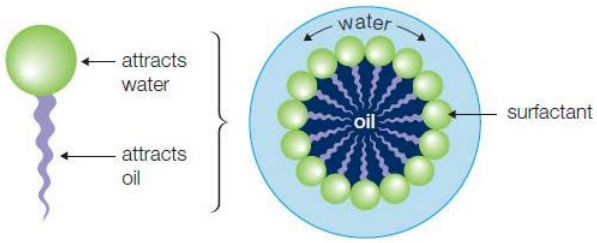

Figure 4.12: Schematic showing the orientation of amphiphillic molecules (with a polar head group and a non-polar tail group) on the surface of oil-in-water emulsions. Figure adapted from [7].

These molecules that form from orientated monolayers at interfaces show certain surface activity and are termed surfactants [7]. Surfactant molar masses range from a few hundreds up to several thousands grams per mole. Since there is a balance between adsorption and desorption (as a result of thermal motion), the interfacial conditions require some time to establish, which, means that surface activity should be considered a dynamic phenomenon [8]. This can be seen by measuring surface tension versus time for a freshly formed surface (an example can be seen in Figure 3.5). Naturally, temperature also has an influence on the stability and properties of PCDs, the adsorption of surfactants at the solid-liquid interface (when the PCM is crystallised/melted) is strongly affected by many factors such as: the nature of the structural groups on the solid surface, whether the surface contains highly charged sites or are essentially non-polar groupings (which is the case for the investigated surfactants in this study) and the nature of the atoms of which these sits or groupings are located [9, 5]. Additionally, the molecular structure of the surfactant being adsorbed, whether it is ionic or non-ionic and whether the hydrophobic group is long or short, straight chained, branched, aliphatic or aromatic [9, 2]. Furthermore another factor which affects the adsorption at the solid-liquid interface is the environment of the aqueous phase, such as the presence of additives, such as short-chain polar solutes, salts, pH and electrolyte concentration (and its temperature) [2, 5]. In this section of the thesis, the effect of the structure of the surfactant and its relative concentration was examined.

After the production method had been examined in Section 4.1.1, the next step was to determine the optimum about of emulsifier for our system, for our pre-selected PCM concentration (16 wt.%). This pre-selection was done to obtain the best capacity flow rate for the PCDs. Following this, a variety of different surfactants were tested. Firstly, it was hypothesised that to create a more stable interface, and to create a more stable PCD in general, that a surfactant with a bulky hydrophilic head group should be used. This is due to the steric hindrance, and steric repulsion that would be created between the individual droplets due to this bulky head group, which was envisioned to prevent coalescence between droplets and thus increase the stability. An investigation subsequently

proceeded selecting five different surfactants, which have different hydrophilic head group sizes, but with the same hydrophobic alkyl chain length (C_{16}) for consistency. The molecular structures of the five surfactants, alongside their commercial names, are shown in Figure 4.26.

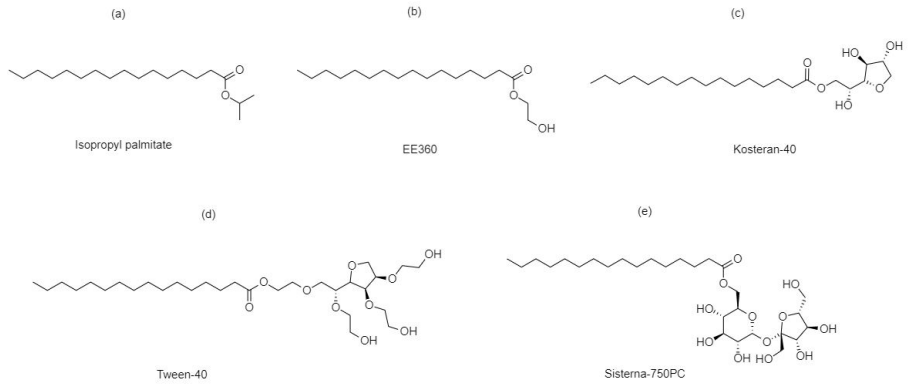

Figure 4.13: Molecular structures of all the investigated surfactants and their commercial names

Each of the five PCD samples were each prepared using the same method shown in Figure 4.1, and were homogenised for 5 minutes at a rotational speed of 6500 rpm. As an initial comparison of how each different head group size affected the properties of the formulated PCDs, the particle size distribution was taken and can be seen in Figure 4.13.

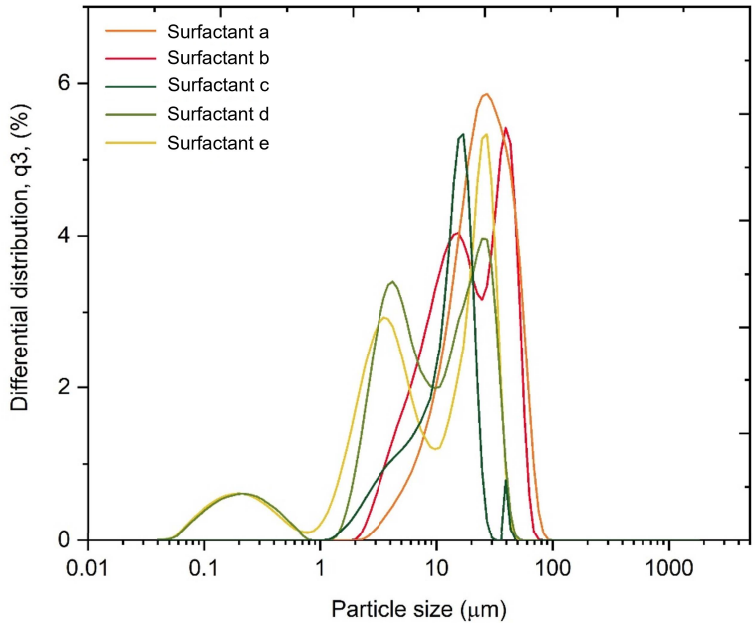

Figure 4.14: The particle size distributions of the five PCD samples formulated with surfactants a-e from Figure 4.13.

From Figure 4.14, it can be immediately observed that each different surfactant results in a different particle size distribution. In part, the particle size distribution provides

indirect information on how well the surfactant has adsorbed onto the PCM droplets during the emulsification process. Large hydrophilic head groups have a harder time adsorbing onto the PCM surface due to steric hindrance, this can be seen in the cases of surfactant c, d and e, which all have bulkier substituent groups and less mono-modal particle size distributions. To observe the adsorption kinetics of each surfactant on the droplet interface, the interfacial tensions of each surfactant system were measured and the time taken to reach an equilibrium for each surfactant was monitored. Figure 4.14 shows the interfacial tensions of each sample formulated with a different surfactant at 24.3℃.

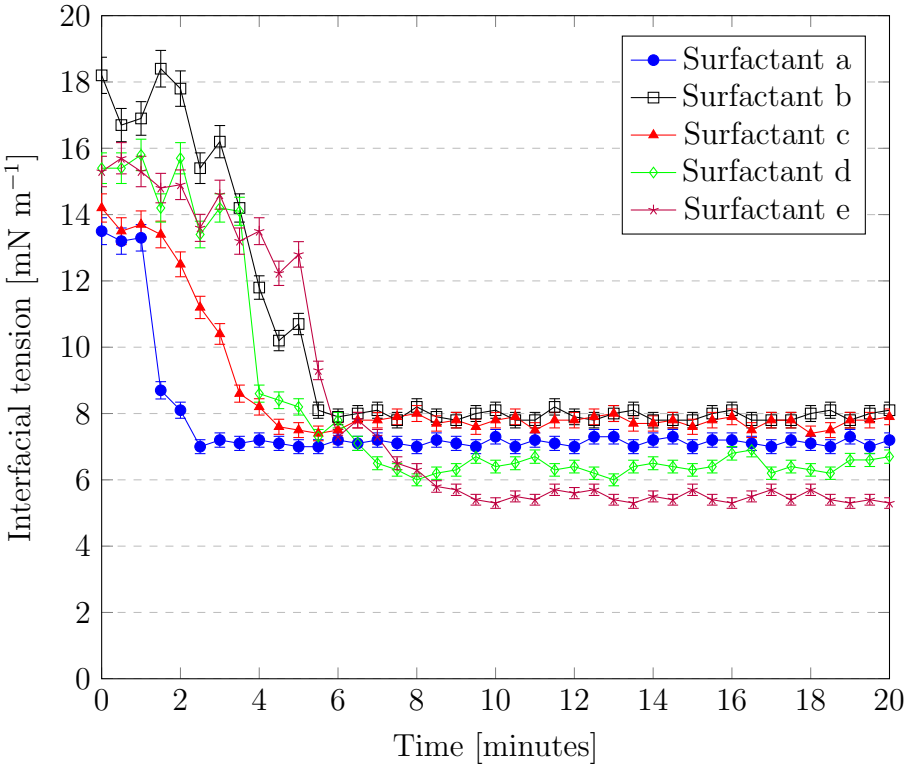

Figure 4.15: The interfacial tensions of PCD samples formulated with surfactants (a-e) against time time taken to reach an adsorption equilibrium of the surfactant on the surface of the PCM droplets.

Figure 4.15 shows that all different PCDs formulated with different surfactants show different times to reach an interfacial tension equilibrium. This is due to the adsorption kinetics of each different surfactant at the interface between the PCM droplet and the water. Surfactant a and surfactant c both reach an equilibrium relatively quickly, with no change in the interfacial tension being observed after approximately four minutes. This can also be seen from the particle sizes distribution curves in Figure 4.14, where both surfactant a and surfactant c show relatively mono-modal particle size distributions after only a short time of emulsification. On the other hand, surfactant b takes approximately 5 minutes and surfactants d takes approximately 8 minutes and surfactant e takes ap-

proximately 9 minutes. This can be explained by the larger head groups of surfactants d and e resulting in slower adsorption kinetics at the interface. However, it can be seen that both of these surfactants reduce the interfacial tension much more than surfactants a,b and c. A lower interfacial tension, and subsequently smaller particle size distributions indicates that the PCDs formulated with surfactants d and e will be more stable against typical emulsion destabilisation mechanisms. Due to surfactant e having the lowest interfacial tension at equilibrium, it was chosen as the surfactant that would create the most stable interface. It must be noted that an additional reason for choosing surfactant e, which is Sisterna-75PC, is that it is biodegradable, which will further help contribute to PCDs being a solution in a sustainable energy model. From the selected surfactant, the mass fraction was varied between 1-4wt.% to observe the optimised concentration of this surfactant for a stable PCD. To understand the effect of each mass fraction on the properties of the PCDs, four different PCDs, which were homogenised for ten minutes at a speed of 6500 rpm were formulated using the Sisterna-750PC surfactant and 16wt% of PCM. The storage stability of each of the samples was then tested in the suspension form (at 5℃) for 48 hours, and in the emulsion form (at 25℃) and pictures were taken after the 48 hour period. These photos can be seen in Figure 4.16 at 25℃ and Figure 4.17 at 5℃.

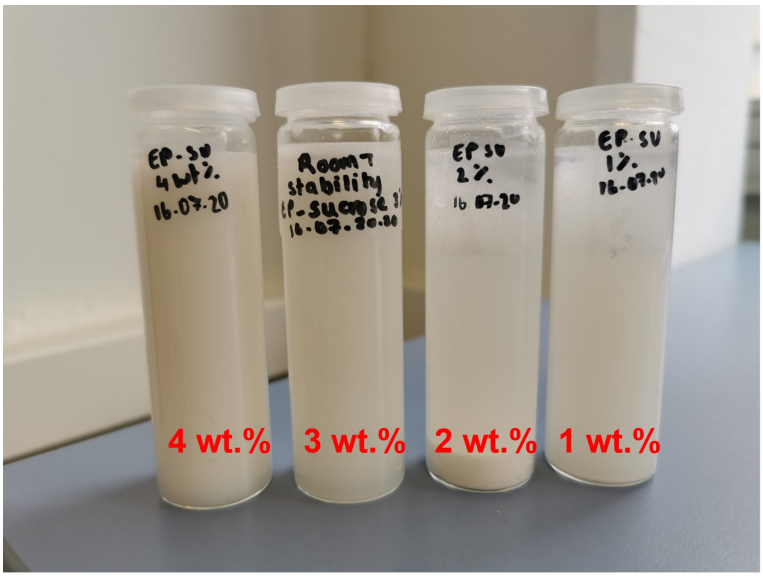

Figure 4.16: Photographs of PCDs formulated with different weight percentages of Sisterna-750PC (1—4 wt.% after 48 hours at 25℃)

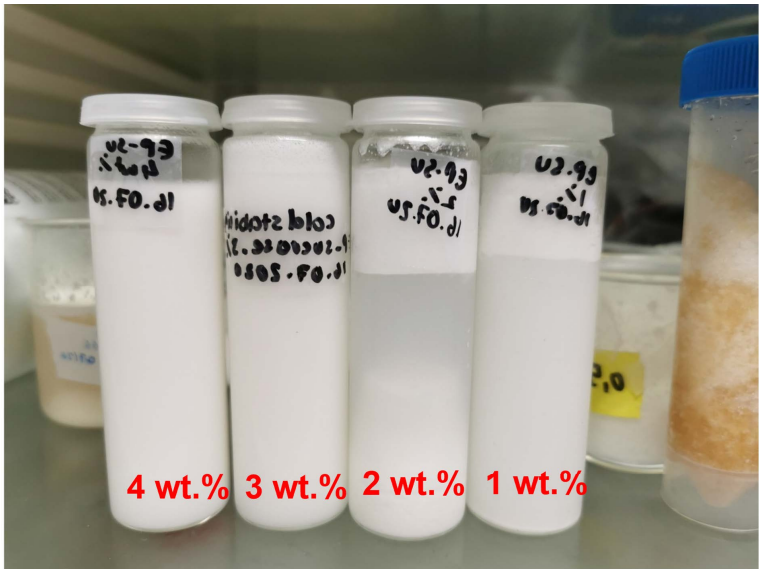

Figure 4.17: Photographs of PCDs formulated with different weight percentages of Sisterna-750PC (1—4 wt.% after 48 hours at 5°C)

From Figures 4.16 and 4.17, it can be seen that 1 and 2 wt% of the Sisterna-750PC was not enough to prevent destabilisation. This can be seen by the separation layers in both of these samples. This is most likely because not enough surfactant was present to cover each PCM droplet surface and prevent creaming. Despite this, the 3 wt.% and 4 wt.% appear to be stable under both temperature conditions. For further investigation of whether the 3 or 4 wt% of surfactant loading was better, two new formulations of PCDs were created with Sisterna-750PC at 3 and 4 wt% respectively. These samples were thermally cycled for seven days and the particle size distributions were monitored and sampled before and after the cycling. Figure 4.18 shows the particle size distributions before and after cycling.

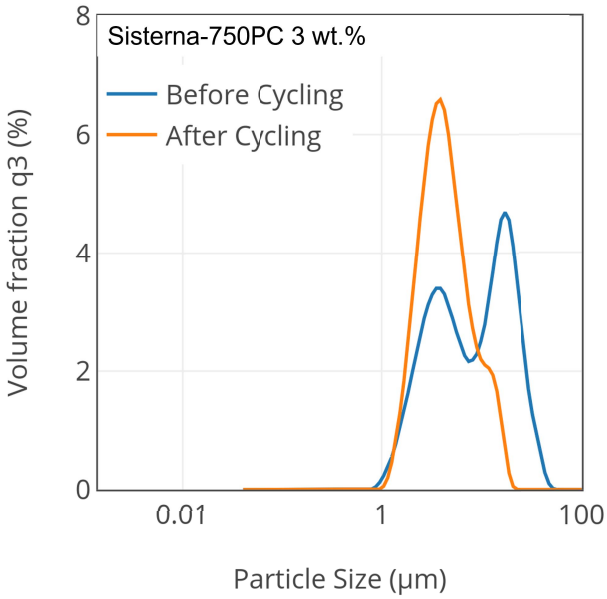

Figure 4.18: The particle size distributions of the PCD formulated with 3 wt.% Sisterna-750PC before and after 7 days of thermal cycles

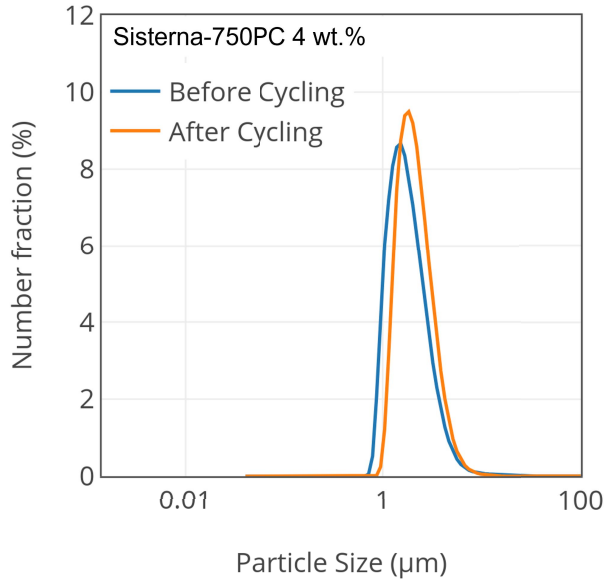

Figure 4.19: The particle size distributions of the PCD formulated with 4 wt.% Sisterna-750PC before and after 7 days of thermal cycles

Figure 4.18 shows that the PCD formulated with 3 wt% showed an increase in the particle size and a less mono-modal particle size distribution after cycling, with two distinct peaks being observed. This change during thermal cycling can be optically seen in the microscope images of the PCD formulated with 3 wt.% Sisterna-750PC before and after thermal cycling in Figure 4.20. The red arrows on the microscope image after cycling shows that large particles have coalesced for form a large droplet of the PCM and additionally there also appears to be areas with extremely small droplet sizes, suggesting Ostwald ripening has occurred, where smaller parts of the particles have broken off during

crystallisation, this is a well documented phenomenon. However, it could be problematic from an application point of view, with the droplet size variability, so will the crystallisation temperatures. Eventually, over multiple melt-crystallisation cycles this could lead to a total separation of the two phases, creaming. On the other hand, the PCD formulated with 4 wt.% of the surfactant showed no distinct changes in the particle size distribution before and after cycling, suggesting that a 4 wt% loading contributes to a much more stable emulsion.

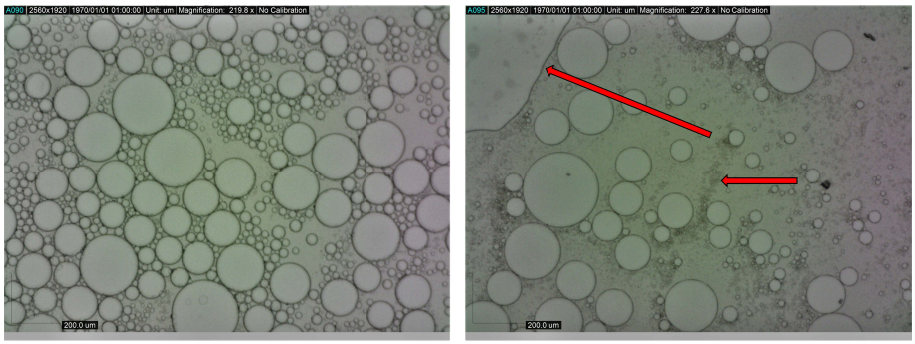

Figure 4.20: Microscope images of the PCD formulated with 3 wt% Sisterna-750PC before and after being thermally cylced for seven days. The red arrows point to obvious signs of destabilisation within the PCD's internal structure.

Overall, a highly stable formulated PCD was produced, with a 4 wt% Sisterna-750PC surfactant system. The interfacial tensions reported were extremely low for the formulation which suggests good adsorption of the surfactant onto the PCM droplets. Additionally, particle size distributions before and after thermally cycling for seven days showed extreme consistency, suggesting no destabilisation occurs. Given this information, for future formulations of PCDs in this chapter, Sisterna-750PC surfactant will be used.

4.2.1 Formulation of Nucleation Sites

Since a stable interface has been created within a PCD, the next step is to eliminate the problem of supercooling that PCDs tend to suffer from. Methods to combat supercooling have been the centre of PCD research for quite some time, with most techniques focusing on seeding [10]. Whilst the most common method to reduce supercooling is to add nucleating agents (NA) directly into the PCM mixture before emulsification, this technique has a lot of drawbacks. For instance firstly, it is hard to ensure that each droplet has a nucleating agent inside, which can cause a spread of crystallisation temperatures, and thus meaning that the latent heat is released over different temperatures and not at a specific temperature (which is required for effective crystallisation) [11, 10]. Additionally, it has been observed that over thermal and thermo-mechanical cycling the nucleating agent which was added into the PCM phase stops working over a certain amount of cycles.

This is suggested to be due to the nucleating agent separating out of the PCM phase with thermal/mechanical cycling [12]. As a result of this, it was envisioned in this section of the chapter, that the degree of supercooling of PCDs could be controlled by modifying the surfactant system in such a way that it would act as a template for nucleation and subsequently crystallisation.

Throughout this work, it was hypothesised, that a more rigid film (between the PCM droplet and the water), would cause a more ordered array of the liquid PCM molecules within the PCM droplet, due to stacking of the liquid molecules in an ordered array to fit within the rigid film. It is well known that a more ordered array of liquid molecules results in a lower degree of supercooling since less energy is required to initiate supercooling due to a larger entropic term in the Gibbs nucleation energy barrier. To form a rigid interface between the PCM droplet and the water phase, a bulky surfactant (such as the one presented in the preceding section, Sisterna-750PC) should be used. To test this hypothesis a preliminary investigation was performed by formulating two PCDs, one with a small surfactant, EE360 (surfactant b in Figure 4.13), which would result in a flexible film interface, and a large, bulky surfactant, Sisterna-750PC (surfactant e in Figure 4.13). The crystallisation behaviour of both surfactants was monitored optically through the use of a hot-stage microscope and can be observed in Figure 4.21.

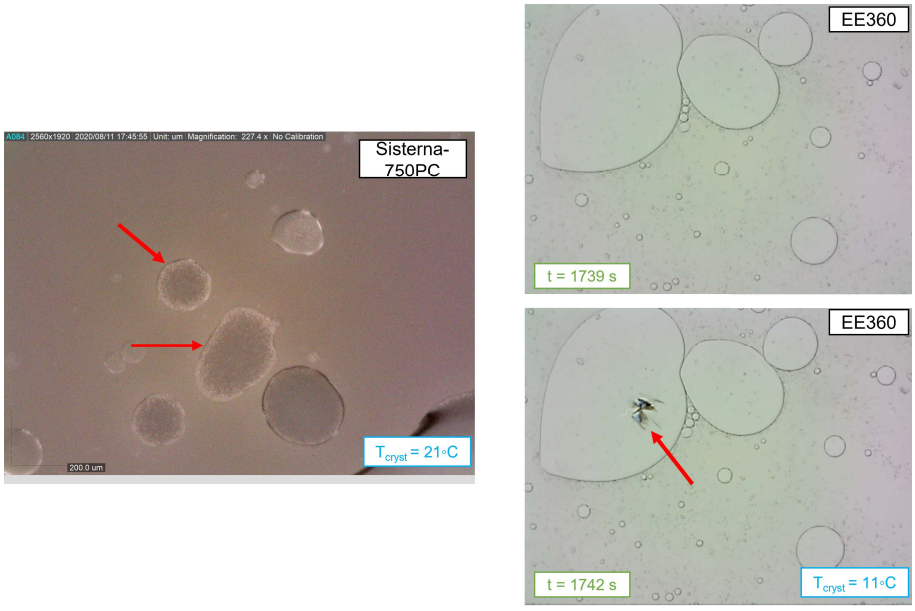

Figure 4.21: Microscope images of the PCDs formulated Right: with Sisterna-750PC and Left: with EE360 before and at the start of crystallisation. The red arrows point to the location crystallisation initiation.

Interestingly, from Figure 4.21, the surfactant appears to have an affect not only on the onset of crystallisation observed from the hot-stage microscope: 21℃ in the case of the rigid-film with Sisterna-750PC, and 11℃ for the flexible-filmed EE360 surfactant based

PCD. Even more interestingly, the surfactant used appears to affect the site where nucleation occurs. With EE360, nucleation appears to initiate from the centre of the droplet, suggesting homogeneous nucleation has occurred, whereas in the case of the Sisterna-750PC nucleation appears to start from the interface of the surfactant and the PCM. Even though the hydrophobic chain length is the same size (which is often hypothesised to initiate nucleation), it appears that it is a change in the hydrophilic head group which changes this affect and the creation of a more rigid template at the interface by this bulky hydrophilic head group. This is hypothesised to be due to the bulky packing of the large sucrose molecules at the interface causing a rigid template of the molecules within the PCM. The crystallisation onset temperature was further investigated using the EasyMax thermal cycling unit and the results can be seen in Figure 4.22, which shows both PCDs formulated with EE360 and Sisterna-750PC.

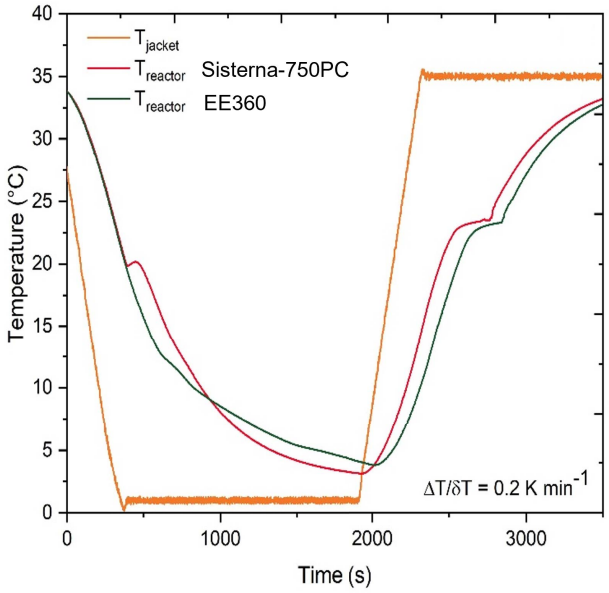

Figure 4.22: The EasyMax thermal cycling analysis of the PCD formulated with Sisterna-750PC and with the EE360 PCD. Note that the two arrows point to the crystallisation temperature of each sample.

Figure 4.22 clearly indicates that the Sisterna-750PC PCD has a much higher crystallisation temperature than the EE360 PCD. There is almost a 10 K difference between the two crystallisation temperatures. This is indicative that the Sisterna-75PC induces heterogeneous nucleation, and shows that certain types of surfactant can reduce supercooling. As aforementioned, both the Sisterna-750PC and the EE360 have the same hydrophobic chain length, so this cannot be the part of the Sisterna-750PC which is initiating nucleation. The only other difference between the two surfactants is the hydrophilic head, suggesting that the sucrose molecule directs the surfactants (and thus the liquid PCM molecules in the PCM) in such a way that it acts as a template for nucleation. Despite

the promising nucleating behaviour of Sisterna-750PC surfactant system, on observation of the physical sample, as shown in Figure 4.23, it appeared to extremely viscous and had a paste-like consistency unlike the sample produced with the EE360 surfactant system. The consistency of this PCD is thought to be as a result of the high rigidity of the film created between the PCM droplet and the water, which resulted in the high stabilities and low degrees of supercooling. These high viscosities render the PCD unusable from an application point-of-view and therefore an optimisation procedure needs to ensue to keep the promising supercooling reduction behaviour of the surfactant but with lower viscosities. This is discussed in the following section.

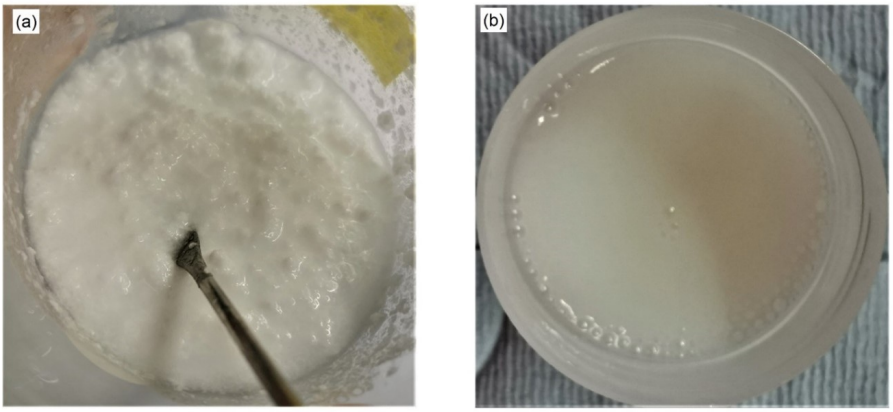

Figure 4.23: Photograph images of (a)the Sisterna-750PC sample and (b) the EE360 sample.

4.2.2 Optimising Formulation Properties

To fine-tune emulsion systems, the concept of co-surfactant systems needs to be introduced. Co-surfactants are molecules which sit between the main surfactant molecules on the PCM droplet interface. The partitioning between where the co-surfactant lays on the droplet surface depends on the strength of the co-surfactant head-group. Weakly polar groups can occupy the droplet centre, or stay at the surface of the droplet. From this, it becomes evident that co-surfactants affect the curvature of the droplets and thus the internal energy and flexibility of the film. Whilst certain investigated surfactants had excellent nucleating-initiating capabilities, such as Sisterna-75PC, with additional high stabilities, they also produced PCDs with extremely large dynamic viscosities. As a result of these high viscosities, an effective screening procedure was performed to find a suitable co-surfactant for the Sisterna-750PC surfactant, to create a new surfactant system, which would retain the nucleating ability of the Sisterna-750PC but lower the viscosity with the aid of a smaller molecular weight co-surfactant. The underlying hypothesis is that by substituting a certain amount of the Sisterna-750PC with a co-surfactant of lower molecular weight, which would sit between the bulky surfactant molecules as shown in the schematic

in Figure 4.24, that the PCD stability could be obtained with a lower viscosity, whilst keeping the original nucleating-inducing ability.

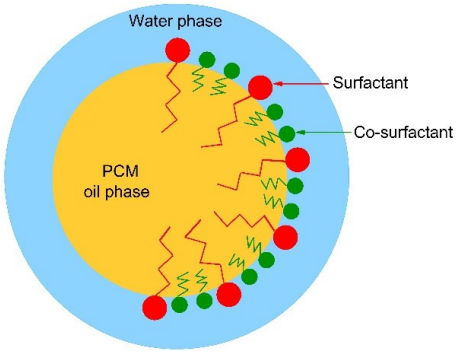

Figure 4.24: Schematic showing the placement of the surfactant and co-surfactant on the interface between the PCM and water phase.

To determine the best lower molecular weight surfactant, a pre-screening study of various co-surfactants was performed to select the most promising candidate, which was found to be the Brij-52 surfactant. This was chosen on accounts of the interfacial tensions, particle size distributions and thermal cycling behaviour. After finding the most promising co-surfactant, the most suitable weight percentage of the Sisterna-750PC and the Brij-52 surfactant had to be chosen. Three different samples, with varying weight percentages were created and tested for their thermal cycling behaviour, viscosity and particle size distributions. From these experiments, the following composition: Sisterna-750PC 1.6 wt.%) and Brij-52 2.4 wt% was chosen on accounts of the most monomodal particle size distribution being obtained; suggesting the best coverage of the PCM droplet with the co-surfactant system. The optimised mass fraction of the co-surfactant system was then subjected to extended thermal cycling on the EasyMax to see if a change in the crystallisation temperature (thermal profile) could be seen, which would indicate instability (particle size changes due to coalescence reducing the degree of supercooling with consecutive cycles). Figure 4.25 shows this extended thermal cycling.

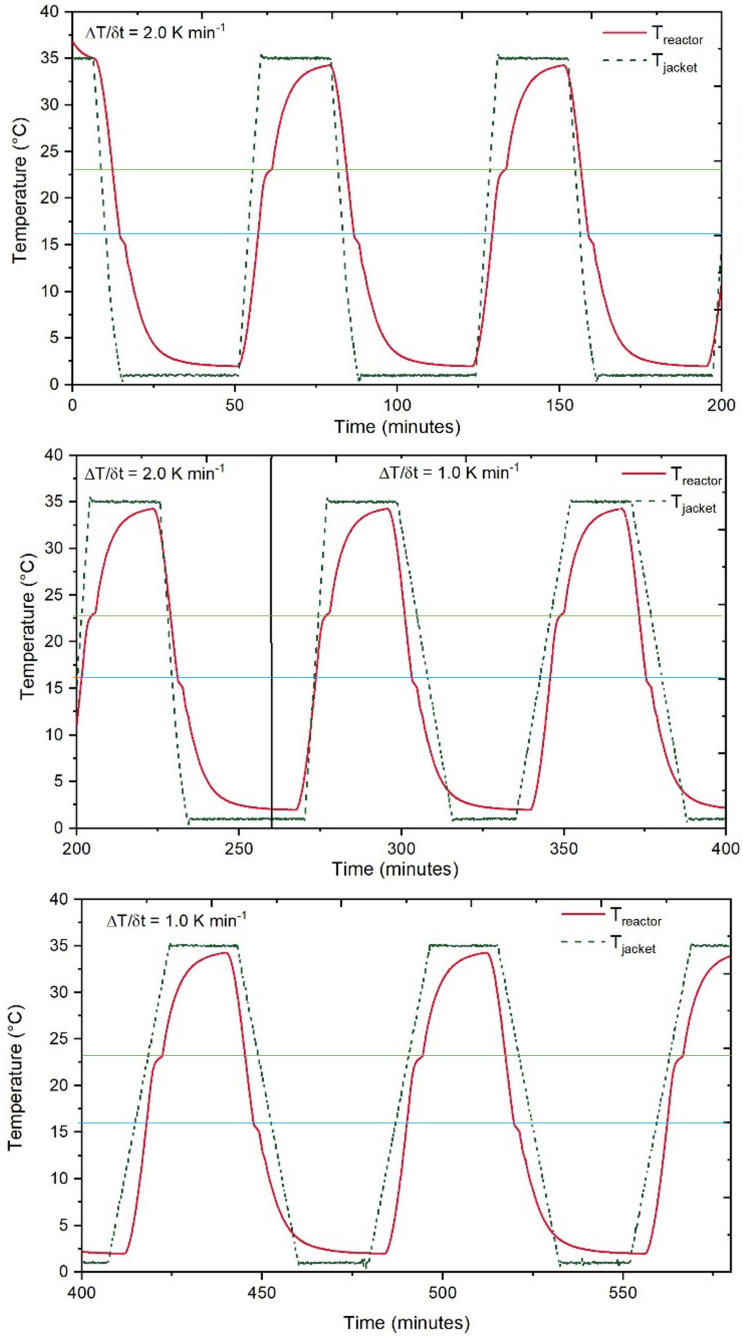

Figure 4.25: EasyMax extended thermal cycling of Sample 1 (40:60 mass ratio of bulky to small surfactant) over 600 minutes with the first 300 minutes at a heating/cooling rate of 2 K min^{-1}, and the last 300 minutes at 1 K min^{-1}

On Figure 4.25 eight crystallisation cycles can be observed. Halfway through the experimentation (denoted by the black line in Figure 4.25), that the heating/cooling rate was changed from 2 K min^{-1} to 1 K min^{-1} to try and further induce instability. However, despite this, in all thermal cycles, the crystallisation temperature is at the same temperature and each crystallisation plateau has the same duration and occurs at the same temperature (as denoted by the blue line in Figure 4.25). This is further indication

that the sample is thermally stable, alongside the same temperature of the melting plateau for each cycle (as denoted by the green line in Figure 4.25). Additionally, the particle size distributions before and after the thermal cycling that no change in the particle size of the PCD occurred. From the EasyMax thermal cycling, it can be observed that whilst the supercooling degree is not as low as when using the pure Sisterna-750PC as the surfactant, it still has a reduction in the supercooling degree compared to the EE360 surfactant system by almost 4 K, which is a 50% reduction in the degree of supercooling. It is postulated that this co-surfactant system has a higher degree of supercooling than the pure Sisterna-750PC surfactant because of the packing of the surfactant layer at the interface. With the co-surfactant system, the interface of the droplet is more flexible, due to the smaller co-surfactants woven between the larger, bulkier surfactants and with the pure Sisterna-750PC surfactant, the interface is more rigid, resulting in a better template for nucleation. However, the flexibility of the interface helps to reduce the dynamic viscosity of the entire PCD. The dynamic viscosity of the co-surfactant PCD can be seen in Figure 4.26, where the stability of the co-surfactant system can be observed by little-to-no change in the values of the dynamic viscosity after one week of thermo-mechanical cycling.

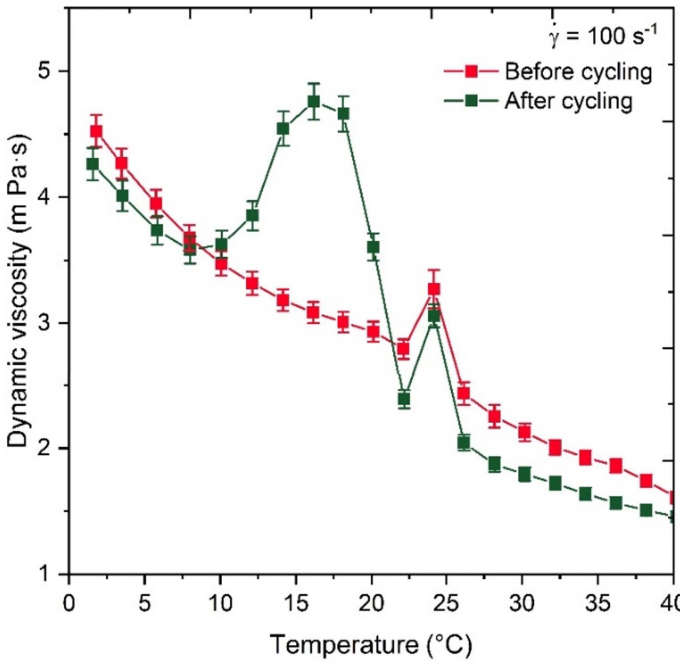

Figure 4.26: The dynamic viscosities of the optimised surfactant system straight after production and after 1 week of continuous thermo-mechanical cycling. The error bars represent the ± 3% uncertainty given by the Rheometer manufacturer

As can be seen in Figure 4.26, the dynamic viscosity is below 5mPas^{-1}, which is extremely low for PCDs, with most formulations having a viscosity higher than 10 when fully crystallised. This is as a result of the flexible film due to the introduction of the

lower-molecular weight co-surfactant. However due to the more flexible and less rigid structure at the interface, the liquid PCM molecules no longer have as a rigid template for nucleation as with the pure Sisterna-750PC. This is one of the instances in PCD formulation were a compromise on properties needs to be made. The PCD needs to be pump-able, and thus the viscosity must be low enough to not cause such an increase in the pumping power and reduce the energy efficiency when using PCD as a HTF, but additionally the supercooling degree should not be so large that a huge amount of energy needs to be put into the system to fully crystallise the PCM droplets within the PCDs. Therefore, this co-surfactant system seems to be an optimised compromise of having a low viscosity, and a slight reduction in the supercooling degree compared to other surfactant systems.

4.2.3 Conclusion on the formulation properties of phase change dispersions

The effect of different formulation conditions, such as shear rate and type of homogenising has been addressed and the best method for producing stable PCDs has been established for the studied PCD systems. Stationary homogenising techniques for a homogenising time of five minutes at a speed of 6500 rpm was the best compromise between the production of stable PCDs, without requiring the addition of too much energy. Additionally, the role of the surfactant has been elucidated and the relationship between the structure of the surfactant and the stability has also been established. Furthermore, the modification of surfactant systems has been employed to try and induce nucleation, and keep a relatively flexible film interface to try and ensure that a low viscosity has been applied. Overall, the formulated co-surfactant system using all the experimental information gathered appears to be extremely promising and in the next chapter, it will be compared for its rheological and heat transfer behaviour in the experimental test-rig discussed in Chapter 5. Overall, since the current methods to reduce supercooling in PCDs involves adding nucleating agents into the droplets, which are unreliable over many cycles and reduce the percentage of PCM used, and thus the heat capacity of the PCD, this chapter presents a novel surfactant system which shows a reduced degree of supercooling. Initial testing of a PCD with a 4 wt.% bulky surfactant system showed promising thermal behaviour in terms of a supercooling reduction of 8 K compared to a reference PCD sample of Tween-80/Span-80 (one of the most common surfactant systems in PCD research). Despite the promising supercooling reduction behaviour of the surfactant system, the PCD was highly viscous, with a paste-like consistency and thus would be unviable for use as a HTF. As a result of this, the bulky main surfactant was paired with a smaller molecular weight co-surfactant. Particle size distribution analysis determined the best composition of the main surfactant and co-surfactant by determining the most mono-modal PSD. Addition-

ally, the dynamic viscosity of the novel co-surfactant system was much lower than the reference sample when the PCM was fully crystallised and fully melted. Furthermore, the novel co-surfactant system was cycled for one week on an experimental test-rig, continuously subjected to both thermal and mechanical loads, and viscosity and DSC analysis showed no distinct change in either the dynamic viscosities or the crystallisation onset temperature. This suggests that there was no distinct growth of PCM droplet sizes after the one week of continuous cycling. The thermal stability of the novel co-surfactant system was further tested through extended cycling on the EasyMax and after 600 minutes of continuous cycling, there was no change in the crystallisation onset temperature. The other promising aspect taken from this investigation is that combinations of bulky surfactants with smaller molecular weight co-surfactants can be used to fine-tune the rheological properties. Despite the experiments presented in this paper show promising results in the direction of surfactant-initiated nucleation, the current formulations still need to be optimised to reduce the degree of supercooling further. From the experiments, it is evident that bulky surfactants can be used to induce heterogeneous nucleation and control the crystallisation behaviour but the mechanisms of how still remain unknown and thus future work should be directed in elucidating these mechanisms.

References

[1] George Gabriel Stokes et al. "On the effect of the internal friction of fluids on the motion of pendulums". In: (1851).

[2] Tharwat F Tadros. *Emulsions*. De Gruyter, 2016.

[3] Santosh Nemichand Kale and Sharada Laxman Deore. "Emulsion micro emulsion and nano emulsion: a review". In: *Systematic Reviews in Pharmacy* 8.1 (2017), p. 39.

[4] Julia Maldonado-Valderrama, Teresa del Castillo-Santaella, Maria José Gálvez-Ruiz, Juan Antonio Holgado-Terriza, and Miguel Ángel Cabrerizo-Vılchez. "Structure and functionality of interfacial layers in food emulsions". In: *Food structure and functionality*. Elsevier, 2021, pp. 1–22.

[5] Changjiu Li, Wenhao Yang, Wen He, Xudong Zhang, and Jiefang Zhu. "Multifunctional surfactants for synthesizing high-performance energy storage materials". In: *Energy Storage Materials* 43 (2021), pp. 1–19.

[6] Duo Wang, Diling Yang, Charley Huang, Yueying Huang, Dingzheng Yang, Hao Zhang, Qi Liu, Tian Tang, Mohamed Gamal El-Din, Tom Kemppi, et al. "Stabilization mechanism and chemical demulsification of water-in-oil and oil-in-water emulsions in petroleum industry: A review". In: *Fuel* 286 (2021), p. 119390.

[7] Jin-Woong Kim, Daeyeon Lee, Ho Cheung Shum, and David A Weitz. "Colloid surfactants for emulsion stabilization". In: *Advanced materials* 20.17 (2008), pp. 3239–3243.

[8] Yuting Guo, Donatas Surblys, Hiroki Matsubara, and Taku Ohara. "A molecular dynamics study of the effect of functional groups and side chain on adsorption of alcoholic surfactant and interfacial thermal transport". In: *Journal of Molecular Liquids* 335 (2021), p. 116243.

[9] Athumani Omari, Ruibo Cao, Zhuoyan Zhu, and Xingguang Xu. "A comprehensive review of recent advances on surfactant architectures and their applications for unconventional reservoirs". In: *Journal of Petroleum Science and Engineering* 206 (2021), p. 109025.

[10] Poppy O'neill, Anastasia Stamatiou, Jocelyn Bonjour, Ludger Fischer, and Rémi Revellin. "The effect of surfactant selection in phase change dispersions". In: *13th IIR PCM Conference*. 2021.

[11] Poppy O'neill, Ludger Fischer, Rémi Revellin, and Jocelyn Bonjour. "Phase change dispersions: A literature review on their thermo-rheological performance for cooling applications". In: *Applied Thermal Engineering* 192 (2021), p. 116920.

[12] Ludger Fischer, Ernesto Mura, Poppy O'Neill, Silvan Von Arx, Jörg Worlitschek, Geng Qiao, Qi Li, and Yulong Ding. "Thermophysical properties of a phase change dispersion for cooling around 50 C". In: *International Journal of Refrigeration* 119 (2020), pp. 410–419.

Chapter 5

Experimental Investigation into the Heat Transfer and Rheological Behaviour of Phase Change Dispersions during melting

5.1 Materials and Methodology

5.1.1 Materials

This chapter presents a comparative investigation into the heat transfer and rheological behaviour of two phase change dispersions during melting. For this, two different PCDs were created and their respective formulation details can be seen in Table 5.1. From here-on-out, the two formulations will be named formulation 1 and formulation 2 respectively.

Table 5.1: The formulation details of all components in each formulation

Formulation	PCM (wt.%)	Surfactant System (wt.%)	Continuous Phase (wt.%)	Nucleating agent (wt.%)
1	Rubitherm 25 HC (16)	EE364 (4)	Water (80)	Myristic acid (3)
2	Crodatherm 24 (16)	Sisterna 750-PC (1.6)/Brij-52 (3.4)	Water (80)	-

From here-on-out, the two formulations will be named formulation 1 and formulation 2 respectively. It should also be noted that formulation 1 is a paraffin-based PCD, and that formulation 2 is a completely bio-based PCD, with all of its components being bio-based.

5.1.2 Heat transfer test-rig

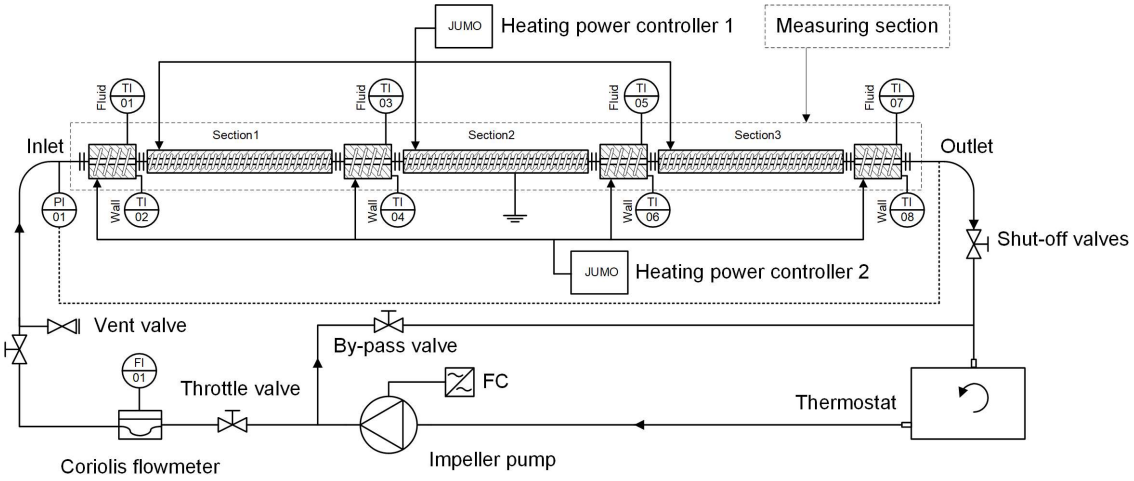

Figure 5.1: Schematic of the experimental test-rig employed in the investigation of determining the heat transfer behaviour during melting.

The main part of this experimental investigation was to determine the heat transfer characteristics of formulation 1 and formulation 2 flowing through a circular tube with constant heat flux boundary condition. Figure 5.1 shows the schematic of the experimental test-rig used to achieve this. The measuring section consists of three stainless steel (1.4301/304) tubes, each with a length of 5.322 m, an inner tube diameter of 14 mm and an outer diameter of 20 mm, that are connected in series with a flange. The total length of the measuring section is 16 m with a total heat exchange area (equivalent to the inner area of the tube with diameter, d) of 0.6 m^2. An inlet section of 0.14 m is arranged in front of the heating section to ensure a fully developed flow regime. Further details of the measuring section within the test-rig are shown in Figure 5.2 and the geometrical details are summarised in Table 5.2.

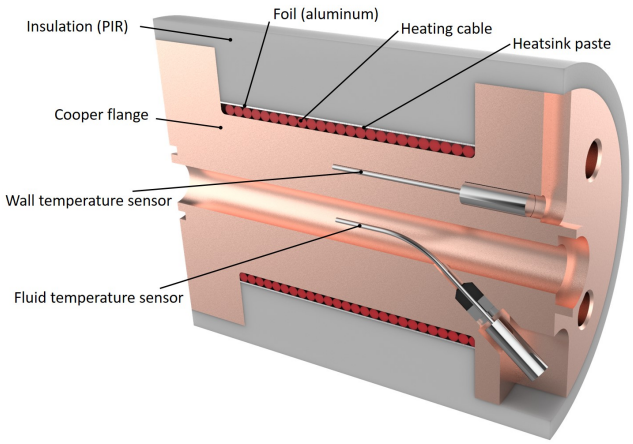

Figure 5.2: Diagram of the placement of the thermocouples and the geometry of the measuring section used to measure the temperatures in the heat-transfer test-rig

Table 5.2: Geometrical details of the components in the experimental test-rig.

Material of the tubes	Stainless steel 1.4301/304
Inner diameter of pipe (d)	14 mm
Wall thickness of pipe	3 mm
Total length of heated part of pipe	15.966 m
Total length of measuring section	16.05 m
Material of the flange	Stainless steel 1.4404/316L
Flange thickness	14 mm
Length of the inlet section	140 mm
Material of the spring	Stainless steel
Diameter of the spring	3 mm
Pitch of the spring	6.36 mm
Thickness of insulation	50 mm

The boundary condition of uniform heat flux is achieved by winding a heating cable (TWIN, Arnold Rak GmbH) along each tube. The heating cable has a diameter of 3.37 mm and a thermal power input of 15 W m^{-1}. The total length of the heating cable is 267 m which leads to a maximum thermal power input of 4 kW, 1.34 kW for each tube section. The cables are held in place by a stainless steel spring that firmly slides onto the pipe. The spring ensures that the cable is mounted symmetrically around the tube. Thermally conductive paste (type OKS 1103) is applied between the spring, cable and the pipe in order to enhance the heat transfer. To minimise heat losses to the ambient, an aluminium foil is wrapped around the spring and heating cable and the whole measuring section is thermally insulated with PIR shells (Swisspor) with a thickness of 50 mm and a thermal conductivity of 0.027 W m^{-1} K^{-1}. The heating cable is powered by a single-phase thyristor power controller, which allows precise regulation of the heat input to the fluid. In order to remove the heat added in the test section, a thermostat (JUMO, Type TYA-201) is connected to the set-up. An impeller pump (Zuwa, Type NIROSTAR/V 2000-B/PT) with a frequency converter as well as a by-pass valve enables the accurate control of the mass flow rate.

Sensors and data aquisition

Table 5.3: Specifications and details of all types of sensors used

Sensor	Manufacturer	Type	Range	Uncertainty
T_b (T101/03/05/07)	Roth+Co AG	PT100 4 wire, A	-65—200°C	± 0.03°C
T_w (T102/04/06/08)	Roth+Co AG	PT100 4 wire, A	-65—200°C	± 0.03°C
Coriolis, $\dot{m}$	Endress+Hauser	F83, Type 4x	0—6500 $\dot{m}$	± 0.004
Electrical power, P_{el}	Jumo GmbH	JUMO TYA 201	0—4 kW	± 0.002 P_{el}

Specifications of all the sensors that were used are summarised in Table 5.3. Temperature sensors were installed the measure the fluid bulk temperatures, T_{bulk} (T101, T103, T105,

T107) and the inner wall temperatures T_{wall} (T102, T104, T106, T108) at the inlet of the first tube section and at the outlet of the second and third tube section. Both fluid and wall temperature sensors were measured with a Pt-100 four-wire thin film sensor (1.2×1.6 mm). The four wires were directly attached to the sensor and thus prevented any measurements error due to temperature variations. As shown in Figure 5.2, each wall temperature sensor was glued to the tip of an M3 screw that was subsequently inserted into the pipe through a hole. After adjusting the sensor position with the screw, such that it did not protrude into the pipe, a synthetic resin was applied to the small gaps next to the sensor to ensure a smooth inner pipe surface. The bulk fluid temperatures were measured at the centreline of the tube. The sensors were placed into ductile tubes with a diameter of 3 mm. These tubes were then inserted into the test-rig tube through a hole in the flange, such that the lower part lies parallel to the flow (see Fig. 5.2). Since the four-wires from the sensor were free to move inside the tube, they were not exposed to any tension during bending. Before attaching both the wall and fluid temperature sensors, the complete system was calibrated in a precise temperature-regulated bath between 15 and 50℃. The measurements uncertainty of each individual temperature sensor was ensured to be in the range of ±0.03℃ after calibration. The mass flow rate of the pumped fluid was measured with a Coriolis flow meter (Type Promass F 83). The heating input was measured with a thyristor power controller (JUMO, Type TYA-201). Temperatures, pressures and mass flow rates were recorded by an NI 9216 module. The data was captured and recorded with LabView.

5.1.3 Quantities of interest

The objective of this experimental work was to investigate the heat transfer behaviour of a PCDs using different operational parameters (applied heat flux and mass flow rate). For this, interest lies in the local heat transfer coefficient between the bulk of the PCD and the tube wall under steady state conditions. Additionally, the local Nusselt numbers (Nu) are also of interest. Firstly, the specific flux density at the wall (q_w) was calculated according to:

$$_w= \frac{P_{el} - Q_{loss}}{A} \tag{5.1}$$

where P_{el} is the electrical power input, A is the inner area of the tube and Q_{loss} was the heat losses which are discussed in the next section of this chapter. Using the specific flux density and the temperature difference between the local wall temperature ($T_{w,x}$) and the local bulk temperature ($T_{b,x}$), the local heat transfer coefficient was calculated as follows:

$$h_x = \frac{q_w}{T_{w,x} - T_{b,x}} \tag{5.2}$$

using h_x, the local Nusselt numbers (Nu_x) was calculated according to:

$$Nu_x = \frac{h_x d}{\lambda} \tag{5.3}$$

where λ is the thermal conductivity of the PCD. Additionally, to calculate the apparent specific heat capacity ($\bar{c}p$) of the PCD during melting in the experimental test set-up to determine the quantity of heat the PCD is able to store during cycling, the average $\bar{c}_p$ over the entire length of the tube was calculated in accordance with:

$$\bar{c}p = \frac{P_{el} - Q_{loss}}{\dot{m}(T_{b,out} - T_{b,in})} \tag{5.4}$$

where $T_{b,out}$ and $T_{b,in}$ are the fluid's bulk temperature at the outlet and inlet of the tube respectively. The specific heat capacity can also be calculated for each section of the tube; section 1 (0-5.3 m), section 2 (5.3-10.6 m) and section 3 (10.6-16.0 m) by dividing the term $P_{el} - Q_{loss}$ by three and taking the bulk fluid's inlet and outlet temperatures at the inlet and outlet of each section respectively.

5.1.4 Validation with water

The first set of results collected from the experimental test-rig discussed in Section 5.1.2 was with water, to accurately calculate heat losses and to check the validity and reliability of the test-rig. This was performed with varying the mass flow rates (and subsequently the Reynolds numbers), heating inputs and inlet temperatures. Firstly, although most of the energy supplied by the heating cable wrapped around the tubing is transferred to the fluid, a small proportion of the energy is transferred to the environment as heat losses through the insulation, which can be seen in Figure 5.3.

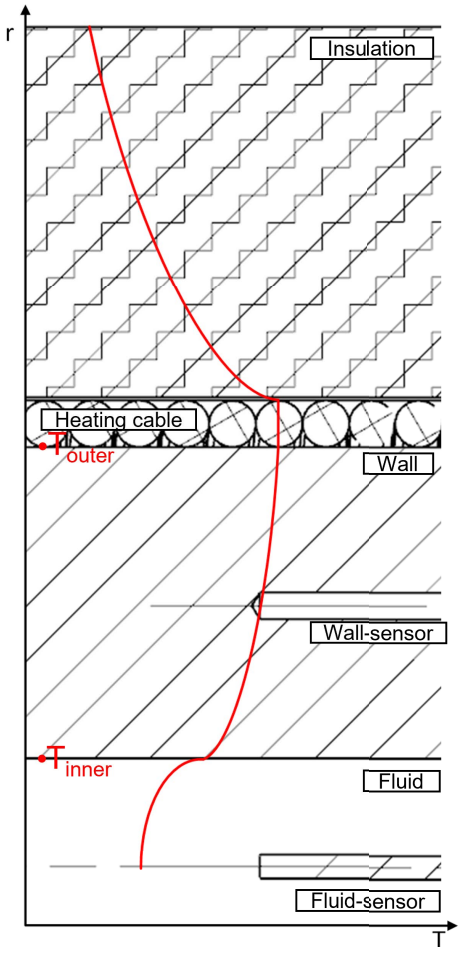

Figure 5.3: Temperature profile in the measuring section of the test-rig

The heat transfer from the heating cable to the fluid passes through the partition by means of conduction and then by convection into the fluid. To calculate these heat losses it was assumed that the temperature in the heating cable was constant over the entire length of the pipe. Additionally, due to the fact that the wall temperature sensors were placed in the centre of the wall (due to the inaccuracies of measuring directly at the flow surface), the recorded temperature and the surface temperature (or wall temperature) of the flow can be calculated. Another assumption was that since the nickel coating of the copper tubing (to prevent against oxidation) was only a few micrometers thick, that its influence on the thermal conductivity can be neglected. The heat flow through the wall can subsequently be calculated according to the following equations:

$$Q = 2\pi l_{pipe}\lambda \frac{T_{outer} - T_{inner}}{ln(\frac{2d_{outer}}{2d_{inner}})} \tag{5.5}$$

and

$$\frac{T_r - T_{inner}}{ln(\frac{2d}{2d_{inner}})} = \frac{T_{outer} - T_{inner}}{ln(\frac{2d_{outer}}{2d_{inner}})} \tag{5.6}$$

For the temperature T_r the wall sensor temperature is used. Subsequently, Equations 5.5

and 5.6 can be arranged and the surface temperature of the fluid at the inner wall of the pipe can be determined using:

$$T_{wall} = T_{inner} = T_{wallsensor} - \frac{Qln(\frac{2d_{wallsensor}}{2d_{inner}})}{2\pi l_{pipe}\lambda_{copper}} \tag{5.7}$$

For the temperature range we investigate (15-50℃) the thermal conductivity of the copper remains constant at $\lambda_{copper} = 394$ W m^{-1} K^{-1}.

The heat losses in the system were determined using the following equation:

$$Q_{loss} = P_{el} - \dot{m}(cp_{out}T_{out} - cp_{in}T_{in}) \tag{5.8}$$

Figure 5.4 shows the heat losses as a function of the temperature difference between the mean temperature of the inlet and outlet of the measuring section and the ambient temperature (T_{amb}). It should be noted that the term heat losses is used for uniformity, but this also encompasses heat gains, where the water absorbs heat from the ambient. As

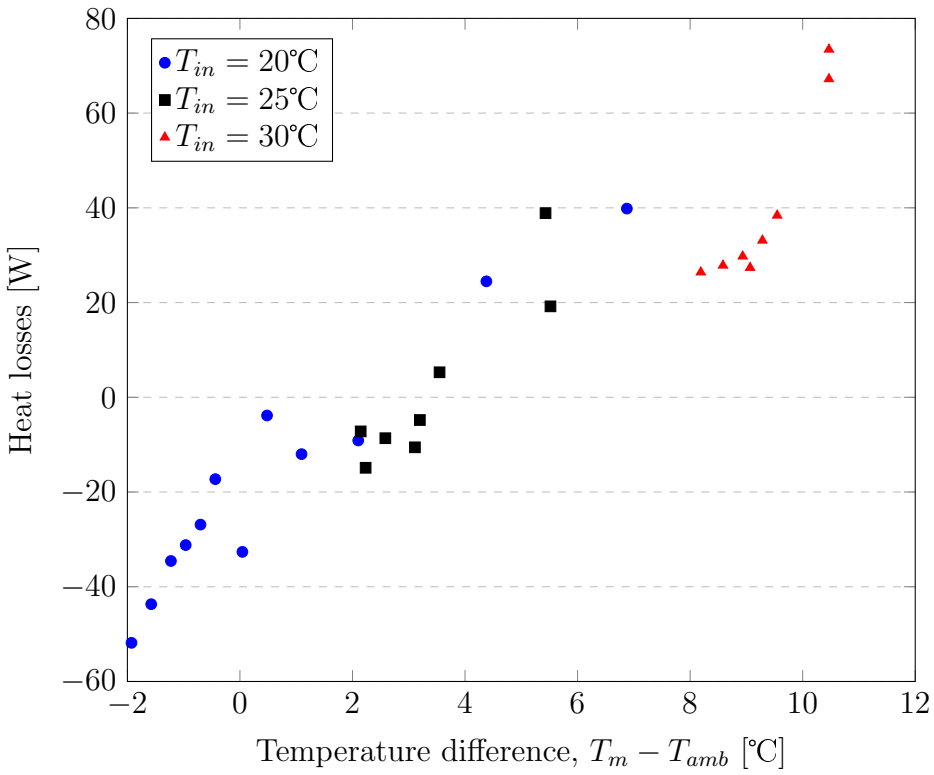

Figure 5.4: The calculated heat losses with Equation 5.8 for water in the experimental test-rig at three different inlet temperatures against the temperature difference between the mean of the inlet and outlet temperatures of the water and the measured ambient temperature.

evident, the ambient temperature has a great influence on the heat losses especially when the ambient is cooler than the fluid (and subsequently there is a negative temperature

difference shown on Figure 5.4) and there is a negative heat flow where the water draws additional energy from the environment. In general however, the heat losses are extremely low, depending on the heat capacity, they amount to less than 3% of the heat supplied. To observe the effect of the heat losses with the mass flow rate, the heat losses were calculated for three different inlet temperatures and plotted against the mass flow rates and can be seen in Figure 5.5. For the measurements with the PCDs, the heat losses were calculated

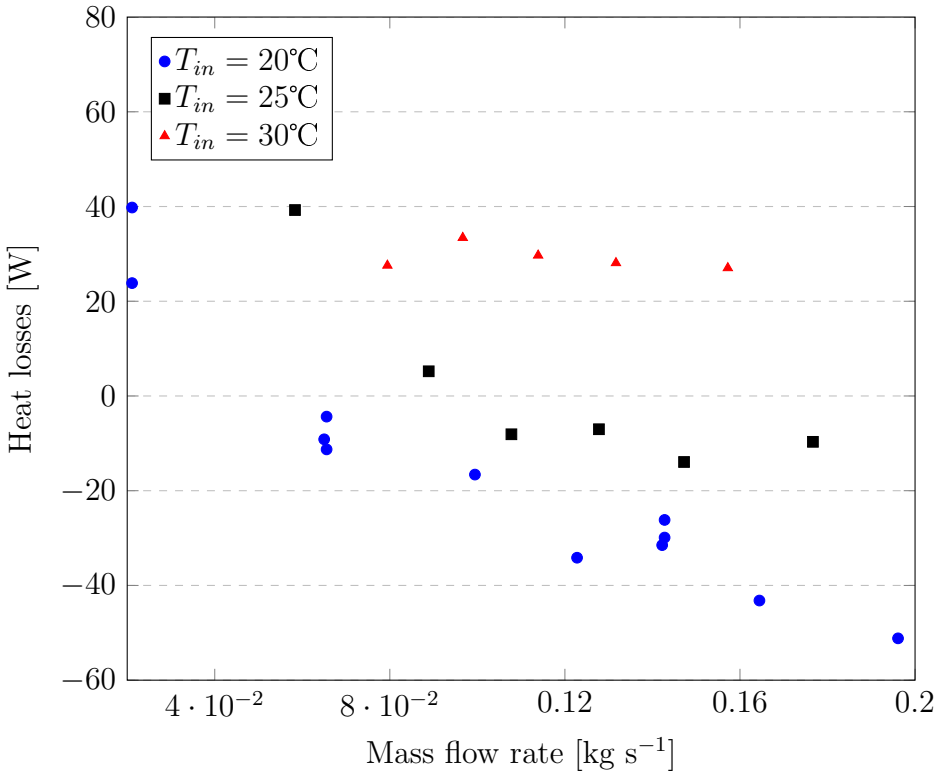

Figure 5.5: The calculated heat losses with Equation 5.9 for water in the experimental test-rig at three different inlet temperatures against the mass flow rate.

based on the water experiments, as a function of the temperature difference according to the following equation:

$$Q_{loss} = a_1 \Delta T_{amb} + a_0 \tag{5.9}$$

For the validation and determination of the reliability of the experimental test-rig, experiments were again conducted with water to calculate experimental Nusselt numbers to compare to Nusselt numbers calculated with correlations for the boundary condition of constant wall heat input in a cylindrical pipe. Within the system, the pipe flow is undergoing forced convection due to the pump. The heat transfer in the system therefore takes place between the water (or PCDs) and the wall. With the measured temperatures and the corrected heat input (with the calculated heat losses), the average heat transfer

coefficient over the length of the pipe can be calculated according to:

$$= \frac{Q}{A} = h\Delta T \tag{5.10}$$

furthermore, the local heat transfer coefficients, h_x at any point on the pipe surface, x, depends on the surface temperature at the wall and in the bulk of the fluid. It is calculated using:

$$q = h_x(T_{wall} - T_{fluid}) \tag{5.11}$$

From the calculated heat transfer coefficients of water, the Nusselt numbers can be calculated. For a pipe flow, the Nusselt number is calculated as:

$$Nu = \frac{hd}{\lambda} \tag{5.12}$$

In the literature, there are various correlations that describe the Nusselt number in cylindrical pipe flow. In order to validate the experimental set-up, the Nusselt numbers from the water measurements were compared to the results from commonly used Nusselt correlations based on the Reynolds number and Prandtl number. The first correlation used was a well-known correlation from Gnielinski [1], with fully developed turbulent flow, where the correlation is as follows:

$$Nu_G = \frac{(\xi/8) \cdot Re \cdot Pr}{1 + 12.7 \cdot \sqrt{\xi/8} \cdot (Pr^{2/3} - 1)} \left[1 + \left(\frac{d_i}{l}\right)^{2/3}\right] \tag{5.13}$$

where

$$\xi = (1.8log_{10}(Re) - 1.5)^{-2} \tag{5.14}$$

The Nusselt curve in the transition area (between the distinct laminar and turbulent flow regime) is obtained as follows:

$$Nu = (1 - \gamma)Nu_{lam,2300} + Nu_{turb,10^4} \tag{5.15}$$

The correlation is valid for Reynolds number ≥ 2400. It should be noted that the type of flow, geometry and surface roughness all influence the development of turbulence after a critical Reynolds number of 2300 has been exceeded (for Newtonian fluids in a cylindrical pipe) and the intermittency factor, γ indicates how high the temporal proportion of turbulent flow is, where $\gamma = 1$ is a permanently turbulent flow. $Nu_{lam,2300}$ can be calculated as follows:

$$Nu_{lam,2300} = [83.326 + (1.953(2300\frac{d}{l})^{1/3} - 0.6)^3 + (0.924Pr^{1/3}(2300\frac{d}{l})^{1/2})^3]^{1/3} \tag{5.16}$$

and $Nu_{turb,10^4}$ can be calculated using:

$$Nu_{turb,10^4} = \frac{38.5Pr}{1 + 12.7\sqrt{0.00385}(Pr^{2/3} - 1)}[1 + (\frac{d}{l})^{2/3}] \tag{5.17}$$

where

$$\gamma = \frac{Re - 2300}{10^4 - 2300} \tag{5.18}$$

where $0 \leq \gamma \leq 1$ for the laminar flow regime, the Gnielinski correlation becomes:

$$Nu = [Nu_{q1^3} + 0.6^3 + (Nu_{q2} - 0.6)^3 + Nu_{q3^3}]^{1/3} \tag{5.19}$$

where

$$Nu_{q1} = 4.364 \tag{5.20}$$

$$Nu_{q2} = 1.953(RePr(\frac{d}{l}))^{1/3} \tag{5.21}$$

$$Nu_{q3} = 0.924Pr^{1/3}(Re(\frac{d}{l}))^{1/2} \tag{5.22}$$

Equations 5.20-5.22 show that for extremely long pipes, the Nusselt number approaches the value Nu_{q1}. An additional correlation used to compare with the experimentally derived Nusselt number is the Hausen and Gnielinski correlation which does not take into account the transition region from laminar to turbulent. The range of validity of the correlation is $1.5 < Pr < 500$ and $2300 < Re < 10^4$. The Hausen and Gnielinski [2] reads as:

$$Nu_{HG} = 0.012(Re^{0.87} - 280)Pr^{0.4}[1 + (\frac{d}{l})^{2/3}] \tag{5.23}$$

There are other common correlations such as Churchill's or Petuhkov's, which yield similar values for the Nusselt number, they can be found in [3, 4]. Figure 5.6 shows the evolution of the two mentioned Nusselt correlations, the Gnielinski and the Hausen-Gnielinski with the Reynolds number as a function of two different Prandtl numbers for water, which was a function of $T_{in} = 19.0$ and $T_{in} = 25.0$. The red dotted lines represent the laminar and turbulent flow regions and in between lies the transition region.

The two Prandtl numbers are calculated based on the thermophysical and transport properties of water at 19 ℃ (Pr=7.0) and 25 ℃ (Pr=6.1). The calculated Nusselt numbers with the Hausen-Gnielinski correlation are somewhat lower than those predicted by the Gnielinski correlation in the turbulent flow regime. However the correlations in the transition region predict almost the same Nusselt number. In order to compare the behaviour of the water measurements with the correlations, several experiments were performed with different flow velocities, so that the behaviour over a wide-range of Reynolds number could be represented. The assumption during calculation was that the average

temperature between the inlet and the outlet of the measuring section remained constant and as a result the Prandtl number also remained constant ($Pr = 6.64$). Figure 5.7 shows the results of the experiments, with the experimentally obtained data being shown as crosses.

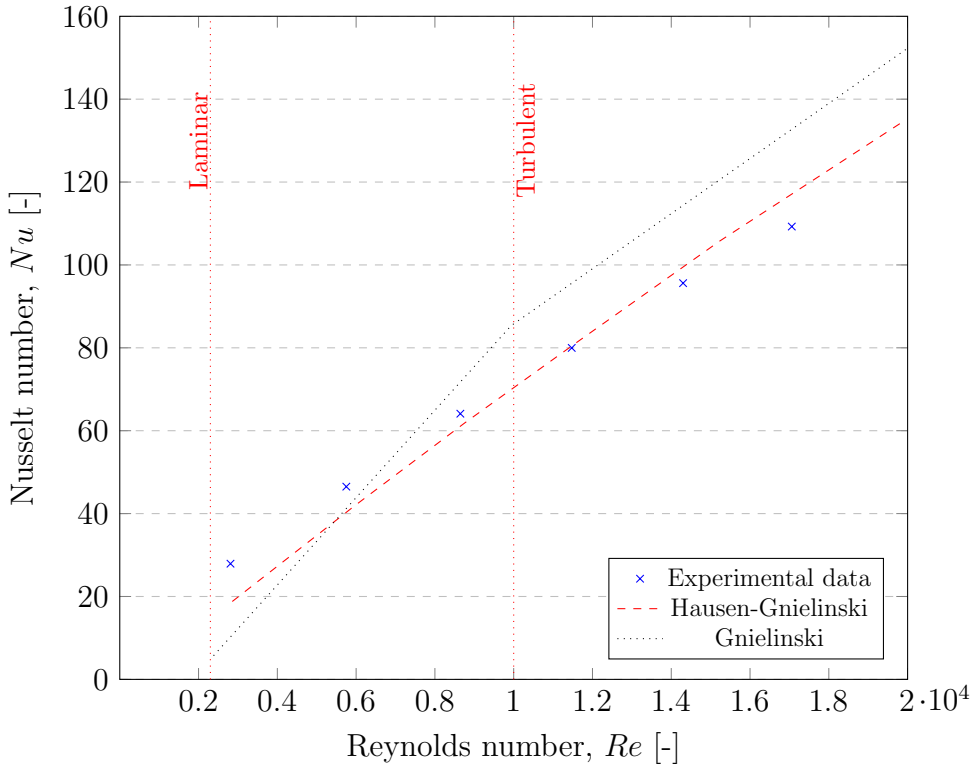

Figure 5.7: The calculated heat losses for water in the experimental test-rig at $T_{in} = 20.0$℃ and $P_e = 2$ kW.

A clear similarity between the Nusselt correlation according to Hausen and Gnielinski can be seen, with less than 15% deviation for all values, except for the lowest Reynolds number. For the correlation according to the Gnielinski correlation. The majority of the measurements lie outside the given a tolerance of 15%. As a result of this, for the experiments with the two formulations of PCD, Reynolds numbers of above 3000 will be used to ensure that the test-rig is validated for all measurements.

5.2 The Effect of Formulation on the Rheological Behaviour of Phase Change Dispersions during Melting

When considering the melting regime, we need to consider the fact that initially, the PCD is in the form of a suspension; solid PCM droplets suspended in water. As the PCD flows,

the applied heating input heats up the fluid and melts the solid PCM droplets so that along the length of the experimental pipe, the PCD is gradually changing from a suspension to an emulsion. This creates a complex rheological behaviour along the length of the pipe and careful consideration must be placed on determining the temperature-dependence of the rheological behaviour. Furthermore, it has been speculated that PCD formulated with different PCM concentrations and surfactant systems act as non-Newtonian fluids [5, 6, 7, 8]. To determine if this was the case for the two formulations presented in this section, the shear rate versus shear stress curves were plotted to identify not only if the formulations were Newtonian or non-Newtonian, but in the case of the latter, to determine which classification of non-Newtonian fluid they belonged to. This information is crucial in accurately determining the heat transfer performance of PCDs with different operational conditions. The type of non-Newtonian fluid class can be elucidated since different types of non-Newtonian fluids have different shear-rate shear stress relationships, as shown by Figure 5.8 which compares the behaviours of non-Newtonian fluids with a Newtonian fluid.

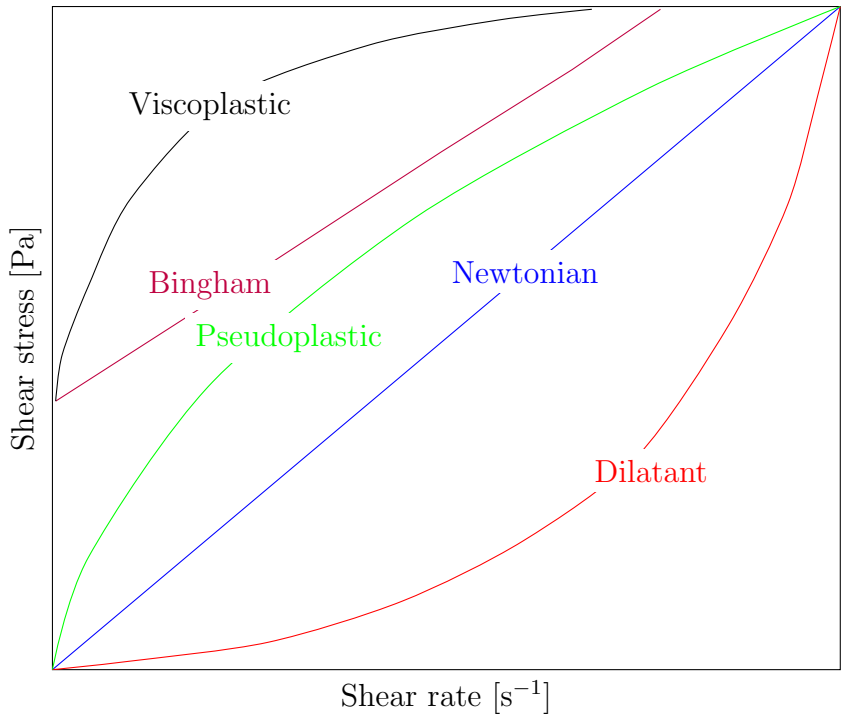

Figure 5.8: Relationship between shear stress and shear rate for different types of non-Newtonian fluids and showing the Newtonian behaviour, adapted from [9].

Figure 5.8 demonstrates that if either of the formulations were to be Newtonian, the relationship between the shear stress and shear rate would be linear. Any deviation from this linear relationship would indicate that the either of the formulation's behave as non-Newtonian fluids. Using the rheometer described in Chapter 3, the shear rate and shear

stress relationships for both formulation 1 and formulation 2 was plotted and can be seen in Figures 5.9(Top) and 5.9(Bottom) respectively.

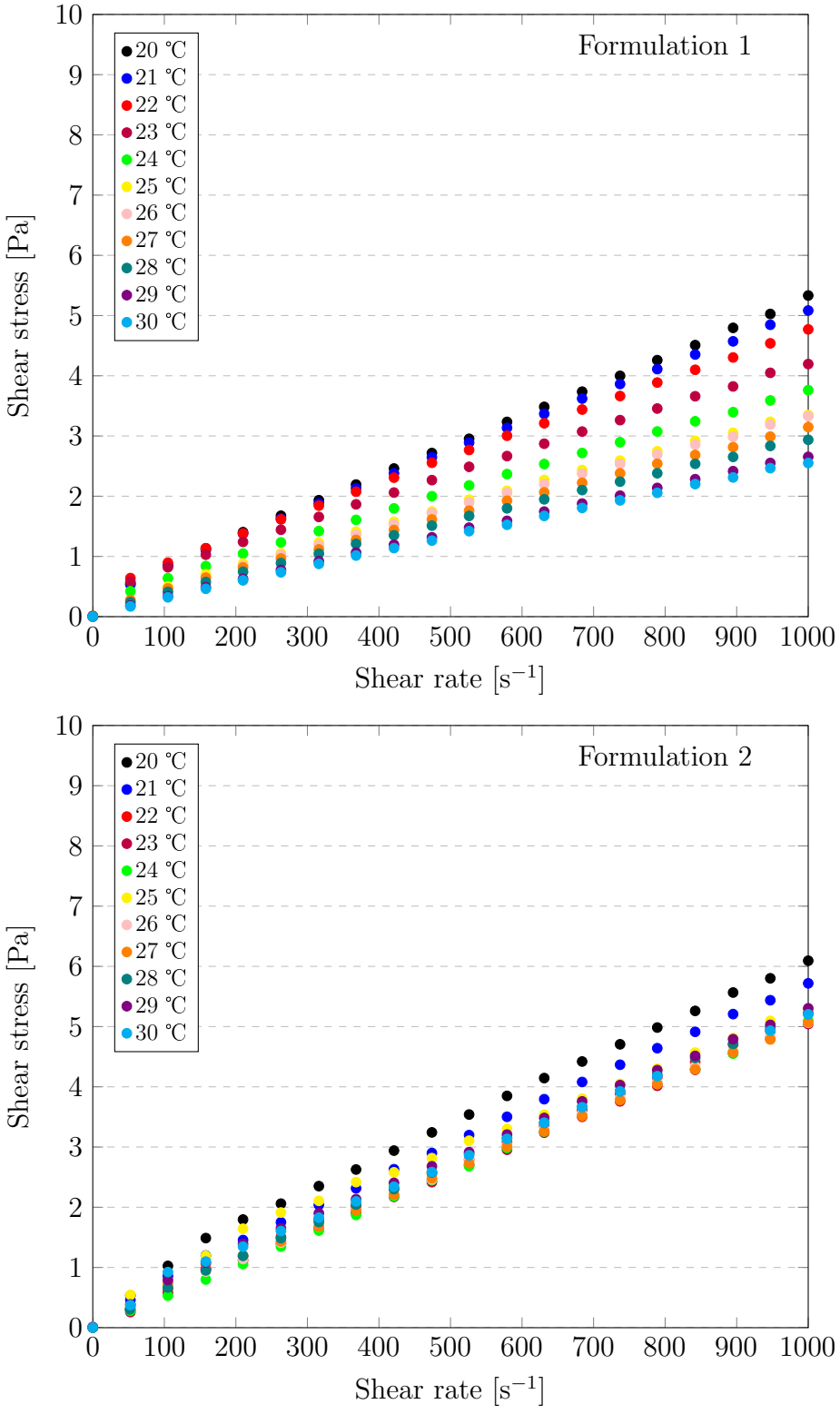

Figure 5.9: Relationship between shear stress and shear rate for Top: formulation 1 and Bottom: formulation 2 at the different temperatures used in the investigation (20—30 ℃).

Interestingly, Figure 5.9 demonstrates that both formulation 1 and formulation 2 de-

viate slightly from the classical Newtonian behaviour, with neither having a completely linear relationship between the shear stress and shear rate, at all investigated temperatures. As related to Figure 5.8, they both seem to show modest pseudo-plastic behaviour. However, it can be seen that the spread of shear-stresses with respect to temperature is much greater for formulation 1 than for formulation 2. This can be explained by the different surfactant system used in both formulations. Formulation 1 contains a standard, single surfactant, which allows a greater flexibility of the interfacial film between the PCM droplets and the water. This flexibility results in a much larger susceptibility to changes in the shear-rate. Formulation 2, on the other hand, contains an extremely bulky surfactant (and a smaller molecular weight co-surfactant) that creates a rigid interface between the PCM droplets and the water phases. This film rigidity results in greater resistance within the PCM droplets of deformation, and makes it much less susceptible to changes in the shear rate. Additionally, formulation 2 appears to show less linear behaviour than formulation 1, particularly at lower shear rates, which indicates it also shows a greater degree of non-Newtonian behaviour. Finally, it appears that temperature does seem to have an influence on the relationship between the shear rate and shear stress for both formulations. Formulation 1, which has a melting point of 24℃, shows a greater degree of linearity after it has melted, e.g. when it is in the emulsion form. Formulation 2, with a melting point of also 24℃, displays a similar trend, but strangely, at the highest investigated temperature, 30℃, the degree of non-linearity appears to increase again. This was further investigated by plotting the dynamic viscosities against the shear rate to see how the viscosity changes with respect to shear rate. This can be observed in Figure 5.10(Top) for formulation 1, and Figure 5.10(Bottom) for formulation 2.

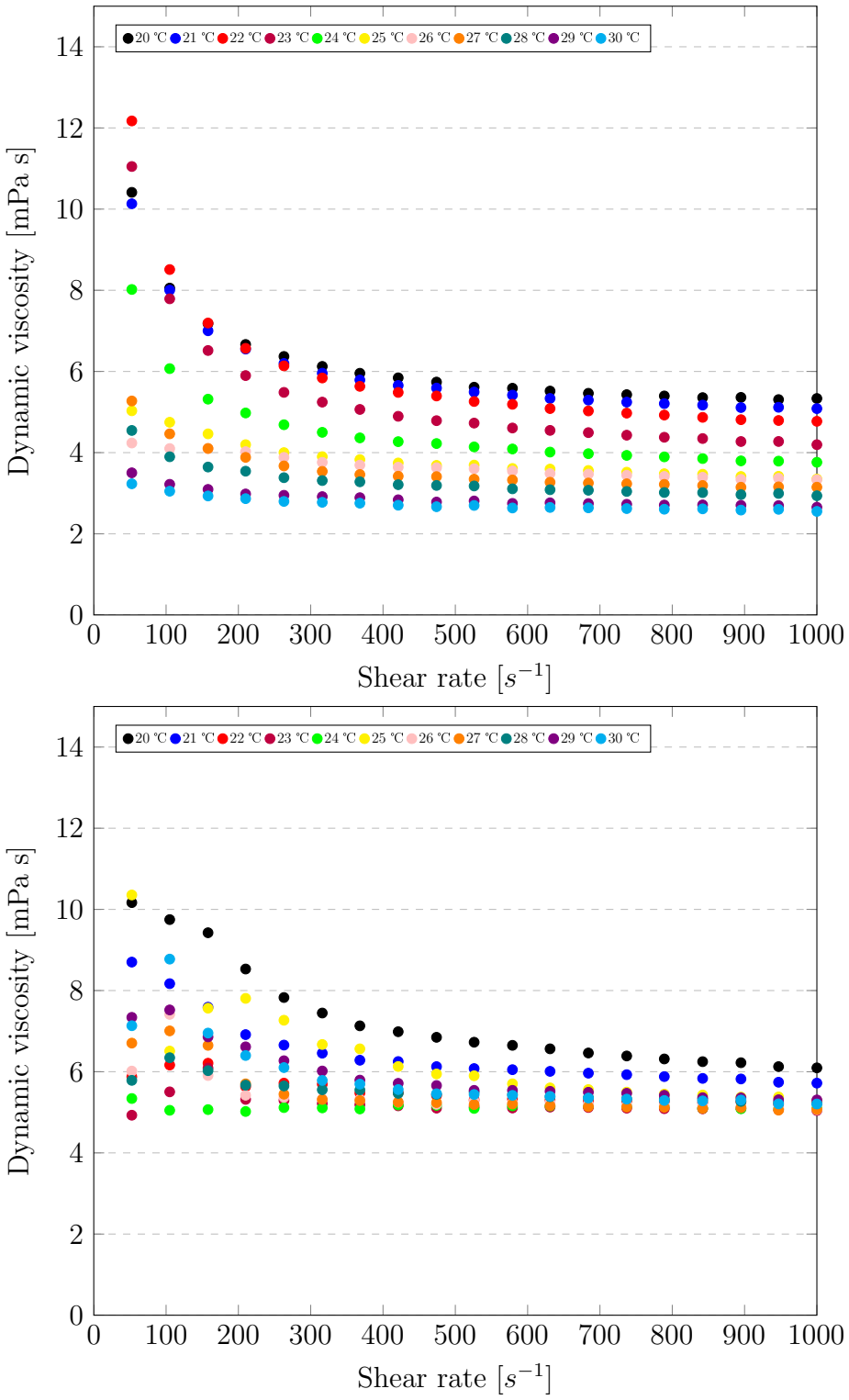

Figure 5.10: The dynamic viscosities of Top: Formulation 1 and Bottom: Formulation 2 for the temperature range (20—30 ℃) and for shear rate range 50—1000 s^{-1}.

From Figure 5.10, the shear-thinning behaviour is evident for both formulations, especially in the region of when the PCD is in the suspension form (below 24℃). Formulation 1 shows a relatively simple trend, at all temperatures shear-thinning behaviour is obvious,

but the degree of shear-thinning behaviour becomes less apparent as the temperature increases, particularly after the melting point. A decrease in the dynamic viscosity with an increase in the temperature can also be seen. Despite this, the trend for formulation 2 is more complex. Firstly, the dynamic viscosity appears to be much less dependent on the temperature, which is due to the inflexible film created by the rigid surfactant structure in formulation 2. Additionally, formulation 2 shows the highest degree of shear-thinning behaviour at the lowest temperature (20℃) and at 25℃, right after melting. This suggests that the interface between the PCM and water phase in formulation 2 is much more dynamic than in formulation 1 during the melting process, and the melting process results in a different adsorption of the surfactants at the interface. In this investigation, this was not studied further, however it is highlighted that this is a current knowledge gap and that further experimentation should be performed to understand the complex behaviour of surfactant adsorption during phase change processes and how this effects the thermophysical and transport properties of PCDs. Despite the evident shear-thinning behaviour for both formulations, after a shear rate of approximately 400 s^{-1} for formulation 1 and 600 s^{-1} for formulation 2, the shear-thinning behaviour becomes less obvious. Overall, the fact that the results show that the formulations are shear-thinning adds extra complexity when calculating relevant heat transfer and rheological parameters, as the analysis of the heat transfer and rheological behaviour is dependent upon viscosity, which in our case, is not only $\mu = f(T)$ as with Newtonian fluids, but $\mu = f(T, \dot{\gamma})$. This further adds complication to the situation, and means that as well as the temperature dependency, consideration of the shear-dependence needs to be determined. To elucidate the degree of non-Newtonian behaviour of both fluids, the n and K coefficients from the Herschel-Bulkley model were calculated:

$$\tau = \tau_0 + K\dot{\gamma}^n \tag{5.24}$$

and subsequently rearranging to the form:

$$log_{10}(\tau - \tau_0) = log_{10}K + nlog_{10}\dot{\gamma} \tag{5.25}$$

A graph was then plotted of $log_{10}\tau$ against $log_{10}\dot{\gamma}$ where the gradient of the linear plot is n and the y-intercept is K. An example of this can be seen in Figure 5.11.

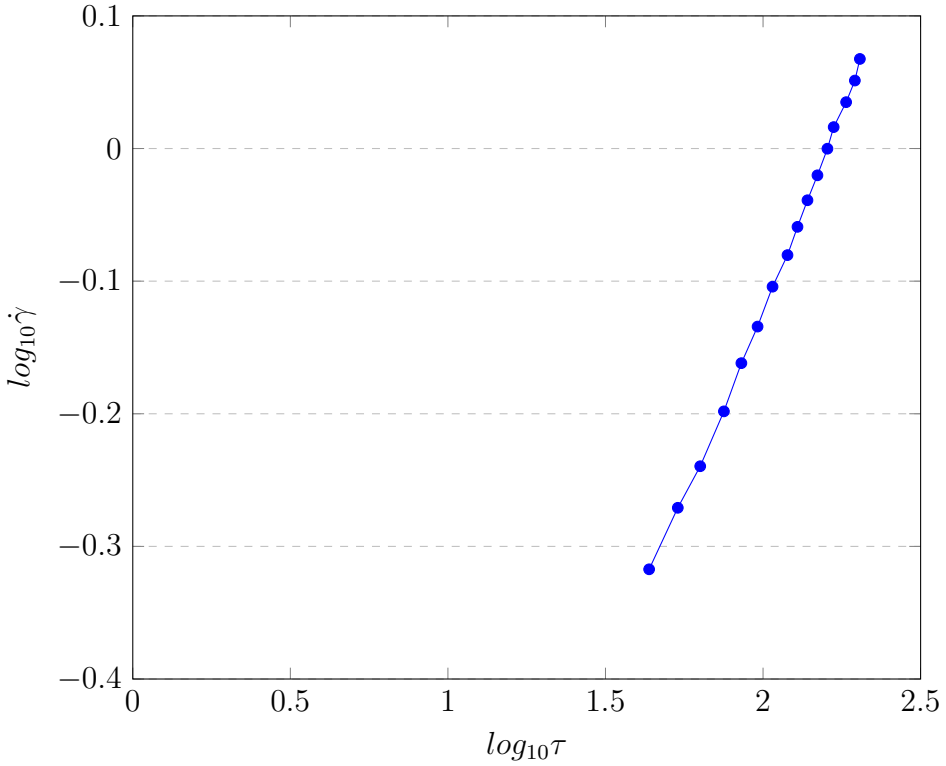

Figure 5.11: Highlighting the method of calculating the n and K parameters from the Herschel-Bulkley model (Equation 5.25).

This methodology was performed for all investigated temperatures and for both formulations and the corresponding n and K values are displayed in Figure 5.12.

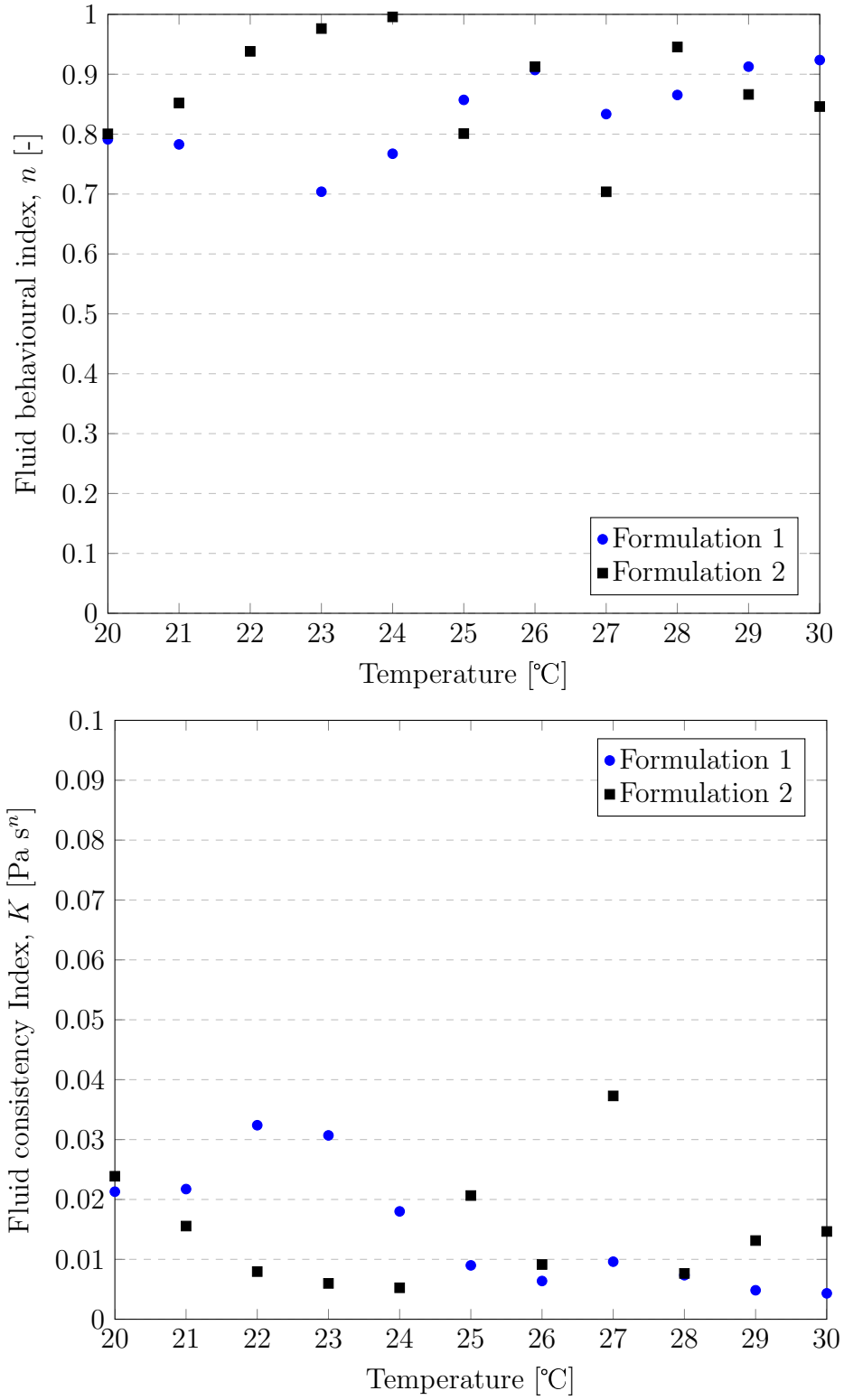

Figure 5.12: Top: The calculated Fluid behavioural index, n, for formulation 1 and formulation 2 in the temperature range of 20—30 °C and Bottom: the calculated fluid consistency index, K, for both formulations in the same temperature range.

Figure 5.12 shows both the n and K values for both formulations at different tem-

peratures. From this, it can be seen that for formulation 1, n generally increases with increasing temperature, with the biggest change being seen around the melting point. After the melting point, the calculated n for formulation 1 appears to be relatively constant. Despite the increasing n value for formulation 1, it never reaches 1, which suggests that the fluid is also non-Newtonian throughout all the temperatures. On the other hand, n for formulation 2 increases until the melting point, where a sudden decrease is observed, which is in line with what was seen in the plot of the dynamic viscosity against the shear rate. This further points in the direction of needing to understand the adsorption kinetics of the surfactants at the interface during the phase change process. Despite this, the n value for formulation 2 also stays below 1, suggesting it also shows non-Newtonian behaviour throughout all the operated temperatures. The fluid consistency index, K, which represents the viscosity of a fluid, shows that for formulation 1, as the temperature decreases so does the K value, this was also seen in the plot of the dynamic viscosities against the shear rate. For formulation 2, the K value decreases initially (20-24℃) and then after the melting point, a stark increase is observed until 27℃ and then the K value decreases. This is also seen in the plot of the dynamic viscosities against the shear rate and points again in the direction of complex surfactant adsorption kinetics of the surfactant system. Overall, the rheological analysis of both formulations show the effect that the surfactant system has on the overall dynamic viscosity, and the relationship between the dynamic viscosity, temperature, phase change phenomenon and shear rate. Whilst in this instance, a clear structure-related causation cannot be elucidated, this is noted as a significant point for future research on the formulation of PCDs. On top of the dynamic viscosity, another important transport property to consider when studying PCDs is the pressure drop. The pressure drop is essential because the pumping power consumption of PCDs accounts for a large part of the total energy required for the PCDs when used in an application, especially where the viscosities of PCDs are higher, which depends on the operational temperature, mass flow rate (and thus shear rate), PCM used within the PCD (and its relative concentration) and the surfactant system used. Most often, the high viscosities of PCDs, compared to single-phase fluids like water, result in higher pressure drops and thus pumping powers, due to this, the pressure drops of the two formulations at different flow velocities was investigated against water, to determine how much higher the pressure drops were. The pressure drops of the two formulations were investigated using the experimental test-rig shown in Figure 5.1, with PI01 being the pressure drop sensor measuring the pressure drop over the entire 16.5 m tube section. The comparison of both formulations and water was based under both the constant flow velocity basis and Figure 5.13 shows this relationship for each formulation and for water.

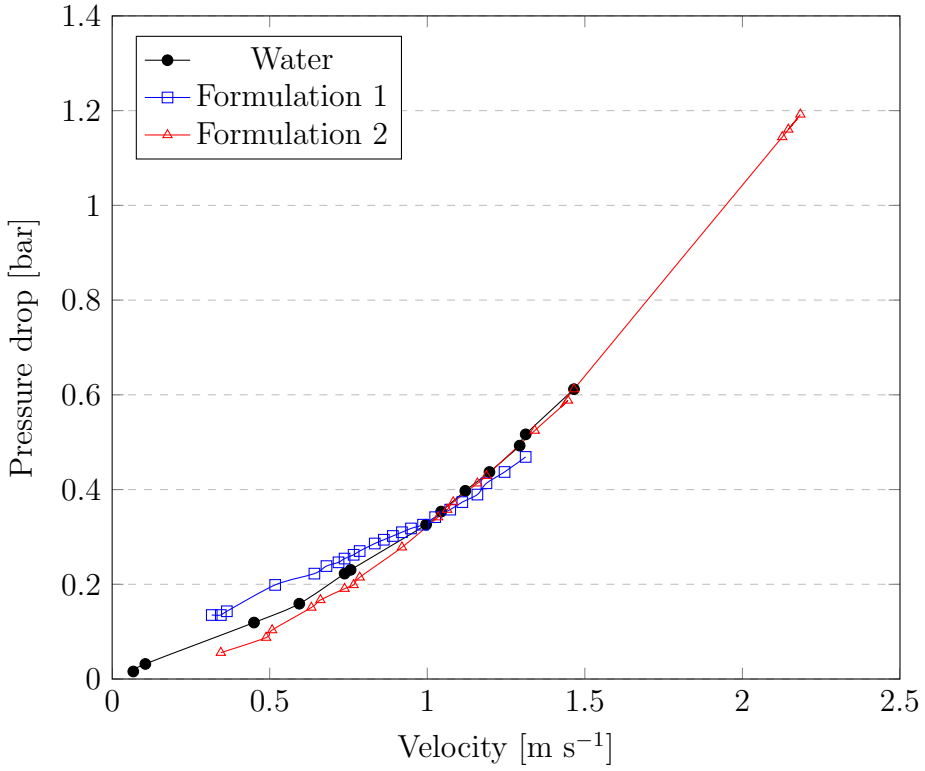

Figure 5.13: The pressure drop measurements collected from the experimental test-rig for water, Formulation 1 and Formulation 2 against the flow velocity at an inlet temperature of approximately 21℃.

The pressure drop depends on the geometry of the test-rig and the effective viscosity of the fluid used. In this case, the geometry of the test-rig used was the same and so the comparison of the pressure drops give an idea of the effective viscosities of both formulations during flow and shear experienced during the experimental investigation. Figure 5.13 shows the the pressure drops at an inlet temperature of 21℃ for both formulations and for water. Ultimately, due to the shear-thinning behaviour of the two formulations, their pressure drops are not that much higher than water. Formulation 1 has a higher pressure drop at lower velocities, and a lower pressure drop at higher flow velocities. Looking at the pressure drops allows for the proper design of operational parameters for utilising specific PCDs, and under which conditions they are beneficial. Another important thermophysical property to consider for a full rheological characterisation, and for calculation of the Reynolds number of the two formulations is the density. The effective density of both formulations was calculated using the following formula and can be seen in Figure 5.14:

$$\rho_{PCD} = \phi_{PCM}\rho_{PCM} + (1 - \phi_{PCM})\rho_{water} \tag{5.26}$$

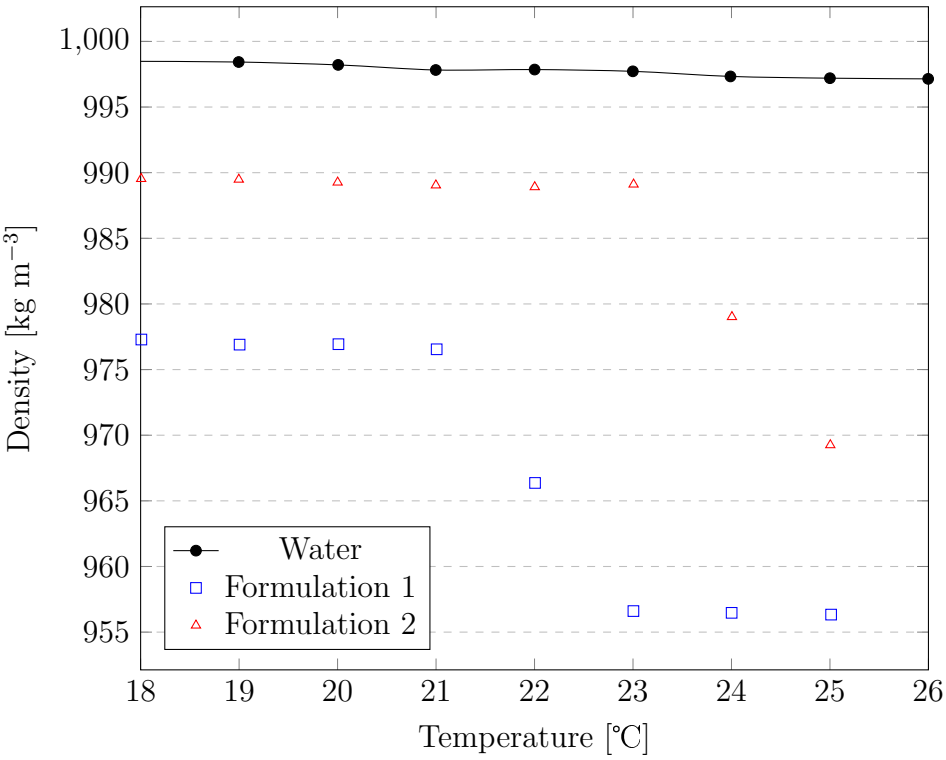

Figure 5.14: Effective densities of formulation 1, formulation 2 using Equation 5.26 for the range of temperatures in the region of interest for the heat transfer experiments. Note, the density of water as found from Coolprop [10] is shown as a comparison.

Figure 5.14 highlights that both formulation 1 and formulation 2 have a lower effective density than for water, due to the lower density of the PCM dispersed phase. Additionally, at the melting point of each formulation, a dramatic decrease in the density can be seen as the PCM is changing from solid to liquid. Overall, both formulations were determined to be non-Newtonian fluids on accounts of their shear-stress, shear-rate relationships, from the observation of the evolution of the dynamic viscosity with shear rate and from the calculation of the flow behavioural index, n. Additionally, the the densities of each formulation at specific temperatures were calculated in order to aid the calculation of dimensionless numbers to help with the heat transfer characterisation, such as the Prandtl number and Reynolds number.

5.3 The Effect of Formulation on the Heat Transfer Behaviour of Phase Change Dispersions during Melting

5.3.1 Determination of the thermophysical properties

The objective of this section of the thesis is to understand the effect of the formulation of PCDs on the heat transfer behaviour during melting. To effectively describe the heat transfer of fluids, and to subsequently compare two different fluids, knowledge of the PCD's thermophysical properties is essential. Not only do the thermophysical properties appear as parameters in the calculation of Reynolds number, Nusselt number and Prandtl number, but they also have a significant impact on the heat transfer performance of a fluid. Specifically, the thermal conductivity, dynamic viscosity, density and specific heat capacity. Whilst for single-phase fluids, such as water, the thermophysical properties have been extensively collected and determined to an extremely high accuracy, for multi-component systems this is not the case and often times research is limited to exhaustive analytical experimentation. It is to be noted that all experimental techniques in this investigation are taken for the "static" case at each temperature (e.g. not under flow), and are therefore experimentally determined values and cannot be assumed to be extremely accurate in the case of the fluid under flow. Alongside the experimental values, the effective values as calculated by means of common correlations will be additionally used for comparison. Firstly, the apparent specific heat capacity was calculated from DSC experiments for both formulations. It is to be noted that the calculated values of the apparent specific heat capacity from the DSC are larger compared to the values obtained by energy balance calculations in the experimental test-rig experiments. Figure 5.15 shows both the specific heat capacities of formulation 1 and formulation 2 during the heating and melting process. The apparent specific heat capacities of both formulations were calculated from the DSC experiments using the following equation:

$$cp = \frac{\delta t}{\Delta T}\frac{Q}{m} \tag{5.27}$$

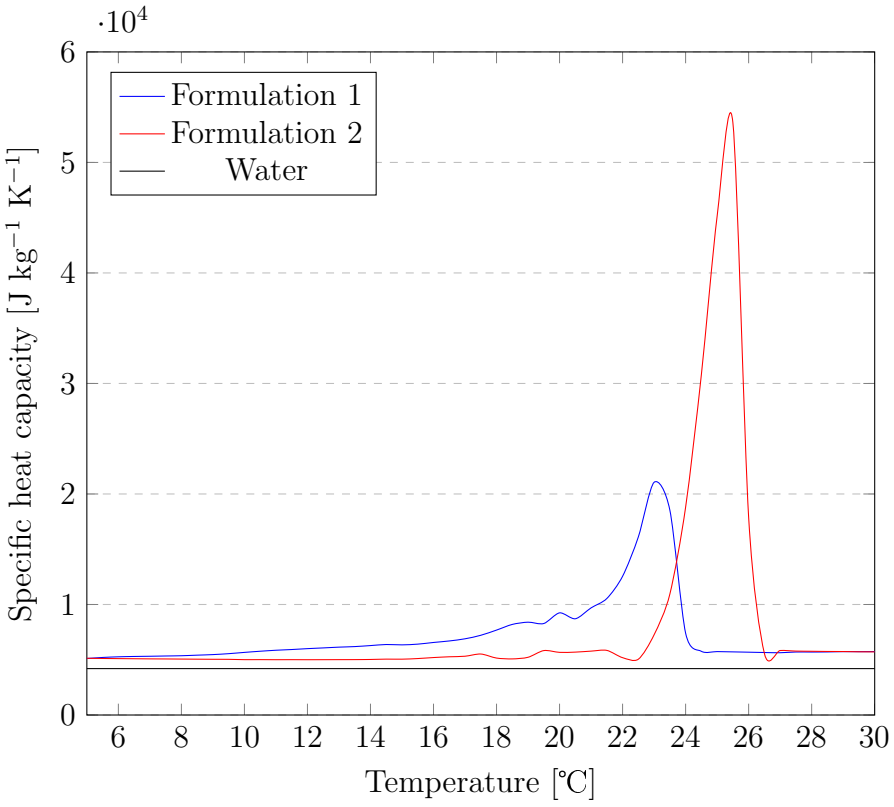

Figure 5.15: The calculated specific heat capacities for formulation 1 and formulation 2 using Equation 5.27 from DSC experiments. Additionally, the apparent specific heat capacity for water is shown for a comparison.

Figure 5.15 shows two main differences in the two formulations, and this is on accounts of the two different PCMs used in their formulations. Firstly, the peak melting temperature of formulation 1 is slightly lower at approximately 24℃ than the peak melting temperature of formulation 2, which is is 25℃. Secondly, the apparent heat capacity of formulation 1 is much lower than for formulation 2, almost three times lower. This is due to the lower enthalpy of fusion of the paraffin-based PCM used in formulation 1, compared to the higher enthalpy of fusion of the fatty acid-based PCM used in formulation 2. An important point to note is that, not only does formulation 2 show higher enthalpies and apparent heat capacities, but the whole formulation (PCM and surfactant system) is completely bio-based, stemming from sustainable feedstocks. The importance of the apparent heat capacity is that for temperature stabilisation applications, a higher apparent heat capacity over a narrower temperature range means that the PCDs will be better. The effect the increased apparent heat capacity has on the heat transfer behaviour of the two formulations will be further acknowledged in the following section of this chapter. The final important thermophysical property which must be taken into consideration when formulating PCDs is the thermal conductivity. In this investigation the thermal conductivity of both formulations was measured using the Linseis THB as described in chapter 3.

In addition to the experimentally determined thermal conductivities, the effective thermal conductivities were also calculated by a common means in the PCD community, through the Maxwell Equation [11]:

$$\lambda_{PCD} = \lambda_{water} \frac{2\lambda_{water} + \lambda_{PCM} - 2\phi(\lambda_{water} - \lambda_{PCM})}{2\lambda_{water} + \lambda_{PCM} + \phi(\lambda_{water} - \lambda_{PCM})} \tag{5.28}$$

where ϕ is the volume fraction of the PCM. Figure 5.16 shows the comparison of the thermal conductivities according to the Maxwell Equation [11] and the measured values of formulation 1 and formulation 2 against those of water taken from CoolProp [10].

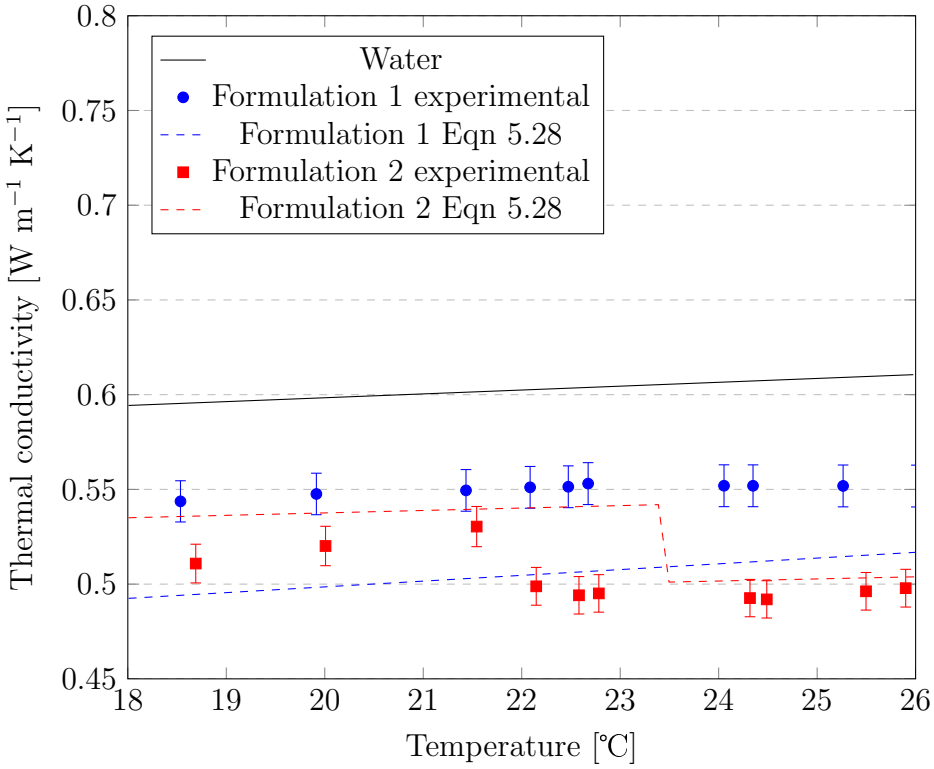

Figure 5.16: The measured thermal conductivities of formulation 1 and formulation 2 alongside the calculated thermal conductivity values for formulation 1 and formulation 2. For comparison, the thermal conductivity of water as given by CoolProp [10] is given.

Figure 5.16 highlights that both formulations have a lower thermal conductivity than water. This is due to both formulations consisting of PCMs that have much lower thermal conductivities than water, with formulation 1 having a slightly higher measured thermal conductivity than formulation 2. Overall, the thermal conductivity of formulation 1 does not appear to be affected by phase change, and it relatively stays the same in the suspension and the emulsion form. This is also what is predicted by the Maxwell equation for formulation 1, due to the manufacturer of the PCM providing the same thermal conductivity when the PCM is in the liquid and the solid state. On the other hand, the thermal

conductivity of formulation 2 decreases on melting, this is normally to be expected as liquids tend to have a lower thermal conductivity than solids. Surprisingly, the decrease in the thermal conductivity upon melting for formulation 2 happens at a much lower temperature than expected, this is due to a calculation-based error. The calculation of the Maxwell equation (Equation 5.29) uses the volume fraction of the PCM, which inherently uses the density of the PCM for it to be calculated. The density decrease occurs from 23℃ according to Figure 5.14. Additionally, the Maxwell equation is an empirical equation based on the effective medium theory and subsequently does not take into account scale-related phenomena, for nano-sized droplets, which include; interfacial resistance, droplet-continuous phase interactions or solid-liquid interactions . Despite this, for formulation 2 the Maxwell appears to precisely predict the thermal conductivity when the PCD is in the emulsion form (when the PCM is liquid), however it overestimates the thermal conductivity in the solid state. This could be due to many factors since the amount of assumptions in the Maxwell equation are high, and it neglects many factors, such as particle size distribution and droplet-droplet interactions [12]. Despite the pronounced use of the Maxwell equation in literature and in research articles studying PCDs, from the experimental data it is recommended that for accurate determination of the thermal conductivity, that an experimental campaign to determine the thermal conductivity of PCDs at different operational temperatures are performed for more accurate heat transfer analysis and Nusselt number calculations. However, it is acknowledged that for calculating the Nusselt number that the static measurements in the laboratory can be used, since the Nusselt number is calculated at the wall where the fluid velocity tends to zero. However, for calculation of the Prandtl number, this may lead to discrepancies, as currently the shear-rate dependence of the thermal conductivity is unknown and thus going forward with the heat transfer analysis, a major assumption made, is that the thermal conductivity used in all analyses is under static conditions.

5.3.2 Local Heat Transfer Behaviour

Once all of the thermophysical properties had been analysed and calculated for all temperatures to be used in the heat transfer investigations, the heat transfer performance of both formulations could ensue. When considering the heat transfer behaviour of PCDs during melting, the most promising applications to be used are for temperature stabilisation. The ability of PCDs to offer isothermal cooling (and thus temperature stabilisation) is a result of the latent heat of phase change associated with the endothermic melting process. As a result of this, the two PCD formulations developed in this investigation were each subjected to three different experimental conditions, alongside water. The operational parameters of each of these experiments can be seen in Table 5.4 for formulation 1 and Table 5.5 for formulation 2.

Table 5.4: Operational parameters used for the three experiments comparing Formulation 1 and water

Experiment number	Heat input (kW)	Inlet temperature PCD (℃)	Reynolds number (-)
1	3	22.5	8400
2	2.2	22.2	2700
3	1.9	22.0	4680

Table 5.5: Operational parameters used for the three experiments comparing Formulation 2 and water

Experiment number	Heat input (kW)	Inlet temperature PCD (℃)	Reynolds number (-)
1	1.9	21.6	10899
2	2.2	21.4	4342
3	4	21.7	8276

During these experiments, the bulk and wall temperatures of both formulations and of water were monitored and plotted, the local heat transfer coefficients were calculated and so where the apparent heat capacities of each formulation in each local tube section in the experimental test-rig. The aim of these experiments was not to directly compare between formulation 1 and formulation 2, but to compare each to water to observe which formulation had the better heat transfer behaviour compared to water. Figure 5.17 shows the local bulk temperatures for formulation 1 and the calculated local heat transfer coefficients for formulation 1.

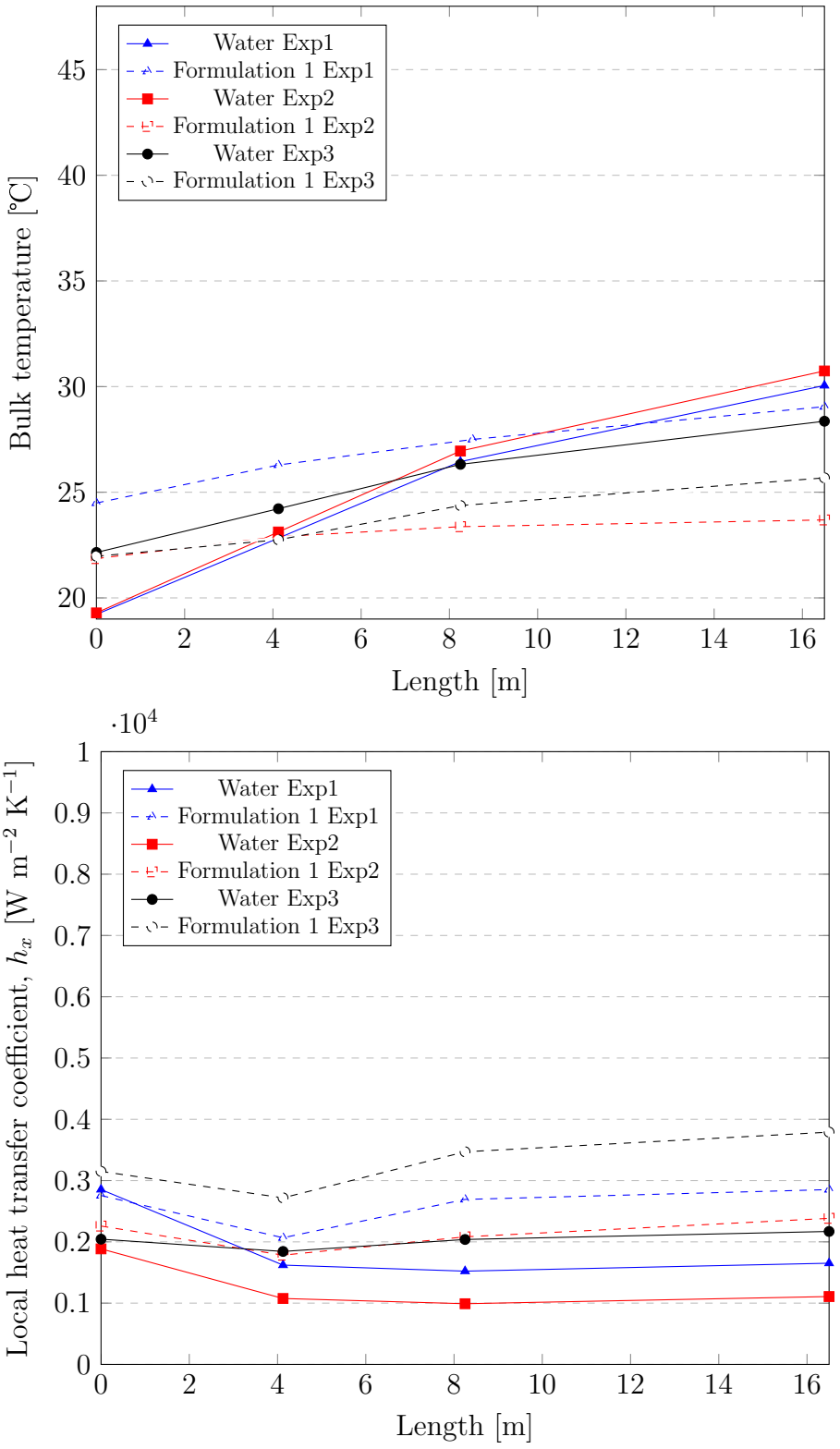

Figure 5.17: Top: The evolution of the bulk temperatures along the length of the cylindrical pipe for formulation 1 Bottom: Local heat transfer coefficients for Formulation 1 and water under the constant velocity comparison basis.

Firstly, from Figure 5.17, the bulk temperatures of formulation 1 are much lower than

for water under the same flow conditions, with a maximum reduction of 8 K along the length of the pipe being found for the conditions in experiment 2. This can be explained by looking at the calculated apparent specific heat capacities for formulation 1, which are shown in Figure 5.18.

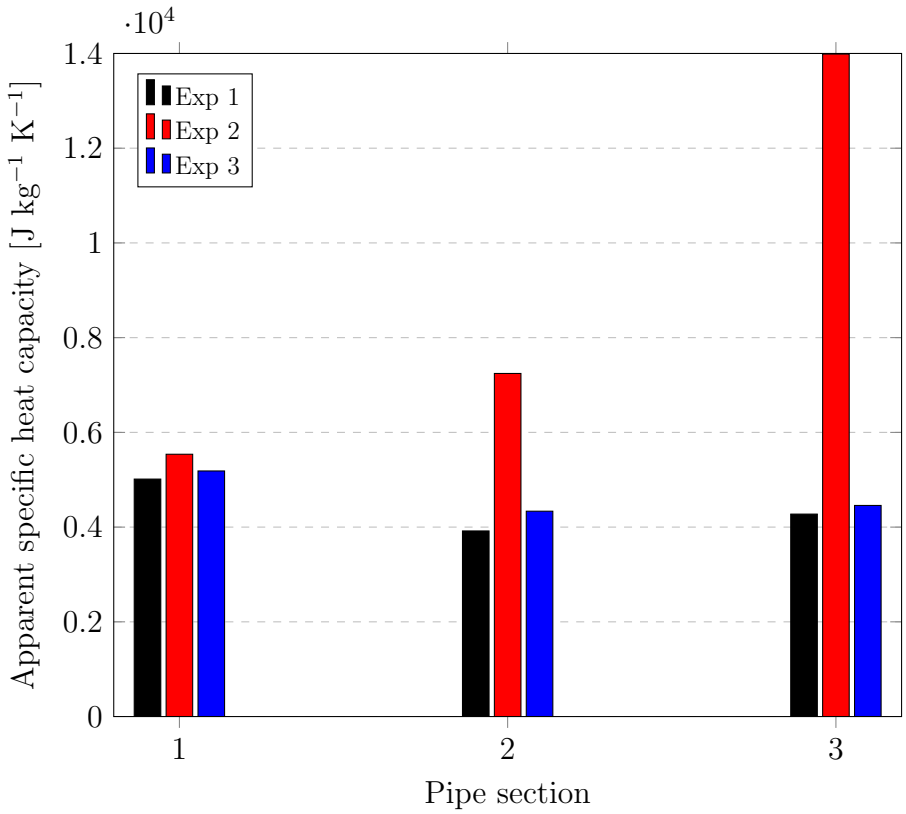

Figure 5.18: The calculated apparent specific heat capacities for formulation 1. Note pipe section 1=0—4.12 m, section 2=4.13—8.25 m and section 3=8.26—16.5 m.

The bar chart in Figure 5.18 demonstrates the apparent specific heat capacities as a function of the pipe section. Experiment 2 has a much larger apparent specific heat capacity in all pipe sections, but especially in pipe section 3. This can be attributed to the lower Reynolds number, meaning a lower mass flow rate and therefore a longer residence time of the PCD in the pipe and subsequently a larger degree of melting and a higher apparent specific heat capacity. The lower mass flow rate (and subsequently Reynolds number) used also explains why even though experiment 2 had the highest apparent specific heat capacity, it does not have the highest local heat transfer coefficients out of all the experiments. This is because the heat transfer behaviour is a function of both the Prandtl number (apparent specific heat capacity) and the flow behaviour (Reynolds number), with lower Reynolds number resulting in lower heat transfer coefficients. On the other hand, on closer inspection of experiment 1, it can be seen that the inlet temperature is extremely close to the melting point of formulation 1, and as a result of this, large

increase in the bulk temperature are observed. This is because the melting process most likely already started when heating up formulation 1 to the correct inlet temperature, and so the bulk temperature is resisting increasing along the pipe length only partially with the latent heat of phase change, and otherwise with the sensible heat of formulation 1. This is reflected in the low apparent specific heat capacities for formulation 1 in the bar chart in Figure 5.18. The local heat transfer coefficient however, is relatively high due to the higher Reynolds number being employed in experiment 1. For experiment 2, the local heat transfer coefficients were the highest, due to the highest Reynolds number being employed in this experiment. Despite this, the increase in the bulk temperatures along the length of the pipe were larger than for experiment 2 and the apparent specific heat capacities were also low, suggesting not much melting occurred along the length of the pipe. This was attributed to the fact that at such high mass flow rates (and thus Reynolds numbers) that the residence time of formulation 1 in the pipe was not so long and therefore the PCD did not have time to fully melt, resulting in incomplete melting along the pipe. Despite all the interplaying parameters that can affect the ability of a PCDs to cool isothermally, in all three experiments formulation 1 showed a lower bulk temperature increase compared to water, higher local heat transfer coefficients and on average, higher apparent specific heat capacities.

From Figure 5.19 we can see the local bulk temperatures and calculated local heat transfer coefficients for formulation 2 and for water for the three experiments.

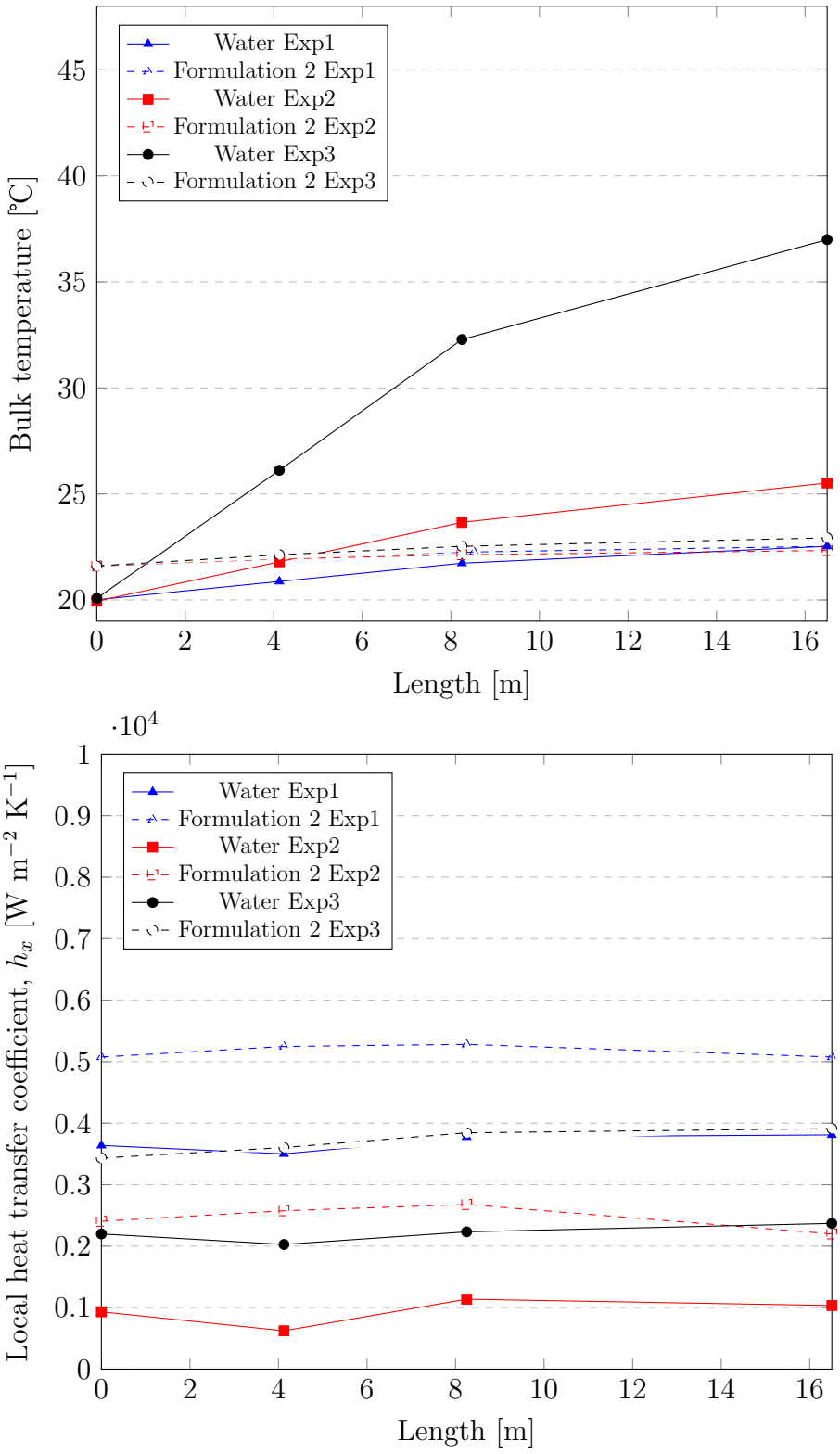

Figure 5.19: Top: The evolution of the bulk temperatures along the length of the cylindrical pipe for formulation 2 and Bottom: Local heat transfer coefficients for formulation 2 and water under the constant velocity comparison basis.

Figure 5.19 demonstrates that for experiment 3, a higher electrical heat input at

the wall was applied and this is reflected in the large temperature increase of the bulk temperature for water. On the other hand, formulation 2 has a very small increase in the bulk temperature across the length of the pipe and as highlighted by Figure 5.20, a large apparent specific heat capacity (more than double water's) across the length of the pipe.

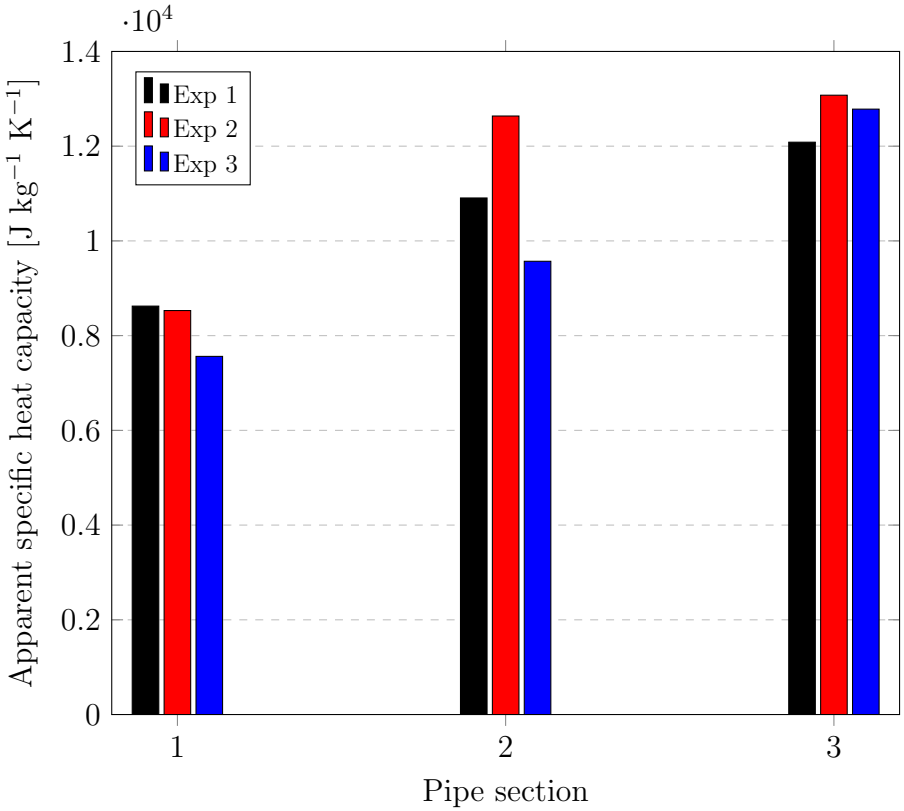

Figure 5.20: The calculated apparent specific heat capacities for formulation 2. Note pipe section 1=0—4.12 m, section 2=4.13—8.25 m and section 3=8.26—16.5.

The local heat transfer coefficient from Figure 5.19 is also almost double water's. The local heat transfer coefficient of formulation 2 is the second highest in experiment 1 out of the three experiments, most likely due to the second highest Reynolds number being employed in that experiment. On the other hand, formulation 2 has the highest apparent specific heat capacities in experiment 2, but has the lowest local heat transfer coefficients, due to a much smaller Reynolds number being used. Experiment 1 has the highest local heat transfer coefficients and the highest Reynolds number used. Overall, in these preliminary experiments, formulation 2 appears to stabilise the bulk temperatures better than formulation 1, and shows much higher apparent specific heat capacities. This could be due to the PCM used in formulation 2, which as shown by the DSC in Figure 5.15, has a higher enthalpy of phase change and subsequently a larger apparent specific heat capacity. However, there are multiple factors playing into the temperature stabilisation abilities of PCDs, and as shown in the analysis of Figures 5.17-5.20, many different op-

erational parameters that must be controlled to ensure the most latent heat of melting is being exploited by each formulation along the length of the pipe. As a result of this, an experimental campaign of over 50 experiments for each formulation was performed; with varying the inlet temperatures, mass flow rates (and thus Reynolds numbers) and electrical heat inputs. The results of these experiments gave the best operational parameters to use for temperature stabilisation using each PCM formulation. Subsequently, the following results from this chapter were performed using the optimised operational conditions. To compare the temperature stabilisation ability of each formulation, the apparent specific heat capacity against the temperature difference between the inlet and the outlet was plotted for both formulation 1 and formulation 2 and can be seen in Figure 5.19.

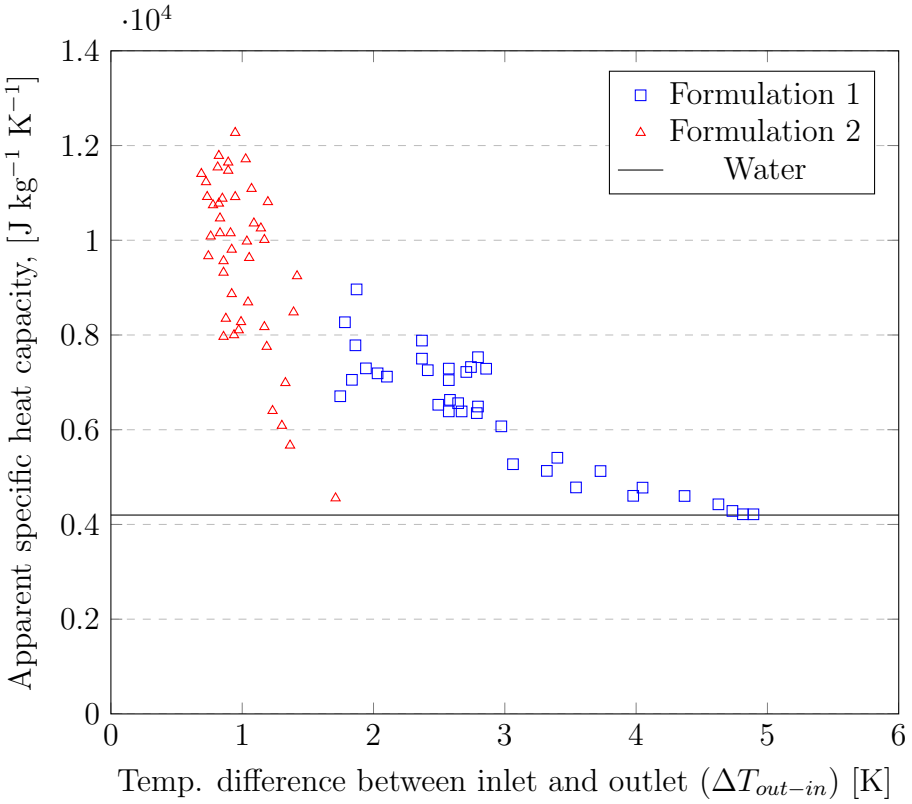

Figure 5.21: The calculated apparent specific heat capacities of both formulation 1 and formulation 2 against the temperature difference between the inlet and outlet of the cylindrical pipe.

From Figure 5.21, it can be seen that higher apparent specific heat capacities and lower temperature differences were found for formulation 2 compared to formulation 1. As aforementioned, this is most likely due to the higher enthalpy of fusion of the PCM used in formulation 2 compared to formulation 1. To investigate the effect of the increased apparent specific heat capacity obtained with formulation 2 on the heat transfer behaviour, the local Nusselt numbers were plotted for each formulation, for each pipe

section against the Reynolds number calculated using the temperature-averaged thermophysical properties for each pipe section (this includes using the densities and the dynamic viscosities of the average temperature between T_{in} and T_{out} of each pipe section). This can be observed in Figure 5.22.

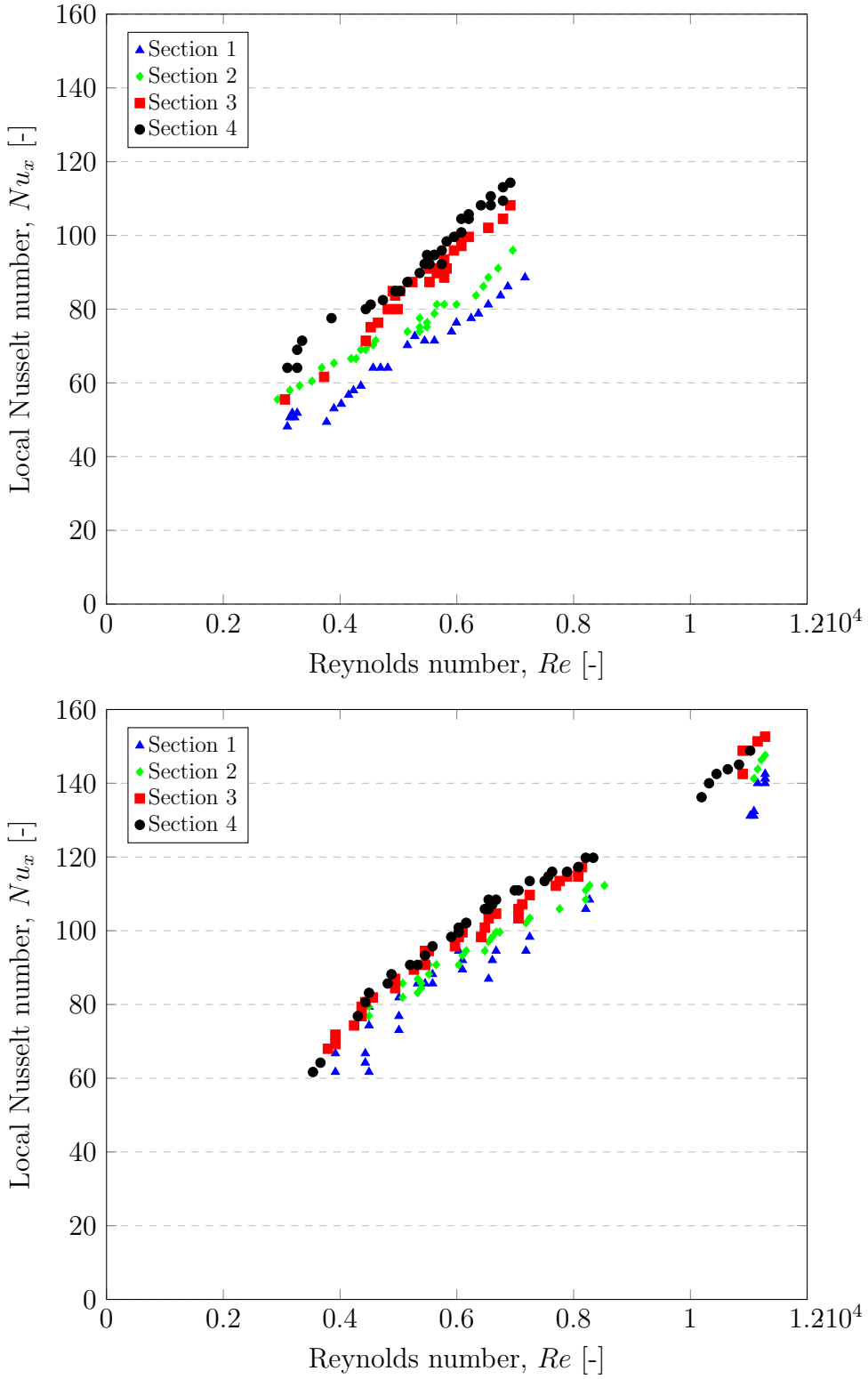

Figure 5.22: The evolution of the local Nusselt numbers, Nu_x with the Reynolds number for each cylindrical pipe section for Top: Formulation 1 and Bottom: Formulation 2.

Figure 5.22 shows an interesting trend of an increase in the local Nusselt numbers with an increase in the pipe section for both formulations. This is hypothesised to be due to an

increased degree of melting along the length of the pipe. This is due to the fact that the apparent specific heat capacity is the highest in the last section of the pipe, which results in a higher Prandtl number, which results in a higher Nusselt number. Furthermore, at the same Reynolds number, the local Nusselt numbers for formulation 2 are higher than for formulation 1, indicating that formulation 2 has a better heat transfer performance. For further distinction of this, the overall heat transfer behaviour of both formulations was analysed.

5.3.3 Overall Heat Transfer Behaviour

The average heat transfer coefficients and average Nusselt numbers for water, formulation 1 and formulation 2 were calculated by averaging the local heat transfer coefficients and local Nusselt numbers for each fluid over the length of the pipe. The average heat transfer coefficients and average Nusselt numbers for all fluids can be seen in Figure 5.213.

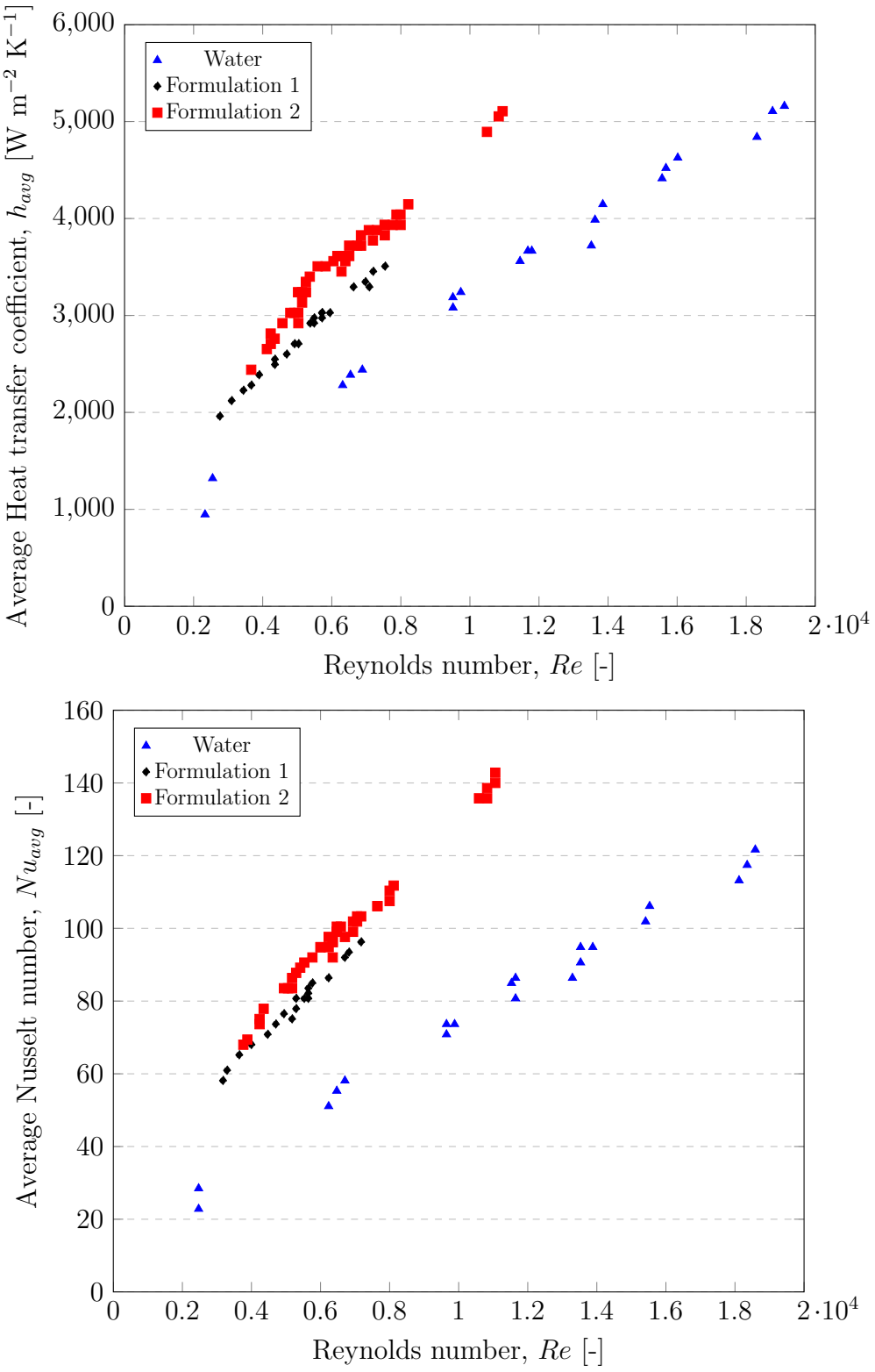

Figure 5.23: Top: The average heat transfer coefficients against the Reynolds number for Formulation 1, Formulation 2 and water and Bottom: The average Nusselt number for Formulation 1, Formulation 2 and water.

Figure 5.23 displays that both formulation 1 and formulation 2 have higher average

heat transfer coefficients and average Nusselt numbers compared to water under the same comparison criteria of constant Reynolds number. The results also indicate that formulation 2 has an improved heat transfer performance than formulation 1 by having higher average heat transfer coefficients and average Nusselt numbers. The increased heat transfer performance of both formulation 1 and formulation 2 compared to water is most likely due to the enhanced apparent specific heat capacity as a result of the melting process of the PCM particles dispersed within the water of both formulations and the higher enthalpy of fusion of formulation 2 results in a better performance than formulation 1. The commonly used Hausen-Gnielinski correlation for turbulent flow in a cylindrical pipe was used to calculate average Nusselt numbers to compare to the experimentally determined Nusselt numbers for both formulation 1 and formulation 2. The Hausen-Gnielinski correlation can be seen in 5.24 and using this correlation, the calculated Nusselt numbers alongside the experimentally obtained Nusselt numbers were plotted and their deviation can be observed in Figure 5.22.

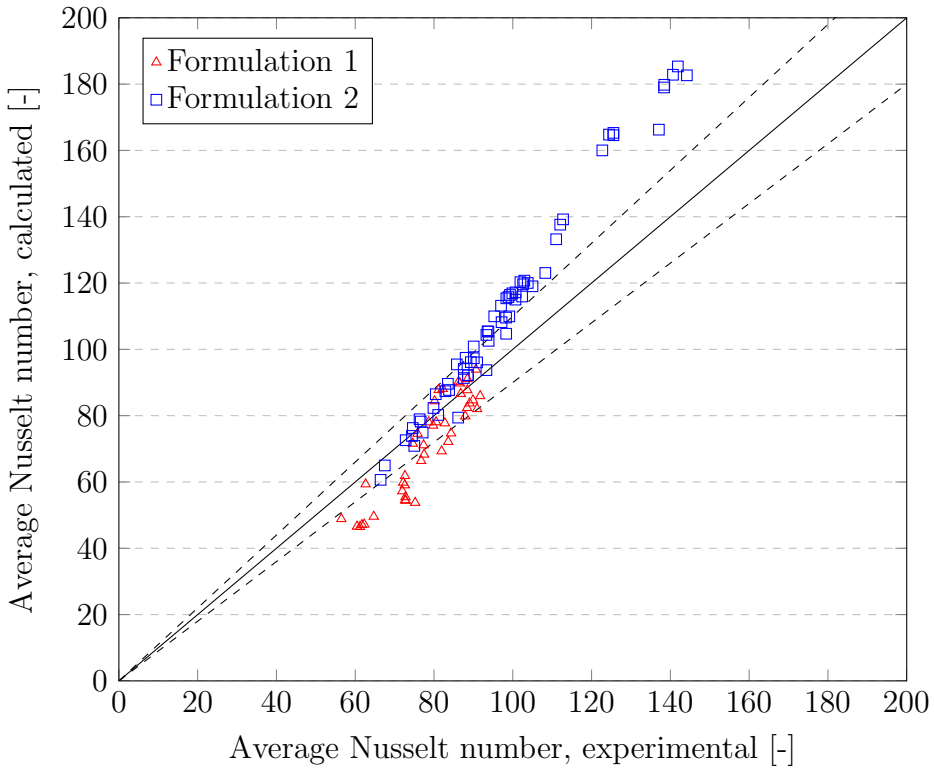

Figure 5.24: The calculated Nusselt numbers using the Hausen-Gnielinski correlation (see Eqn 5.23) against the experimentally determined Nusselt numbers for both formulation 1 and formulation 2.

Figure 5.24 shows that the Hausen-Gnielinski equation over predicts the average Nusselt numbers compared to the experimentally determined Nusselt numbers for both formulations given the following conditions: the Reynolds number is calculated based on the

shear-rate dependent and temperature dependent dynamic viscosity, the temperature-dependent density is used and secondly and for the Prandtl number, the thermal conductivity is taken from the static analytical experiments. For accuracy, the thermal conductivity of both formulations under shear rate is unknown and so here the value of the Prandtl number was optimised and a correction factor was produced for each different Reynolds number for both formulation 1 and formulation 2. This was achieved by setting the $Nu_{H\&G}$ equal to Nu_{exp} with an unknown factor v as shown below:

$$Nu_{exp} = 0.012(Re^{0.87} - 280)vPr^{0.4}(1 + (\frac{d}{L})^{2/3}) \tag{5.29}$$

Subsequently, the equation was re-arranged for v, the correction factor to the Prandtl number, and Figure 5.24 displays v for each Reynolds number for each formulation.

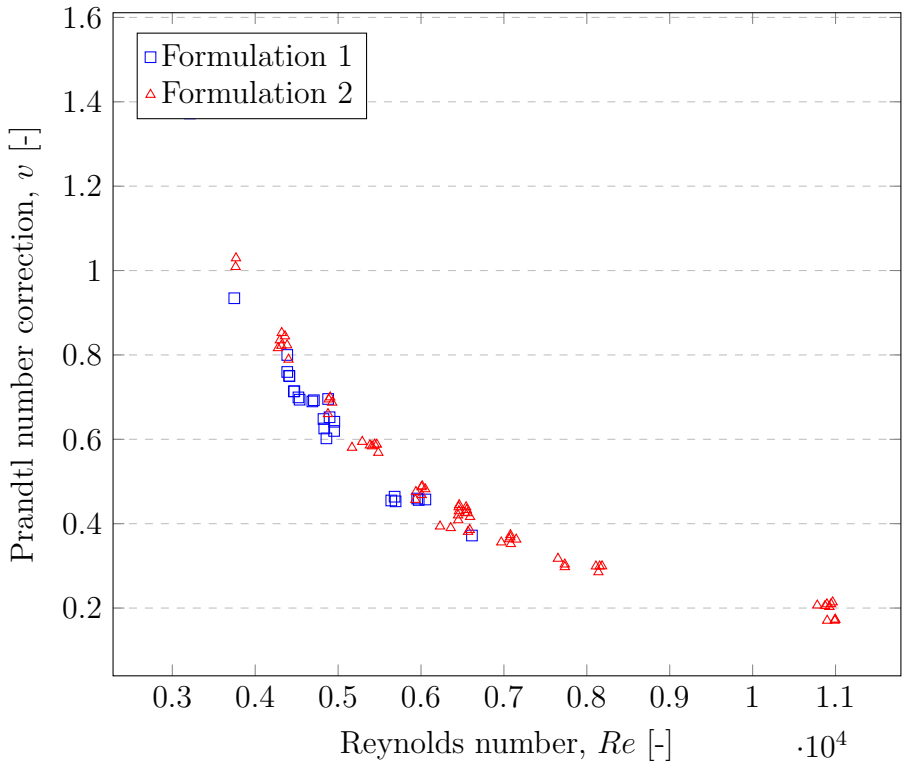

Figure 5.25: The calculated Prandtl number correction factor, v, against the Reynolds number for both Formulation 1 and 2.

As suspected, with an increase in shear-rate, the correction factor decreases, meaning the Prandtl number will also decrease. This is to be expected, as with an increase in the shear-rate, the thermal conductivity is expected to increase. The Prandtl correction factors were then applied to the Prandtl number and Figure 5.25 displays the re-calculated Nusselt numbers using the Hausen Gnielinski correlation with the corrected Prandtl numbers against the experimentally determined Nusselt numbers.

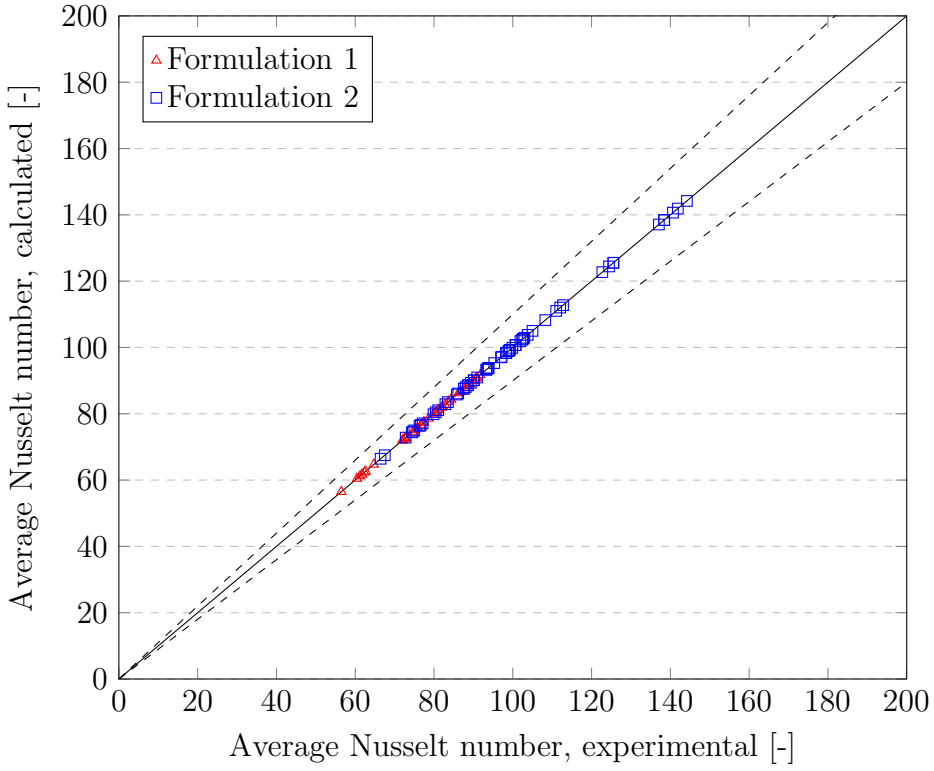

Figure 5.26: The calculated Nusselt numbers using the Hausen-Gnielinski correlation (see Eqn 5.23) against the experimentally determined Nusselt numbers for both formulation 1 and formulation 2 taking into consideration the Prandtl correction factor

These Prandtl correction factors are valid for both formulation 1 and formulation 2. However, with further investigation in the future, this methodology can act as a design guideline for future PCDs, whereby the thermal conductivity of the PCD under flow is unknown.

5.4 Conclusions

Overall, this chapter focuses on the heat transfer and rheological behaviour of two differently formulated phase change dispersions during melting. Firstly, a detailed explanation of the experimental test-rig used for the determination of the heat transfer performance of the two formulations was given and the test-rig was validated with water. Rheological analysis showed that both formulation 1 and formulation 2 showed non-Newtonian, shear-thinning behaviour whereby the degree of non-Newtonian behaviour was affected in both formulations by the temperature. In formulation 2, due to the nature of the surfactant system used, the melting process also affected the rheological behaviour and the degree of non-Newtonian exhibited by the fluid. Alongside this, pressure drop measurements showed that both fluids showed only slightly higher pressure drops than water at high

Reynolds numbers, due to the shear-thinning behaviour of the fluids. The thermophysical properties of both fluids, such as the density, dynamic viscosity, thermal conductivity and apparent specific heat capacity were experimentally determined for both fluids at different temperatures during the melting process. The higher enthalpy of fusion of the PCM used in formulation 2 resulted in formulation 2 having higher apparent specific heat capacities and ultimately a better heat transfer performance, in terms of higher average heat transfer coefficients and higher average Nusselt numbers than formulation 1. Despite this, both formulation 1 and formulation 2 had improved heat transfer coefficients and Nusselt numbers than compared to water. Finally, a modified version of the Hausen-Gnielinski equation, with a scaled Prandtl number, to account for the shear-rate dependence of the thermal conductivity calculated the experimentally determined average Nusselt number for both formulation 1 and formulation 2 within ±10%.

References

[1] Volker Gnielinski. "New equations for heat and mass transfer in turbulent pipe and channel flow". In: *Int. Chem. Eng.* 16.2 (1976), pp. 359–368.

[2] Helmuth Hausen. "Heat Transfer in Counterflow, Parallel Flow and Cross Flow." In: *McGraw-Hill Book Company, xx+ 515, 23 x 16 cm, illustrated, pounds sterling 45. 25* (1983).

[3] Stuart W Churchill. "Comprehensive correlating equations for heat, mass and momentum transfer in fully developed flow in smooth tubes". In: *Industrial & Engineering Chemistry Fundamentals* 16.1 (1977), pp. 109–116.

[4] BS Petukhov. "Heat transfer and friction in turbulent pipe flow with variable physical properties". In: *Advances in heat transfer*. Vol. 6. Elsevier, 1970, pp. 503–564.

[5] L. Huang and M. Petermann. "An experimental study on rheological behaviors of paraffin/water phase change emulsion". In: *Int. J. Heat Mass Transf.* 83 (2015), pp. 479–486.

[6] Yijie Zhuang, Zibiao Liu, and Wenbin Xu. "Experimental investigation on the non-Newtonian to Newtonian rheology transition of nanoparticles enhanced phase change material during melting". In: *Colloids and Surfaces A: Physicochemical and Engineering Aspects* 629 (2021), p. 127432.

[7] Mohammad Ghalambaz, SAM Mehryan, Ali Tahmasebi, and Ahmad Hajjar. "Non-Newtonian phase-change heat transfer of nano-enhanced octadecane with mesoporous silica particles in a tilted enclosure using a deformed mesh technique". In: *Applied Mathematical Modelling* 85 (2020), pp. 318–337.

[8] Poppy O'neill, Jocelyn Bonjour, Ludger Fischer, and Rémi Revellin. "Experimental study on the heat transfer and rheology of a phase change dispersion during crystallization". In: *13th IIR PCM Conference*. 2021.

[9] Rajendra P Chhabra. "Non-Newtonian fluids: an introduction". In: *Rheology of complex fluids*. Springer, 2010, pp. 3–34.

[10] Ian H. Bell, Jorrit Wronski, Sylvain Quoilin, and Vincent Lemort. "Pure and Pseudo-pure Fluid Thermophysical Property Evaluation and the Open-Source Thermophysical Property Library CoolProp". In: *Industrial & Engineering Chemistry Research* 53.6 (2014), pp. 2498–2508.

[11] James Clerk Maxwell. *A treatise on electricity and magnetism*. Vol. 1. Clarendon press, 1873.

[12] David Cabaleiro, Filippo Agresti, Simona Barison, Marco A Marcos, Jose I Prado, Stefano Rossi, Sergio Bobbo, and Laura Fedele. "Development of paraffinic phase change material nanoemulsions for thermal energy storage and transport in low-temperature applications". In: *Applied Thermal Engineering* 159 (2019), p. 113868.

Chapter 6

Experimental investigation into the heat transfer and rheological behaviour during crystallisation

Thus far in literature, studies on the heat transfer and rheological behaviour of PCDs during crystallisation are extremely limited and are subsequently poorly understood. It was suggested by Morimoto et al. [1] that this was due to the unpredictability of complex crystallisation kinetics as a result of supercooling making the prediction of crystallisation temperatures difficult. As a result of this, this chapter is dedicated to understanding the heat transfer and rheological behaviour of a PCD during the cooling, and crystallisation process. This is because it is essential for the design of heat exchangers, piping networks and cooling systems, which will host PCDs, that a full understanding of the whole melt-crystallisation behaviour is achieved. As a result of this, this chapter presents an experimental investigation into the rheological and heat transfer behaviour of a PCD during the cooling and crystallisation process. This chapter includes the description of the experimental test-rigs used to determine the rheological behaviour of Formulation 1 from Chapter 5, and the heat transfer behaviour, the validation of the test-rigs with water, the results for formulation 1 and a detailed explanation of the phenomena observed.

6.1 Materials and Methodology

Formulation 1, as shown in Table 5.1 in Chapter 5 is the PCD used for all the analysis presented throughout this chapter.

6.1.1 Rheology test-rig

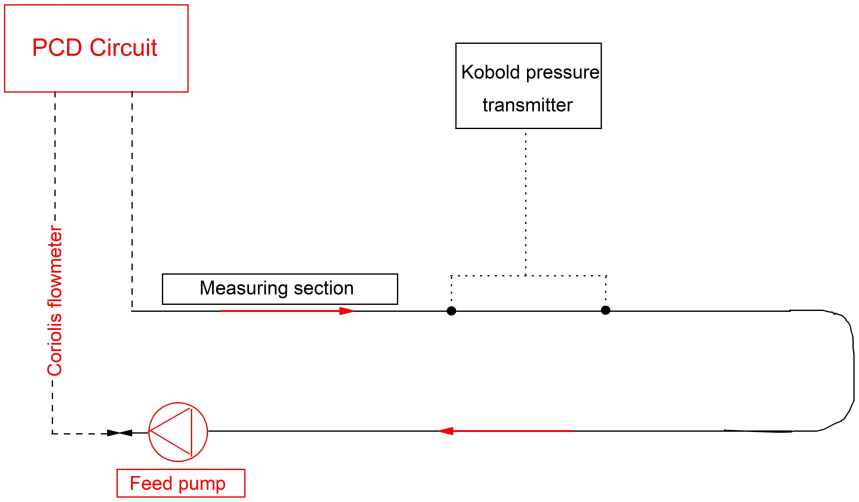

Figure 6.1: Schematic of the experimental test-rig to determine the rheological behaviour.

The experimental test-rig used for the rheological experiments can be seen in Figure 6.1. The measuring section is composed of copper tubing with an inner diameter of 8 mm. The PCD is pumped around the circuit in the direction shown in Figure 6.1 with a PQA60 Pedrollo pump. A Kobold smart pressure transmitter was installed with pressure tapings 1 m apart as shown in Figure 6.1 to measure the pressure drop of the PCDs. To understand the rheological behaviour of formulation 1 during cooling, the temperature, mass flow rate and pressure drop were all measured and the specifications of all the installed sensors used for the rheological characterisation can be seen in Table 6.1.

Table 6.1: Specifications of the installed sensors used in the rheological investigation

Sensor	Manufacturer	Type	Range	Uncertainty
Flow rate, $\dot{m}$	Micromotion	Coriolis	0—1.5 kg s^{-1}	± 0.006 kg s^{-1}
Pressure drop, Δp	Kobold	Smart Pressure Transmitter	1—600 bar	± 0.015 bar
Temperature ($T_{in,PCD}$ and $T_{out,PCD}$)	-	Type K thermocouples	273—323 K	± 0.3 K

The procedure for determining the rheological behaviour was as follows, the mass flow rate of the PCD was varied using a manual control valve and in consequence so was the shear rate acting on the PCD. This was performed at different operational temperatures of the PCD (20—5 ℃) by cooling the PCD down to the correct temperature for each experiment using an ethanol cooling loop which is discussed further in Section 6.1.2.

Quantities of interest

The main objective of the rheological investigation was to understand the flow behaviour of the PCD, its viscosity and subsequently the pressure drop. This is because the pumping

power consumption of PCDs accounts for a large part of the energy consumed for PCD applications, especially when viscosities are higher, which most often occurs at lower temperatures and during crystallisation. For the experimental test-rig in Figure 6.1, the shear stress (τ) and the shear rate ($\dot{\gamma}$) were calculated using:

$$\tau = \frac{D\Delta p}{4l} \tag{6.1}$$

$$\dot{\gamma} = \frac{3n+1}{4n}\frac{8u}{D} \tag{6.2}$$

where D is the pipe diameter, l is the length between the pressure sensors, Δp is the pressure drop and u is the flow velocity. Subsequently, the n and K coefficients were calculated for formulation 1 during cooling using Equation 5.25 and plotting graphs such as the one in Figure 5.11.

Additionally, from the experimentally determined values of the pressure drop (Δp), the dimensionless friction factor (f) were determined using the Darcy-Weisbach equation:

$$f = \frac{\Delta p}{\frac{l}{D}\frac{\rho}{2}u^2} \tag{6.3}$$

6.1.2 Heat transfer test-rig

The purpose of the heat transfer test-rig was to characterise the heat transfer of a PCD, during the cooling process, flowing through a rectangular channel under transient cooling. The cooling of the rectangular channel, through which the PCD flows was achieved by a circulating ethanol loop, which flowed in an external channel counter current to the PCD flow. Figure 6.2 shows the schematic of the PCD circuit in the experimental test-rig alongside the PCD flow direction.

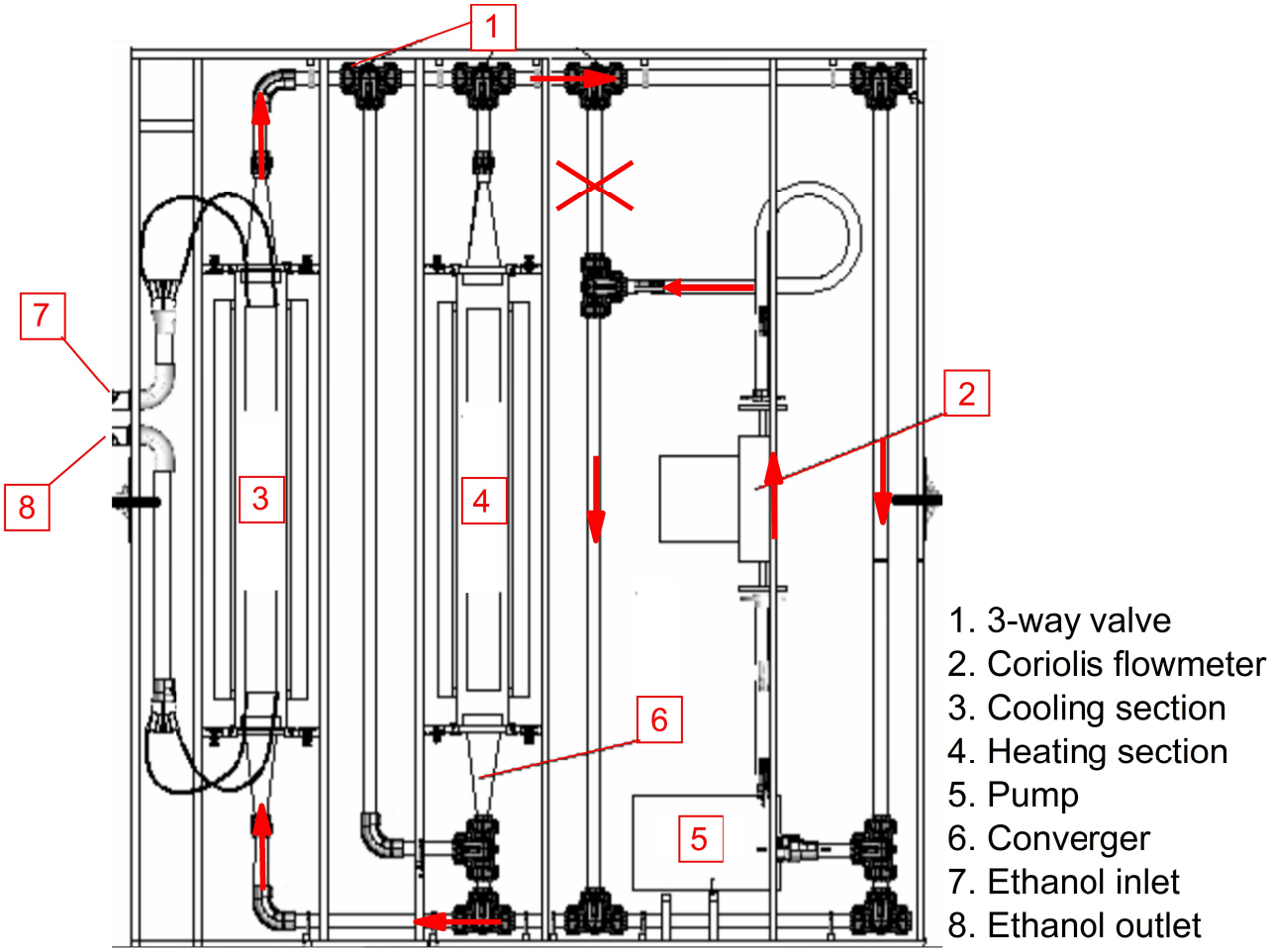

Figure 6.2: Schematic of the test-rig used to determine the heat transfer performance of PCDs.

The PCD circuit is comprised of transparent PVC tubes with an internal diameter of 56 mm, with three-way valves to control the PCD flow direction. A vortex pump (TURO EGGER T21-32 HF4 LB1) is used for the flow of the PCD and the flow rate is adjusted using a frequency converter (DANFOSS type VL103) with a rotational speed of 600—3000 rev min^{-1} (10-50 Hz). There are two main measuring sections on the experimental test-rig, the heating section (where the PCD is heated up) and the cooling section (where the PCD is cooled down using the circulating ethanol loop). The measuring section used in this investigation is the cooling section. The cooling section is composed of three channels, a central channel where the PCD flows and the two outer channels where the ethanol flows in counter current. The PCD enters through the bottom of the central channel and exits through the top of the channel as shown in Figure 6.2. The PCD channel consists of two stainless steel (304) plates (width = 130 mm, thickness = 4.5 mm and length = 1100 mm) with a thickness between them of 6 mm which is set by two polyethylene spacers. The two outer channels (ethanol channels) are 1000 mm long, 80 mm wide and 4 mm thick. The ethanol flow through these channels is ensured to be uniform with the aid

of five supply tubes at the inlet and outlet. To understand the heat transfer behaviour of formulation 1 during cooling, the temperatures, mass flow rates and densities were measured. A detailed description of each measurement is given in the following sections.

Temperature measurements

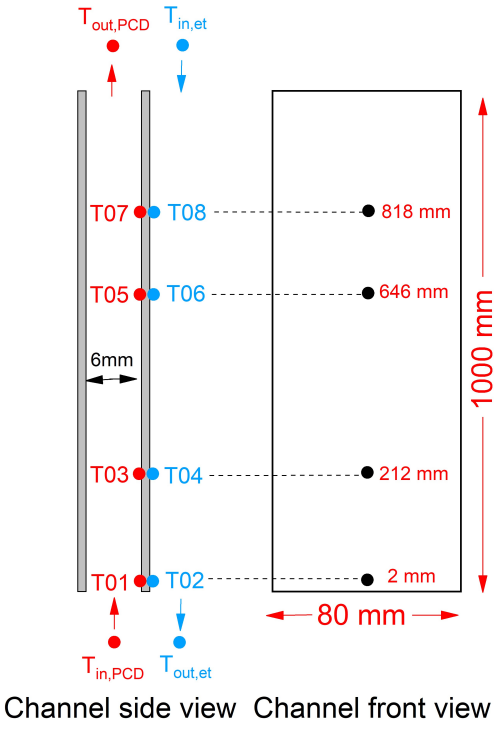

Figure 6.3: Schematic of the test-section used to determine the heat transfer performance of PCDs.

To determine the heat transfer behaviour, temperature sensors were installed at the inlet and outlets of the ethanol and water channels and along the walls as seen in Figure 6.3. The bulk inlet and outlet temperatures of the ethanol and PCD ($T_{in,PCD}$, $T_{out,PCD}$, $T_{in,et}$ and $T_{out,et}$ in Figure 6.3) were measured with type K thermocouples, which were calibrated against the temperature of a resistance temperature detector (RTD) over the temperature range used in this investigation. Type K thermocouples were also installed to measure the inner wall temperatures of the PCD cooling section (T01, 03, 05 and 07 in Figure 6.3) and the ethanol channel inner wall (T02, 04, 06 and 08 in Figure 6.3). The wall temperatures were calibrated against the reference RTD and static measurements showed that all thermocouples (bulk inlet and outlet and wall) were within 0.3 K of each other. The thermocouples were paired on both sides of the measuring wall (on the ethanol inner wall and the PCD inner wall). It is to be noted that there is symmetry within the channel, whereby it is equipped with the same eight thermocouples on either side of the plate (so that the plate has a total of 16 thermocouples) to observe the symmetry of the

temperature profile along the channel. This also acts as an additional mean to reinforce the temperature measurements if one thermocouple along the length of the plate is not working.

Mass flow rate measurements

The mass flow rate of the PCD and ethanol flowing through the cooling loop is performed using two different flow meters. The flow rate of the PCD is measured using a Coriolis mass flow rate meter (Micro motion) which is placed just after the pump and can be seen in Figure 6.2 showing the schematic of the experimental test set-up. It directly measures the mass flow rates without the need for correction. The mass flow rate of the ethanol in the cooling loop is measured using a vortex flow meter (Rosemount 8800) which measures the frequency of the vortex's detachment which is produced by a bar that is perpendicular to the direction of the ethanol flow. The flow meter subsequently converts the frequency into a 4-20 mA signal that is converted into a flow rate by the central data acquisition.

Density measurements

The density measurements are performed using the transmitter used to show the mass flow rate of the PCD which is equipped with a digital output that provides a frequency (in the range of 0-40 kHz) that is proportional to the density of the fluid. Taking the frequency output and the density displayed by the transmitter, the density of the PCD flowing through the heat transfer test-rig can be determined. To determine the accuracy of the density measurements as measured with the transmitter, the values of water at different temperature are plotted against those values given with CoolProp, and from this, it can be seen that the variation in the density for all temperatures between the CoolProp values and the transmitter values are less than 5% and subsequently show that the density can be measured quite accurately using the transmitter.

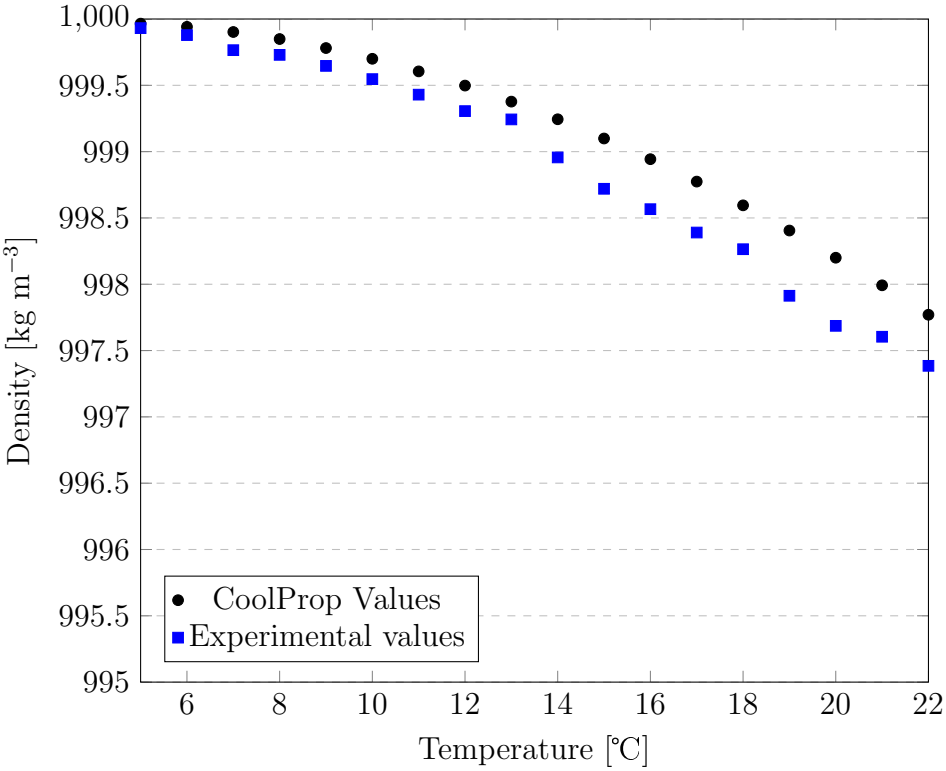

Figure 6.4: Comparison between the density values for water as given by CoolProp [2] and experimentally obtained values.

Quantities of interest

One of the objectives of this experimental work was to investigate the heat transfer performance of a PCD during crystallisation. Firstly, the local heat transfer coefficients (h_x) were calculated using:

$$h_x = \frac{\phi_x}{T_{b,PCD,x} - T_{w,PCD,x}} \tag{6.4}$$

where ϕ_x is the local wall heat flux at the axial location x, $T_{b,PCD,x}$ is the bulk mixed mean temperature of the PCD at the axial location x, and $T_{w,PCD,x}$ is the inner wall temperature of the PCD channel at the axial location x (T01/T03/T05/T07). ϕ_x is calculated according to:

$$\phi_x = \frac{\lambda_{plate}}{e}(T_{w,PCD,x} - T_{w,et,x}) \tag{6.5}$$

where λ_{plate} is the thermal conductivity of the plate, which was taken to be 15 W m^{-1} K^{-1}, e is the thickness of the plate (4.5 mm), and $T_{w,et,x}$ is the inner wall temperature of the ethanol channel at the axial location x (T02/T04/T06/T08). The bulk mixed mean temperatures of the PCD ($T_{b,PCD,x}$) were calculated using:

$$T_{b,PCD,x} = T_{b,PCD,x-1} - \left(\frac{1}{\frac{\dot{m}}{2}c_p}\right)\frac{\phi_{x-1} + \phi_x}{2}(x_i - x_{i-1})a \tag{6.6}$$

where $\dot{m}$ is the mass flow rate of the PCD, x is the distance from the inlet, i=01/03/05/07 (as shown in Figure 3) and a is the width of the channel. It is to be noted that for x=0 (the entrance of the PCD channel), the bulk mixed mean temperature of the fluid, $T_0 = T_{in,PCD}$, and for x = 1000 mm (the outlet of the channel), $T_{1000} = T_{out,PCD}$. From h_x, the local Nusselt numbers (Nu_x) were calculated using:

$$Nu_x = \frac{h_x D_h}{\lambda_{PCD}} \tag{6.7}$$

where D_h is the hydraulic diameter of the channel (0.011 m) and λ_{PCD} is the thermal conductivity of the PCD. The average Nusselt number (Nu_{avg}) was thus calculated by integrating the local Nusselt numbers over the entire length of the plate as follows:

$$Nu_{avg} = \frac{1}{L}\int_0^L Nu(x)\,dx \cong \frac{1}{L}\left[\sum_{i=1}^{4}\frac{Nu_i + Nu_{i+1}}{2}(x_{i+1} - x_i) + x_{07}\right] \tag{6.8}$$

Validation with water

To verify that the measuring instruments were functioning well, verification experiments with water were performed. Firstly, an experiment was conducted at ambient temperature under stationary conditions (no flow within the water or the ethanol circuits) to observe the deviation in temperatures on each side of the plates in the channel. The channels are positioned vertically and the fluids were stationary. The experiment was performed at an ambient temperature of approximately 20℃ without cooling or heating for the static single-phase HTF (water). Figure 6.5 shows the evolution of the temperatures on each side of the plates (A/B and C/D) representing the temperatures of the ethanol and water sides respectively. The maximum deviation observed between the thermocouples on each side of the plate was in the order of 0.3K which is below the uncertainty of K-type thermocouples and therefore suggests that the thermocouples are valid in representing fluxometers for future measurements. Due to the stratification within the channel, the temperature difference between the inlet of the channel and the outlet (x = 2mm and x = 860mm) was also approximately 0.3 K. Additionally, compared to the resistance temperature detector (RTD) which was used as an external measuring thermocouple, the values of all temperature sensors deviated less than 0.3 K.

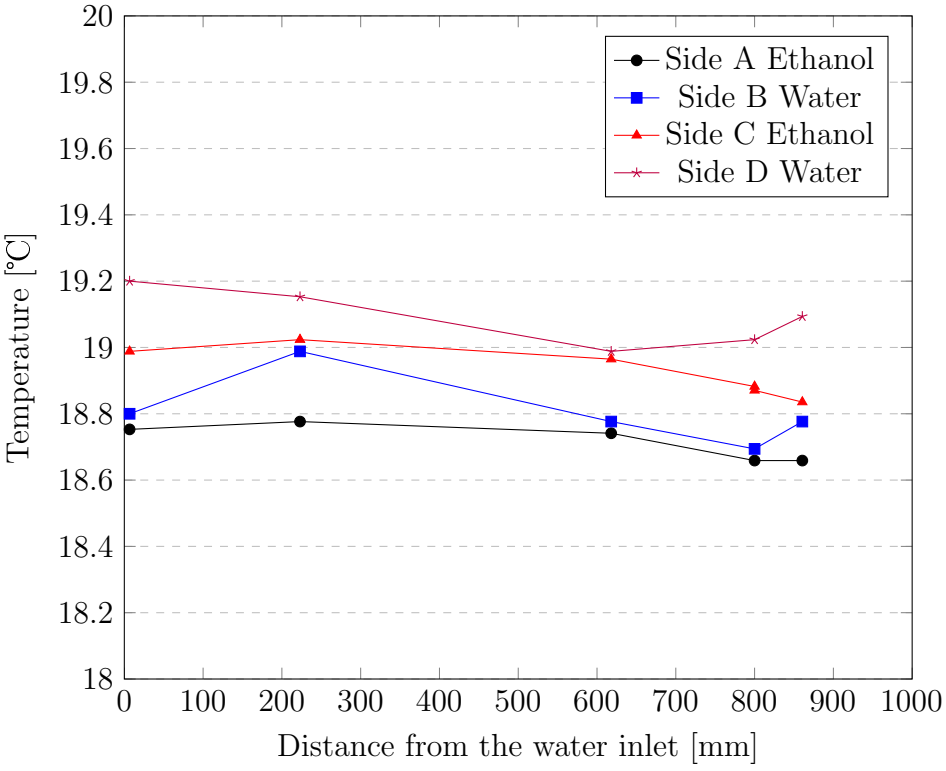

Figure 6.5: Temperature measurements taken for the thermocouples along each side of the plate (for both the ethanol and water wall-side temperatures of the channel) under the static condition (no flow in the ethanol or water channel).

Subsequently, to validate the whole measuring system for the PCD, water was again used as single-phase HTF and experiments were performed under flow (flow in both the ethanol and water circuits). The thermal balance between the water and the ethanol was checked in the cooling channel. An investigation was performed with a mass flow of the water between 760 and 3235 kg h^{-1}, with an inlet temperature into the channel between 21.7 and 23.1℃ . The mass flow of the alcohol was fixed at a value of 4121 kg h^{-1} and an inlet temperature of -15℃ was used. The thermal power for the water and the alcohol are given by the following energy balances respectively:

$$\dot{Q}_{water} = \dot{m}_{water} cp_{water} (T_{water,in} - T_{water,out}) \tag{6.9}$$

and

$$\dot{Q}_{ethanol} = \dot{m}_{ethanol} cp_{ethanol} (T_{ethanol,out} - T_{ethanol,in}) \tag{6.10}$$

In Figure 6.6 the results from this experiment can be seen. The maximum deviation between the values of the thermal power was in the order of 15%. The deviation between the energy balances on the ethanol and water side becomes more apparent at mass flow rates higher than 2250 kg h^{-1}. However, despite this deviation it is still considered to be

in the acceptable range and going forward with PCD experiments, mass flow rates below 2500 kg h^{-1} are to be used.

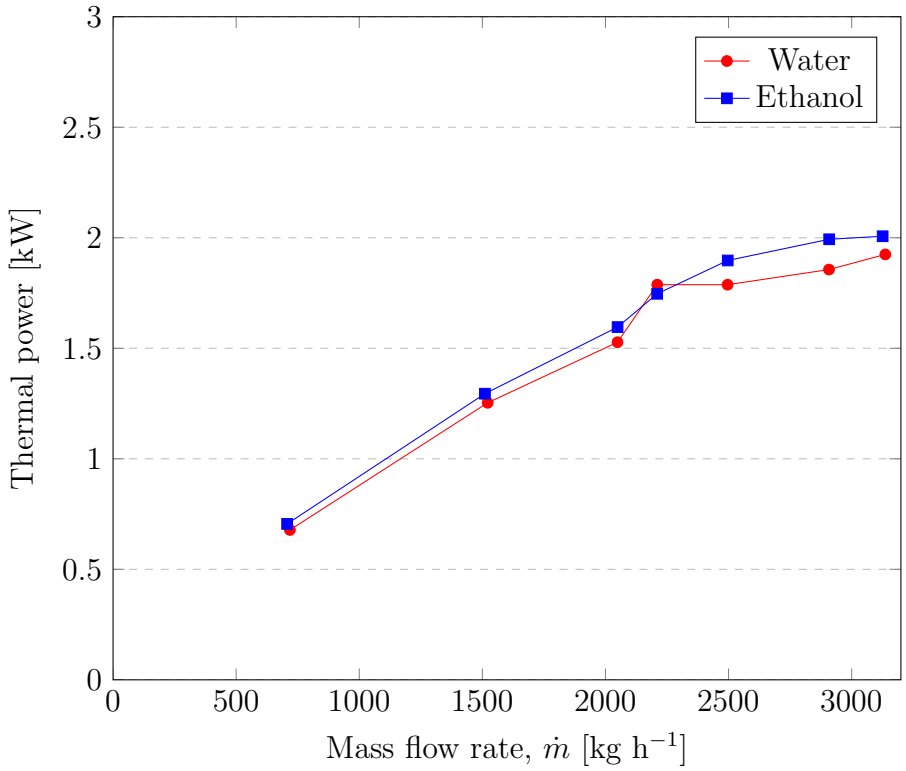

Figure 6.6: Thermal power exchange under steady-state for water and for a range of mass flow rates

After the validation of the experimental equipment was performed, the experimental methodology was validated by firstly calculating the local heat transfer coefficients of water at different mass flow rates (and thus Reynolds number) for the same inlet temperature, which was approximately 18℃. The mass flow rates chosen coincided with Reynolds numbers which were in the laminar flow regime, so the test-rig could be properly validated and correlations applied without considering the effect of turbulence. The values of the local heat transfer coefficients were calculated using Equation 6.4. Ten experiments were performed with water during cooling in the cold channel and the local heat transfer coefficients for the different Reynolds number as a function of distance from the water inlet can be seen in Figure 6.7.

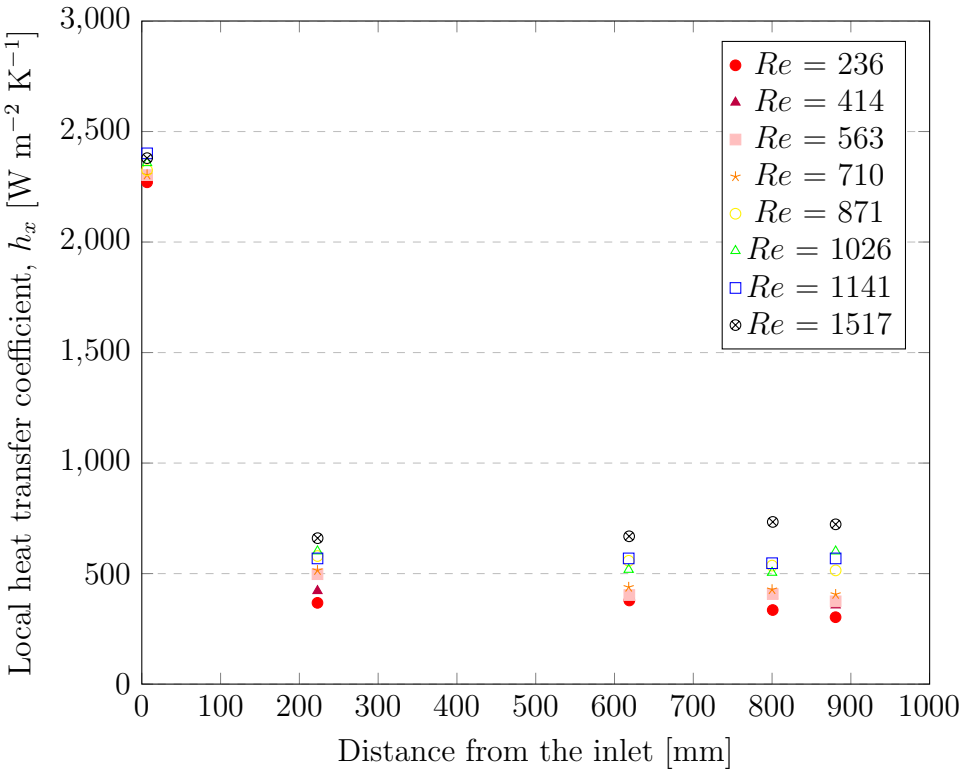

Figure 6.7: Local heat transfer coefficients for water at a range of different Reynolds numbers.

From Figure 6.7, it is evident that the local heat transfer coefficient is the highest in the entry length of the channel, which is known to be due to the growing of the thermal boundary layer, and then a sharp decrease within the first 200 mm of the channel followed by a stabilisation of the local heat transfer coefficient values from approximately 200 mm, which suggests that the thermal boundary layer is fully established. However, interestingly, there appears to be a dependence of the local heat transfer coefficients on the Reynolds number, which contradicts the analytical solution presented by Shah and London [3] for water in laminar flows in rectangular channels. To examine this further, the average Nusselt numbers of water were calculated using Equation 6.10 and can be seen in Figure 6.8.

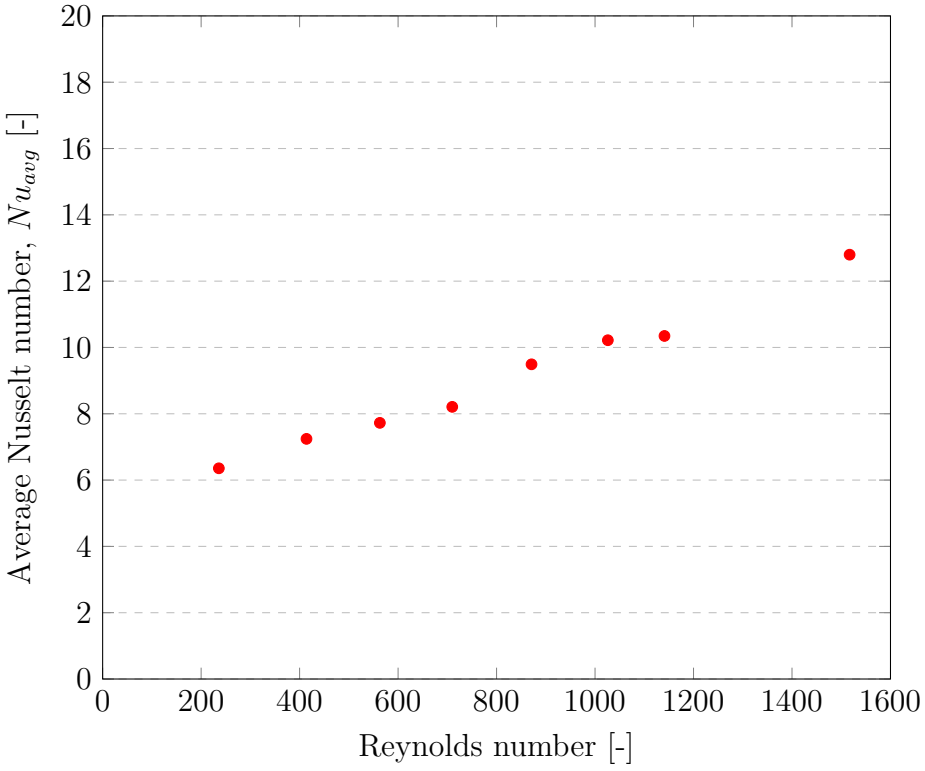

Figure 6.8: Average Nusselt numbers calculated for water using Equation 6.8, against the Reynolds number

Figure 6.8 also highlights the increase of the average Nusselt number for water with an increase in the Reynolds number. However, this is under the assumption of constant fluid velocity, which cannot be assumed in our rectangular channel and most likely leads to a dependency of the Reynolds number on the flow regime.

6.2 The effect of crystallisation on the rheological behaviour

To establish the flow behaviour of formulation 1 during cooling, a rheological investigation was launched, which would subsequently allow for the correct treatment of the results from the heat transfer experimental campaign. This includes determining if the PCD is non-Newtonian, which changes the way that the Nusselt number as a function of the Reynolds number and Prandtl number is assessed. Additionally, important transport properties such as the density and dynamic viscosity need to be established and subsequently so does the pressure drop and friction factors for determining the merit of using PCDs as replacement HTFs. Firstly, the relationship between the shear stress and shear rate was elucidated using the rheometer as described in Section 3.2. Five different operating temperatures were used; 20, 18, 11, 8 and 5℃, to determine the rheological

behaviour throughout the entire cooling process. During the experiments, isothermal temperature conditions were used for each specific experiment and the shear rate was varied between 1-200 s^{-1}. It is important to note that the different experiments with different temperatures were performed in temperature-decreasing order (e.g. starting at 20℃ and proceeding to 18℃) , this is because of the hysteresis between the melting and crystallisation temperature (due to supercooling), that during the cooling down process at 20℃ the PCD is in the form of an emulsion (liquid droplets suspended in liquid water). Starting from the lower temperature (5℃) and increasing the temperature would result in the PCD being in the suspension form at 20℃ since the melting point is not until 24℃ and so care needs to be taken when determining the correct transport properties. Figure 6.9 (Top) shows the shear stress-shear rate relationship.

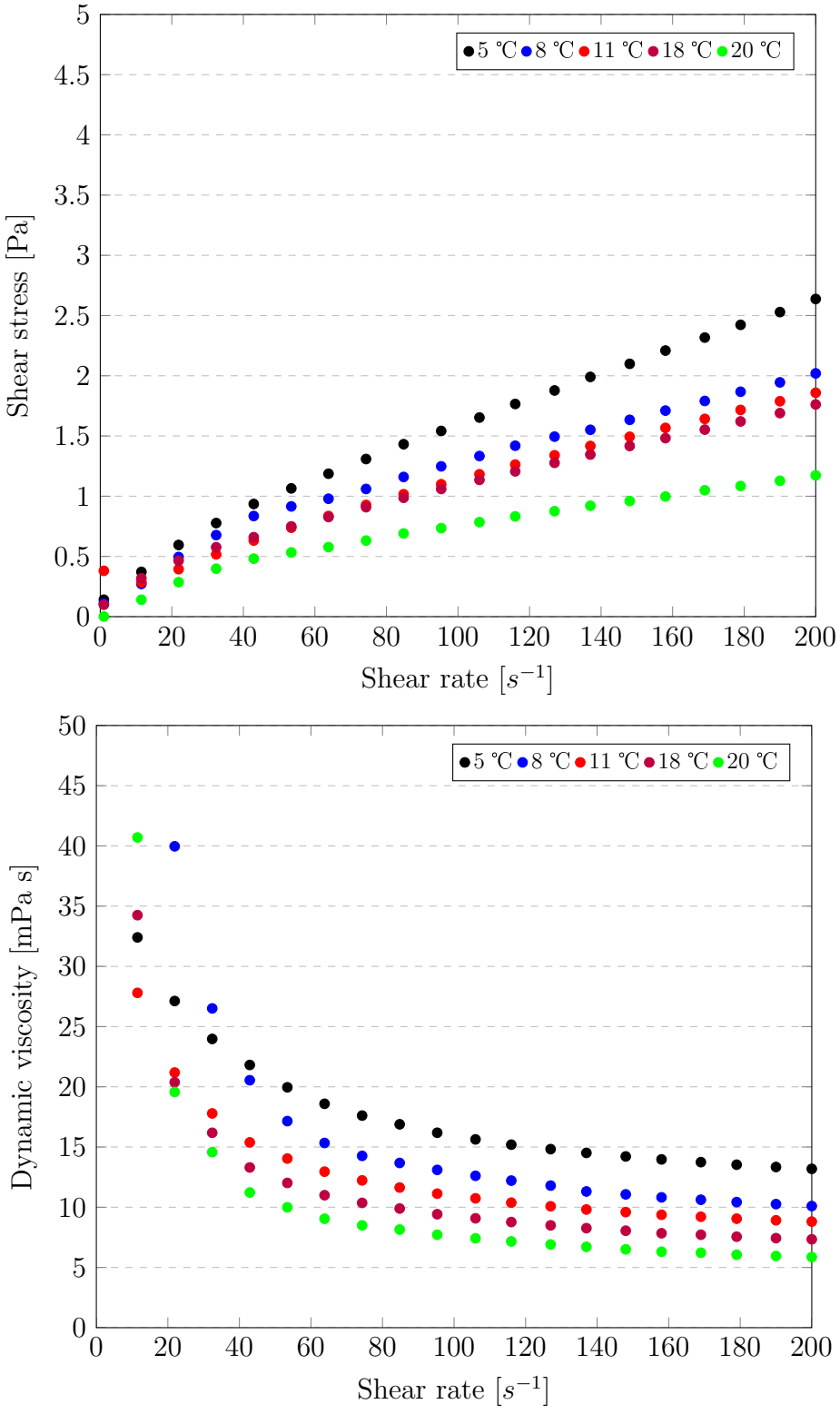

Figure 6.9: Top: The shear rate versus shear stress for formulation 1 at 20, 18, 11, 8 and 5℃ and bottom: The dynamic viscosities of formulation 1 against the shear rate (in the range of 1—200 s^{-1}) at temperatures of 20, 18, 11, 8 and 5℃.

If a fluid is a Newtonian fluid, the relationship between the shear stress and shear rate

is linear, however as is clear from Figure 6.9, at all temperatures, formulation 1 shows a non-linear relationship between the shear rate and shear stress. This suggests that the PCD is non-Newtonian and the relationship between the shear rate and shear stress indicates that the PCD is a pseudo-plastic fluid. This is further exhibited by plotting the dynamic viscosities of the PCD against the shear rate, which can be seen in Figure 6.9 (bottom). Here, the dependency of the viscosity on the shear rate can be observed and the shear-thinning behaviour of the PCD is evident. For quantification of the non-Newtonian behaviour, the flow behavioural index, n and the consistency factor K from the Herschel-Bulkley equation for pseudo-plastic fluids can be determined by plotting the natural logarithm of the shear rate and the shear stress. Here, two different methods were performed to calculate n and K for formulation 1 at the five different temperatures used during the cooling process. The first method involved the rheological test-rig described in Section 6.1.1, by setting the temperature of the PCD fluid in the circuit using the ethanol cooling circuit, and adjusting the flow rate so that different shear rates could be obtained. The shear stresses and shear rates were then calculated with Equations 6.1 and 6.2 respectively and from a plot of the natural logarithms of the calculated shear rates and shear stresses, the n and K values were determined. The second method involved plotting the natural logarithm of the shear rate and stress from the rheometer experiments discussed previously. The determined n and K values for both methods can be seen in Figure 6.10.

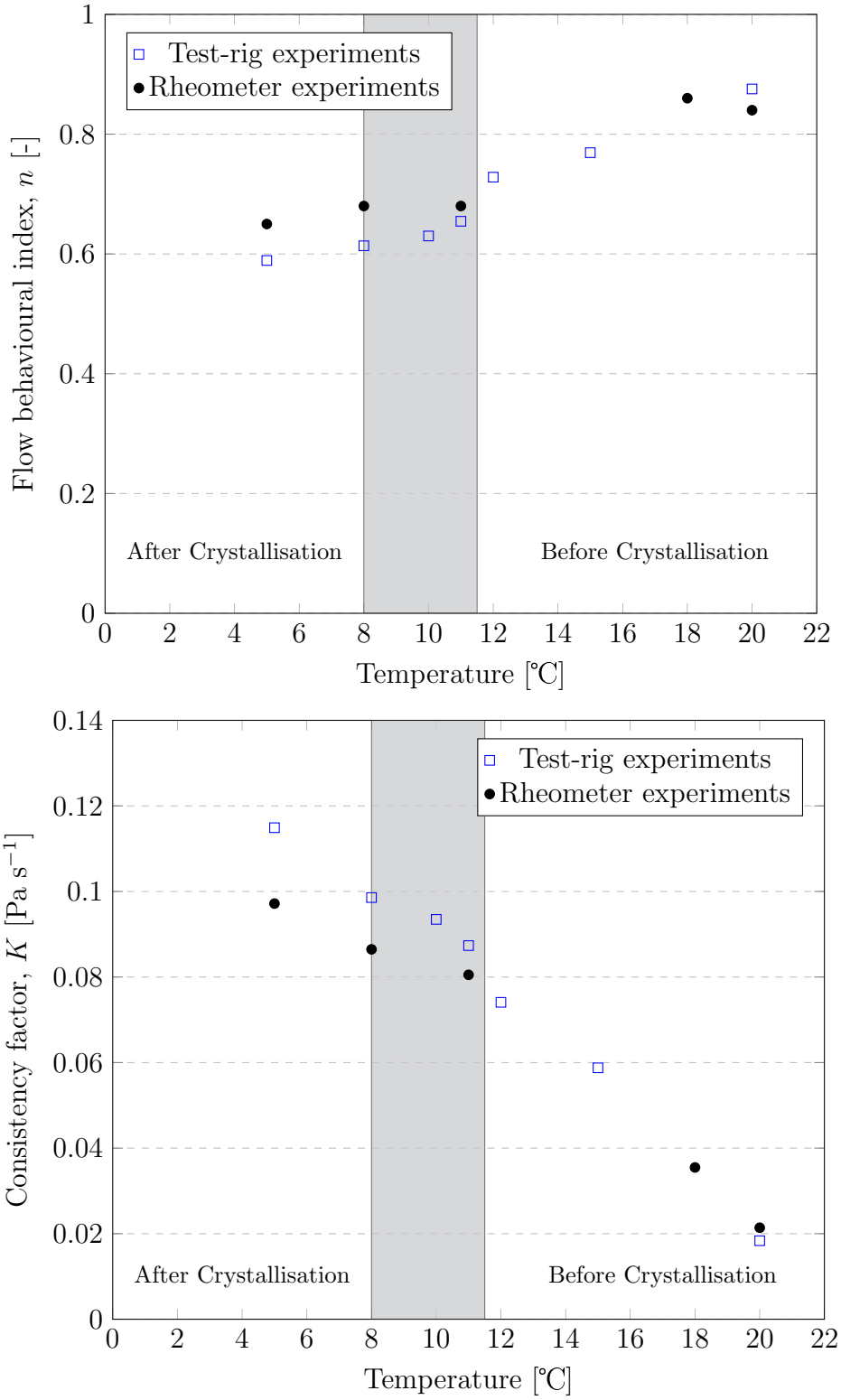

Figure 6.10: Top: The fluid behavioural index, n, for formulation 1 at a range of different temperatures calculated from data both in the experimental test-rig and from the rheometer and Bottom: the consistency coefficients, K, for formulation 1 at a range of different temperatures undergoing the cooling process calcualted from data both in the experimental test-rig and from the rheometer. Note that the shaded region indicates the crystallisation region as identified from the DSC.

Figure 6.10 demonstrates that at all temperatures, the PCD showed non-Newtonian behaviour as $n < 1$ at all temperatures and lies in the range of 0.6-0.9. Additionally, it can be observed that n decreases when the temperature decreases suggesting that the degree of non-Newtonian behaviour increases with a decrease in temperature. This is particularly noticeable during the phase change, which is most likely due to the PCD changing from a two-phase liquid-liquid fluid (emulsion) to a two-phase liquid-solid fluid (suspension) during crystallisation. Figure 6.10 also displays K against temperature, where it can be seen that K increases as the temperature decreases which is owing to the increasing viscosity as the PCD is cooled down. Furthermore, the rheometer experiments show similar values to those obtained from the experimental test-rig and subsequently suggest that the values obtained are correct. An additional thermophysical property needs to be determined for a full characterisation of the PCD and this is the density of the PCD. In literature, one of the common methods to analytically calculate the density of oil-in-water emulsions is determined using a weighted-average of both the oil and water component. For formulation 1, this was experimentally obtained from the Coriolis flow meter and can be observed in Figure 6.11.

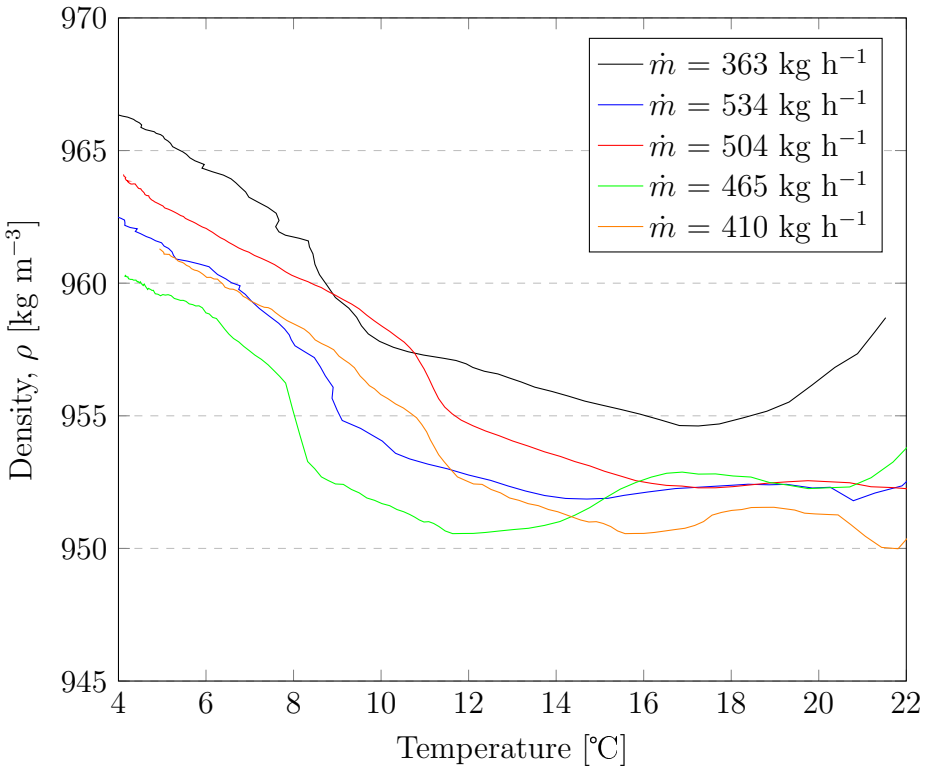

Figure 6.11: The evolution of the density of formulation 1 against the inlet temperature of the channel for five different mass flow rates.

Figure 6.11 shows the evolution of the density of formulation 1 for different temperatures at different mass flow rates to observe if shear rate influences the density and

interestingly, the higher the mass flow rate the lower the density which could be attributed to less crystallisation occurring during higher mass flow rates, or alternatively could point toward a shear-rate dependence of the density. This will be examined in the following subchapter, where the calculated apparent specific heat capacity at different flow rates will allow for a determination of the relationship between the flow rate and the degree of crystallisation occurring at each inlet temperature.

Given that formulation 1 has shown non-Newtonian behaviour at all investigated temperatures during the cooling process, and subsequently the shear rate as a function of both temperature and shear rate has been elucidated and the density determined, a discussion on the calculation of the Reynolds number is presented. A common way in literature to deal with calculation of Reynolds for non-Newtonian pseudo-plastic fluids is the generalisation method presented by Metzner and Reed [4]. This method involves creating a generalised viscosity and subsequently a generalised Reynolds number, using the calculated fluid behavioural index, n, and the consistency factor, K. The Reynolds number as presented by Metzner and Reed (Re_{MR}) can be calculated using [4]:

$$Re_{MR} = \frac{\rho D_h^n u^{2-n}}{K((3n+1)/(4n))^n 8^{n-1}} \tag{6.11}$$

Whilst many generalisation methods have been presented since, the method presented by Metzner and Reed was valid for rectangular ducts and will therefore be used in this investigation. Here, a new method is presented, using the creation of a look-up table for $\mu = (T, \dot{\gamma})$ and calculating the Reynolds number with the viscosity as a function of shear rate and temperature, according to the normal Reynolds number calculation (see equation 2.3). Figure 6.12 presents a comparison of the Reynolds number calculated with the generalisation method presented by Metzner and Reed [4] and the novel method against the mass flow rate for three different channel inlet temperatures. The method of creating a look-up table for the dynamic viscosity as a function of the temperature and shear rate, also has the added benefit of being able to be used in the calculation of the Prandtl number in non-isothermal flows for the subsequent chapter on the determination of the heat transfer behaviour.

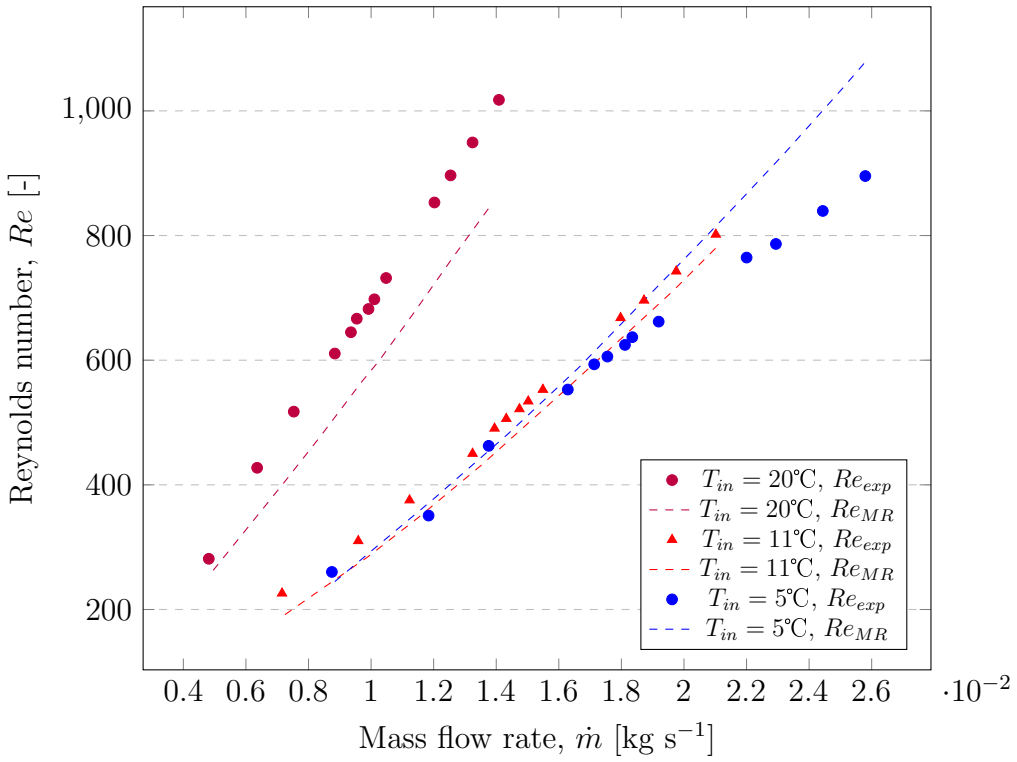

Figure 6.12: The Reynolds number versus the mass flow rate for three different channel inlet temperatures calculated using the experimentally determined viscosity (μ_{exp}) and using the method presented by Metzner and Reed (μ_{MR}).

Firstly, it is evident that the influence of temperature on the Reynolds number for a given mass flow rate is large, with 20 ℃ having larger Reynolds numbers than 11 and 5℃ for a given mass flow rate due to lower viscosities. In most experimental campaigns of PCDs in literature, this is not taken into consideration and this calculation highlights the importance of taking the correct transport and thermophysical properties at the right temperature for fluids. Additionally, the deviation between the predicted Reynolds number using the method by Metzner and Reed and the Reynolds number using the experimentally determined viscosity, is smaller at low mass flow rates and at lower temperatures (11 and 5℃). However, due to the larger deviations at higher mass flow rates, and at 20℃ in the rest of this experimental campaign, the experimentally determined viscosity will be used to determine the Reynolds number. Despite this, it is recognised that using the n and K coefficients can rather accurately predict the dynamic viscosity, and subsequently Reynolds number for pseudo-plastic PCDs under certain operating conditions, which could potentially lead to reduced experimental time in the future.

Furthermore, the influence of the cooling process was investigated on the pressure drop of formulation 1 by measuring the pressure drop of the fluid using the experimental test-rig described in Section 6.1.1 against the Reynolds number for different bulk flow temperatures. Figure 6.14 shows the pressure drop of formulation 1 and water for different

Reynolds numbers and temperatures.

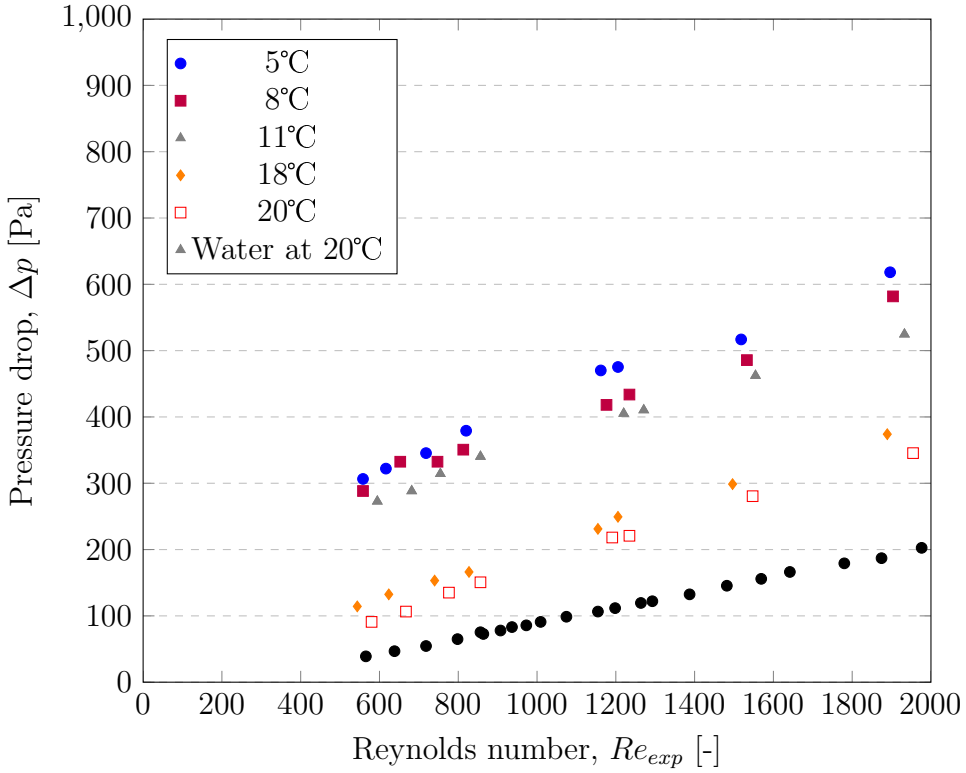

Figure 6.13: The pressure drop of formulation 1 for five different temperatures at different experimental Reynolds number, and additionally the pressure drop of water at 20°C.

Two distinct influences can be seen from the pressure drop against the Reynolds number. Firstly as the temperature is decreased, the pressure drop increases, most likely due to the increased viscosity of the PCD as it is cooled down. Secondly, the pressure drop also increases as the mass flow rate (and subsequently Reynolds number) is increased, despite the shear-thinning behaviour of the PCD. At lower Reynolds numbers, the pressure drop increase is proportional to the increase in the Reynolds number, particularly for 20 and 18°C, which is common for fluids in the laminar flow regime. However, at lower temperatures, and at higher Reynolds numbers, the relationship becomes less linear for the PCD, suggesting some kind of transition. This is discussed further in the subsequent chapter. Once the pressure drop is known, the friction factor of PCDs can be calculated using the Darcy-Weisbach equation:

$$f = \frac{\Delta p}{\frac{l}{D}\frac{\rho}{2}u^2} \tag{6.12}$$

The friction factors of formulation 1 at different temperatures during the cooling process, alongside the approximation given for fluids in a laminar flow, using the relation $f = 16/Re$, can be seen in Figure 6.15. The relationship between the friction factors and the

Reynolds number can be elucidated at the three different temperatures that represent; before crystallisation, during crystallisation and after crystallisation.

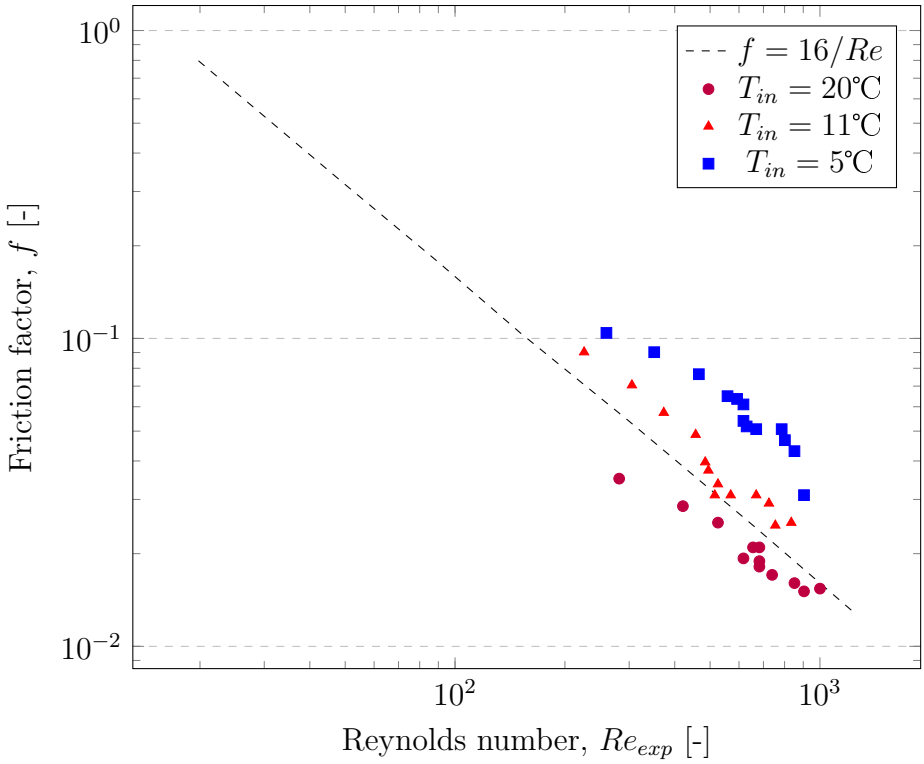

Figure 6.14: The calculated friction factors for three different channel inlet temperatures; 20, 11 and 5 ℃ for formulation 1.

Theoretically, when there is no surface roughness in the channel, the friction factors should collapse onto a single-curve. However, in our case we see deviations of the friction factors from the standard $f = 16/Re_{exp}$, and this is thought to be due to surface roughness in the experimental set-up channel. Additionally, it can be noted that the PCD has the lowest friction factor when the PCM is fully melted, at 20℃ and has the highest friction factor at 5℃ when the PCM is fully crystallised.

6.3 The effect of crystallisation on the heat transfer behaviour of PCDs

6.3.1 Determination of the thermophysical properties

Firstly, the specific heat capacity of formulation 1 was determined from DSC heat flow curves against temperature, during cooling down, using Equation 5.28. The specific heat capacity can be seen in Figure 5.15.

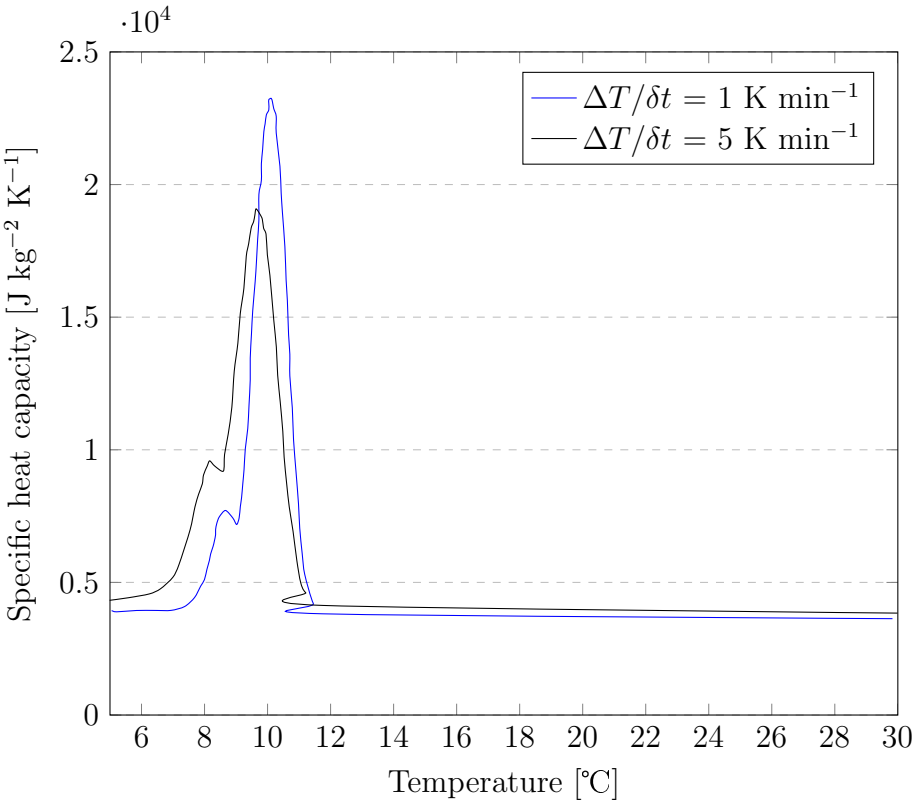

Figure 6.15: The calculated apparent specific heat capacities from the DSC experiments for formulation 1 during crystallisation. The cooling rate used was 2 K min^{-1}.

From the DSC, the onset crystallisation temperature appears to be at approximately 12℃and the peak crystallisation temperature at 9-10℃depending on the heating rate used. As previously discussed, the heating/cooling rate of 1 K min^{-1} should be taken due to the influence of the DSC crucible and the imperfect heat transfer within the DSC. Before and after crystallisation, formulation 1 has a specific heat capacity slightly lower than water (which as a specific heat capacity of 4180 W m^{-2} K^{-1} in the same temperature range), but during crystallisation, the specific heat capacity increases by a factor of 5.5 compared to water. This increase during crystallisation is a combination of the sensible heat of the water and PCM and the latent heat of crystallisation of the PCM. In this investigation, the thermal conductivities of formulation 1 were measured with the Linseis Transient Hot Bridge (for further description see Chapter 3, section 3.2), during the cooling process at five different temperatures (20, 18, 11, 8 and 5℃). For comparison, experimental values for water and the CoolProp values for water were also investigated. Due to the aforementioned problems, and time-consuming manner of experimentally determining thermal conductivities of PCDs, in literature, the effective thermal conductivity of PCDs is most often calculated by the modified version of the first-order approximation Maxwell equation, as shown by Equation 5.29. Figure 6.16 displays the experimental thermal conductivity values for water and for formulation 1,

the Maxwell Equation calculated values for formulation 1 and the CoolProp values[2] for water.

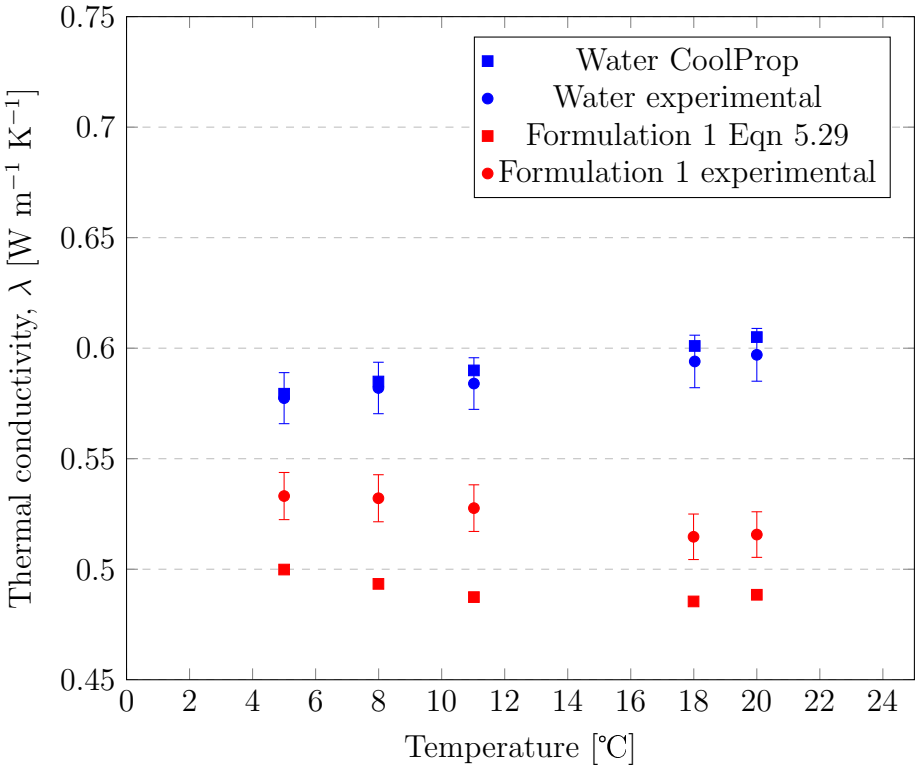

Figure 6.16: The thermal conductivity of formulation 1 during the cooling process measured with the THB and calculated with the Maxwell equation. Additionally, the thermal conductivities of water as found with Coolprop [2] are shown as a comparison.

The error bars shown in Figure 6.16 represent the standard instrument errors as given by the manufacturer. For water, the measured thermal conductivity values fall within the standard instrument errors. As expected, the thermal conductivity values for water, at all temperatures, are higher than for the PCD. This is due to the organic PCM having a much lower thermal conductivity than water. Generally, thermal conductivity increases with an increase in temperature, however as shown in Figure 6.16, the thermal conductivity of formulation 1 increases with a decrease in temperature, this is because the PCM is changing phase and solids have a larger thermal conductivity than liquids. Furthermore, it can be seen that the effective thermal conductivities calculated by the Maxwell equation [5], are much lower than the experimentally measured values.

Following the collection of the relevant thermophysical properties, the dimensionless analysis of the heat transfer behaviour, in terms of Reynolds number calculation, Nusselt number calculation and Prandtl number calculation can be performed. The following section discusses the heat transfer behaviour of formulation 1 during the cooling, and crystallisation, process.

6.3.2 Local heat transfer behaviour

The heat transfer experiments were performed for formulation 1 for different experimental Reynolds numbers and at different channel inlet temperatures, to understand the behaviour of formulation 1 during the whole cooling down and crystallisation process. The different channel inlet temperatures used were; 20, 18, 11, 8 and 5℃ . A novel method for the the analysis for these temperatures was performed. The data acquisition system recorded each temperature sensor measurement every 16 s and when the inlet temperature of the PCD was within 0.9℃ of the selected temperature for analysis (e.g. 19.5-20.4℃ for 20℃), the calculated values of the local heat transfer coefficients (for every 16 s). This data reduction relies on the assumption that the inertia effects in the system can be neglected against the instantaneous heat exchanges. This assumption was validated using the same method for water. Before the heat transfer behaviour is tackled, an understanding of the experimental heat transfer test-rig as described in Section 6.1.2 is required. Figure 6.17 shows the evolution of the inlet and outlet temperatures of the ethanol and PCD during cooling in the cooling section of the experimental test-rig. A mass flow rate was imposed on the ethanol, flowing in the outer two channels within the cooling section, and the temperature of the ethanol was set to 2℃. The cooling of the PCD and the ethanol took place in parallel. The plateau, which can be observed at approximately 1000 s, represents the crystallisation of the PCM within the PCD and separates the cooling curve into three distinct regions. In the first region, from t = 0–1000s, the emulsion is fully liquid. The second region shows the crystallisation of the PCM in the form of a plateau in the cooling curve and when it is finished, the temperature decreases until it reaches a steady state which is the third region. Figure 6.17 also serves as an additional mean to observe the existence of the supercooling. From the plateau in the cooling curve, crystallisation appears to initiate at 11℃ which conforms to the DSC in Figure 6.15. It has been suggested, that shear rate can have an influence on the degree of supercooling (lu2012), however during the experiments performed in this investigation, there was no change in the degree of supercooling observed for different mass flow rates, and thus shear rates.

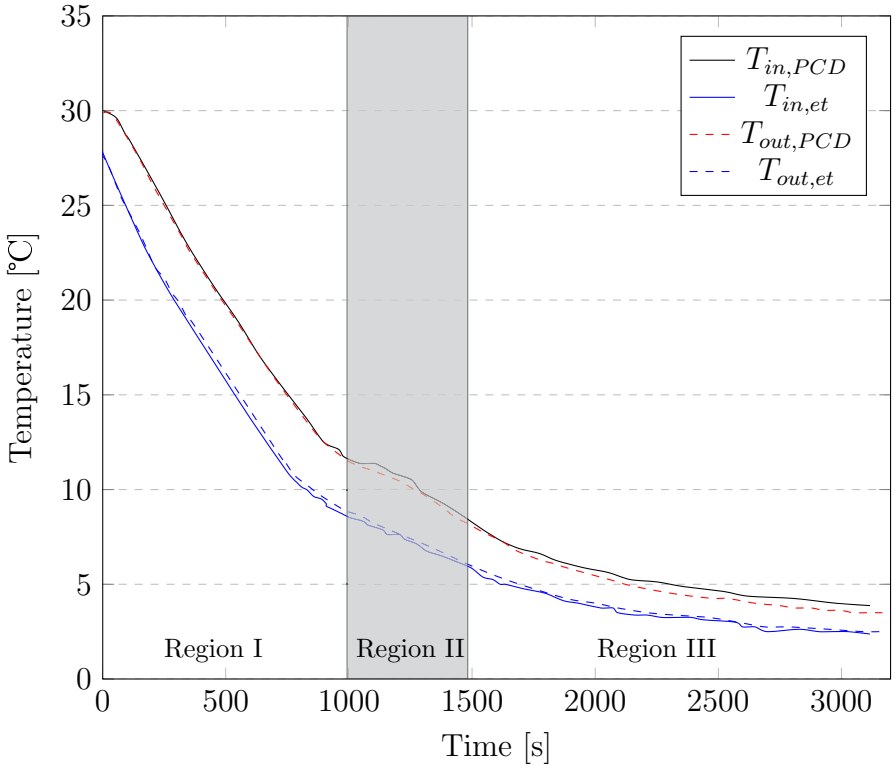

Figure 6.17: Temperature versus time profile for the PCD showing the inlet and outlet temperatures of the PCD and ethanol channels respectively. Note that the shaded region indicates the crystallisation region as identified from the DSC.

Firstly, the influence of the inlet temperature and the experimental Reynolds number on the local heat transfer behaviour and development of the thermal boundary layer was examined by calculating the local heat transfer coefficients according to Equation 6.6 and plotting them against the distance from the PCD inlet of the channel. Figure 6.18 shows the development of these local heat transfer coefficients, with the top graph showing the influence of the experimental Reynolds number and the bottom graph displaying the influence of the inlet temperature. The top graph in Figure 6.18, indicates quite clearly a relationship between the experimental Reynolds number and the local heat transfer coefficients with an increase in the experimental Reynolds number resulting in an increase of the local heat transfer coefficients. Interestingly, whilst all experimental Reynolds numbers show a decrease in the local heat transfer coefficients at the entrance of the channel (0-200 mm), this effect is larger at lower experimental Reynolds numbers. This decrease at the beginning of the channel can be attributed to the development of the thermal boundary layer, which decreases in thickness as the mass flux (and subsequently experimental Reynolds number) is increased because of a more efficient transport and mixing of heat.

From the bottom graph in Figure 6.18, a relationship between the PCD inlet tem-

perature and the local heat transfer coefficient can also be seen. The highest local heat transfer coefficients are observed for an inlet temperature of 20℃ and interestingly, the next highest local heat transfer coefficients are observed for 11℃, which is where the DSC indicates crystallisation initiates. The local heat transfer coefficients at an inlet temperature of 8 and 18℃ are very similar, again due to crystallisation resulting in an increase in the heat transfer at 8℃. The lowest inlet temperature also has the lowest local heat transfer coefficients and with the smallest decrease in the local heat transfer coefficient at the inlet of the channel. The development of the thermal boundary layer appears to be relatively different for most of the inlet temperatures, other than 18 and 11°, this is due to the temperature dependency of the transport and thermophysical properties of the PCD. This influence is discussed further in the subsequent section.

From the local heat transfer coefficients, the local Nusselt numbers were calculated, according to Equation 6.9 for the different experimental Reynolds numbers and inlet temperatures used and can be seen in Figure 6.19.

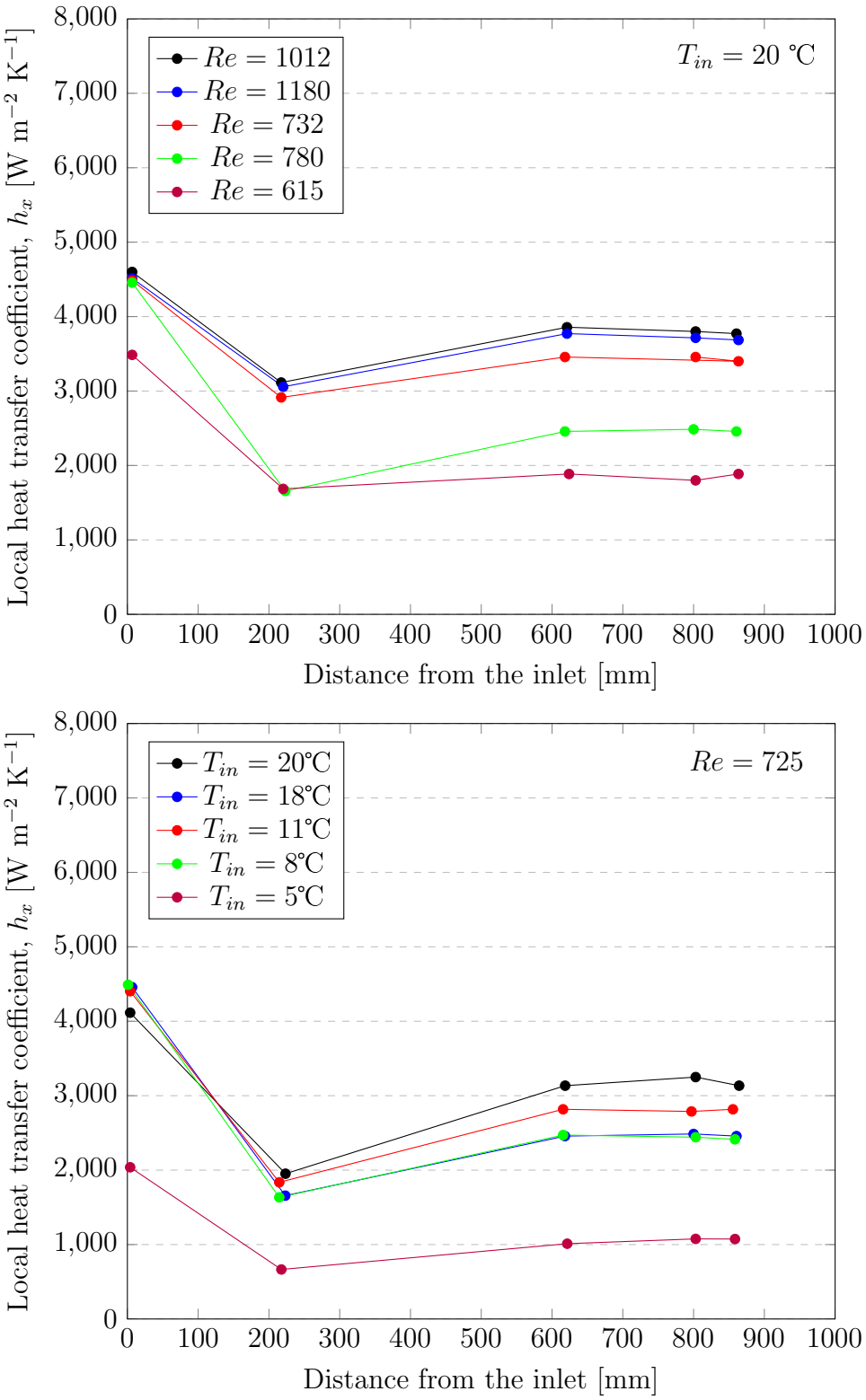

Figure 6.18: Top: The influence of the experimental Reynolds number on the local heat transfer coefficients of formulation 1 and bottom: The influence of the channel inlet temperature on the local heat transfer coefficients of formulation 1.

As with the local heat transfer coefficients, the local Nusselt numbers for both the

varying experimental Reynolds number and the varying inlet temperature conditions follow the same trend. It must be noted, that in this instance, the local Nusselt numbers were calculated using the experimentally determined thermal conductivities as shown in Figure 6.16, since it is for the calculation of the Nusselt number, the thermal conductivity can be taken under the static condition, since it is the Nusselt number at the wall of the tube, where the fluid velocity tends towards 0. In this specific case, the effect of shear-rate on the thermal conductivity does not need to be considered. For a Newtonian fluid, in a fully developed laminar flow, the Nusselt number is constant and independent of the experimental Reynolds and Prandtl number (Pr). For a rectangular channel, with an a/b ratio of 13.3 (the case for our experimental test-rig), Shah and London [3] proposed the constant value of the Nusselt number to be 7.5 for a constant wall temperature boundary condition. This is indicative of the complex physical and heat transfer mechanisms occurring in two-phase flows and must be taken into consideration when using a rudimentary explanation of classical heat transfer behaviour in single-phase Newtonian flow.

The local Nusselt numbers were subsequently compared to those of water to observe if the development of the local Nusselt number along the length of the channel was different between formulation 1 and water. The local Nusselt numbers were then plotted alongside correlations created by Vasile et al. [6] . The first correlation is valid for $200 \leq Re \leq 500$ and $Pr \leq 160$ and is:

$$Nu_x = 0.37 Re^{0.427} Pr^{0.33} x*^{-0.238} \tag{6.13}$$

where $x*$ is the dimensionless axial distance, which is defined as;

$$x* = \frac{x}{D_h} \tag{6.14}$$

The second correlation developed by Vasile et al. [6] is valid for $200 \leq Re \leq 900$ and $Pr \leq 160$ and the correlation is:

$$Nu_x = 0.28 Re^{0.427} Pr^{0.33} (\frac{x}{x + D_h})^{-0.59} \tag{6.15}$$

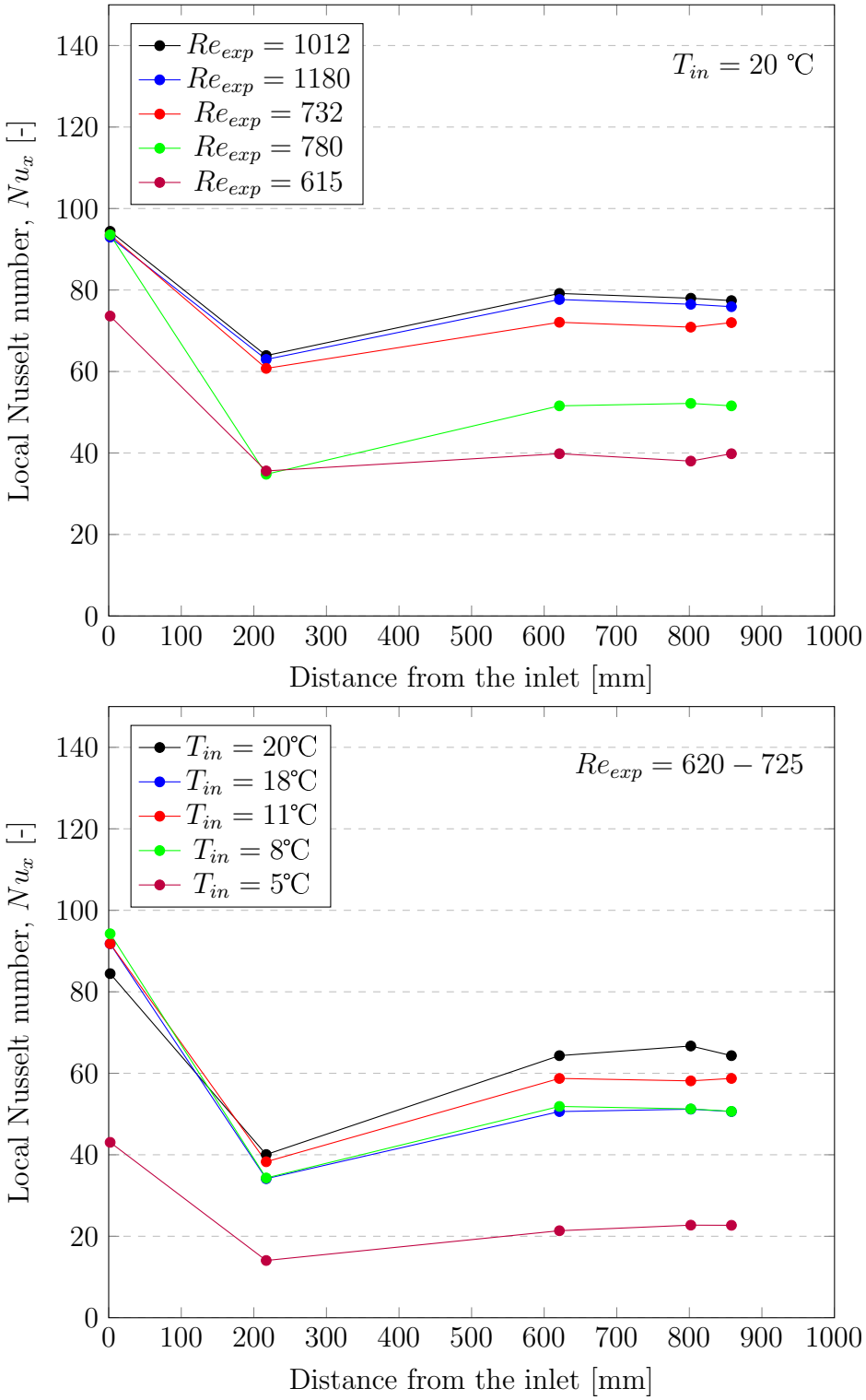

Figure 6.19: Top: The influence of the Reynolds number on the local Nusselt numbers of formulation 1 and bottom: The influence of the channel inlet temperature on the local Nusselt numbers of formulation 1.

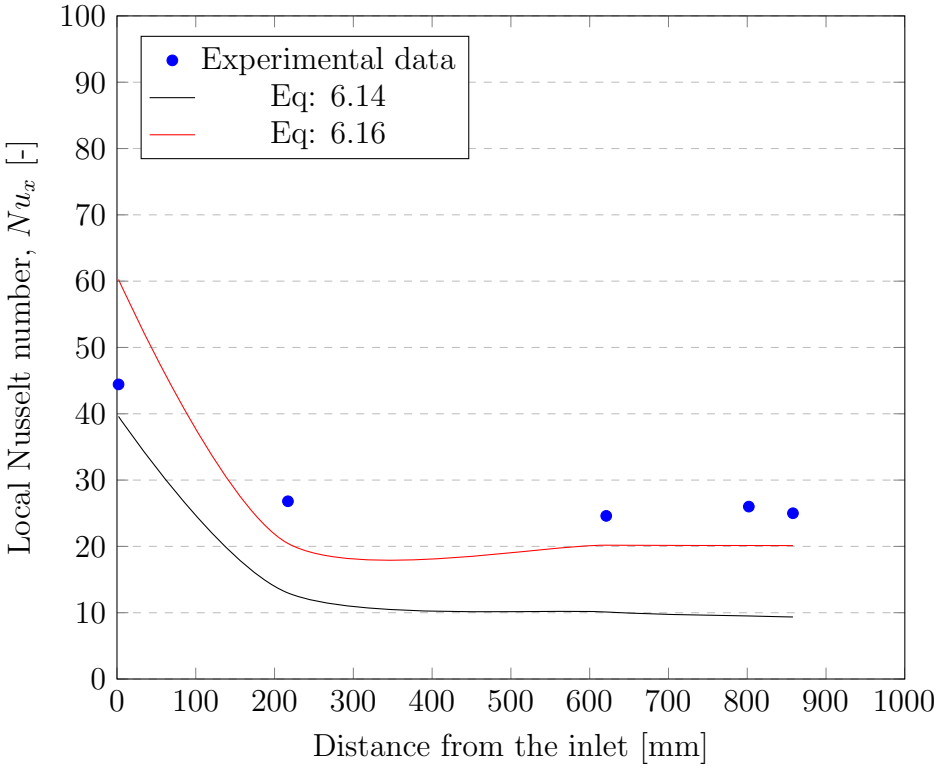

Figure 6.20: Comparison of experimental data for the conditions; $Re = 410$, $T_{in} = 5$℃ for formulation 1 with the two correlations proposed by Vasile et al. [6].

It was previously stated by Vasile et al. [7] that since the PCM concentration remains constant in the PCD the Prandtl number variations should be weak along the length of the channel. However, changes in the shear-rate and temperature along the length of the channel will ultimately change the Prandtl number, and it is believed now that the assumption of a constant Prandtl along the length of the channel is not possible. This effect of the changing Prandtl number is more evident during the crystallisation process, where the degree of crystallisation along the length of the channel is unknown.

6.3.3 Overall heat transfer behaviour

The effect of the channel inlet temperature (and subsequently the Prandtl number) and the experimental Reynolds number was also examined by determining the effects of both of these parameters on the average heat transfer coefficients and average Nusselt numbers. Firstly, Figure 6.21 shows the average Nusselt numbers for five different experimental Reynolds number against the inlet temperature of the channel. Note that the experimental Reynolds numbers given are shown as a range, since for each separate temperature, even for the same mass flow rate, the experimental Reynolds number will change as a result of the changing dynamic viscosity and densities at each different temperatures.

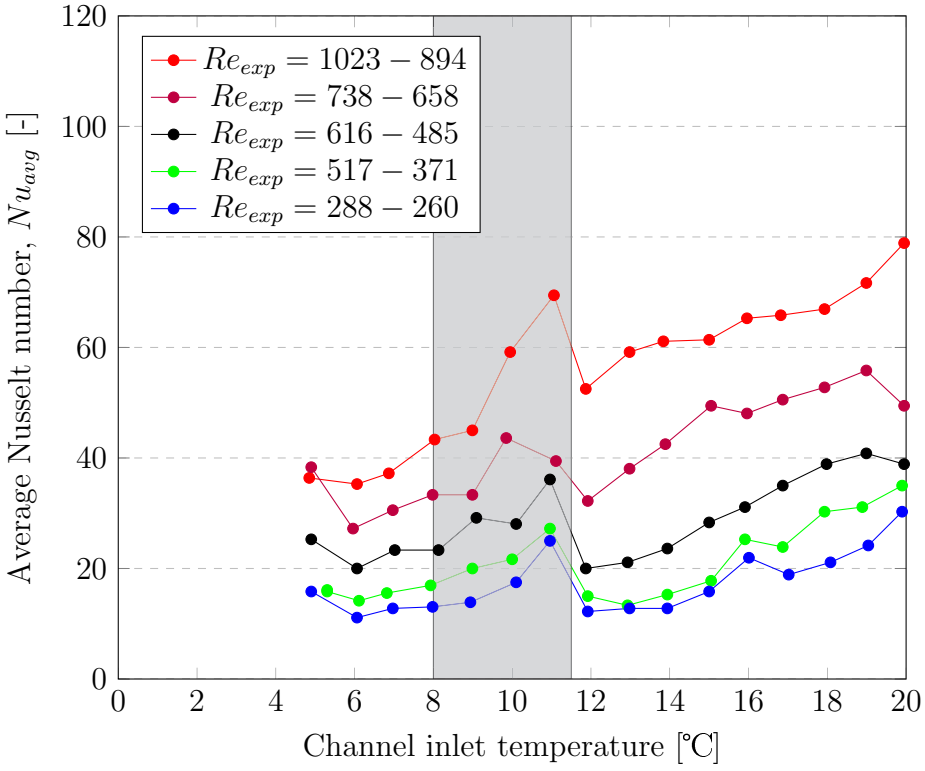

Figure 6.21: The average Nusselt numbers of formulation 1 against the channel inlet temperature for five different experimental Reynolds numbers. Note that the shaded region indicates the crystallisation zone as identified from the DSC.

Theoretically, one would expect the Nusselt numbers to be higher at lower temperatures, due to the apparent specific heat capacity remaining the same at 5°C as 20°C (after and before crystallisation), the dynamic viscosity being higher at 5°C than 20°C and a small change in the thermal conductivity. The general trend appears to be that, for all experimental Reynolds numbers, the average Nusselt number decreases as the inlet temperature channel decreases. However, as the PCD begins to crystallise, which is highlighted by the shaded region in Figure 6.21, the average Nusselt numbers begin to increase as the amount of crystallised PCM within the PCD increases. This is an indication that crystallisation of the PCM induces an enhanced heat transfer performance. After the crystallisation has finished, the average Nusselt number decreases again. Figure 6.21 also demonstrates the increase of the average Nusselt number with an increase in the experimental Reynolds number. These results show that the Nusselt numbers of PCDs during crystallisation are influenced by both the flow regime and the thermophysical properties of the PCD itself. During the process of cooling down the PCD, a few of these effects may overlap or interfere with each other, thus presenting as if there was no influence at all (or a mixed influence). From Figure 6.21, the steep increase in the Nusselt number for different experimental Reynolds number within the inlet temperature region of 9-12°C

is a clear indication of the crystallisation of the dispersed PCM droplets. The Prandtl number, as defined by:

$$Pr = \frac{cp\mu}{\lambda} \tag{6.16}$$

allows for the following interpretation; whilst crystallising, the apparent specific heat capacity of the PCD is drastically increasing, which leads to a strong increase in the Prandtl number and therefore in the Nusselt number. This effect is limited to the temperature range of the phase change and is thus only visible as a peak in Figure 6.21. For further examination of this, the apparent specific heat capacity of formulation 1 flowing through the channel was calculated according to the following energy balance equation:

$$cp = \frac{Q}{\dot{m}\Delta T} \tag{6.17}$$

The calculated specific heat capacities can be observed in Figure 6.22.

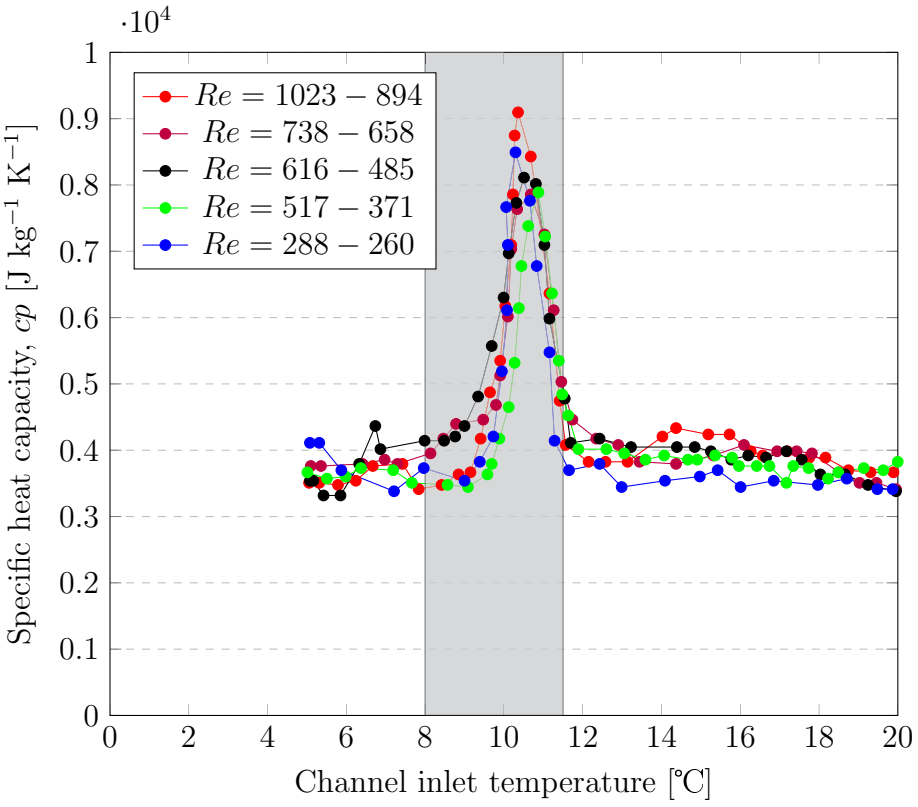

Figure 6.22: The calculated specific heat capacities of formulation 1 against the channel inlet temperature for five different experimental Reynolds numbers. Note that the shaded region indicates the crystallisation zone as identified from the DSC.

Figure 6.22 highlights the reason for the increase in the average Nusselt number using the Prandtl analogy. Furthermore, when the PCD crystallises and the PCM changes from liquid to solid, the viscosity and density increases, but only slightly and therefore their

influence on the Prandtl number is of minor importance in this instance. The influence of the dynamic viscosity is higher at lower Reynolds numbers (due to a lower shear rate and thus a higher dynamic viscosity). This is reflected in Figure 6.21 by the little-to-no change in the Nusselt numbers right before phase change and right afterwards.

To further examine the relationship between the average Nusselt number and the Reynolds number, the average Nusselt number was plotted against the Reynolds number, which was calculated using the shear-rate and temperature dependence of the thermo-physical properties. Figure 6.23 displays the average Nusselt numbers for three inlet temperatures; 20, 11 and 5℃.

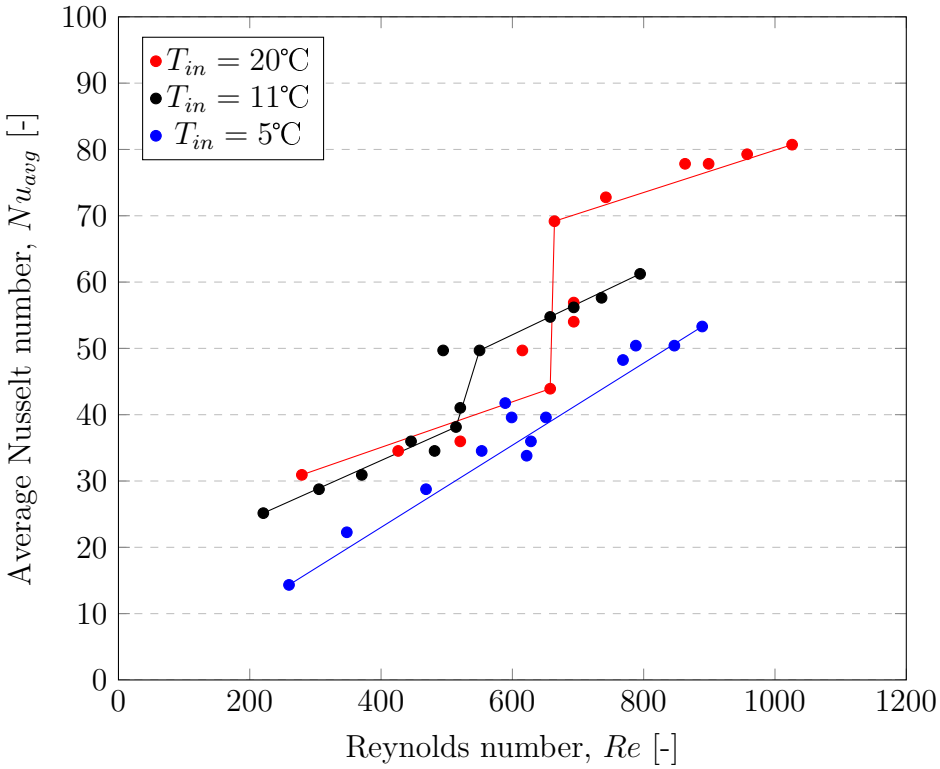

Figure 6.23: The average Nusselt numbers of formulation 1 against the experimental Reynolds number calculated for three different temperatures to represent before crystallisation (20℃), during crystallisation (11℃) and after crystallisation (5℃). The trend curves are drawn to display the important phenomenon.

As evident from Figure 6.22, the Nusselt number is strongly dependent on the experimental Reynolds number, with increasing flow rates (and subsequently experimental Reynolds number) leading to an in increase in the Nusselt number. The dependence of the Nusselt number on the experimental Reynolds number is different, depending on the inlet temperature of the channel and the mass flow rate (and thus shear rate) used, which indicates not only the influence of higher momentum exchange at the boundary layer due to velocity, but also due to an even stronger influence at the boundary layer with increas-

ing temperature or experimental Reynolds number. However, this is not always the case, for example, the Nusselt numbers are higher at higher temperatures (disregarding the phase change), which suggests that the values of the thermal conductivity that we use for static measurements are not accurate for use in the quantification of the heat transfer behaviour. Additionally, it can be noticed that for the higher experimental Reynolds numbers, the decrease of the average Nusselt number (from higher to lower temperatures) is more profound. From Figure 6.23, the increase in the Nusselt number at an experimental Reynolds number of approximately 750 for 20℃ and 500 for 11℃ is most likely caused by a transition in the flow behaviour. At 20 and 11 ℃, a strong increase in the heat transfer is visible in this "transition" regime, which slightly deviates for different experiments (due to the temperature and shear-rate dependence of the viscosity) but also due to other changing thermophysical properties (such as the specific heat capacity). For example, at 5℃ , there is no phase change, the PCD enters the channel already in the suspension form (solid PCM droplets) where the viscosity is relatively high and it can be observed that the transition happens at a lower degree for 5℃ than for 11 and 20℃Ṫhe critical experimental Reynolds number (Re_{crit}) determining the transition from laminar to turbulent flow, of approximately 2300, is valid for Newtonian fluids in cylindrical tubes and is well understood. However, any deviation from this (in terms of geometry, surface roughness of the channel and transport properties of the fluid) will change this critical experimental Reynolds number. In the experimental test-rig used in this investigation, the channel has a width of 80 mm and a thickness of 4.5 mm leading to a calculated hydraulic diameter of 0.0116 m. Therefore, for the flow in our rectangular channel, the value of $Re_{crit} = 2300$ is not valid and for our case with the specific fluid, not even known. From Figure 6.23, the increase in the Nusselt number at an experimental Reynolds number of approximately 500-750 (depending on inlet temperature) is most likely caused by a change in the flow behaviour. Despite this, the deviation of the critical experimental Reynolds number between all three investigated temperatures is extremely low since the influence of the thermophysical properties on the flow regime is not permanent. These findings suggest that further investigation into the calculation of the experimental Reynolds number and the critical experimental Reynolds number of this PCD in the specific geometry needs to be performed. Previous correlations exist to describe the evolution of the average Nusselt number with respect to the Prandtl number and the experimental Reynolds number; two correlations were produced for the specific test-rig and geometry used in this investigation. These correlations were presented by El Boujaddaini et al [8]:

$$Nu = 0.893 Re^{0.68} Pr^{0.34} \tag{6.18}$$

and is valid for $400 \leq Re \leq 2500$ for $30 \leq Pr \leq 110$ and $L/D_h \leq 20$. The other

correlation was produced by Vasile et al [7]:

$$Nu = 0.13Re^{0.56}Pr^{0.33} \tag{6.19}$$

which is valid for $200 \leq Re \leq 900$ and $Pr \leq 160$. Figure 6.24 show the experimental data for an inlet temperature of 11℃ alongside the calculated Nusselt numbers from the two correlations presented in Equation 6.20 and 6.21. Additionally, a new correlation was developed, which can be seen in Equation 6.22 to describe the heat transfer behaviour at 11℃ by modifying the Prandtl number's power, to account for the shear-rate dependence of the thermophysical properties, which would result in a higher Prandtl number than calculated with the experimental values.

$$Nu = 0.893Re^{0.68}Pr^{0.4} \tag{6.20}$$

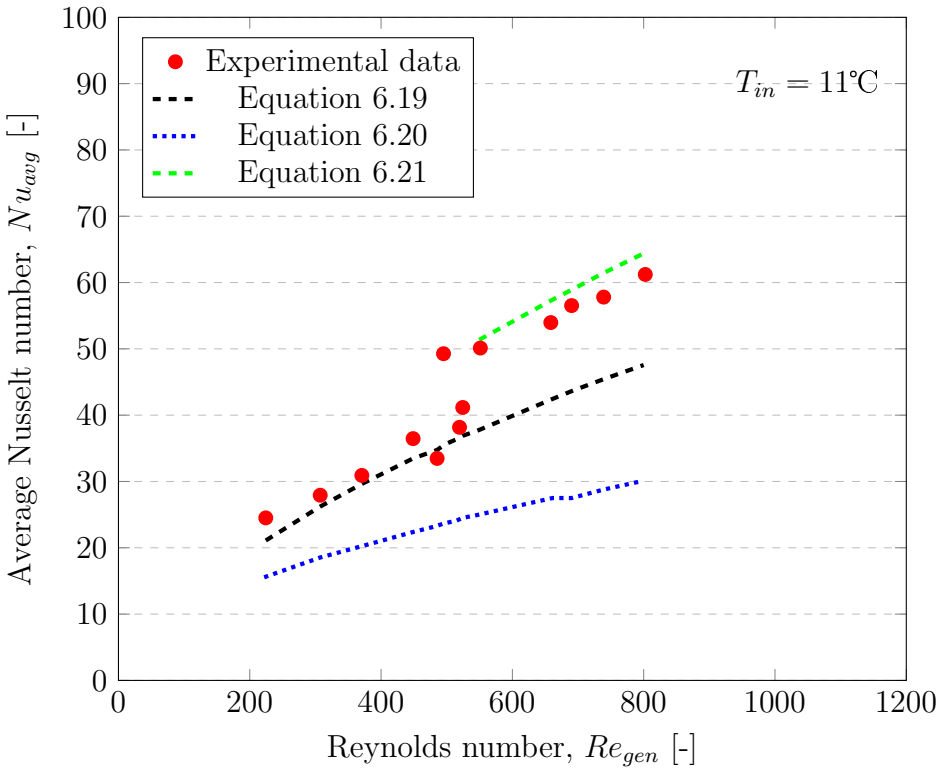

Figure 6.24: The average Nusselt numbers of formulation 1 against the generalised Reynolds number for 11℃ alongside the correlations presented in Equation 6.18 and 6.19 and alongside the new correlation for after the transition as seen in Equation 6.20.

it is evident from the correlations for 11℃ that a transition is occurring and that the correlation presented in Equation 6.20 can be used in the case of 11 to describe the Nusselt number until a Reynolds number of approximately 500. After this, the change in

gradient is most likely due to a transition in the flow.

6.4 Conclusions

Currently a major issue is when using correlations for single-phase fluids such as water, the thermophysical and transport properties have been well established in the literature due to years of research and experimentation. However, for two phase fluids, either complex experimental techniques have to be used and perform static measurements, or analytical equations to predict the thermophysical properties have to be used. Ultimately, this will lead to errors in the actual heat transfer behaviour and the calculated heat transfer performance using statically measured values and/or those calculated from analytical solutions. In this chapter, a complete characterisation was performed on a paraffin-in-water PCD during crystallisation in a rectangular channel using a novel data reduction method. A significant degree of supercooling (11 K) was observed in DSC analysis, which was confirmed by the temperature versus time profile in the experimental test set-up. Nusselt numbers at different temperatures in the cooling and crystallisation process were investigated for an experimental Reynolds number in the range of 200 to 1100 and it was found that 20℃ had the highest Nusselt numbers and that an increase in the experimental Reynolds number resulted in an increase in the average Nusselt numbers. Additionally at experimental Reynolds number below the normal transition experimental Reynolds number (2300), an unexpected transition, characterised by a large increase in the average Nusselt number was observed for all temperatures. An interesting and novel discussion was presented in an attempt to theoretically explain this phenomenon. For single-phase flows, such as water, the transition regime of the experimental Reynolds number has been extensively investigated and validated. However, with the two-phase fluid studied, in a rectangular channel, the transition regime is unknown. It is expected that this transition regime is influenced by the channel geometry, the surface roughness of the channel, the thermophysical properties of the PCD and ultimately the stability of the PCD. Despite this, it is suggested that this behaviour needs more future focus and analysis to properly describe the heat transfer behaviour of non-Newtonian fluids in rectangular channels. The 16 wt.% paraffin in water emulsion showed non-Newtonian behaviour, whereby the non-Newtonian degree increased as the temperature was decreased. Additionally, the friction factors were found to be higher than those for water.

References

[1] T. Morimoto, K. Suzuki, and H. Kumano. "Heat transfer characteristics of phase change emulsions with solidification of phase change material particles in a circular tube". In: *Int. J. Refrig.* 114 (2020), pp. 1–9.

[2] Ian H. Bell, Jorrit Wronski, Sylvain Quoilin, and Vincent Lemort. "Pure and Pseudo-pure Fluid Thermophysical Property Evaluation and the Open-Source Thermophysical Property Library CoolProp". In: *Industrial & Engineering Chemistry Research* 53.6 (2014), pp. 2498–2508.

[3] RAMESH KESHAVLAL SHAH. *Laminar Flow Forced Convection Heat Transfer and Flow Friction in Straight and Curved Ducts–A Summary of Analytical Solutions.* Stanford University, 1972.

[4] AB Metzner and JC Reed. "Flow of non-newtonian fluids—correlation of the laminar, transition, and turbulent-flow regions". In: *Aiche journal* 1.4 (1955), pp. 434–440.

[5] James Clerk Maxwell. *A treatise on electricity and magnetism.* Vol. 1. Clarendon press, 1873.

[6] Virginia Vasile, Horia Necula, Adrian Badea, Rémi Revellin, Jocelyn Bonjour, and Phillipe Haberschill. "Experimental study of the heat transfer characteristics of a paraffin-in-water emulsion used as a secondary refrigerant". In: *International Journal of Refrigeration* 88 (2018), pp. 1–7.

[7] Virginia Vasile. "Experimental study of the thermal and rheological behaviour of paraffin-in-water emulsions used as a secondary refrigerants". PhD thesis. Université de Lyon; Universitatea politehnica (Bucarest), 2019.

[8] Mohamed Najib El Boujaddaini, Abdelaziz Mimet, and Philippe Haberschill. "Forced Convective Heat Transfer Study of Paraffin Slurry Flowing in a Vertical Rectangular Channel". In: *International Journal of Fluid Mechanics Research* 40.5 (2013).

Chapter 7

Numerical investigation into the heat transfer performance of phase change dispersions

This chapter establishes the development of a numerical model that captures the heat transfer behaviour of a PCD during crystallisation. The model works on the premise of a quasi-homogeneous fluid which has temperature adaptive properties, which are ultimately the transport properties of the PCD (as measured under static conditions). The heat transfer behaviour is addressed through an energy balance, taking into account the crystallisation apparent specific heat capacity during the cooling process. Firstly, a literature review was performed to grasp the current state of the art in numerical modelling of phase change dispersions, and subsequently a model was developed using ANSYS Fluent. Once the equations had been established, the numerical validation was performed with experimental results obtained for water. The numerical analysis was then executed using the PCD fluid (formulation 1) and compared to the experimentally obtained results.

7.1 Literature study on numerical investigations

Thermal energy storage and transport with PCDs combines several physical processes and subsequently modelling challenges e.g. phase change, dispersion flow dynamics and convective/conductive heat transfer [1, 2]. Additionally, large differences in the scale between dispersed PCM droplet sizes and the channel/pipe's diameter or length presents as difficult [3]. The first numerical study on the heat transfer properties of PCDs was performed by Kasza and Chen using the dirac σ-function to study the heat transfer of a phase change dispersion over a plate at constant temperature [4]. This model was further elaborated on by Charuyakorn et al. [5] to take into account the increase in the thermal conductivity as a result of particle-fluid interactions. The heat gain due to the phase

change was also incorporated as a source term into the energy equation [5]. From this numerical investigation, it was found that the Nusselt number was the highest at the inlet of the pipe and was 2-4 times higher than for water [5]. Zhang and Faghri [6] developed a new model which incorporated the initial subcooling of the PCD into the quasi-steady method, which eliminated the problem of the over-estimation of the simulation. This was due to assuming a melting range of the PCD droplets, and not a fixed melting point [6]. Roy and Avanic [7] then used the effective heat capacity model to investigate the heat transfer behaviour of a PCD in laminar forced convection. In previous investigations, the specific heat functions were taken as rectangular functions, such that the temperature-dependent specific heat step function only occurred during phase change. The effective heat capacity model, was improved by Alisetti and Roy [8] by incorporating the phase change effects of the PCM directly into the energy equation by assuming the specific heat capacity of the PCM to be a function of the temperature. Choi et al. [9] proposed a three-region melting model, with regions taking into account the initial subcooling, melting and a region of no melting.

Generally, numerical models of PCDs can be split into two main categories, those that use a quasi-homogeneous single-phase model with modified thermophysical and transport properties, and the two-phase, Euler-Euler numerical model, which treats both the dispersed PCM phase and the continuous water phase separately.

7.1.1 Single-phase model

Single-phase modelling approaches consider the dispersed PCM droplets and the continuous phase as a single homogeneous fluid with respect to its effective properties [10, 11]. Serale et al. [12] simulated a solar thermal collector with a PCD as the heat transfer fluid and developed auxiliary equations for the PCD by using mass averaged properties of the PCM and continuous phase. Subsequently, the model was well validated with experimental results [12]. It was suggested by Li et al. [1] that a single-phase quasi-homogeneous model has better thermal prediction than the two-phase models for phase change dispersions, with significantly lower computational costs. The single-fluid model is the least computational demanding and easy to implement, however single-fluid models have been shown to be inadequate at modelling phase redistributions that can occur for larger particle sizes with buoyancy effects [1, 2]. Akbari et al. [13] concluded in their comparative assessment of single and two-phase models for numerical studies of nano-fluids that since the single-phase model is simpler to implement and requires less computer memory that it is more appropriate for studying nano-fluids. This comparison was also performed by Goktepe et al. [11] where it was summarised that the type of model to be used depends on a case-by-case basis. In the instance that detailed knowledge about each phase needs to be known, the two phase modelling approach should be undertaken.

7.1.2 Two-phase model

Two-phase modelling approaches for PCDs treat the continuity, momentum and energy equations for the dispersed PCM particles and the continuous phase with two different approaches. The first approach, and the most common, is the Eulerian-Mixture model, whereby the momentum and energy equations are solved for the mixture, coupled with the continuity equation for each phase, with the velocities of each phase related to each other by the use of empirical equations [14, 11]. The second approach is generally used where the interactions between the two phases are not well defined or understood, and is named the Eulerian-Eulerian model. In this model, the continuity, momentum and energy equations are solved separately for each phase [11, 15, 16]. Currently, state-of-the-art contributions have shown that the mixture two fluid model is the most accurate when specific empirical data (such as measured thermophysical properties) and that the two phase model is preferable when limited data is available.

7.2 Methodology and Geometry

The list of assumptions used in the numerical investigation include:

1. The flow is laminar and steady
2. The crystallisation process takes place over a range of temperatures, which is predefined by the experimental inlet temperatures taken
3. The PCM droplets and the continuous phase are considered as a new quasi-homogeneous phase, with averaged transport and thermophysical properties.
4. The bulk properties are assumed constant spatially, but the thermal conductivity, dynamic viscosity, density and specific heat capacity are functions of temperature

7.2.1 Geometry

This model is based on the test-rig described in Section 6.1.2 and the fluid (either water or PCD) flows vertically in the rectangular channel from the bottom of the channel to the top. The ethanol channel, which cools down the PCD/water, flows in counter-current. The vertical flow is to ensure that gravity produces no concentration gradients and that the PCD flow can be considered homogeneous along the length of the channel. The model can be seen alongside a schematic of the actual experimental test-rig in Figure 7.1, it is a 2D planar model with symmetry in the y-axis. The coordinate system is defined as x in the horizontal, the y is the vertical and is pointing upwards (in the opposite direction of gravity, and the way in which the PCD flows).

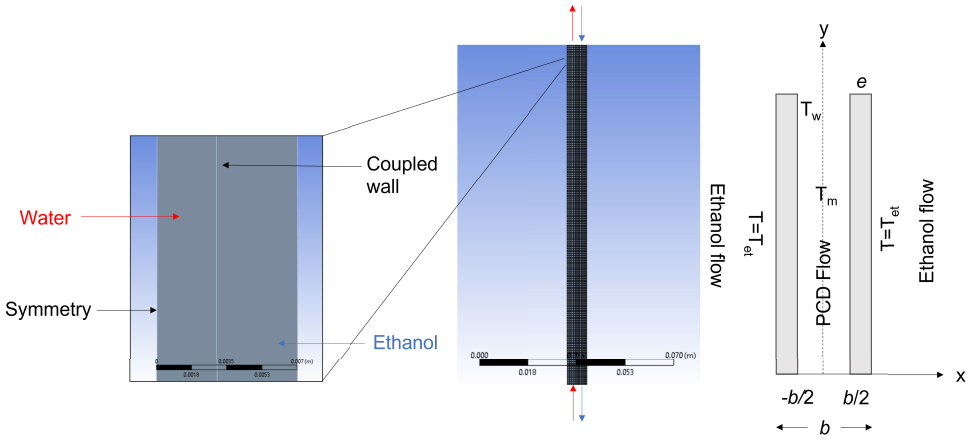

Figure 7.1: The simulation model and the actual geometry used in the numerical investigation

7.2.2 Mesh

The 2D domain is fabricated from hexahedral cells throughout the channel with refinement near the channel walls, and inlets and outlets, this is to ensure that the wall coordinate y+ near the walls is near 1 in the sublayer. The mesh was optimised to accurately carry out the calculation without consuming too much computational power.

7.2.3 Boundary conditions

For flow inside the rectangular channel, the velocity was considered to be 0 at the walls. The inlet temperature was set as a transient table taken from the experimental data, and $T = T_{in,PCD}$ at the inlet for the water/PCD and $T = T_{in,et}$ for the ethanol inlet. The external walls were considered adiabatic and the internal wall (between the ethanol and water/PCD side of the channel) was a coupled wall. The velocities of both the ethanol and PCD flows in the channel are given in the form of a transient table at the inlet of the channel.

7.2.4 Solution methods and discretisation

The pressure-velocity coupling using the SIMPLE scheme was used and the spatial discretisation was used as follows: for the gradient, the least squares cell based, for the pressure second order scheme, for the momentum second order upwind and for the energy second order upwind. The residuals from all the numerical investigations were below 10^{-8} and the energy residuals were less than 10^{-16} for the solution to be considered fully converged at every time-step.

7.3 Validation with water

7.3.1 Validation of temperature profiles

To initiate the validation of the numerical model, firstly the experimental temperature profiles obtained for water were compared to the numerically determined result. Since the inlet temperatures of the ethanol and water channels were set with a user-defined function in the form of a transient table, the outlet temperatures of the ethanol and water channels were monitored with respect to different time-steps (flow-time). This was performed for a Reynolds numbers of 641 and the deviation between the experimentally obtained results and the numerical results can be seen in Figure 7.2 below.

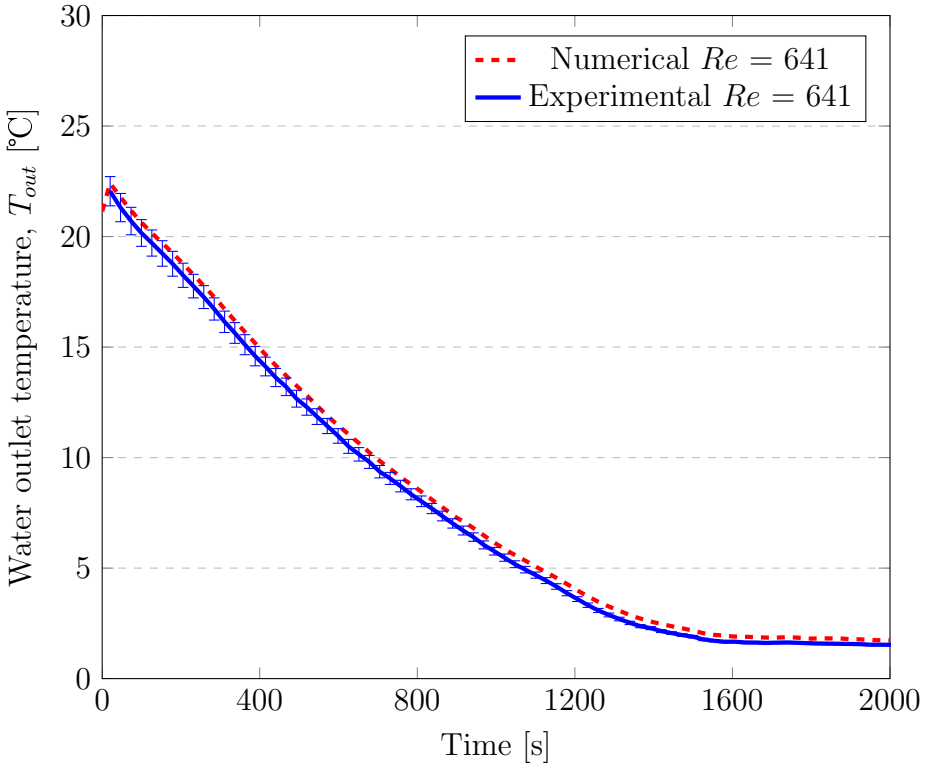

Figure 7.2: Comparison of the numerical and experimental water outlet temperatures at Reynolds numbers of 710. Additionally, the error bars for the experimental values are shown.

It can be seen that the maximum deviation between the experimentally measured outlet temperatures of water and the numerically determined determined outlet temperatures are below the uncertainty of the measured values (0.3 K) at all time steps. The local temperature profiles, at specific time steps (flow times) were then compared to observe how well the numerical model can capture the bulk temperatures of the fluid along the length of the rectangular channel. The numerically determined values were compared to

the experimentally obtained bulk temperatures , which were calculated from the experimentally measured temperatures based on an energy balance using Equation 6.6. The local comparison can be seen for two different flow times, 400 and 1200 s.

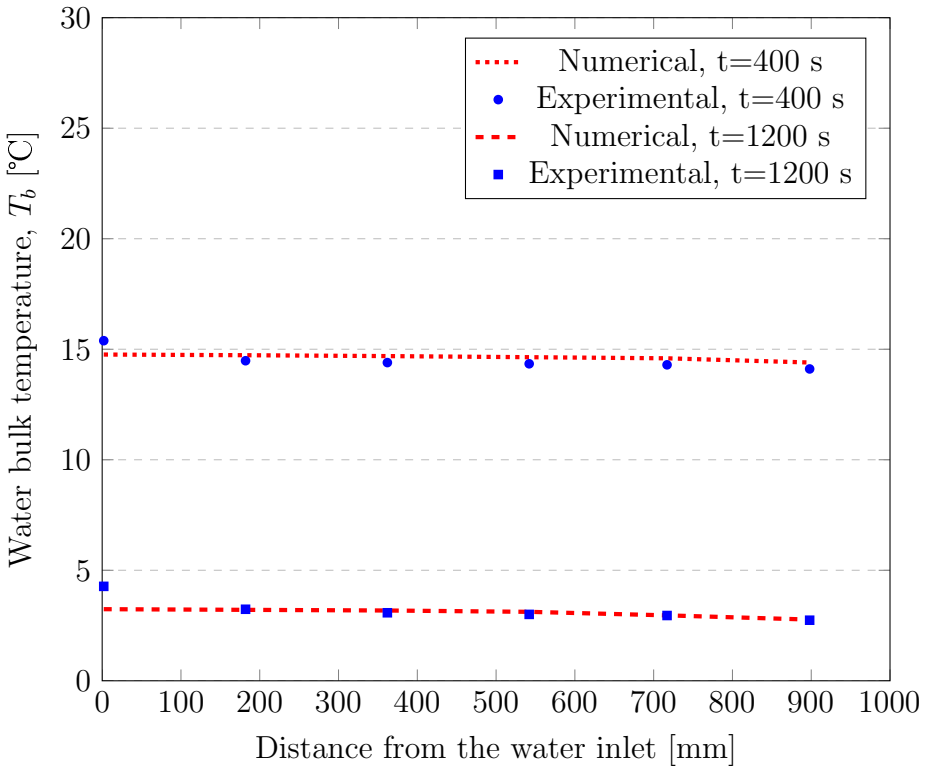

Figure 7.3: Comparison of the numerical and experimental water local bulk temperatures, at a Reynolds number of 710 and for two different time steps: at time 400 s and at time 1200 s. Additionally, the error bars are shown for the experimental values.

From Figure 7.3, it can be seen that there is a good agreement between the numerical results and the experimental results with an exception of the first calculated bulk temperature. The reasoning for this, is that at the inlet of the channel, there is more area for exchange with the ambient, suggesting that there could be an absorption of heat from the atmosphere near the inlet of the experimental channel. The numerically calculated bulk temperatures are just above the 0.3 K error of the experimentally determined bulk temperatures. It has been suggested that using the single-phase model can result in temperatures higher than those obtained experimentally due to the accuracy of the simulation by the wall.

7.3.2 Local heat transfer coefficients

Following the validation of the temperatures at both the outlet and in the bulk, the calculation of the water-side heat transfer coefficients were calculated using the numerical

model through the following equation:

$$h_x = \frac{q_f}{T_b - T_w} \tag{7.1}$$

where q_f is the heat flux computed through Fourier's law applied at the walls as:

$$q_f = \lambda_f (\frac{dt}{dn})_{wall} \tag{7.2}$$

where n is the local coordinate normal to the wall. For a Reynolds number of 641, the local heat transfer coefficients were calculated for water using the simulation and compared to the experimental results calculated in Chapter 6. Figure 7.4 displays the local heat transfer coefficients determined both experimentally and with the model.

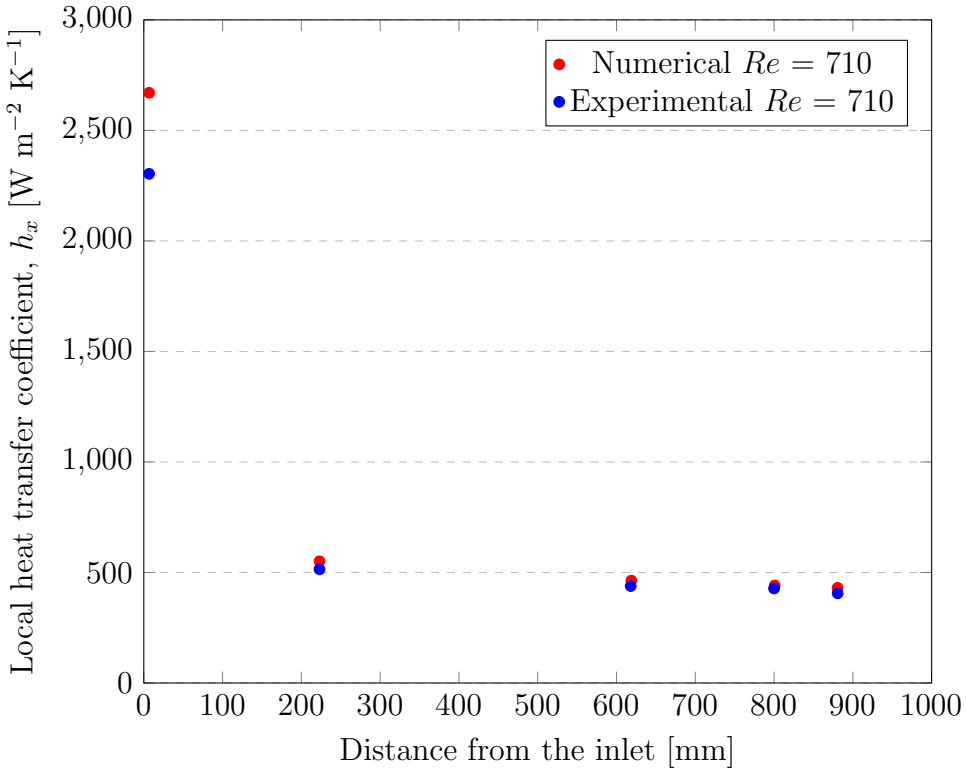

Figure 7.4: Comparison of the numerical and experimental water local heat transfer coefficients for a Reynolds numbers of 710. Additionally, the error bars are shown for the experimental values.

Figure 7.4 highlights the discrepancy between the heat transfer coefficient at the inlet determined experimentally and calculated with the model. This is thought to be as a result of the model's over-prediction of the first temperature at the inlet, as highlighted in Figure 7.3. This is most likely as a result of neglecting the thermal resistances in the simulation. Despite this, after the thermal boundary layer had been established after

approximately 200 mm, the values between the experimental and numerical results were much closer.

7.4 Results with formulation 1

Once the model was performing well with water, a numerical investigation into the heat transfer behaviour of formulation 1 ensued. The dynamic viscosity, specific heat capacity, density and thermal conductivity were all modified to be temperature dependent (since only one mass flow rate was investigated with the PCD, the shear-rate dependence of the dynamic viscosity was not taken into consideration). Firstly, as with water, since the inlet temperatures were set with a user-defined function in the form of a transient table from the experimental data, the outlet temperatures of the PCD channel was monitored with respect to different time-steps (flow times). The Reynolds number of 710 was chosen, to compare with water, and the results of the thermal profile of the PCD (formulation 1) both experimentally, and with the numerical model can be seen in Figure 7.5.

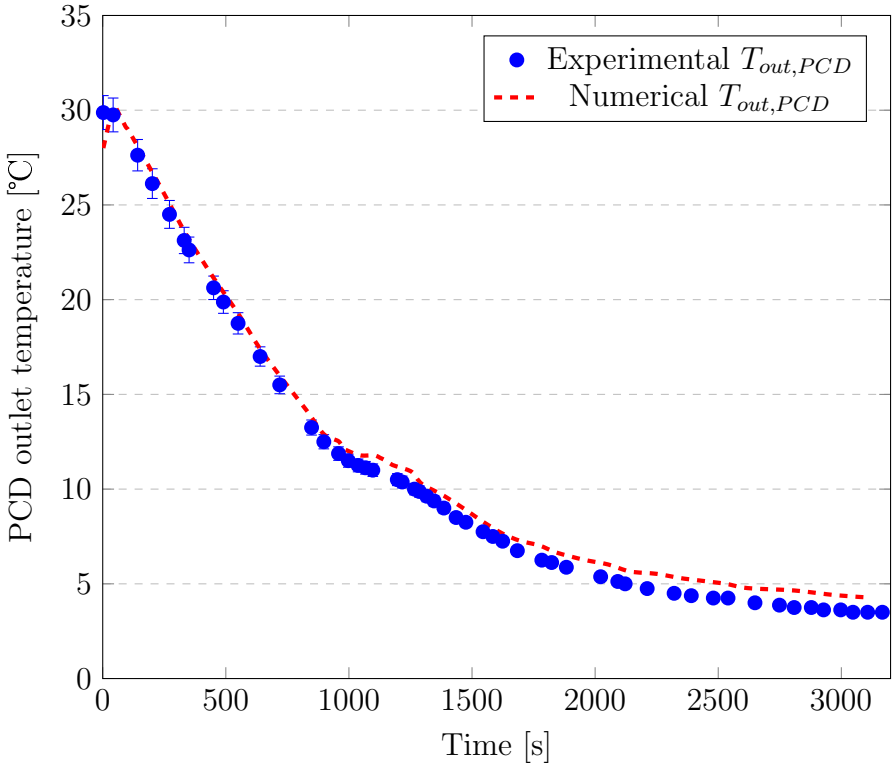

Figure 7.5: Comparison of the numerical and experimental PCD outlet temperatures at Reynolds numbers of 710. Additionally, the error bars for the experimental values are shown.

It can be seen from Figure 7.5 that before the phase change, from $t = 0$ until $t = 800s$, the deviation between the numerical model and the experimental values are within the

0.3K experimental error. This is with the exception of $t = 0$, which corresponds to the initialisation of the numerical simulation. However, it can be seen that there is a delay in the phase change plateau in the numerical model results compared to the experimentally determined results, where the deviation also exceeds the 0.3K experimental uncertainty. After the phase change, it also appears that the deviation is larger. This can most likely be attributed to thermal resistances being ignored in the simulation.

For closer inspection of the thermal behaviour at specific time steps, the local temperature profiles, over the length of the channel for $t = 450s$ and $t = 2000s$ were compared from both the numerical model and the experimental results. The results of the local bulk PCD temperatures determined both experimentally and numerically are displayed in Figure 7.6.

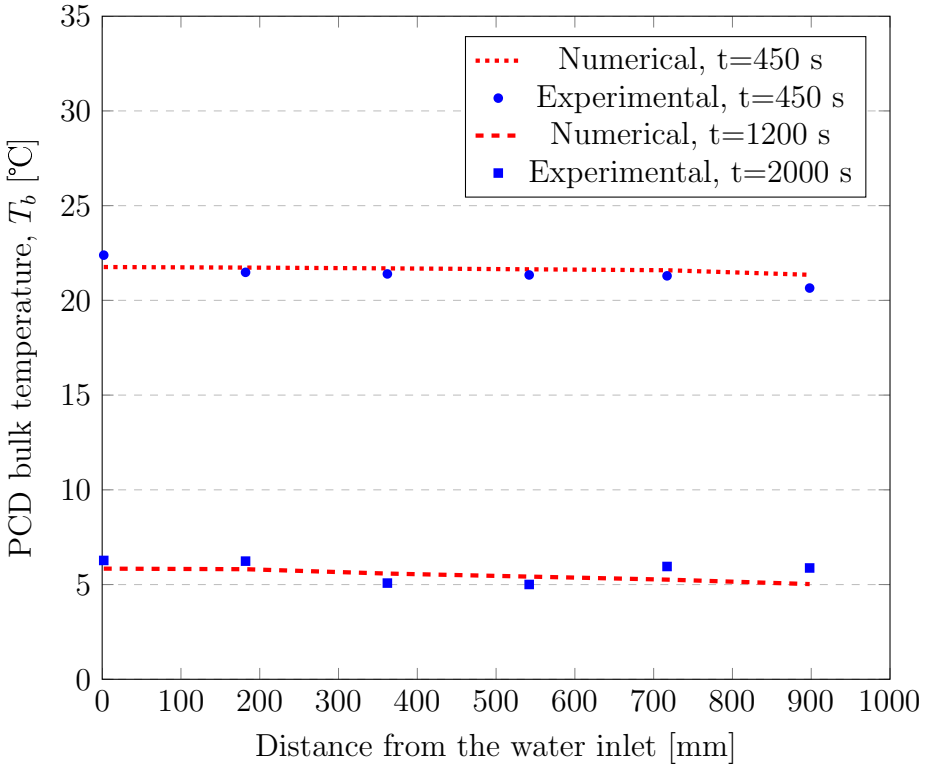

Figure 7.6: Comparison of the numerical and experimental PCD local bulk temperatures, at a Reynolds number of 710 and for two different time steps: at time 450 s and at time 2000 s. Additionally, the error bars are shown for the experimental values.

From Figure 7.6 it can be observed that there is a good agreement between the numerical values and the experimental values at $t = 450s$, which is further evidenced by the thermal profiles of the outlet temperatures in Figure 7.5. There is a discrepancy between the the first thermocouple measurement (at 2 mm) compared to the numerical result. This was the same as what was observed in the local water bulk temperatures. It is expected that as with the case with water, in the experiments, there is a larger exchange

with the ambient, suggesting heat gains from the environment. In the case of $t = 2000s$, the experimental values fluctuate significantly, most likely due to the low temperatures.

7.4.1 Local heat transfer coefficients

Using equations 7.1 and 7.2, the PCD-side local heat transfer coefficients were calculated from the numerical model for a Reynolds number of 710, and for an inlet temperature of 20 ℃.These values were subsequently compared to the experimentally determined values for the same boundary conditions.

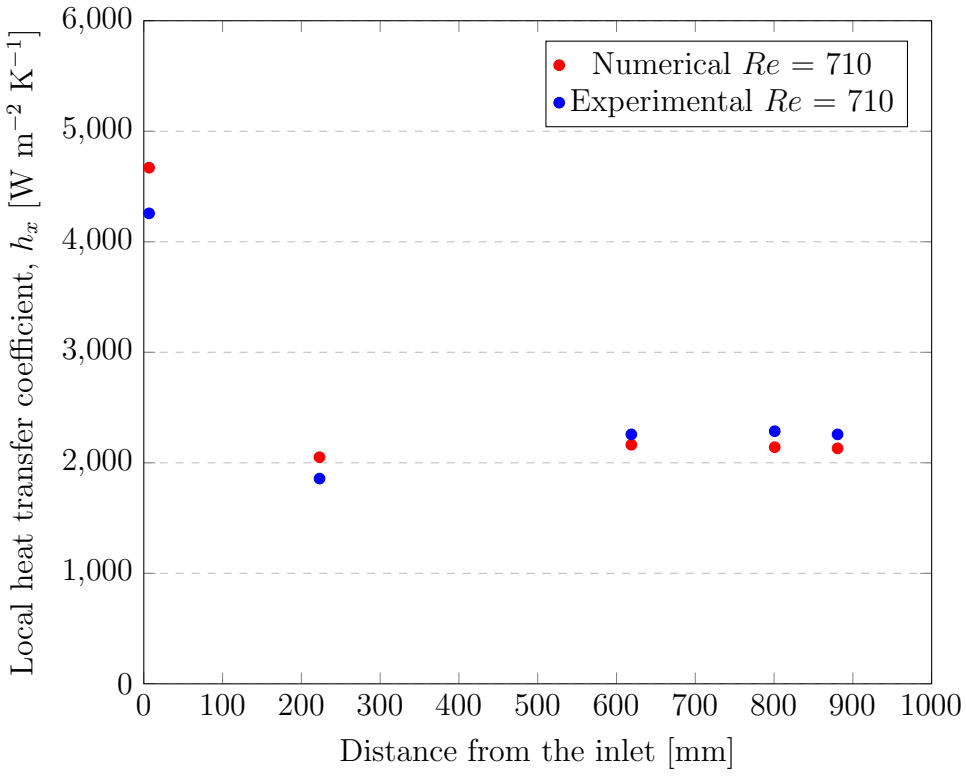

Figure 7.7: Comparison of the numerical and experimental PCD local heat transfer coefficients for a Reynolds numbers of 710. Additionally, the error bars are shown for the experimental values.

From Figure 7.7, the local heat transfer coefficients for the PCD determined experimentally and numerically are displayed. Before the thermally developed region, there is a larger discrepancy between the local heat transfer coefficients, which again is most likely due to the inlet phenomenon. This suggests further investigation needs to be taken into understanding this and how to correct it in the numerical model.

7.5 Conclusions and future perspectives

In this chapter, a rudimentary numerical model has been created for elucidation of the heat transfer behaviour of phase change dispersions flowing through a rectangular channel. The numerical model was based on the quasi-homogeneous single-phase fluid approach, and executed with ANSYS Fluent. The boundary inlet conditions for the simulation was based on a transient table using the velocities and temperatures from the experimental campaign. Validation of the model was performed with water, with low deviations between the experimental and numerical values for the water outlet temperatures, local bulk temperatures and local heat transfer coefficients. There was slight deviations noticed between the numerical simulation and the experimentally determined values at the first thermocouple measurement from the inlet. This was named the inlet phenomenon. Despite this, the numerical model was run for a PCD, formulation 1 from Chapter 5, and the PCD used in Chapter 6. The thermal profile of the PCD outlet temperature against time showed that before the phase change, the discrepancy between the simulation and the experimental results was smaller than after the phase change. It was also noticed that the phase change detected by the model, was delayed. The bulk PCD temperatures also showed good accordance with each other, as did the local heat transfer coefficients. However, for future development of the model it is suggested that the inlet phenomenon is looked at more carefully and the model and geometry modified to take this into account. Additionally, it must be noted that the simulation is not well optimised for cost efficiency, with each simulation requiring long-time frames due to the adaptive transient time-steps used. For future, this must be improved upon before the simulation can be used effectively.

References

[1] Qi Li, Geng Qiao, Ernesto Mura, Chuan Li, Ludger Fischer, and Yulong Ding. "Experimental and numerical studies of a fatty acid based phase change dispersion for enhancing cooling of high voltage electrical devices". In: *Energy* 198 (2020), p. 117280.

[2] Qi Li, Ludger Fischer, Geng Qiao, Ernesto Mura, Chuan Li, and Yulong Ding. "High performance cooling of a HVDC converter using a fatty acid ester-based phase change dispersion in a heat sink with double-layer oblique-crossed ribs". In: *International Journal of Energy Research* 44.7 (2020), pp. 5819–5840.

[3] F. Wang, J. Cao, Z. Ling, Z. Zhang, and X. Fang. "Experimental and simulative investigations on a phase change material nano-emulsion-based liquid cooling ther-

mal management system for a lithium-ion battery pack". In: *Energy* 207 (2020), p. 118215.

[4] KE Kasza and MM Chen. "Improvement of the performance of solar energy or waste heat utilization systems by using phase-change slurry as an enhanced heat-transfer storage fluid". In: (1985).

[5] Pongtorn Charunyakorn, S Sengupta, and SK Roy. "Forced convection heat transfer in microencapsulated phase change material slurries: flow in circular ducts". In: *International journal of heat and mass transfer* 34.3 (1991), pp. 819–833.

[6] Yuwen Zhang and Amir Faghri. "Analysis of forced convection heat transfer in microencapsulated phase change material suspensions". In: *Journal of thermophysics and heat transfer* 9.4 (1995), pp. 727–732.

[7] SK Roy and BL Avanic. "Laminar forced convection heat transfer with phase change material emulsions". In: *International communications in heat and mass transfer* 24.5 (1997), pp. 653–662.

[8] Edwin L Alisetti and Sanjay K Roy. "Forced convection heat transfer to phase change material slurries in circular ducts". In: *Journal of thermophysics and heat transfer* 14.1 (2000), pp. 115–118.

[9] C. Eunsoo, Y. Cho, and H. Lorsch. "Forced convection heat transfer with phase-change-material slurries: turbulent flow in a circular tube". In: *Int. J. Heat Mass Transf.* 37.2 (1994), pp. 207–215.

[10] Sidi El Bécaye Maıga, Cong Tam Nguyen, Nicolas Galanis, and Gilles Roy. "Heat transfer behaviours of nanofluids in a uniformly heated tube". In: *Superlattices and Microstructures* 35.3-6 (2004), pp. 543–557.

[11] Sinan Göktepe, Kunt Atalık, and Hakan Ertürk. "Comparison of single and two-phase models for nanofluid convection at the entrance of a uniformly heated tube". In: *International Journal of Thermal Sciences* 80 (2014), pp. 83–92.

[12] Gianluca Serale, Francesco Goia, and Marco Perino. "Numerical model and simulation of a solar thermal collector with slurry Phase Change Material (PCM) as the heat transfer fluid". In: *Solar energy* 134 (2016), pp. 429–444.

[13] M Akbari, N Galanis, and A Behzadmehr. "Comparative assessment of single and two-phase models for numerical studies of nanofluid turbulent forced convection". In: *International Journal of Heat and Fluid Flow* 37 (2012), pp. 136–146.

[14] R Lotfi, Y Saboohi, and AM Rashidi. "Numerical study of forced convective heat transfer of nanofluids: comparison of different approaches". In: *International Communications in Heat and Mass Transfer* 37.1 (2010), pp. 74–78.

[15] Mohammad Kalteh, Abbas Abbassi, Majid Saffar-Avval, and Jens Harting. "Eulerian–Eulerian two-phase numerical simulation of nanofluid laminar forced convection in a microchannel". In: *International journal of heat and fluid flow* 32.1 (2011), pp. 107–116.

[16] T Ahmad, SL Plee, and JP Myers. "FLUENT Theory Guide". In: *ANSYS Inc* (2010).

Chapter 8

Conclusions and Future Perspectives

The main objective of this thesis was to analyse the different formulation and operational conditions on the heat transfer and rheological performance of phase change dispersions for different applications. Firstly, a literature study was conducted, which highlighted that the application of PCDs into the cooling network has been limited due to large degrees of supercooling because of the small particle sizes and issues with stability both in storage and during cycling. Additionally, a more comprehensive understanding of the heat transfer performance is required to push PCDs into industrial systems. Furthermore, the literature review highlighted the conflicting information given in literature on the effect of the different formulation properties and operational conditions on the heat transfer performance of PCDs.

Chapter four addressed the effect of different formulation conditions, such as shear rate and type of homogenising on the stability of PCDs. Here, it was found that stationary homogenising techniques, for a homogenising time of five minutes and a speed of 6500 rpm was the best compromise between the production of stable PCDs, whilst using a lower energy input. The role of surfactants in controlling the stability of PCDs was elucidated and the relationship between the structure of the surfactant and the stability was established. It was found that larger, bulkier head groups of the surfactants increased the steric-hindrance between droplets and prevented them from suffering from coalescence. The structure of surfactants and their effect on the nucleation behaviour of PCDs was also investigated. Here, the results displayed that the bulky head group of surfactants can induce nucleation through acting as templates by creating rigid-film interfaces. Despite the promising behaviour of choosing surfactants with bulky head groups, for increasing stability and decreasing supercooling, the rigid interface as a result of these head groups resulted in highly viscous, unpump-able PCDs. To rectify this, a novel surfactant system was engineered, which comprised of an optimised mixture of a bulky head group surfactant and a smaller co-surfactant. When using this surfactant system, the PCD had high stabilities, low degrees of supercooling and low viscosities. A theory was suggested

to explain how surfactant systems can be chosen and designed to better optimise the thermophysical properties of PCDs. This chapter should act as a future guideline in the design and formulation of PCDs and emulsions with tailored properties.

The influence of the surfactant systems and formulation properties was elucidated in Chapter four, and then in Chapter five, on the heat transfer and rheological behaviour of PCDs. Overall, Chapter five displayed an experimental heat transfer and rheological campaign that was executed for two different PCDs in a cylindrical pipe during melting. The rheological analysis showcased that both PCD formulations, which both consisted of a 16 wt.% PCM and a 4 wt.% surfactant system had non-Newtonian, shear-thinning behaviour. The degree of the non-Newtonian behaviour was affected by temperature, due to the different natures of the surfactant system used. This was also affected by the melting of the PCM droplets in the PCD. The two different PCD formulations also had different heat transfer behaviour, with formulation 2 having higher heat transfer coefficients and Nusselt numbers. This was attributed to a higher enthalpy of fusion and apparent specific heat capacity of the PCM used in formulation 2 compared to formulation 1. Despite this, both formulations showed higher Nusselt numbers compared to water under the comparison criterion of the same Reynolds number. Interestingly, a never-before-seen phenomenon of a shear-rate dependence of the thermal conductivity was observed and corrected for by using the Hausen-Gnielinski correlation.

As discussed in the literature review in Chapter two, there has been extremely few experimental campaigns looking into the physical phenomena occurring during the crystallisation of PCDs. As a result of this, Chapter six focused on a complete characterisation of formulation 1 during crystallisation in a rectangular channel using a novel data reduction method. Nusselt numbers at different temperatures in the cooling and crystallisation process were investigated for a Reynolds number in the range of 200 to 1100 and it was found that 20℃ had the highest Nusselt numbers and that an increase in the Reynolds number resulted in an increase in the average Nusselt numbers. Additionally at Reynolds numbers below the normal transition Reynolds number (2300), an unexpected transition, characterised by a large increase in the average Nusselt number was observed for all temperatures. An interesting and novel discussion was presented in an attempt to theoretically explain this phenomenon. For single-phase flows, such as water, the transition regime of the Reynolds number has been extensively investigated and validated. However, with the two-phase fluid studied, in a rectangular channel, the transition regime is unknown. It is expected that this transition regime is influenced by the channel geometry, the surface roughness of the channel, the thermophysical properties of the PCD and ultimately the stability of the PCD. Despite this, it is suggested that this behaviour needs more future focus and analysis to properly describe the heat transfer behaviour of non-Newtonian fluids in rectangular channels.

The same fluid and geometry from Chapter six was then the basis for a numerical

simulation ran in Chapter seven. In this chapter, a basic numerical model was created for elucidation of the heat transfer behaviour of phase change dispersions flowing through a rectangular channel. The numerical model was based on the quasi-homogeneous single-phase fluid approach, and executed with ANSYS Fluent. The boundary inlet conditions for the simulation was based on a transient table using the velocities and temperatures from the experimental campaign. Validation of the model was performed with water, with low deviations between the experimental and numerical values for the water outlet temperatures, local bulk temperatures and local heat transfer coefficients. There was slight deviations noticed between the numerical simulation and the experimentally determined values at the first thermocouple measurement from the inlet. This was named the inlet phenomenon. Despite this, the numerical model was run for a PCD, formulation 1 from Chapter 5, and the PCD used in Chapter 6. The thermal profile of the PCD outlet temperature against time showed that before the phase change, the discrepancy between the simulation and the experimental results was smaller than after the phase change. It was also noticed that the phase change detected by the model, was delayed. The bulk PCD temperatures also showed good accordance with each other, as did the local heat transfer coefficients. However, for future development of the model it is suggested that the inlet phenomenon is looked at more carefully and the model and geometry modified to take this into account. Additionally, it must be noted that the simulation is not well optimised for cost efficiency, with each simulation requiring long-time frames due to the adaptive transient time-steps used. For future, this must be improved upon before the simulation can be used effectively.

FOLIO ADMINISTRATIF

THESE DE L'INSA LYON, MEMBRE DE L'UNIVERSITE DE LYON

NOM : O'NEILL DATE de SOUTENANCE : 02.09.2022

Prénoms : Poppy

TITRE : Phase change dispersions as high performance heat transfer fluids

NATURE : Doctorat Numéro d'ordre : 2022ISAL0073

Ecole doctorale : ED162 : Mécanique, Énergétique, Génie civil, Acoustique (MEGA)

Spécialité : Mécanique de fluide

RESUME : This thesis focuses on the heat transfer, transport, and rheological behaviour of novel two-phase fluids, named phase change dispersions. Phase change dispersions consist of phase change material dispersed into a continuous phase with the aid of surfactants. The optimal formulation procedure for phase change dispersions with high stabilities, low supercooling degrees and high apparent specific heat capacities is discussed and an innovative approach in fine-tuning the thermophysical properties of phase change dispersions with the use of cosurfactants is defined. Two of the developed formulations were then chosen for a heat transfer and rheological behaviour comparison to observe the effect that surfactants have on the transport and heat transfer properties during heating. This was performed using a test-rig to measure the bulk fluid and inner wall temperatures of the phase change dispersions flowing through a cylindrical tube under the constant heat flux boundary condition. The crystallisation heat transfer and rheological behaviour of a phase change dispersion was also examined through calculation of heat balances in a rectangular duct. During melting and crystallisation, an interesting phenomenon was discovered, that the transition from laminar to turbulent with phase change dispersions was much lower than those predicted for Newtonian fluids. By regression of the experimental results, correlations for the average Nusselt numbers for laminar and turbulent flow are presented, using a modified Reynolds number and a Prandtl number correction factor. A numerical model for the thermal behaviour studies of a phase change dispersion during its cooling in laminar flow through a rectangular duct was developed and is based on the quasi-homogeneous single fluid approach. The evolution of the experimental and theoretical values shows good agreement and the model satisfactorily predicts the behaviour, with variations of less than 5%.

MOTS-CLÉS : Transfert de chaleur, dispersion à changement de phase (PCD), matériau à changement de phase (PCM), rhéologie, débit biphasé

Laboratoire (s) de recherche : CETHIL

Directeur de thèse: Professeur Rémi Revellin
Co-directeur de thèse : Professeur Jocelyn Bonjour

Président de jury : Professeur Jérôme Bellettre

Composition du jury : Professeure Monica Siroux, Professeur Matthias Kind, Professeur Ludger Fischer, Professeur Phillipe Haberschill, Dr. Anastasia Stamatiou